Lower Jurassic organic matter accumulation in the Bächental basin: Global to regional controls

Doctoral Thesis

Dipl.-Ing. Stefan Neumeister, BSc

Supervisor

Ao.Univ.-Prof. Mag. et Dr.rer.nat. Hans-Jürgen Gawlick

Department of Applied Geosciences and Geophysics

Chair of Petroleum Geology

Montanuniversitaet Leoben

Leoben, 2016

Affidavit

I declare in lieu of oath, that I wrote this thesis and performed the associated research myself, using only literature cited in this volume.

(Dipl.-Ing. Stefan Neumeister, BSc)

Fertig?

Nein, nur ein Zwischenschritt.

Es gibt noch viel zu tun!

Danksagung

Wem alles danken? Es gibt so viele Personen, die mich unterstützt, gefördert, motiviert, angetrieben, aufgefangen, abgelenkt, im positiven Sinne belehrt und weiter gebracht haben. Personen, die mir geholfen und Wissen vermittelt haben, die mir Beistand und Rückhalt waren, die mit mir diskutiert und mich auf neue, frische Gedanken und Wege gebracht haben. Personen, die rücksichtvoll, geduldig und verständnisvoll waren. Personen, die mich aus meiner Komfortzone gebracht und Ausreden und Ausflüchte schamlos aufgedeckt haben. Kurz: Personen, die in fachlicher oder privat-emotionaler Hinsicht am erfolgreichen Abschluss dieser Arbeit mitgewirkt haben. Im Anschluss eine Liste ohne Gewähr auf Vollständigkeit:

Professor Hans-Jürgen Gawlick. Danke, dass du mich auf die Idee für diese Doktorarbeit gebracht und intensiv am ursprünglichen Einreichprojekt mitgearbeitet hast. Danke auch für die Anregungen zum kritischen Hinterfragen und Nachdenken, für die Herstellung von vielen hilfreichen Kontakten, für die allgemeine und fachliche Unterstützung während der letzten Jahre und dafür, dass du mir verschiedene Länder des Balkans näher gebracht hast.

Professor Reinhard F. Sachsenhofer. Danke für dein Interesse an meiner Arbeit, deine Lösungsorientiertheit, die intensive erdölgeologische Unterstützung, die vielen fachlichen Gespräche und Diskussionen, die Fähigkeit, komplizierte Sachverhalte einfach darzustellen, die immens wichtige Mitwirkung an den Veröffentlichungen und für das ständige Antreiben.

Professor Werner Piller. Danke, dass Sie bei Bedarf immer Zeit für ein Gespräch am Lehrstuhl in Graz gehabt haben, bei denen ich neben fachlichen auch private Themen – ganz im Sinne eines echten „Mentoring“ – offen ansprechen und mit Ihnen diskutieren konnte.

Prof. Tom Algeo. Danke für die anorganischen-geochemischen Analysen und deinen wichtigen Beitrag als „native speaker“ für unsere Publikationen. Deine typisch amerikanische „straight forward“-Mentalität und dein Blick für das große Ganze haben der Arbeit gut getan und den Horizont dieser Dissertation erweitert.

Dr. Reinhard Gratzer. Die Arbeit im Geochemie- und im Isotopenlabor und die Auswertung der dazugehörigen Daten hast du mir näher gebracht. Du hast in vielerlei Bereichen mitgearbeitet und mitgeholfen. Deine Hilfsbereitschaft, Offenheit und Direktheit sowie dein

technisches Verständnis habe ich immer geschätzt, damit warst du am Institut eine meiner wichtigsten Bezugspersonen. Danke, du bist ein echter Tausendsassa!

Dr. Achim Bechtel. Dein Wissen hinsichtlich organisch-geochemischer Parameter und deren Bedeutung ist die Basis vieler Interpretationen dieser Arbeit. Danke für die Unterstützung.

Dr. Doris Groß. Wann immer ich etwas gebraucht habe, warst du da. Kohlenpetrographie, Leco, Rock Eval – ohne deine Unterstützung undenkbar. Danke auch für die vielen Gespräche über Daten und die dazugehörigen Interpretationen sowie über die anderen wichtigen Dinge des Lebens.

Dr. Sylvain Richoz. Danke für die vielen fachlichen Diskussionen, welche meinen Horizont im Besonderen hinsichtlich Ozeanologie, Klimatologie und Isotopie erweitert und damit ganz wesentlich zum Gelingen dieser Arbeit beigetragen haben. Ich habe dich im Rahmen meiner Dissertation kennengelernt und du bist ein sehr guter Freund geworden, auch dafür möchte ich dir hier danken.

Ursula Schmid. Ich will und muss Ihnen für so Vieles danken, das sprengt den Rahmen dieser Danksagung. Für mich sind Sie das Herz und die Seele des Instituts. Also, einfach „Herzlichen Dank“!

Sabine Feuchter. Danke für die vielen Stunden, in denen du mir bei der Probenpräparation und mit den Dünn- und Anschliffen geholfen hast. Besonders danken möchte ich dir aber auch für die unzähligen Gespräche über verschiedenste Themen während unserer gemeinsamen Arbeit. Du schaffst es mit deiner Art, dass selbst ein Dünnschlifflabor ein angenehmer Aufenthaltsraum ist und abgeschliffene Fingerkuppen erträglich sind.

Meine ausländischen Kooperationspartner: *Prof. Igor Vlahovic* (Zagreb) und *Prof. Nenad Banjac* (Belgrad). Danke für die Unterstützung bei etlichen Probennahmen und interessante, lehrreiche und kurzweilige Tage in Kroatien, Bosnien-Herzegowina und Serbien.

Danke an: *Prof. Gerd Rantitsch* für die Unterstützung im Labor, *Franz Seidl* für die Durchführung der RDA-Messungen und für die Mithilfe bei der Auswertung, meine *studentischen Kolleginnen und Kollegen* für die freundlichen und lustigen Gespräche, die fachliche Unterstützung und für die gute Zusammenarbeit im Allgemeinen.

Gertrude und Erwin Neumeister, meine Eltern. Danke für die Unterstützung während meines gesamten Bildungswegs. Diesbezüglich konnte und durfte ich immer machen, was ich wollte bzw. was mir vorschwebte. Ohne euch wäre diese Dissertation nicht möglich gewesen. Tja, es hat doch einige Zeit gedauert. Danke für die Geduld.

Nina, Lorenz, Simon und mein dritter, noch ungeborener, Sohn. Meine Familie, mein Rückhalt.

Abstract

The Bächental bituminous marls (Bächentaler Bitumenmergel) belonging to the Sachrang Member of the Lower Jurassic Middle Allgäu Formation were investigated using a multi-analytical (microscopy, XRD analysis, bulk geochemistry, stable isotopy, and organic geochemistry) approach to determine environmental, depositional, and diagenetic controls on the formation of organic-rich deposits in a semi-restricted basin of the NW Tethys during the Early Jurassic. The marls were subdivided into three discrete units (Units 1-2a-2b-3 from base to top) on the basis of mineralogical composition, source-rock parameters, redox conditions, salinity variations, and diagenetic processes. Redox proxies indicate varying suboxic to euxinic conditions during deposition of the Bächental section. In suboxic Units 1 and 3, organic matter (OM) was intensely degraded by Mn reduction. This process additionally triggered the formation of kutnohorite featuring abnormally negative carbonate-C isotope values at the chemocline. In contrast, sulfate reduction was the dominant degradation process in anoxic-euxinic Unit 2 and Mn-bearing calcite formed below the chemocline and containing small amounts of isotopically light C is the main diagenetic carbonate phase. Redox variations were mainly controlled by sea-level fluctuations with the tectonically complex bathymetry of the Bächental basin determining watermass exchange with the Tethys Ocean. Accordingly, strongest anoxia and highest TOC content occur in the middle part of the section coincident with a flourishing of algal and planktonic organisms during a period of relative sea-level lowstand that induced salinity stratification in a stagnant basin setting. This level corresponds to the time interval of the lower Toarcian oceanic anoxic event. However, the absence of the widely observed lower Toarcian negative carbon isotope excursion in the study section questions its unrestricted use as a global chemostratigraphic marker. The onset of reducing conditions in the Bächental basin coincided with the occurrence of charred OM and an influx of volcaniclastic detritus that was possibly connected to complex rifting processes of the Alpine Tethys and with a globally observed eruption-induced extinction event. The level of maximum OM accumulation corresponds to the main eruptive phase of the Karoo-Ferrar LIP, confirming its massive impact on global climate and oceanic conditions during the Early Jurassic. The study section is thus a record of the complex interaction of global (i.e., LIP) and local (e.g., redox and salinity variations, basin morphology) factors that caused reducing conditions and OM enrichment in the Bächental basin. These developments resulted in highly inhomogeneous environmental conditions in semi-restricted basins of the NW Tethyan domain during the Early Jurassic.

Kurzfassung

Der Bächentaler Bitumenmergel (Sachrang Member der unterjurassischen Mittleren Allgäu Formation) wurde unter Anwendung eines multi-analytischen Ansatzes (Mikroskopie, Röntgendiffraktometrie, Muttergesteinsparameter, Isotopie, organische und anorganische Geochemie) hinsichtlich der Umwelt-, Ablagerungs- und Diagenesebedingungen, welche die Bildung von organisch reichen Ablagerungen in eingeschränkten Becken der NW Tethys kontrollierten, untersucht. Die Mergel können auf Basis von Mineralogie, Muttergesteinsparameter, Redoxbedingungen, Salinität und diagenetischen Prozessen in drei Einheiten unterteilt werden (Units 1-2a-2b-3 von Liegend nach Hangend). Redoxparameter indizieren variierende suboxische bis euxinische Bedingungen während der Ablagerung des Bächentalprofils. Manganreduktion bewirkte den intensiven Abbau von organischem Material in den suboxischen Units 1 und 3. Dieser Prozess induzierte zusätzlich die Bildung von Kutnohorit mit abnormal negativen Werten für karbonatischen Kohlenstoff an der Chemokline. In der anoxisch-euxinischen Unit 2 war Sulfatreduktion der dominante Abbauprozess und manganhaltiger Kalzit mit geringen Mengen an isotopisch leichtem Kohlenstoff, welcher unter der Chemokline gebildet wurde, repräsentiert die Hauptkarbonatphase. Meeresspiegelschwankungen im Zusammenspiel mit der komplexen Beckengeometrie bestimmten den Wasseraustausch mit der Tethys und die Redoxvariationen im Bächentalbecken. Folglich ist der mittlere Teil des Profils, welcher während einer Periode erhöhter Bioproduktivität von algalen und planktonischen Organismen und eines relativen Meeresspiegeltiefstandes, der stagnierende Beckenbedingungen und eine Salinitätsschichtung verursachte, abgelagert wurde, durch Anoxia und höchste TOC Gehalte charakterisiert. Dieser Bereich entspricht dem Zeitintervall des ozeanischen anoxischen Ereignisses des Unteren Toarcium. Das Fehlen der im unteren Toarcium weit verbreiteten negativen Kohlenstoffisotopieexkursion im untersuchten Profil stellt ihre uneingeschränkte Anwendung als chemostratigraphischer Marker in Frage. Die Ausbildung reduzierender Bedingungen im Bächentalbecken erfolgt zeitgleich mit dem Auftreten von verkohltem organischen Material und dem Eintrag von vulkanoklastischem Detritus, welche potentiell mit den komplexen Riftingprozessen der Alpinen Tethys und mit einem globalen eruptions-induzierten Massensterbeereignis zusammenhängen. Das Intervall mit der höchsten Anreicherung von organischem Material korreliert mit der Haupteruptionsphase der Karoo-Ferrar Large Igneous Province (LIP), was deren massiven Einfluss auf die globalen klimatischen und ozeanischen Bedingungen während des Unteren Jura bestätigt. Das untersuchte Profil dokumentiert das

komplexe Zusammenspiel zwischen globalen (z.B. LIP) und lokalen (z.B. Redox- und Salinitätsvariationen, Beckenmorphologie) Faktoren, welche reduzierende Bedingungen und die Anreicherung von organischem Material im Bächentalbecken kontrolliert haben. Diese Entwicklungen bewirkten die höchst inhomogenen Bedingungen in den eingeschränkten Becken der NW Tethys während des Unteren Jura.

Table of contents

GENERAL PART OF DOCTORAL THESIS

GENERAL PART OF DOCTORAL THESIS

1 General Introduction

1.1 Oceanic anoxic events

The concept of oceanic anoxic events (OAEs) was firstly introduced by Schlanger and Jenkyns (1976) for Cenomanian-Turonian strata. Whereas several OAEs were additionally identified for Cretaceous deposits in the meantime, (Schlanger and Jenkyns, 1976; Coccioni et al., 1987; Arthur et al., 1990; Leckie et al., 2002; Erba et al., 2004; Baudin, 2005), only one OAE occurred during the remaining Mesozoic Era, namely in the Early Toarcian (~183 Ma; T-OAE; Jenkyns, 1980, 1985, 1988; see Fig. 1.1). In contrast, a number of such events was recognized for the Paleozoic time period (Büggisch, 1991).

The length of OAEs was suggested to be in the range of just a few hundred thousand years based on data from cyclostratigraphy and biostratigraphy (Sageman et al., 2006; Li et al., 2008; Suan et al., 2008; Voigt et al., 2008; Sabatino et al., 2009). These time intervals were typically characterized by massive perturbations of the global carbon cycle inducing the accumulation of organic-rich deposits (black marls, black shales) on global scales (see Jenkyns, 2010 for references) and associated with global mass-extinction events (Parente et al., 2008; Jenkyns, 2010; Caruthers et al., 2013). Thickness and organic-matter (OM) contents of deposits, connected to time intervals of OAEs, vary significantly from each other (Jenkyns, 2010). This is clearly visible for sections corresponding to the Cenomanian to Turonian Bonarelli OAE. Whereas this interval is reflected by a 1-m-thick black shale layer featuring up to 30 % total organic carbon (TOC) in Gubbio, Italy (Bonarelli, 1891; Arthur and Premoli Silva, 1982; Tsikos et al., 2004; Bernoulli and Jenkyns, 2009), coeval sediments contain less than 2 % TOC in Tibet (Wang et al., 2001) and are only ~2 cm thick in the Mariana Basin (Schlanger et al., 1987), respectively.

The present study addresses the Lower Jurassic Bächental bituminous marls, deposited in the time period of the T-OAE. Thus, driving forces and impact of this particular event are discussed in the following.

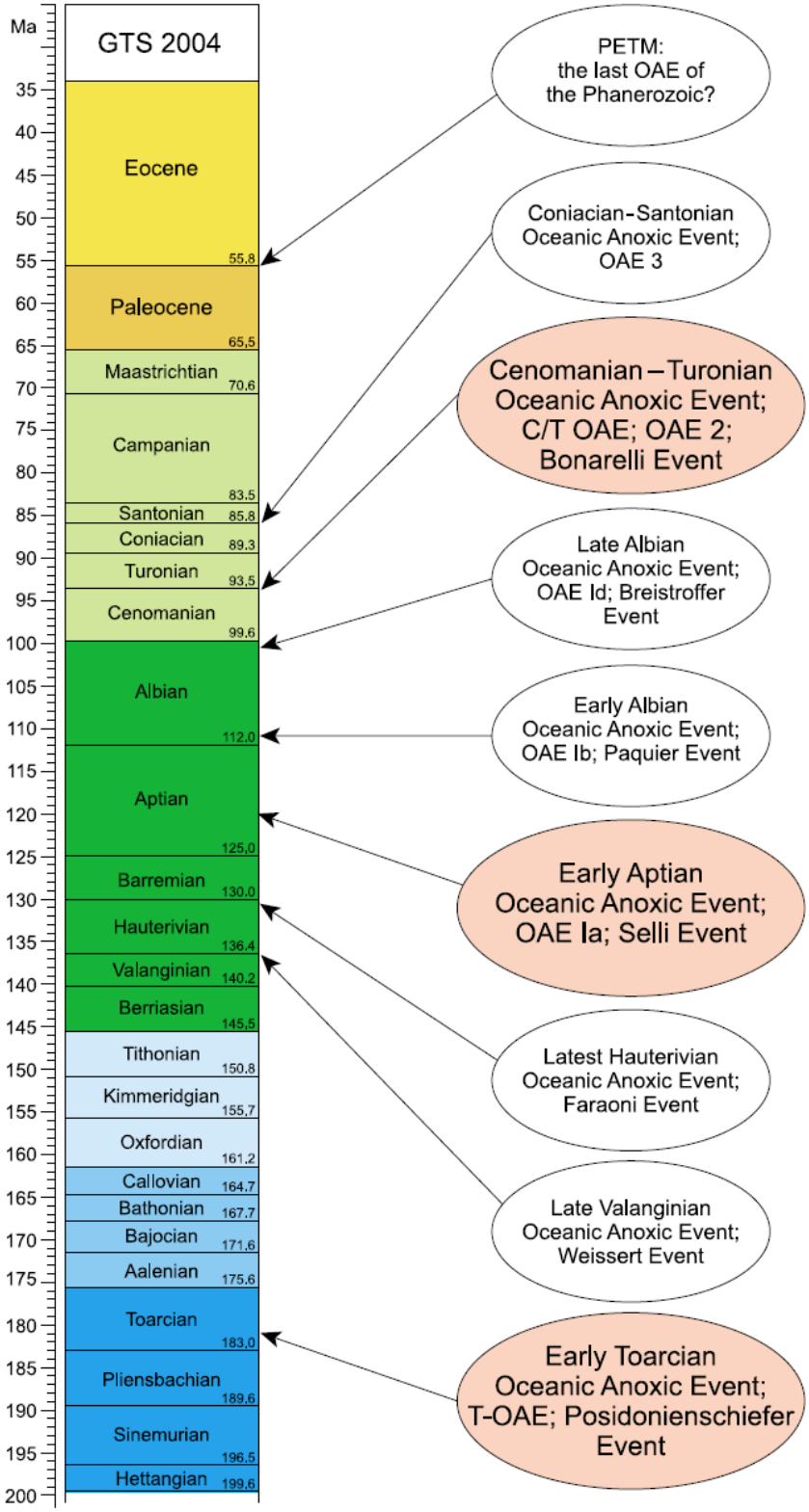

Fig. 1.1: Stratigraphic position and nomenclature of OAEs identified by now (Gradstein et al., 2005; Jenkyns, 2010). Whereas red circles mark events of global imprint, OAEs mentioned in white circles were particularly described for the Tethyan domain (see Jenkyns, 2010).

Sediments deposited in the course of the T-OAE are limited to sections corresponding to former shelves and continental margin settings due to the absence of Lower Jurassic crust on the planet (Jenkyns, 2010). Nevertheless, marine deposits associated to this event (Fig. 1.2) have been reported from sections in NW Europe and the Mediterranean (e.g., Röhl et al., 2001; Jenkyns et al., 2001; Kemp et al., 2005; Hesselbo et al., 2007; Sabatino et al., 2009; Kafousia et al., 2014), the NE paleo-Pacific ocean (Caruthers et al., 2011), South America (Al-Suwaidi et al., 2010; Mazzini et al., 2010; Sell et al., 2014), and northwestern Panthalassa (Izumi et al., 2012). Sections located in Northern (Austria, Germany, France, Britain) and Southern Europe (Italy, Slovenia, Croatia, Greece), respectively, show distinct differences regarding TOC contents. Whereas black shales from the former areas, deposited in epicontinental settings, contain up to 20 % OM (Küspert, 1982; Jenkyns and Clayton, 1997; Ebli et al., 1998; Röhl et al., 2001), sediments from the latter locations, reflecting pelagic depositional environments of the Tethys Ocean, generally feature less than 5 % TOC (Jenkyns, 1985, 1988; Jenkyns et al., 2001; Pancost et al., 2004; Sabatino et al., 2009, 2013).

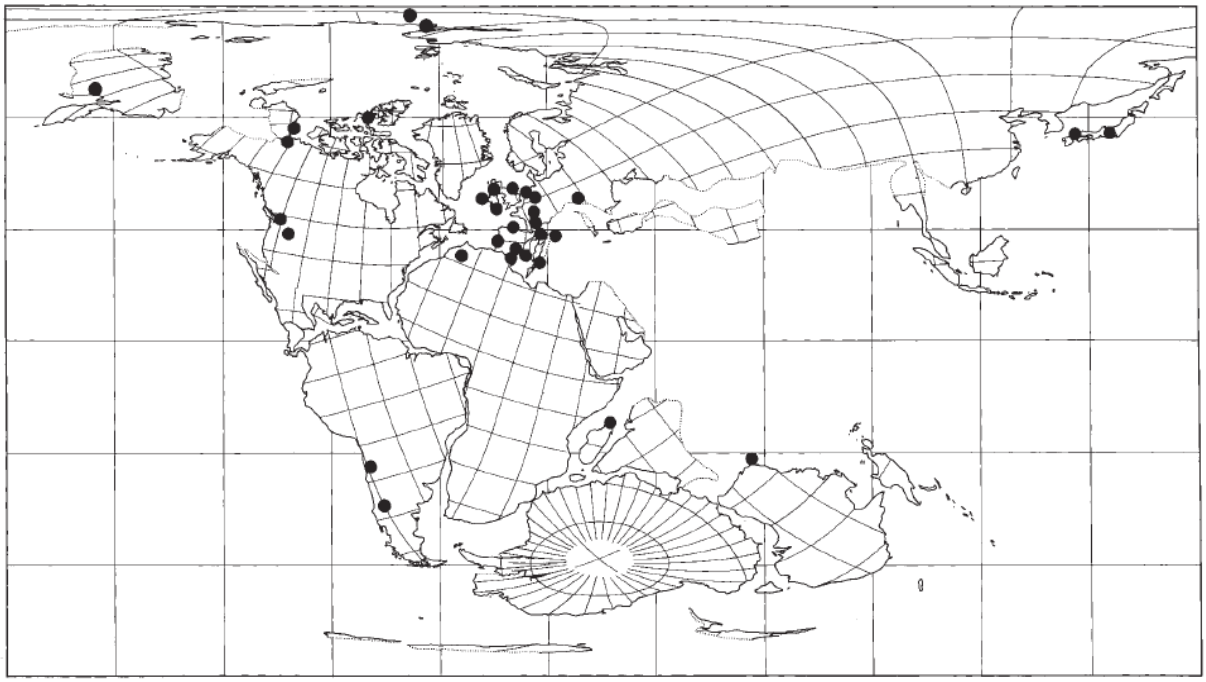

Fig. 1.2: Global distribution of organic-rich marine deposits connected to the T-OAE (after Jenkyns et al., 2002).

There exists a general agreement that the occurrence of OAEs was linked to climatic conditions characterized by significantly elevated global surface temperatures (e.g., Jenkyns, 2003). The release of large quantities of greenhouse gases during the CAMP eruptions (~201 Ma; Marzoli et al., 1999; Whiteside et al., 2007) caused significant climatic warming

beginning at the Triassic/Jurassic boundary. After interim periods of global cooling during late Pliensbachian (Price, 1999; Morard et al., 2003), magmatic activity of the Karoo-Ferrar large igneous province (LIP) commencing at ~186 Ma (Jourdan et al., 2008) induced further climatic warming from the Pliensbachian/Toarcian boundary onwards culminating in "greenhouse Earth" conditions during the Lower Toarcian (Palfy and Smith, 2000; Weissert, 2000; Jenkyns, 2003). The effect of the contemporaneous break-up of the Ligurian-Penninic oceanic realm commencing in the Toarcian (e.g., Ratschbacher et al., 2004) is not well documented and its volcanic contribution therefore probably underestimated. The prevailing subtropical climate was accompanied by an accelerated hydrological cycle with heavy monsoonal rainfalls and intense continental weathering that triggered an extensive supply of nutrients for ocean-surface waters, enhancing primary productivity (Parrish and Curtis, 1982; Parrish, 1993; Cohen et al., 2004). These changes operated in concert to produce conditions conducive to marine anoxia and black shale accumulation during the Early Jurassic.

Despite intense research activity on the T-OEA (e.g., Röhl et al., 2001; Jenkyns et al., 2002; Sabatino et al., 2009, 2011; Caruthers et al., 2011; Izumi et al., 2012; Sell et al., 2014), the main factors governing OM accumulation on local and global scales during the late Pliensbachian and early Toarcian remain controversially discussed. The worldwide occurrence of OM-enriched marine deposits has been attributed to [i] upwelling connected with an oxygen-minimum zone (Jenkyns, 1985, 1988; see summary in Jenkyns, 2010), [ii] a surface-water layer with reduced salinity that caused intensified water-column stratification in epicontinental areas of the western Tethyan realm (Praus and Riegel, 1989; Littke et al., 1991; Sælen et al., 1996), and [iii] minor sea-level fluctuations that controlled watermass exchange and, hence, dissolved oxygen levels in semi-restricted basins within the western European epicontinental sea located on the northern side of the Alpine Atlantic (Röhl et al., 2001; Schmid-Röhl et al., 2002; Frimmel et al., 2004). The latter model can also be adapted to the southern side of the Alpine Atlantic, i.e., the "Lower Austroalpine margin". For any of these mechanisms, short-term variation in OM accumulation may have been modulated by orbital forcings (Ikeda and Hori, 2014). The preservation and dilution of OM in those sediments was distinctly affected by local variations in depositional and diagenetic conditions among which the occurrence of sulfidic bottom waters may be critical (Tsikos et al., 2004; Meyers, 2007).

C-isotope chemostratigraphy has been widely used to correlate and date sections with poor biostratigraphic control (see Weissert, 2013 for summary). This approach is particularly

significant for Lower Toarcian successions due to the commonly observed occurrence of a distinct negative carbon-isotope excursion (CIE) recorded by both marine carbonates and marine and terrestrial OM (e.g., Sabatino et al., 2009; Gröcke et al., 2011; Fig. 1.3).

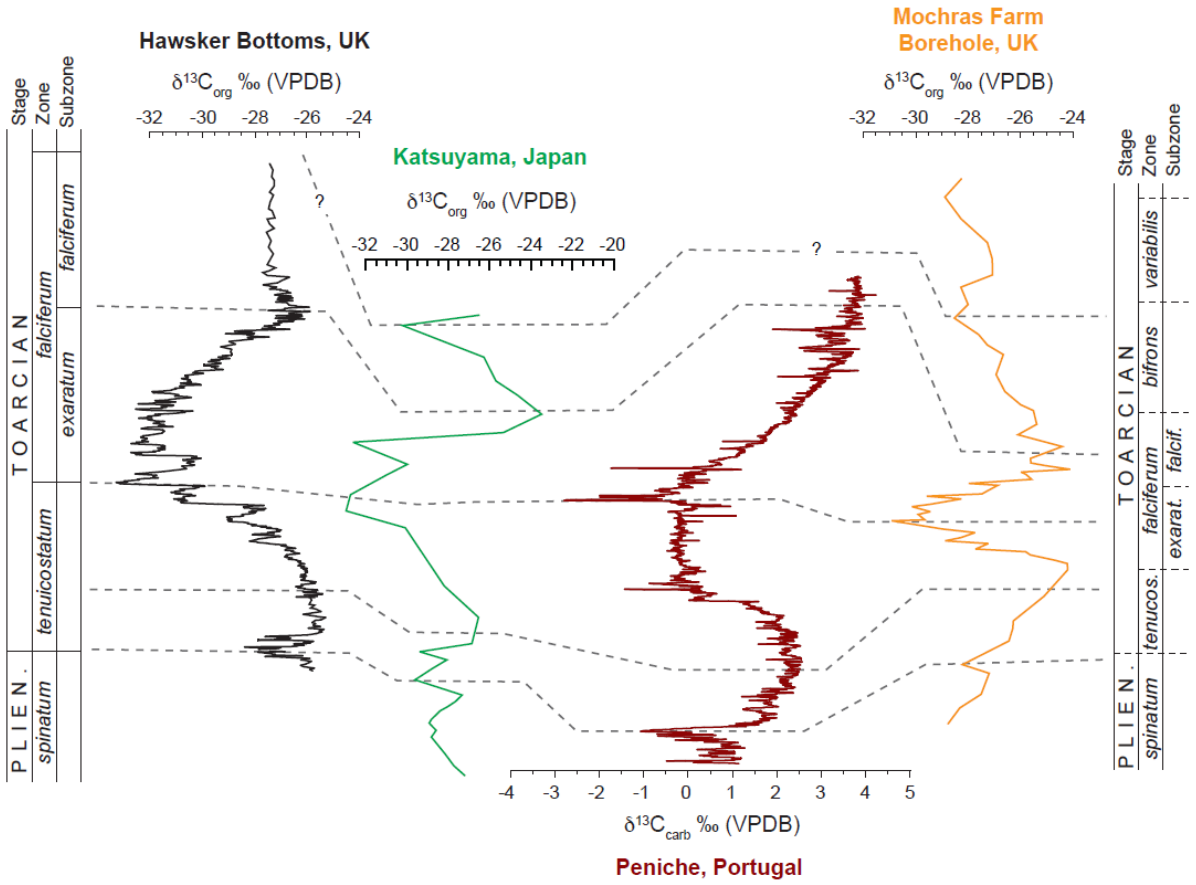

Fig. 1.3: Comparison of $\delta^{13}C$ profiles for the Pliensbachian-Toarcian time interval (adapted from Gröcke et al., 2011). Data for the individual sections from Jenkyns et al. (2001), Kemp et al. (2005), Hesselbo et al. (2007), Littler et al. (2009), and Gröcke et al. (2011).

The Toarcian CIE has been related to [i] a rapid release of biogenic methane by dissociation of methane hydrates (e.g., Hesselbo et al., 2000, 2007; Jenkyns et al., 2002; Kemp et al., 2005), [ii] the release of large volumes of CO_2 due to the emplacement of the Karoo-Ferrar LIP (Palfy and Smith, 2000), [iii] thermogenic methane resulting from the intrusion of igneous rocks into Gondwanan coals (McElwain et al., 2005; Svensen et al., 2007), [iv] the recycling of OM ("recycling model"; Küspert, 1982, 1983; Röhl et al., 2001), and [v] to the contribution of OM deriving either from calcareous or organic-walled plankton (Jenkyns and Clayton, 1986) and is typically used as chemostratigraphic marker to recognize the time interval of the T-OAE (e.g., Röhl et al., 2001; Sabatino et al., 2009; Mazzini et al., 2010; Caruthers et al., 2011; Gröcke et al., 2011; Izumi et al., 2012; Fig. 1.3).

1.2 Oil shales: Definitions and resources

Oil shale (Fig. 1.4) is an organic-rich fine-grained sedimentary rock which contains inorganic matrix, bitumen, and kerogen. The inorganic fraction of the rock may involve a wide variety of minerals including quartz, feldspars, clay minerals, carbonates, and pyrite (Cane, 1976). Whereas oil shales vary significantly regarding their mineral content, chemical composition, age, type of kerogen, and depositional history (Altun et al., 2006), all of the corresponding rocks are characterized by their low solubility in organic solvents and by their ability to generate liquid organic products on thermal decomposition (Urov and Sumberg, 1999). The most useful classification for oil shales in estimating yield and composition of extracted oil is based on the environment of the initial biomass deposit as terrestrial, lacustrine, or marine oil shales (Hutton, 1987; Dyni, 2006, 2010).

Fig. 1.4: Oil shale from the Bächental containing the ammonite *Cleviceras exaratum*.

Oil-shale deposits occur around the world (Fig. 1.5). Global resources are estimated to be in the range of ca. 5 trillion barrels of oil in place (Dyni, 2010).

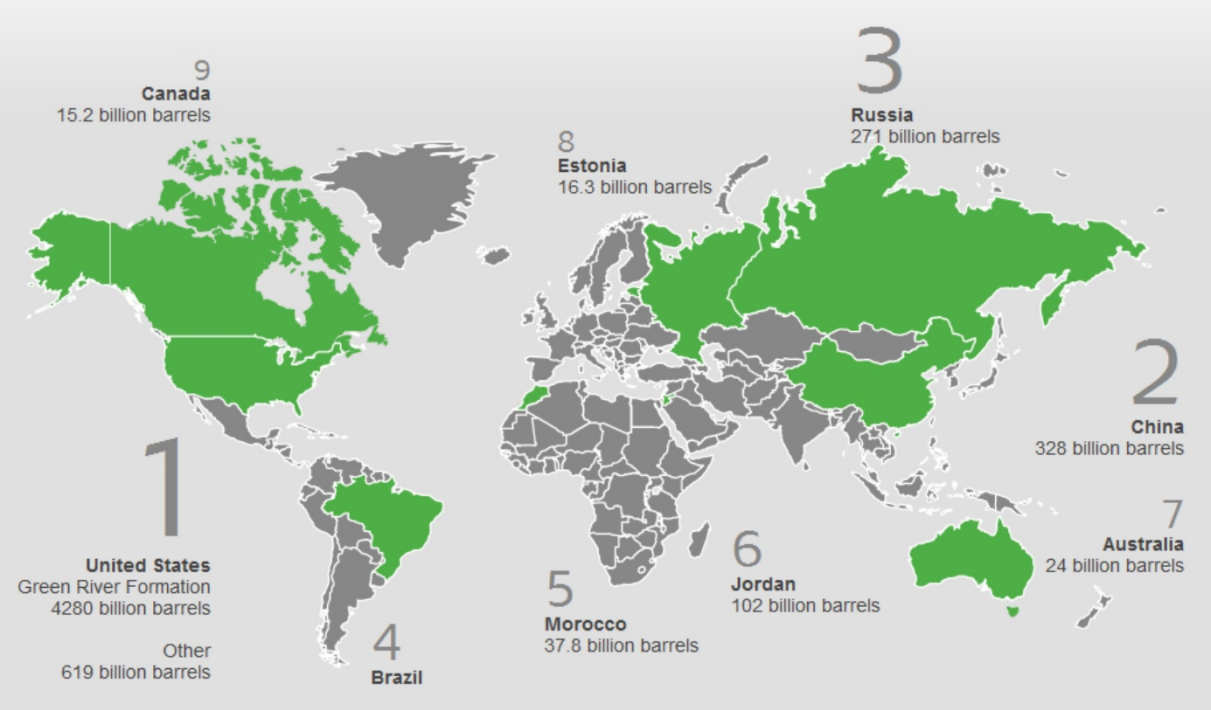

Fig. 1.5: Countries with large oil shale resources (from www.enefit.com).

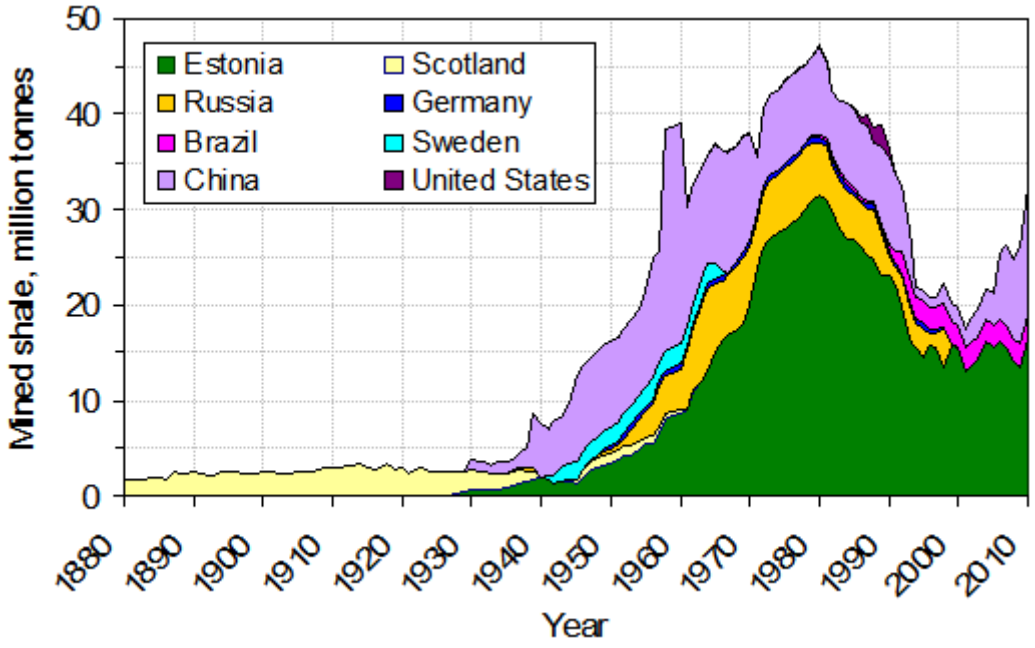

Fig. 1.6: Production of oil shale (in millions of metric tons) referring to the main producing countries (Allix and Burnham, 2010).

Shale oil is mined in several countries with Estonia, Russia, and China representing the main producers (Fig. 1.6). The extracted rock is used for oil production, power generation,

cement production, and chemical industries (Dyni, 2010; Alali, 2006; Yin, 2006; Francu et al., 2007).

1.3 Bituminous rocks of Austria

Several studies addressed the occurrence of bituminous rocks in Austria (e.g., Bitterli, 1962; Heinrich, 1980; Kodina et al., 1988; Lobitzer et al., 1988). Sedimentary successions involving OM-enriched rocks were deposited during various time periods (Lobitzer et al., 1988; Fig. 1.7) including the Miocene (clays of Mataschen; Styria), the Oligocene (marls and marly limestones belonging to the Häringer Schichten; Tyrol), the Pliensbachian-Toarcian (Bächental bituminous marls, Tyrol), and the Norian (Seefelder Schichten, Tyrol).

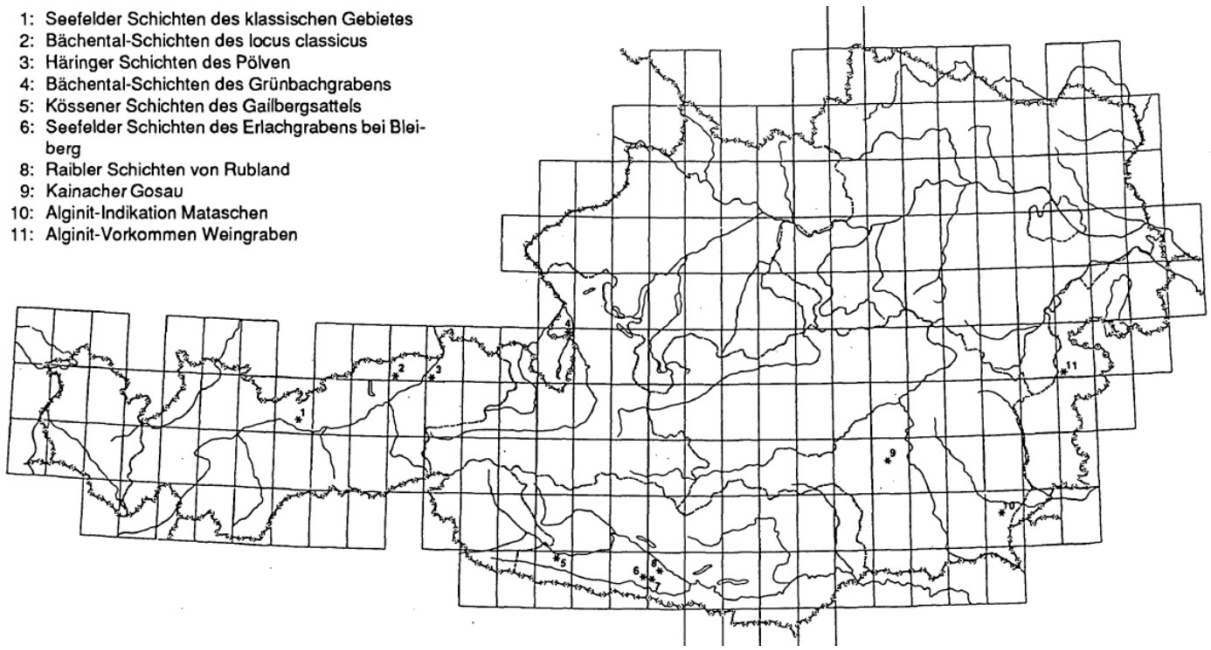

Fig. 1.7: Outcrops of bituminous rocks in Austria (Lobitzer et al., 1988).

Whereas OM-enriched rocks were commonly used as industrial raw material in Austria (e.g., cement production; Lobitzer et al., 1988), oil shales outcropping in the Bächental (up to 13 % TOC; Neumeister et al., 2015) and in Seefeld (up to 50 % TOC; Köster, 1989), respectively, can be used to generate rock oil via pyrolysis. The Seefelder Schichten were mined for several centuries (~1350-1964) to produce petroleum, asphalt, and "ichthyol", a potential remedy traditionally applied in folk medicine (Hörmann, 1872). In contrast, Bächental bituminous marls are still mined and subsequently heated to extract rock oil by the Tiroler Steinöl ® company. The extracted oil is further processed to cosmetic and pharmaceutical products.

1.4 Innovative aspects and importance of the expected results

Studies from various fields address marine and lacustrine OM-enriched deposits of different settings. Beside investigations focusing on economic issues (e.g., source rock potential, maturity), such sediments, commonly providing an excellent record of paleoenvironmental conditions during deposition, are in the scope of scientific research dealing with diverse topics including paleoclimate, biodiversity and mass extinction events, oceanography, and paleodepositional conditions (e.g., Jenkyns, 2003; Frimmel et al., 2004; Harnik et al., 2012; Caruthers et al., 2013).

The Upper Pliensbachian and Lower Toarcian was an interval subjected to major perturbations of the carbon cycle potentially connected to an oceanic anoxic event (T-OAE) and reflected by the global occurrence of OM-rich deposits in marine systems (e.g., Jenkyns, 1985, 1988; Jenkyns et al., 2002; Jenkyns, 2010; Pearce et al., 2008). However, the main controls on OM production and preservation at that time are still controversially discussed. The study section in the Bächental valley (Northern Calcareous Alps) containing OM-rich marls (Bächental bituminous marls; Bächentaler Bitumenmergel) belonging to the Sachrang Member of the Lower Jurassic Middle Allgäu Formation represents the best-exposed equivalent of this event in Austria. Thus, the Bächental bituminous marls provide a unique possibility to determine the main factors effective on local and global scales, controlling onset and duration of OM accumulation in semi-restricted basins of the northwestern Tethyan domain during the Upper Pliensbachian and Lower Toarcian.

Although some work was done on sedimentology (Spieler and Brandner, 1989), stratigraphy (Klebelsberg, 1935), and organic geochemistry (Kodina et al., 1988; Köster, 1995), a detailed investigation of the depositional environment of the Bächental bituminous marls as well as exact data regarding onset and duration of its accumulation are still missing. Hence, the aims of this doctoral thesis are:

- the determination of the source rock potential of Bächental bituminous marls,

- the detailed investigation of prevailing depositional conditions (e.g., redox conditions, degree of watermass restriction, salinity conditions) in the Bächental basin and stratigraphic changes thereof,

- the determination of main factors effective on local to global scales controlling the onset and duration of OM accumulation in semi-restricted basins of the NW Tethyan realm during the Upper Pliensbachian and Lower Toarcian,

- the assessment of the impact of prevailing environmental conditions on OM production and preservation, OM sources, mineralogical composition, watermass redox state, degree of watermass restriction, salinity conditions, diagenesis,

- the application of a comprehensive approach to calibrate proxies from diverse fields (e.g., sedimentology, inorganic geochemistry, biomarker analysis) commonly used for interpretation of environmental conditions.

To reach the goals, the Bächental section is sampled with high resolution and all samples are investigated using a multi-analytical approach. This enables the combined interpretation of data derived from diverse scientific fields in order to maximize the significance of interpretations. The investigation of the Bächental section, reflecting a highly variable carbonate-dominated hemipelagic depositional environment, will provide new insights into the dominant factors controlling the formation of OM-rich marine deposits during the Lower Jurassic.

2 Geological setting

The investigated section is situated in the Bächental valley, which is part of the Karwendel Mountains of northern Tyrol (Fig. 2.1; GPS: 47°30'31.38"N; 11°37'46.00"E). In this area, lithostratigraphic units of Triassic to Jurassic age belonging to the Lechtal nappe of the Bavaric Unit, a tectonic domain of the Northern Calcareous Alps, are exposed.

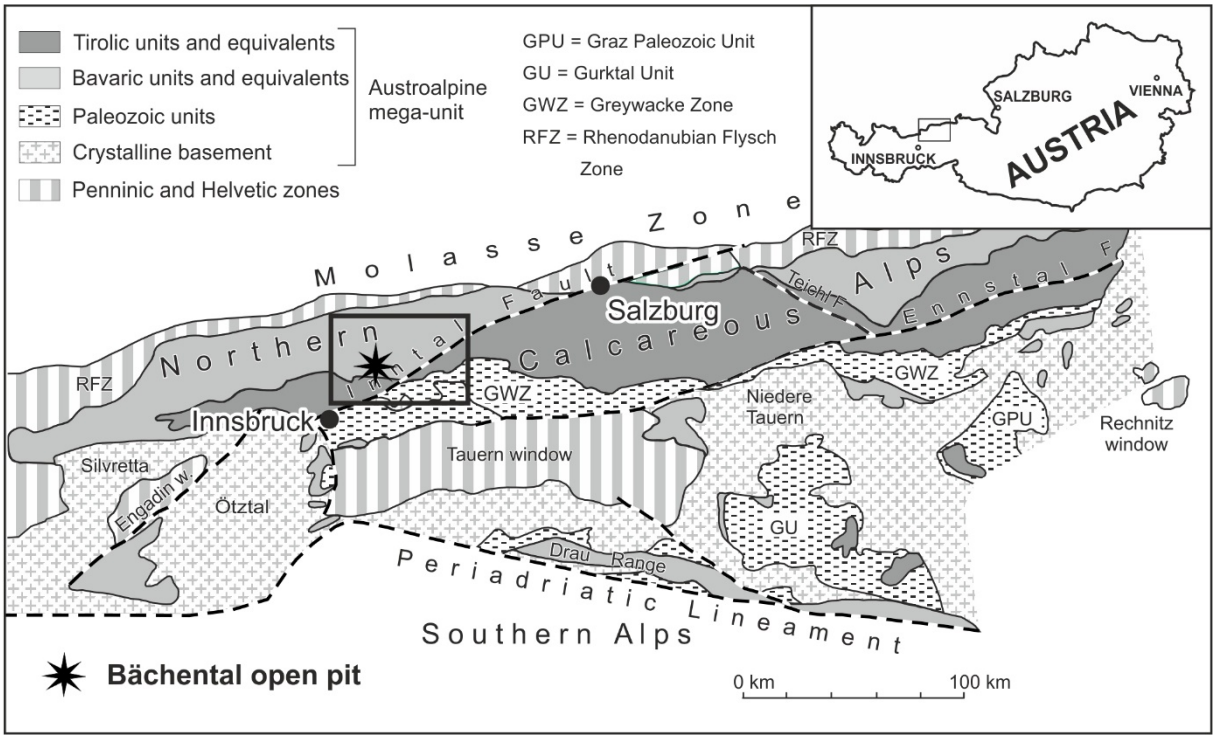

Fig. 2.1: Schematic tectonic map of the Eastern Alps after Frisch and Gawlick (2003). The position of the studied section in the Bächental valley is indicated.

In the late Early Jurassic, the study area was situated at the northwestern continental margin of the Neotethys Ocean and the southeastern newly formed passive margin of the Alpine Atlantic (Figs. 2.2A, B). This area was affected by extensional tectonics, related to late Hettangian rifting and Toarcian oceanic break-up in the Alpine Atlantic (Penninic) realm (e.g., Ratschbacher et al., 2004), that resulted in formation of synrift basins such as the Bächental basin. The final configuration of the roughly north-south-trending Bächental basin developed during late Hettangian to Sinemurian time (Schlager and Schöllnberger, 1973). The basin exhibits tilt block tectonics and antithetic step faults, producing a half-graben geometry with a depocenter in its northern part (Fig. 2.3; Spieler and Brandner, 1989). Deposition of

bituminous marls during the Lower Jurassic was limited to the poorly ventilated deepest part (depocenter) of the Bächental basin (Fig. 2.3; Spieler and Brandner, 1989).

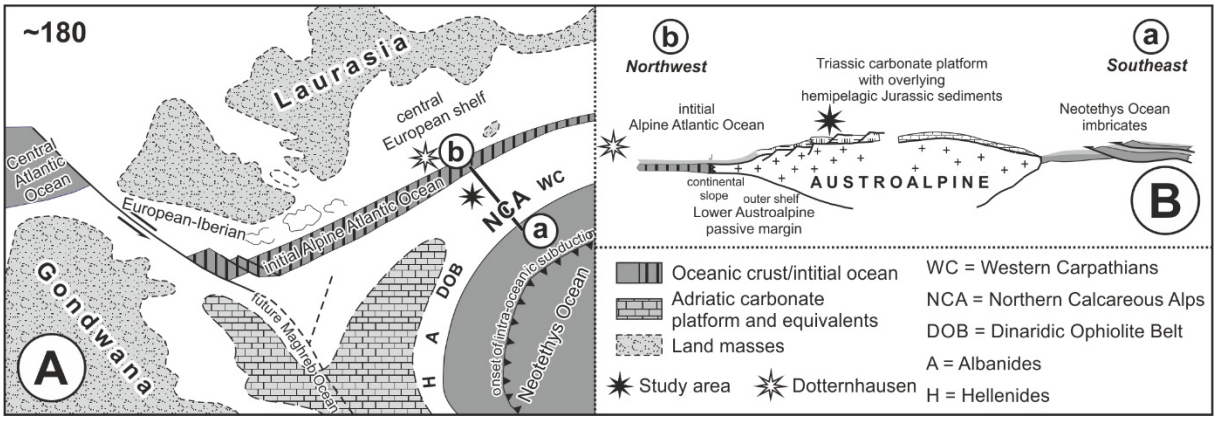

Fig. 2.2: (A) Palaeogeographic position of the study section as part of the Northern Calcareous Alps within the Austroalpine domain in late Early Jurassic time (modified after Gawlick et al., 2009). (B) Schematic cross section (line a-b in A) showing the passive continental margin of the Lower Austroalpine domain (modified after Gawlick et al., 2009). Rifting and spreading of the Alpine Atlantic commencing in the late Early Jurassic affected the Austroalpine domain by the formation of extensional, asymmetric basins exhibiting horst-and-graben structure (cf. Bernoulli and Jenkyns, 1974).

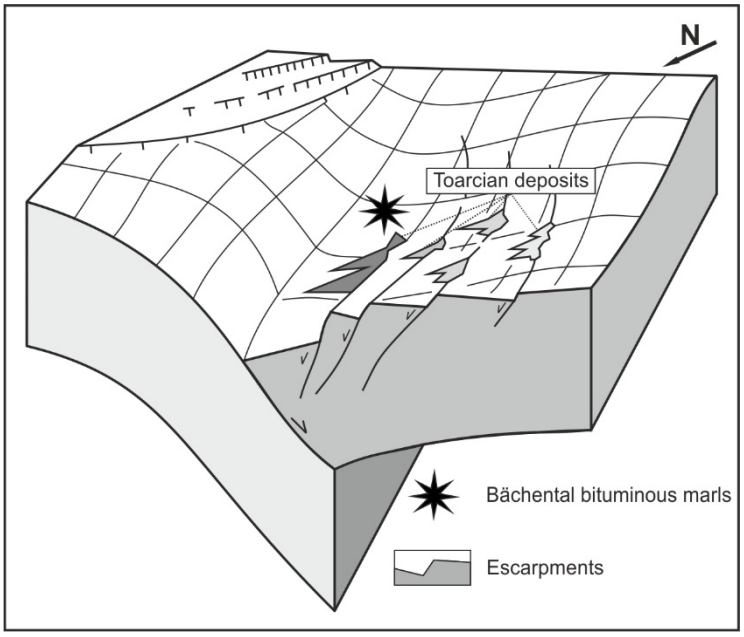

Fig. 2.3: Paleogeography of the depositional area of Bächental bituminous marl in the Lower Jurassic (Spieler and Brandner, 1989; Brandner, 2011). The accumulation of organic-rich rocks was restricted to the deepest parts of a basin with half-graben geometry.

The study section has an overall thickness of 35.54 m (Fig. 3.1) and is well exposed in large parts due to its position in an open-pit mine. At its base, limestone beds with a total thickness of 4.00 m occur. These strata are assigned to the Scheibelberg Formation (Sinemurian to Pliensbachian) and were deposited in water depths of several hundred meters at the transition of distal slope to basin (Spieler and Brandner, 1989). Directly above a 0.25-m-thick weathered mudstone, the Bächental bituminous marls of the Sachrang Member of the Lower Jurassic Middle Allgäu Formation (?upper Pliensbachian to lower Toarcian; Tollmann, 1976; Ebli, 1991; Ebli et al., 1998; Gawlick et al., 2009; Neumeister et al., 2015; Suan et al., 2016) are exposed with a total thickness of 23.70 m. The alternating sequence of limestone and marl with a thickness of 4.69 m forming the top of the succession belongs to the Upper Allgäu Formation (upper Toarcian to early Middle Jurassic; Spieler and Brandner, 1989). The dating of the Bächental bituminous marls to the Toarcian was originally based on the occurrence of *Harpoceras* sp. (Klebelsberg, 1935). This is consistent with the presence of *Cleviceras exaratum* in the middle part of the section (Fig. 3.1), a taxon associated with the early Toarcian *falciferum* Zone (Neumeister et al., 2015). Kodina et al. (1988) and Lobitzer et al. (1988) inferred that bituminous marl sedimentation began during the late Pliensbachian based on the occurrence of *Arieticeras* sp. and, possibly, *Leptaleoceras* sp. Neumeister et al. (2015) proposed that the deposition of the Sachrang Member in the Bächental basin lasted from late Pliensbachian (*margaritatus* Zone) to early Toarcian (*bifrons* Zone) based on correlation of C_{27}/C_{29} sterane data from Bächental and Dotternhausen (epicontinental Posidonia Shale) sections with sea level. However, new biostratigraphic data – including the reexamination of the ammonites published by Kodina et al. (1988) – indicate that Units 2 and 3 solely belong to the Lower Toarcian *falciferum*-Zone, whereas data for the basal part of the section is missing (Suan et al., 2016). At its type locality in Bavaria, deposition of the Sachrang Member commenced at the base of the *tenuicostatum* Zone and continued through the entire early Toarcian (Ebli et al., 1998). Suan et al. (2016) recently published new stratigraphic data for Toarcian organic-rich deposits of the Alpine Tethys. Implications on the present study arising from this publication are discussed in detail in chapter 10.

3 Samples and analytical methods

Samples were collected from fresh exposures in a trench that was dug up to 4 m deep. A total of 68 samples was collected for geochemical analyses (Fig. 3.1). The Scheibelberg Formation at the base of the study succession is represented by six samples. The Sachrang Member, including a basal mudstone, bituminous marls, and a 1-meter-thick debrite layer (Fig. 3.1), is represented by 52 samples resulting in an average sampling interval of ca. 0.50 m. Ten samples at intervals of 0.10 to 0.90 m were collected from the Upper Allgäu Formation at the top of the section.

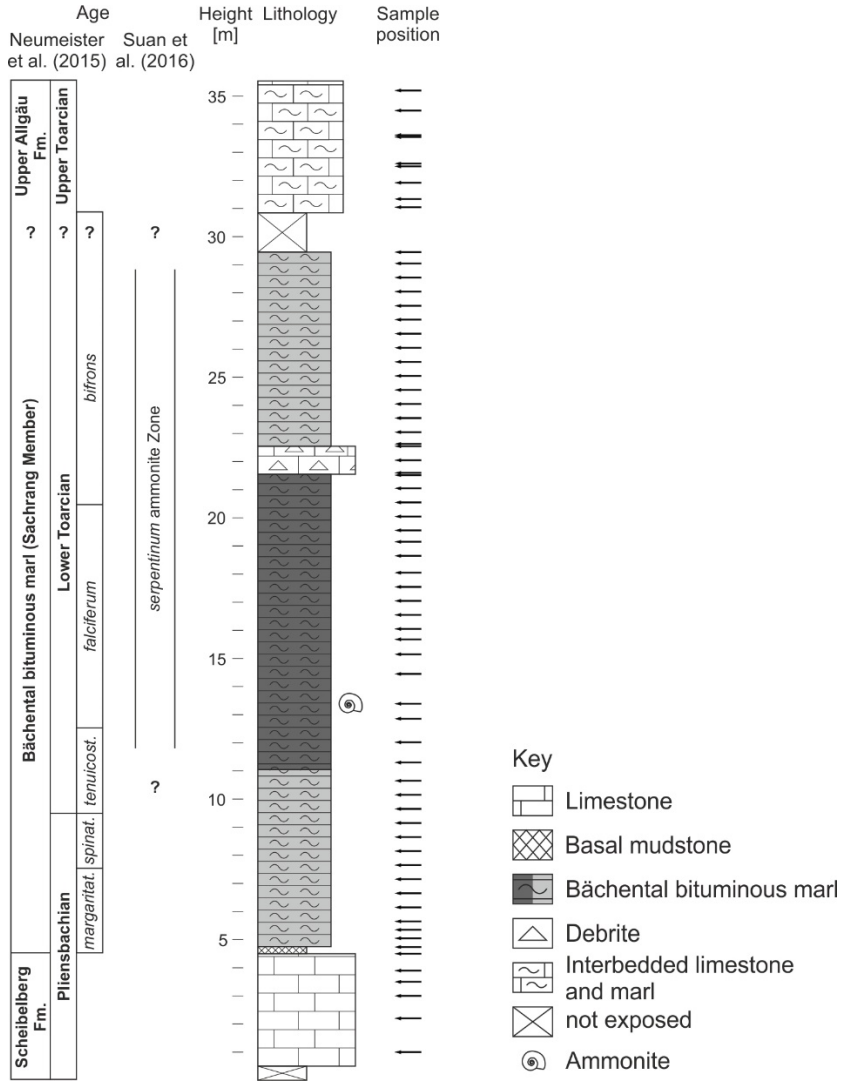

Fig. 3.1: Lithological profile of the investigated Bächental section containing rocks of the Scheibelberg Fm., the Sachrang Member (Middle Allgäu Fm.) and the Upper Allgäu Fm. Stratigraphy based on results of Neumeister et al. (2015) and Suan et al. (2016). Positions of the 68 investigated samples are displayed next to the lithological profile.

3.1 Thin sections and polished sections

A total of 28 thin sections of carbonates and marls were made for analyses via transmitted light microscopy. Polished blocks of 12 samples were prepared for maceral analyses that were performed with a Leica MPV microscope using white and fluorescent light.

3.2 Carbon and sulfur analysis

Total carbon (TC) and sulphur (S) contents were measured with a Leco 300 CSTM analyser. For the determination of TOC sample material was pre-treated with concentrated hydrochloric acid to remove the carbonate-bound carbon. Total inorganic carbon (TIC = TC – TOC) was used to calculate calcite equivalent percentages (Cc_{eq} = TIC x 8.33).

3.3 Rock Eval pyrolysis

Rock Eval pyrolysis was carried out using a Delsi Rock Eval RE II+ instrument. By means of this method the amount of free hydrocarbons (S_1; mg HC/g rock) released at a constant temperature as well as the amount of pyrolysate (S_2; mg HC/g rock) generated from non-volatile OM during subsequent gradual heating of the rock powder in a helium stream can be measured. These values are used to calculate the production index [$PI = S_1/(S_1 + S_2)$] and the hydrogen index [$HI = (S_2/TOC) \times 100$]. The temperature of maximum hydrocarbon generation (T_{max}) can be used as maturity indicator.

3.4 X-ray diffraction

X-ray diffraction (XRD) was carried out using Philips X-pert equipment with the following measuring conditions: [i] bulk samples, 2 to 65° 2θ, random powder mount; [ii] clay mineral analysis of clay-rich samples, oriented powder mounts (smear on glass; Vortisch, 1982), 2 to 38° 2θ, untreated, ethylene glycol-treated, heat-treated, 350 °C/2 h, 550 °C/2 h; and [iii] bulk samples, 25 to 35° 2θ, random powder mount. The powder used for XRD was hand milled by means of an agate mortar.

3.5 X-ray fluorescence

Major- and trace-element (TE) concentrations were determined on whole-rock samples using a wavelength-dispersive Rigaku 3040 X-ray fluorescence spectrometer at the University of Cincinnati. Raw intensities were calibrated using a set of 65 standards from the USGS, the National Bureau of Standards, and internal lab standards that were analyzed by XRAL Incorporated using XRF and INAA. Analytical precision based on replicate analyses was better than ±2 % for major and minor elements and ±5 % for trace elements, and detection limits were 1 to 2 ppm for most trace elements.

3.6 Microprobe

Quantitative analyses of carbonates were performed on selected samples by using an electron microprobe (Superprobe Jeol JXA 8200) installed at the "Eugen F. Stumpfl Laboratory" at the University of Leoben, Austria, operated in WDS mode and applying 15 kV accelerating voltage and 10 nA beam current. The counting times for peak and both backgrounds (left and right) were 20 and 10 sec, respectively. The beam diameter was ~1 μm. Natural diopside, apatite, magnetite, rhodochrosite, and strontianite were used as standards for magnesium (Mg), calcium (Ca), iron (Fe), manganese (Mn), and strontium (Sr). The X-ray lines used were: Kα for Mg, Ca, Fe, and Mn as well as Lα for Sr. Following diffracting crystals were selected: TAP for Mg, PETJ for Ca, LIFH for Fe and Mn, and PETH for Sr. The subsequently quoted detection limits (all in ppm) are automatically calculated by the microprobe software: Mg = 100, Ca = 150, Fe = 200, Mn = 150, and Sr = 200.

3.7 Stable isotope composition of carbonate minerals

Inorganic carbon ($\delta^{13}C_{carb}$) and oxygen isotope ($\delta^{18}O_{carb}$) measurements were carried out for all samples. For the decomposition of carbonates for mass spectrometric analysis, portions of the samples were weighed in glass vials that were subsequently flushed with helium. Inorganic carbon and oxygen isotope measurements were performed by adding 100 % H_3PO_4 to samples heated at 70 °C in an online system (Gasbench II with carbonate option) for determination of $\delta^{13}C_{carb}$ and $\delta^{18}O_{carb}$. Analysis was carried out with a ThermoFisher DELTA V isotope ratio mass spectrometer. The results are reported relative to the Vienna Pee Dee Belemnite (V-PDB) standard for both $\delta^{13}C_{carb}$ and $\delta^{18}O_{carb}$. Reproducibility was better than 0.2 ‰.

3.8 Stable isotope composition of OM

All samples were analysed for their organic carbon isotope composition at the University of Leeds using an Elementar Pyrocube coupled to an Isoprime IRMS. Samples were weighed into tin capsules in sufficient quantity to produce peaks of between 1 and 10nA and combusted at 1150 °C in a helium stream (CP grade) enriched with pure oxygen (N5.0). The resulting gases were passed over tungstic oxide (also at 1150 °C) and excess oxygen and water removed using copper wires held at 850 °C and Sicapent respectively. All solid reagents were sourced from Elemental Microanalysis, UK, and all gases were sourced from BOC, UK. CO_2 was separated from other gases using a temperature controlled adsorption/desorption column. The $\delta^{13}C$ of the sample is derived from the integrated mass 44, 45 and 46 signals from the pulse of sample CO_2, compared to those in an independently introduced pulse of CO_2 reference gas (CP grade). Samples were run in batches of 12-16 bracketed by in-house C4 sucrose and urea standards. These were assigned values of -11.93 ± 0.24 and -46.83 ± 0.22 ‰ respectively based on 10 replicate analyses and calibration using LSVEC lithium carbonate (-46.479 ‰), IAEA-CH7 polyethylene (-31.83 ‰), IAEA-CH6 sucrose (-10.45 ‰) and IAEA-CO1 Carrara marble (2.48 ‰). Samples were batch corrected using a simple linear equation.

3.9 Compound-specific stable isotope geochemistry

Analysis of the C-isotopic composition of acyclic isoprenoids was performed using a Trace GC Ultra attached to a Delta V IRMS via a combustion interface (GC IsoLink) and an autodilution unit (ConFlow IV), all from Thermo-Fisher. For calibration, a CO_2 standard was injected at the beginning and end of each analysis. The GC coupled to the IRMS was equipped with the column described above and the temperature program was the same as for conventional GC-MS analysis. Isotopic compositions are reported in the δ notation relative to the VPDB standard.

3.10 Biomarker analysis

For organic geochemical analyses, samples were extracted using dichloromethane in a Dionex ASE 200 accelerated solvent extractor (temperature: 75 °C; pressure: 50 bar). After separation of asphaltenes, the hexane soluble fractions were separated into NSO compounds,

saturated hydrocarbons and aromatic hydrocarbons using medium pressure liquid chromatography with a Köhnen-Willsch instrument (Radke et al., 1980). The saturated and aromatic hydrocarbon fractions were analysed with a GC equipped with a 30 m DB-1 fused-silica capillary column (i.d. 0.25 mm; 0.25 µm film thickness) coupled to a Finnigan MAT GCQ ion trap mass spectrometer. The oven temperature was programmed from 70 to 300 °C at 4 °C/min, followed by an isothermal period of 15 min. Helium was used as carrier gas. The spectrometer was operated in the electron ionization mode over a scan range from m/z 50 to 650. Relative percentages and absolute concentrations of different compound groups in the saturated and aromatic hydrocarbon fractions were calculated using peak areas in the total ion current chromatograms in relation to those of internal standards (deuterated n-tetracosane and 1,1´-binaphthyl, resp.), or by integration of peak areas in appropriate mass chromatograms using response factors to correct for the intensities of the fragment ion used for quantification of the total ion abundance. The concentrations were normalized to TOC.

4 Summary of publications

4.1 Publication I: Oceanic response to Pliensbachian and Toarcian magmatic events: Implications from an organic-rich basinal succession in the NW Tethys

During the Lower Jurassic, significant environmental changes effective variably at global (i.e., eruptions of the Karoo-Ferrar LIP, opening of the Atlantic Ocean, climate warming - "greenhouse Earth" conditions) to local (e.g., redox and salinity variations, basin morphology) scales operated in concert to produce conditions favorable to marine anoxia and resulting in deposition of organic-rich sediments in marine systems globally (e.g., Jenkyns, 1985, 1988; Jenkyns et al., 2002; Pearce et al., 2008), including the Bächental bituminous marls (Bächentaler Bitumenmergel).

The marls, belonging to the Sachrang Member of the Lower Jurassic Middle Allgäu Formation and outcropping in an open pit in the Bächental in Northern Tyrol, were investigated to determine environmental controls on the formation of organic-rich deposits in a semi-restricted carbonate-dominated basin of the NW Tethys during the Early Jurassic. To reach the goal, high-resolution sampling and a multidisciplinary approach (microscopy, XRD analysis, carbon and sulfur analysis, Rock Eval pyrolysis, isotopy of carbonate minerals and OM, compound-specific stable isotope geochemistry, biomarker analysis) was applied.

The use of a variety of proxies yielded information on source and thermal maturity of OM, redox conditions, salinity, water-column stratification, sea-level fluctuations, diagenetic processes, and volcanic influences enabling the subdivision of the marls into three distinct units (Units 1-2-3 from base to top) on the basis of mineralogical composition, source-rock parameters, redox conditions, salinity variations, and diagenetic processes. The comprehensive interpretation of the gained data permitted the establishment of an overall model for the deposition of the Bächental bituminous marls.

Redox proxies indicate varying suboxic to euxinic conditions during deposition of the Bächental section. Redox variations were mainly controlled by sea-level fluctuations with the tectonically complex bathymetry of the Bächental basin determining watermass exchange with the Tethys Ocean. Accordingly, strongest anoxia and highest TOC contents (up to 13%)

occur in the middle part of the profile, coincident with an increase in surface-water productivity during a period of relative sea-level lowstand that induced salinity stratification in a stagnant basin setting. This level corresponds to the time interval of the T-OAE. However, the absence of the widely observed lower Toarcian negative CIE in the study section questions its unrestricted use as a global chemostratigraphic marker.

Stratigraphic correlation of the thermally immature Bächental bituminous marls with the Posidonia Shale of SW Germany on the basis of C_{27}/C_{29} sterane ratio profiles and ammonite data suggests that deposition of OM-rich sediments in isolated basins in the Alpine realm commenced earlier (late Pliensbachian *margaritatus* Zone) than in regionally proximal epicontinental seas (early Toarcian *tenuicostatum* Zone). The late Pliensbachian onset of reducing conditions in the Bächental basin coincided with an influx of volcaniclastic detritus that was possibly connected to complex rifting processes of the Alpine Tethys and with a globally observed eruption-induced extinction event. The level of maximum OM accumulation in the Bächental basin corresponds to the main eruptive phase of the Karoo-Ferrar LIP, confirming its massive impact on global climate and oceanic conditions during the Early Jurassic.

Thus, the Bächental bituminous marls provide new insights concerning the role of global events as well as the influence of local basinal factors on onset and duration of OM accumulation in semi-restricted basins (e.g., Bächental basin) of the NW Tethyan domain characterized by highly inhomogeneous environmental conditions during the late Pliensbachian and early Toarcian.

4.2 Publication II: Redox conditions and depositional environment of the Lower Jurassic Bächental bituminous marls (Tyrol, Austria)

Redox variation is a key feature of any depositional system that influences the accumulation and formation of OM, TEs, and diagenetic phases. TEs are only stable within a defined range of oxygen availability (e.g., Piper and Calvert, 2009) and several of these redox-sensitive elements show an affinity to anoxic to euxinic paleoenvironments (“euxinic affinity”; e.g., Brumsack, 2006; Tribovillard et al., 2006; Piper and Calvert, 2009). Thus, beside redox proxies derived from organic geochemistry, microscopy, and bulk parameters, inorganic geochemical data (TE concentrations, TE ratios) is most frequently applied for

determination of depositional conditions of both, ancient and modern oxygen-depleted marine environments (e.g., Dean et al., 1999; Yarincik et al., 2000; Morford et al., 2001; Tribovillard et al., 2006; Algeo and Tribovillard, 2009).

The Lower Jurassic Bächental bituminous marls (Bächentaler Bitumenmergel) belonging to the Sachrang Member of the Middle Allgäu Formation in the Northern Calcareous Alps, provide an excellent opportunity to compare proxies based on redox-sensitive TEs with the redox interpretations previously generated on the basis of sedimentologic and organic geochemical data (Neumeister et al., 2015). The goal of the study, therefore, was to evaluate the utility of multiple redox-sensitive TEs as proxies for watermass redox conditions in a carbonate-dominated basinal setting subjected to a complex set of environmental, depositional, and diagenetic factors.

A suite of TEs characterized by an affinity to reducing environments (Mo, U, V, Cu, and Ni), was applied to investigate secular variations in environmental redox conditions during deposition of the Bächental bituminous marls (Bächentaler Bitumenmergel). The use of Al-normalized TE concentrations and TE concentration ratios enabled the subdivision of OM-enriched marls into discrete units (Units 1-2-3 from base to top) which correspond to major shifts in depositional redox conditions. Whereas removal of TEs to the sediment was connected to fine-grained siliciclastics, diagenetic processes, and OM accumulation during deposition of suboxic to transiently anoxic Units 1 and 3, TE enrichment was linked to adsorption onto OM in strictly anoxic Unit 2 featuring strongest TE enrichments and peak TOC contents up to 13 %.

Moreover, the comparison of inorganic and organic geochemical proxies for environmental conditions provides the possibility to detect periods with elevated surface-water bioproductivity. Accordingly, a flourishing of algal and planktonic organisms contributed to the significant increase of TOC content at the base of Unit 2. This corresponds well to the time-equivalent T-OAE characterized by the global occurrence of organic-rich sediments.

4.3 Publication III: Diagenesis of organic-rich marls under shifting suboxic to euxinic conditions

Organic-rich marine deposits are subjected to a variety of early diagenetic processes affecting OM preservation and authigenic mineral precipitation. In such environments, early

diagenetic OM degradation is controlled by a sequence of redox-dependent, microbially mediated aerobic and anaerobic processes using inorganic electron acceptors (e.g., Froelich et al., 1979; Thamdrup, 2000; Jørgensen, 2000). These oxidation processes can create pore-water conditions that are favorable for precipitation of a variety of authigenic mineral phases (Wright and Oren, 2005; Wacey et al., 2008) including dolomite and Mn-bearing carbonates, which are common in both modern and ancient OM-rich successions (e.g., Compton, 1988; Jenkyns, 1988; Mazzullo, 2000; Heiser et al., 2001; Polgári et al., 2004; Sabatino et al., 2011; Meister et al., 2013). However, despite intensive research, the nature and sequence of the reactions governing the formation of authigenic carbonates during diagenesis of OM-rich sediments remain incompletely known.

The Bächental basin was subjected to strong environmental changes during the deposition of the Lower Jurassic Bächentaler Bitumenmergel resulting in pronounced stratigraphic variation of rock parameters. This and the use of a multi-analytical approach based on microscopy, XRD analysis, bulk geochemistry, stable isotopy, and organic geochemistry provided the basis for subdivision of the study section into three units (Units 1-3; Neumeister et al., 2015, 2016). These units represent distinct redox states that were closely linked to the nature and intensity of early diagenetic processes controlling [i] OM degradation and preservation, [ii] pH and alkalinity conditions in pore waters, [iii] occurrence, time of formation, amount, and mineralogical composition of the individual secondary carbonate phases present, [iv] dissolution of biogenic quartz, and [v] alteration of pyrite in the study section. Hence, the Bächentaler Bitumenmergel provides a valuable opportunity to investigate differences regarding the relative significance of diagenetic processes and products associated with OM oxidation in a marine setting subjected to highly variable depositional conditions.

During deposition of Units 1 and 3, predominating suboxic conditions enabled the activity of aerobic and denitrifying microbes in sediment surface layers in addition to anaerobic reduction of Mn and Fe oxides and sulfate. The availability of abundant Mn oxides resulted in strong Mn reduction, causing a maximum OM loss in the range of 0.9 to 1.5 % and a lowering of HI values by up to 400 mg HC/g TOC. In contrast to Units 1 and 3, sulfate reduction was the dominant degradation process in anoxic-euxinic Unit 2. However, natural sulphurization of organic matter under Fe-limited conditions induced an early termination of sulfate reduction, contributing to enhanced OM preservation in Unit 2, as reflected in a more limited decrease of HI values (by 100 mg HC/g TOC).

OM oxidation processes caused an increase of pH values (up to >9) and alkalinity in pore waters. These changes initiated redox-dependent precipitation of diagenetic carbonate phases in all samples and caused advanced dissolution of biogenic silica and incipient alteration of pyrite exclusively in the anoxic-euxinic and radiolarian-silica-rich Unit 2. Dolomite formation, occurring in the sediment surface layers, was favored by suboxic conditions and mediated by aerobic and denitrifying bacteria. Whereas low-temperature dolomite precipitation was not influenced by sulfate concentrations in pore waters and anaerobic reduction processes, it was distinctly impeded during periods of anoxia. Anaerobic Mn reduction triggered the release of isotopically light carbon and Mn supersaturation of pore waters, which was especially significant in suboxic Units 1 and 3. This caused a transition from dolomite to kutnohorite (Mn carbonate) precipitation. Kutnohorite was precipitated at the chemocline during maximum OM degradation and, hence, features abnormally negative carbonate-C isotope values derived from Mn reduction. Mn-bearing siderite occurs solely within a 3-m-thick interval at the base of suboxic Unit 3 characterized by the predominance of Fe over sulfate reduction. In Unit 2, anoxia inhibited kutnohorite precipitation, and Mn-bearing calcite is the dominant secondary carbonate phase instead. This mineral contains small amounts of isotopically light C derived from sulfate reduction, and it was formed at later diagenetic stages when OM oxidation rates were lower. Thus, diagenetic carbonates formed rapidly and exclusively above the chemocline under suboxic conditions, whereas carbonate precipitation persisted for longer periods and occurred mainly below the chemocline under anoxic conditions. These results highlight the highly complex diagenetic processes occurring in semi-restricted marine environments subjected to shifting redox conditions. Mn was the main factor controlling early diagenesis in oxygen-depleted marine basins located at the NW Tethyan realm during the late early Jurassic.

5 General conclusions

The Bächental bituminous marls belonging to the Sachrang Member of the Lower Jurassic Middle Allgäu Formation were sampled in high resolution and investigated using a multi-analytical approach. The results permitted the comprehensive interpretation of environmental, depositional and diagenetic factors effective on global to local scales and controlling the accumulation of organic-rich deposits in the hemipelagic and carbonate-dominated Bächental basin during early Jurassic time. The gained data yielded information to aspects as follows:

[i] Classification and subdivision of the study section

- In the Bächental, the Sachrang Member includes a 25-cm-thick basal mudstone, the OM-enriched Bächental bituminous marls (23.7 m thick) and a 1-m-thick debrite layer. Whereas hemipelagic carbonates of the Scheibelberg Formation occur below the Sachrang Member, overlying limestones and marls are assigned to the Upper Allgäu Formation.

- Strong environmental changes during the deposition of the Bächental bituminous marls resulted in pronounced stratigraphic variation providing the basis for subdivision into three distinct units (suboxic Unit 1 – anoxic-euxinic Subunits 2a and 2b – Unit 3 from base to top).

[ii] Stratigraphy

- The occurrence of *Cleviceras exaratum* in the middle part of the section (13.40 m; base of Subunit 2a) suggests a stratigraphic age of early Toarcian (*falciferum* Zone) for that interval. Accordingly this level corresponds well to the time interval of the globally observed T-OAE.

- Chemostratigraphic correlation of the Bächental bituminous marls with both the time-equivalent SW German Posidonia Shale of Dotternhausen and the global sea-level curve for the Lower Jurassic suggests that deposition of OM-rich sediments in the Alpine realm potentially commenced earlier (?late Pliensbachian) than in proximal epicontinental areas (early Toarcian)

[iii] Sources and thermal maturity of OM, bioproductivity

- The basal mudstone contains mainly amorphous OM. High reflectivity suggests the presence of charred land-plant material. In addition, inertinite occurs together with traces of liptinite.

- Intervals with predominantly suboxic depositional conditions in the Bächental basin (Units 1 and 3) typically feature low HI and TOC values (HI: ~300-550 mg HC/g TOC; TOC: ~1.5-2.2 %). In contrast, samples from anoxic-euxinic Unit 2 are generally characterized by elevated HI and TOC values (HI: ~620-690 mg HC/g TOC; TOC: ~3.5-12.9 %). Variations in HI values, especially striking in suboxic Units 1 and 3, reflect an early diagenetic overprint rather than multiple OM sources

- OM of Bächental bituminous marls mainly derived from marine algal and planktonic sources whereas terrestrial input generally was of minor importance. Lamalginite is the dominating maceral in the organic fraction in the samples, telalginite, sporinite and fish remains are present with slightly varying, but always low amounts. Terrestrial inertinite and vitrinite occur rarely with tiny irregularly shaped particles.

- A flourishing of marine algae and bacterioplankton contributed to the significant TOC increase at the base of Subunit 2a. This unit is also characterized by the occurrence of large amounts of 4-methylsteranes signifying elevated commonness of halophilic microorganisms.

- According to bulk geochemical and organic geochemical proxies the OM of Bächental bituminous marls is thermally immature corresponding to a vitrinite reflectance in the range of ~0.45 to 0.55 % R_o.

[iv] Mineralogical and sedimentological characteristics of the Bächental bituminous marls

- Greyish marls of suboxic Units 1 and 3 are laminated to bioturbated wackestones containing mainly radiolarians and subordinated filaments (*Bositra*), ostracods, sponge spicules, and some foraminifera.

- Black and finely laminated strata from Subunit 2a represent mudstones comprising mainly radiolarians and additionally *Bositra*, sponge spicules, ostracods, and foraminifera. Small channels, onlap structures as well as low energetic, fine-grained turbidites with carbonate detritus are present. Radiolarian wackestones occur occasionally in the middle and upper parts of Subunit 2a

- The most striking characteristic in Subunit 2b is the presence of re-deposited carbonate detritus layers containing abundant pyrite. These layers become thicker and more frequent towards the top of the unit.

[v] TE enrichment in the Bächental basin

- The enrichment of TEs was connected to siliciclastic input (Mo, U, V, Cu, Ni) and potentially to precipitation of diagenetic Mn-rich carbonates (Mo, V) and adsorption onto OM (Cu, Ni) under suboxic conditions (Units 1 and 3).

- In contrast, the removal of TEs to the sediment was linked mainly to adsorption onto OM in anoxic-euxinic Unit 2, reflecting control of TE enrichment by the availability of an organic substrate.

[vi] Global and local factors controlling the onset and duration of OM accumulation in the Bächental basin

- Redox and salinity variations in the tectonically complex Bächental basin were determined mainly by sea-level fluctuations that controlled marginal sill depths and the degree of bottom-water ventilation. Agreement between the sea-level curve and inferred variations in redox conditions and salinity demonstrate this influence.

- During deposition of Units 1 and 3, frequent mixing and ventilation of the water column of the Bächental basin prevented the establishment of a stratified water mass and permanent anoxic conditions.

- In anoxic-euxinic and mainly Fe-limited Subunit 2a, a stagnant basin setting during a period of relative sea-level lowstand triggered the establishment of strong anoxia, a salinity-stratified watermass, and a flourishing of surface-water productivity that jointly enhanced OM accumulation.

- In Subunit 2b infrequently occurring carbonate turbidity currents triggered pyritization and, in addition, served to transiently mix bottom waters and disrupt water-column stratification, although anoxic conditions continued to prevail in the sediment.

[vii] Diagenesis under shifting suboxic to anoxic-euxinic conditions in the Bächental basin

- The dominant diagenetic processes in the Bächental basin were markedly redox-dependent and varied strongly between sediments that accumulated under suboxic versus anoxic-euxinic conditions.

- The carbonate C-isotope profile of the study section has been strongly influenced by diagenetic processes, resulting in a signal mainly derived from secondary carbonate phases.

- In suboxic Units 1 and 3, the availability of abundant Mn oxides resulted in strong Mn reduction, causing a maximum OM loss in the range of 0.9 to 1.5 % and a lowering of HI values by up to 400 mg HC/g TOC.

- Sulfate reduction was the dominant OM oxidation process in anoxic-euxinic Unit 2 containing high amounts of hydrogen-rich OM (TOC: up to 12.9 %; HI: ca. 580-690 mg HC/g TOC). However, natural sulfurization of OM induced the early termination of sulfate reduction, contributing to enhanced OM preservation in Unit 2, as reflected in a more limited decrease of HI values (by 100 mg HC/g TOC). An increase of alkalinity and pH (>9) conditions due to sulfate reduction caused the advanced dissolution of biogenic quartz and incipient alteration of pyrite.

- Under suboxic conditions the activity of aerobic microbes and denitrifying bacteria within the sediment surface layer (<1 cm) favored the precipitation of dolomite whereas anaerobic Mn reduction triggered the release of isotopically light carbon and Mn supersaturation of pore waters causing a transition from dolomite to kutnohorite precipitation. Kutnohorite was precipitated at the chemocline during maximum OM degradation and, hence, features abnormally negative carbonate-C isotope values derived from Mn reduction. The formation of Mn-bearing siderite was limited to an

interval in which the exceptionally high availability of Mn and Fe oxides triggered Mn and Fe reduction and suppressed sulfate reduction.

- Whereas dolomite and kutnohorite precipitation were significantly impeded under anoxic-euxinic conditions in Unit 2, Mn-bearing calcite, formed below the chemocline, is the main carbonate phase. The mineral contains small fractions of isotopically light carbon, derived from sulfate reduction, and was formed at late stages of OM decay

- Diagenetic carbonates formed rapidly and exclusively above the chemocline under suboxic conditions, whereas carbonate precipitation persisted for longer periods and occurred mainly below the chemocline under anoxic conditions.

[viii] Applicability of proxies from diverse scientific fields for interpretation of depositional conditions

- In general, the interpretation of redox proxies based on bulk geochemical parameters, biomarker data as well as TE concentrations and TE concentration ratios results in a consistent stratigraphic redox trend for the Bächental bituminous marls.

- Ratios of pristane versus phytane are obviously controlled by prevailing redox conditions and bioproductivity. Thus, the comparison of vertical trends of geochemical redox proxies provides a means to detect intervals characterized by elevated surface-water productivity.

- The variations of sterane and hopane rations in the study section confirm the questionability of applying isomerization ratios as maturity proxies to sections deposited under hypersaline conditions or strongly variable salinities such as Subunit 2a.

[ix] Broader implications

- The occurrence of charred OM and volcaniclastics in the carbonate-free basal mudstone at the base of the study section suggests that a possibly regional volcanic event was the trigger for onset of OM accumulation. Continued inputs of volcanic

detritus (smectite) during marl deposition confirm ongoing volcanic activity during the early Jurassic in the NW Tethyan domain.

- Mn was the main factor controlling early diagenesis in oxygen-depleted marine basins located at the NW Tethyan realm during the late early Jurassic. Exceptionally high Mn concentrations probably derived from volcanic inputs and from the activity of hydrothermal vents connected to rifting and spreading of the Alpine Atlantic.

- Intervals with peak TOC contents in the study section probably correspond to the main magmatic stage of the Karoo and Ferrar Large Igneous Provinces, suggesting a massive effect on coeval marine productivity.

- The observed salinity variations suggest that global climate processes were overprinted by local factors within the Bächental basin, e.g., mixing of water bodies by turbidites, which also influenced the intensity of water-column anoxia.

- The potential earlier onset of OM accumulation in the Alpine realm compared to epicontinental areas indicates a rapid oceanic response to the major environmental perturbations caused by the activity of Karoo and Ferrar LIPs and complex rifting of the Alpine Tethys in local basins that were prone to the development of water-column stratification and deepwater anoxia because of their geometry or paleogeographic setting.

- The early Toarcian negative CIE that is observed in age-equivalent sections worldwide is not visible in either the carbonate or organic carbon $\delta^{13}C$ profiles of the study section. Thus, this chemostratigraphic marker cannot be used in correlation of the Bächental bituminous marls. Consequently, the unrestricted applicability of the early Toarcian negative CIE as a ubiquitous chemostratigraphic marker for this time interval has to be questioned.

To sum up, significant environmental changes effective variably at global (i.e., eruptions of the Karoo-Ferrar LIP, opening of the Atlantic Ocean, climate warming - "greenhouse Earth" conditions) to local (e.g., redox and salinity variations, basin morphology) scales operated in concert to produce conditions favorable to marine anoxia and black shale accumulation in hemipelagic basins of the NW Tethys Ocean during early Jurassic time.

6 References

Alali, J. (2006). Jordan oil shale, availability, distribution, and investment opportunity. International Oil Shale Conference, Amman, Jordan.

Algeo, T.J., Tribovillard, N. (2009). Environmental analysis of paleoceanographic systems based on molybdenum-uranium covariation. Chemical Geology 268, 211-225.

Allix, P., Burnham, A.K. (2010). Coaxing Oil from Shale. Oilfield Review (Schlumberger) 22 (4): 6.

Al-Suwaidi, A.H., Angelozzi, G.N., Baudin, F., Damborenea, S.E., Hesselbo, S.P., Jenkyns, H.C., Manceñido, M.O., Riccardi, A.C. (2010). First record of the Early Toarcian Oceanic Anoxic Event from the Southern Hemisphere, Neuquén Basin, Argentina. Journal of the Geological Society, London 167, 633-636.

Altun, N.E., Hiçyilmaz, C., Hwang, J.-Y., Suat Bağci, A., Kök, M.V. (2006). Oil shales in the world and Turkey; reserves, current situation and future prospects: a review. Oil Shale. A Scientific-Technical Journal (Estonian Academy Publishers) 23, 211-227.

Arthur, M.A., Premoli Silva, I. (1982). Development of widespread organic carbon-rich strata in the Mediterranean Tethys. In: Schlanger, S.O., Cita, M.B. (Eds.), Nature and Origin of Cretaceous Carbon-Rich Facies. Academic, London, pp. 7-54.

Arthur, M.A., Jenkyns, H.C., Brumsack, H.-J., Schlanger, S.O. (1990). Stratigraphy, geochemistry, and paleoceanography of organic-carbon-rich Cretaceous sequences. In: Ginsburg, R.N., Beaudoin, B. (Eds.), Cretaceous Resources, Events and Rhythms. NATO ASI Ser., vol. 304, Kluwer Acad., Dordrecht,

Baudin, F. (2005). A Late Hauterivian short-lived anoxic event in the Mediterranean Tethys: The 'Faraoni event' (2005). C. R. Geosci. 337, 1532–1540.

Bernoulli, D., Jenkyns, H.C. (1974). Alpine, Mediterranean and Central Atlantic Mesozoic facies in relation to the early evolution of the Tethys. In: Dott, R.H., Shaver, R.H. (Eds.), Modern and Ancient Geosynclinal Sedimentation, a Symposium. Special Publication of the Society of economic Paleontologists and Mineralogists 19, pp. 129-160.

Bernoulli, D., Jenkyns, H.C. (2009). Ancient oceans and continental margins of the Alpine-Mediterranean Tethys: deciphering clues from Mesozoic pelagic sediments and ophiolites. Sedimentology 56,149-190.

Bitterli, P. (1962). Studien an bituminösen Gesteinen aus Österreich und benachbarten Gebieten. Erdöl-Z. 78, 405-416.

Bonarelli, G. (1891). Il territorio di Gubbio. Notizie geologiche. Tipogr. Econ., Rome, 38 pp.

Brandner, R. (2011). In: Geologie des Achenseegebiets. Tagungsband der Arbeitstagung der Geologischen Bundesanstalt, Wien: 220-224.

Brumsack, H.J. (2006). The trace metal content of recent organic carbon-rich sediments: implications for Cretaceous black shale formation. Palaeogeography Palaeoclimatology Palaeoecology 232, 344-361.

Büggisch, W. (1991). The global Frasnian-Famennian 'Kellwasser event'. Geologische Rundschau 80, 49-72.

Cane, R.F. (1976). The origin and formation of oil shale. In: Teh, F.Y., Chilingar, G.V. (Eds.), Oil Shale. Elsevier, Amsterdam, pp. 1-12.

Caruthers, A.H., Gröcke, D.R., Smith, P.L. (2011). The significance of an Early Jurassic (Toarcian) carbon-isotope excursion in Haida Gwaii (Queen Charlotte Islands), British Columbia, Canada. Earth and Planetary Science Letters 307, 19-26.

Caruthers, A.H., Smith, P.L., Gröcke, D.R. (2013). The Pliensbachian-Toarcian (Early Jurassic) extinction, a global multi-phased event. Palaeogeography, Palaeoclimatology, Palaeoecology 386, 104-118.

Coccioni, R., Nesci, O., Tramontana, C.F., Wezel, C.F., Moretti, E. (1987). Descrizione di un livello guida "Radiolaritico-Bituminoso-Ittiolitico" alla base delle Marne a Fucoidi nell'Appennino Umbro-Marchigiano. Boll. Soc. Geol. Ital. 106, 183-192.

Cohen, A.S., Coe, A.L., Harding, S.M., Schwark, L. (2004). Osmium isotope evidence for the regulation of atmospheric CO_2 by continental weathering. Geology 32, 157-160.

Compton, J.S. (1988). Degree of supersaturation and precipitation of organogenic dolomite. Geology 16, 318-321.

Dean, W.E., Piper, D.Z., Peterson, L.C. (1999). Molybdenum accumulation in Cariaco basin sediment over the past 24 k. y.: A record of water-column anoxia and climate. Geology 27, 507-510.

Dyni, J.R. (2006). Geology and resources of some world oil shale deposits. Scientific Investigations Report 2005. United States Department of the Interior, United States Geological Survey.

Dyni, J.R. (2010). Oil Shale. In: Clarke, A.W., Trinnaman, J.A. (Eds.), Survey of Energy Resources. 22nd World Energy Council.

Ebli, O. (1991). Beiträge von Draxler, I., Klein, P., Kodina, L.A., Lobitzer, H., Schwaighofer, B. Fazies, Paläontologie und organische Geochemie der Sachranger Schiefer (Untertoarcium) im Mittelabschnitt der Nördlichen Kalkalpen zwischen Isar und Saalach. Jahrbuch der Geologischen Bundesanstalt 134/1, 5-14.

Ebli, O., Vetö, I., Lobitzer, H., Sajgò, C., Demény, A., Hetényi, M. (1998). Primary productivity and early diagenesis in the Toarcian Tethys on the example of the Mn rich black shales of the Sachrang Formation, Northern Calcareous Alps. Organic Geochemistry 29, 1635-47.

Erba, E., Bartolini, A., Larson R.L. (2004). Valanginian Weissert oceanic anoxic event, Geology 32, 149-152.

Francu, J., Harvie, B., Laenen, B., Siirde, A., Veiderma, M. (2007). A study on the EU oil shale industry viewed in the light of the Estonian experience. A report by EASAC to the Committee on Industry, Research and Energy of the European Parliament. European Academies Science Advisory Council, pp. 12–13; 18–19; 23–24; 28.

Frimmel, A., Oschmann, W., Schwark, L. (2004). Chemostratigraphy of the Posidonia Shale, SW Germany I. Influence of sea-level variation on organic facies evolution. Chemical Geology 206, 199-230.

Frisch, W., Gawlick, H.-J. (2003). The nappe structure of the central Northern Calcareous Alps and its disintegration during Miocene tectonic extrusion – a contribution to understanding the orogenic evolution of the Eastern Alps. International Journal of Earth Sciences 92, 712-727.

Froelich, P.N., Klinkhammer, G.P., Bender, M.L., Luedtke, N.A., Heath, G.R., Cullen, D., Dauphin, P., Hammond, D., Hartman, B., Maynard, V. (1979). Early oxidation of organic matter in pelagic sediments of the eastern equatorial Atlantic: suboxic diagenesis. Geochimica et Cosmochimica Acta 43, 1075-1090.

Gawlick, H.-J., Missoni, S., Schlagintweit, F., Suzuki, H., Frisch, W., Krystyn, L., Blau, J., Lein, R. (2009). Jurassic Tectonostratigraphy of the Austroalpine Domain. Journal of Alpine Geology 50, 1-152.

Gradstein, F.M., Ogg, J.G., Smith, A.G. (2005). A Geologic Time Scale 2004. Cambridge Univ. Press, Cambridge, 610 pp.

Gröcke, D.R., Hori, R.S., Trabucho-Alexandre, J., Kemp, D.B., Schwark, L. (2011). An open ocean record of the Toarcian oceanic anoxic event. Solid Earth 2, 245-57.

Harnik, P.G., Lotze, H.K., Anderson, S.C., Finkel, Z.V., Finnegan, S., Lindberg, D.R., Liow, L.H., Lockwood, R., McClain, C.R., McGuire, J.L., O'Dea, A., Pandolfi, J.M., Simpson, C., Tittensor, D.P. (2012). Extinctions in ancient and modern seas. Trends Ecol. Evol. 27, 608–617.

Heinrich, M. (1980). Ölschiefer. In: Oberhauser, R. (Eds.), Der Geologische Aufbau Österreichs. Springer, Win-New York, pp. 547-548.

Heiser, U., Neumann, T., Scholten, J., Stüben, D. (2001). Recycling of manganese from anoxic sediments in stagnant basins by seawater inflow: a study of surface sediments from the Gotland Basin, Baltic Sea. Marine Geology 177, 151-166.

Hesselbo, S.P., Gröcke, D.R., Jenkyns, H.C., Bjerrum, C.J., Farrimond, P., Morgans Bell, H.S., Green, O.R. (2000). Massive dissociation of gas hydrate during a Jurassic oceanic anoxic event. Nature 406, 392-395.

Hesselbo, S.P., Jenkyns, H.C., Duarte, L.V., Oliviera, L.C.V. (2007). Carbon-isotope record of the Early Jurassic (Toarcian) Oceanic Anoxic Event from fossil wood and marine carbonate (Lusitanian Basin, Portugal). Earth and Planetary Science Letters 253, 455-470.

Hörmann, L. (1872). Steinölträger und Steinölbrenner. In: Amthor, E. (Eds.), Der Alpenfreund, Monatshefte für Verbreitung von Alpenkunde unter Jung und Alt in populären Schilderungen aus dem Gesamtgebiet der Alpenwelt und mit praktischen Winken zur genußvollen Bereisung derselben, 4. Band. Gera, 321 pp.

Hutton, A.C. (1987). Petrographic classification of oil shales. Internat. J. Coal Geol. 8, 203-231.

Ikeda, M., Hori, R.S. (2014). Effects of Karoo-Ferrar volcanism and astronomical cycles on the Toarcian Anoxic Events (Early Jurassic). Palaeogeography, Palaeoclimatology, Palaeoecology 410, 134-142.

Izumi, K., Miyaji, T., Tanabe, K. (2012). Early Toarcian (Early Jurassic) oceanic anoxic event recorded in the shelf deposits in the northwestern Panthalassa: Evidence from the Nishinakayama Formation in the Toyora area, west Japan. Palaeogeography, Palaeoclimatology, Palaeoecology 315-316, 100-108.

Jenkyns, H.C. (1980). Cretaceous anoxic events: From continents to oceans, Journal of the Geological Society 137, 171-188.

Jenkyns H. C. (1985). The Early Toarcian and Cenomanian–Turonian anoxic events in Europe: comparisons and contrasts. Geologische Rundschau 74, 505-518.

Jenkyns, H.C. (1988). The Early Toarcian (Jurassic) anoxic event: stratigraphic, sedimentary, and geochemical evidence. American Journal of Science 288, 101-151.

Jenkyns, H.C. (2003). Evidence for rapid climate change in the Mesozoic–Palaeogene greenhouse world. Philosophical Transactions of the Royal Society of London 361 A, 1885-1916.

Jenkyns, H.C. (2010). The geochemistry of oceanic anoxic events. Geochemistry Geophysics Geosystems 11, Q03004, doi: 10.1029/2009GC002788.

Jenkyns, H.C., Clayton, C.J. (1986). Black shales and carbon isotopes in pelagic sediments from the Tethyan Lower Jurassic. Sedimentology 33, 87-106.

Jenkyns, H.C., Clayton, C.J. (1997). Lower Jurassic epicontinental carbonates and mudstones from England and Wales: chemostratigraphic signals and the early Toarcian anoxic event. Sedimentology 44, 687-706.

Jenkyns, H.C., Gröcke, D.R., Hesselbo, S.P. (2001). Nitrogen isotope evidence for water mass denitrification during the early Toarcian (Jurassic) ocean anoxic event. Paleoceanography 16, 593–603.

Jenkyns, H.C., Jones, C.E., Gröcke, D.R., Hesselbo, S.P., Parkinson, D.N. (2002). Chemostratigraphy of the Jurassic System: applications, limitations and implications for palaeoceanography. Journal of the Geological Society of London 159, 351-378.

Jørgensen, B.B. (2000). Bacteria and marine biogeochemistry. In: Schulz, H.D., Zabel, M. (Eds.), Marine Geochemistry. Springer Verlag, Berlin, pp. 173-207.

Jourdan, F., Féraud, G., Bertrand, H., Watkeys, M.K., Renne, P.R. (2008). The $^{40}Ar/^{39}Ar$ ages of the sill complex of the Karoo large igneous province: implications for the Pliensbachian-Toarcian climate change. Geochemistry, Geophysics, Geosystems 9, 1-20.

Kafousia, N., Karakitsios, V., Mattioli, E., Kenjo, S., Jenkyns, H.C. (2014). The Toarcian Oceanic Anoxic Event in the Ionian Zone, Greece. Palaeogeography, Palaeoclimatology, Palaeoecology 393, 135-145.

Kemp, D.B., Coe, A.L., Cohen, A.S., Schwark, L. (2005). Astronomical pacing of methane release in the early Jurassic period. Nature 437, 396-399.

Klebelsberg, R.v. (1935). Geologie von Tirol. Gebr. Borntraeger, Berlin.

Kodina, L.A., Bogatecheva, M.P., Lobitzer, H. (1988). An anorganic geochemical study of Austrian bituminous rocks. Jb. Geol. B.-A. 131, 291-300, Wien.

Köster, J. (1989). Organische Geochemie und Organo-Petrologie kerogenreicher und bituminöser Einschaltungen im Hauptdolomit (Trias, Nor) der Nördlichen Kalkalpen. Dissertation Geol. Inst. TU., 262 S., Clausthal.

Köster, J., Schouten, S., Sinninghe Damsté, J.S., de Leeuw, J.W. (1995). Reconstruction of the depositional environment of Toarcian marlstones (Allgäu Formation, Tyrol/Austria) using biomarkers and compound specific carbon isotope analysis. In: Grimalt, J.O., Dorronsoro, C. (Eds.), Organic Geochemistry: Developments and Applications to Energy, Climate, Environment and Human History. A.I.G.O.A., San Sebastian, pp. 76–78.

Küspert, W. (1982). Environmental changes during oil shale deposition as deduced from stable isotope ratios. In: Einsele, G., Seilacher, A. (Eds.), Cyclic and Event Stratification. Springer, Berlin, pp. 482-501.

Küspert, W. (1983). Faziestypen des Posidonienschiefers (Toarcium, Süddeutschland): Eine isotopen-geologische, organisch-chemische und petrographische Studie. Ph.D. Thesis, Tübingen University.

Leckie, R.M., Bralower, T.J., Cashman, R. (2002). Oceanic anoxic events and plankton evolution: Biotic response to tectonic forcing during the mid-Cretaceous, Paleoceanography 17, doi:10.1029/2001PA000623.

Li, Y.-X., Bralower, T.J., Montañez, I.P., Osleger, D.A., Arthur, M.A., Bice, D.M., Herbert, T.D., Erba, E., Premoli Silva, I. (2008). Toward an orbital chronology for the early Aptian oceanic anoxic event (OAE1a, ~120 Ma). Earth and Planetary Science Letters 271, 88-100.

Littke, R., Rotzal, H., Leythaeuser, D., Baker, D.R. (1991). Organic facies and maturity of Lower Toarcian Posidonia Shale in Southern Germany (Schwäbische Alb). Erdöl & Kohle Erdgas Petrochemie/Hydrocarbon Technology 44, 407-414.

Littler, K., Hesselbo, S.P., Jenkyns, H.C. (2009). A carbon-isotope perturbation at the Pliensbachian–Toarcian boundary: evidence from the Lias Group, NE England. Geological Magazine 147, 181-192.

Lobitzer, H., Kodina, L.A., Solti, G., Schwaighofer, B., Surenian, R. (1988). Fazies, Geochemie und Stratigraphie ausgewählter Vorkommen österreichischer organisch reicher Gesteine – ein Zwischenbericht. Geologische und Paläontologische Mitteilungen Innsbruck 15, 85-107.

Marzoli, A., Renne, P.R., Piccirillo, E.M., Ernesto, M., Bellieni, G., De Min, A. (1999). Extensive 200 million-year-old continental flood basalts of the central Atlantic magmatic province. Science 284, 616-618.

Mazzini, A., Svensen, H., Leanza, H.A., Corfu, F., Planke, S. (2010). Early Jurassic shale chemostratigraphy and U–Pb ages from the Neuquén Basin (Argentina): implications for the Toarcian Oceanic Anoxic Event. Earth Planet. Sci. Lett. 297, 633–645.

Mazzullo, S.J. (2000). Organogenic dolomitization in peritidal to deep-sea sediments. Journal of Sedimentary Research 70, 10-23.

McElwain, J.C., Murphy, J.W., Hesselbo, S.P. (2005). Changes in carbon dioxide during an oceanic anoxic event linked to intrusion of Gondwana coals. Nature 435, 479–483.

Meister, P., McKenzie, J.A., Bernasconi, S.M., Brack, P. (2013). Dolomite formation in the shallow seas of the Alpine Triassic. Sedimentology 60, 270-291.

Meyers, S.R. (2007). Production and preservation of organic matter: The significance of iron. Paleoceanography 22, PA4211, doi:10.1029/2006PA001332.

Morard, A., Guex, J., Bartolini, A., Morettini, E., De Wever, P. (2003). A new scenario for the Domerian-Toarcian transition. Bulletin de la Société géoloique France 174, 351-356.

Morford, J.L., Russell, A.D., Emerson, S. (2001). Trace metal evidence for changes in the redox environment associated with the transition from terrigenous clay to diatomaceous sediments, Saanich Inlet, BC. Marine Geology 174, 355-369.

Neumeister, S., Gratzer, R., Algeo, T.J., Bechtel, A., Gawlick, H.-J., Newton, R.J., Sachsenhofer, R.F. (2015). Oceanic response to Pliensbachian and Toarcian magmatic events: Implications from an organic-rich basinal succession in the NW Tethys. Global and Planetary Change 126, 62-83.

Pálfy, J., Smith, P.L. (2000). Synchrony between Early Jurassic extinction, oceanic anoxic event, and the Karoo–Ferrar flood basalt volcanism. Geology 28, 747-750.

Pancost, R.D., Crawford, N., Magness, S., Turner, A., Jenkyns, H.C., Maxwell, J.R. (2004). Further evidence for the development of photic-zone euxinic conditions during Mesozoic oceanic anoxic events, Journal of the Geological Society 161, 353-364.

Parente, M., Frijia, G., di Lucia, M., Jenkyns, H.C., Woodfine, R.G., Baroncini, F. (2008). Stepwise extinction of larger foraminifers at the Cenomanian-Turonian boundary: A shallow-water perspective on nutrient fluctuations during oceanic anoxic event 2 (Bonarelli event). Geology 36, 715-718.

Parrish, J.T. (1993). Climate of the supercontinent Pangaea. Journal of Geology 101, 215-233.

Parrish, J.T., Curtis, R.L. (1982). Atmospheric circulation, upwelling, and organic-rich rocks in the Mesozoic and Cenozoic areas. Palaeogeography, Palaeoclimatology, Palaeoecology 40, 31-66.

Pearce, C.R., Cohen, A.S., Coe, A.L., Burton, K.W. (2008). Molybdenum isotope evidence for global ocean anoxia coupled with perturbations to the carbon cycle during the Early Jurassic. Geology 36, 231–234.

Piper, D.Z., Calvert, S.E. (2009). A marine biogeochemical perspective on black shale deposition. Earth Science Reviews 95, 63-96.

Polgári, M., Szabó-Drubina, M., Szabó, Z. (2004). Theoretical model for Jurassic manganese mineralization in Central Europe, Úrkút, Hungary. Bulletin of Geoscience 79, 53-61.

Praus, M., Riegel, W. (1989). Evidence from phytoplanktonic associations for causes of black shale formation in epicontinental seas. N. Jb. Geol. Paläontol. Mh. 11, 671-682.

Price, G.D. (1999). The evidence and implications of polar ice during the Mesozoic. Earth Science Reviews 48, 183-210.

Radke, M., Willsch, H., Welte, D.H. (1980). Preparative hydrocarbon group type determination by automated medium pressure liquid chromatography. Analytical Chemistry 52, 406-411.

Ratschbacher, L., Dingeldey, C., Miller, C., Hacker, B.R., McWilliams, M.O. (2004). Formation, subduction, and exhumation of Penninic oceanic crust in the Eastern Alps: time constraints from $^{40}Ar/^{39}Ar$ geochronology. Tectonophysics 394, 155-170.

Röhl, H.J., Schmid-Röhl, A., Oschmann, W., Frimmel, A., Schwark, L. (2001). The Posidonia Shale (Lower Toarcian) of SW-Germany: an oxygen-depleted ecosystem controlled by sea level and palaeoclimate. Palaeogeography, Palaeoclimatology, Palaeoecology 165, 27-52.

Sabatino, N., Neri, R., Bellanca, A., Jenkyns, H.C., Baudin, F., Parisi, G., Masetti, D. (2009). Carbon-isotope records of the Early Jurassic (Toarcian) Oceanic Anoxic Event from the Valdorbia (Umbria-Marche Apennines) and Monte Mangart (Julian Alps) sections: palaeoceanographic and stratigraphic implications. Sedimentology 56, 1307-1328.

Sabatino, N., Neri, R., Bellanca, A., Jenkyns, H.C., Masetti, D., Scopelliti, G. (2011). Petrography and high-resolution geochemical records of Lower Jurassic manganese-rich deposits from Monte Mangart, Julian Alps. Palaeogeography, Palaeoclimatology, Palaeoecology 299, 97-109.

Sabatino, N., Vlahović, I., Jenkyns, H.C., Scopelliti, G., Neri, R., Prtoljan, B., Velić, I. (2013). Carbon-isotope record and palaeoenvironmental changes during the early Toarcian oceanic anoxic event in shallow-marine carbonates of the Adriatic Carbonate Platform in Croatia. Geological Magazine 150, Issue 6, 1085-1102.

Sælen, G., Doyle, P., Talbot, M.R. (1996). Stable-isotope analysis of belemnite rostra from the Whitby Mudstone Fm., England: Surface water conditions during deposition of a marine black shale. Palaios 11, 97-117.

Sageman, B.B., Meyers, S.R., Arthur, M.A. (2006). Orbital time scale and new C-isotope record for Cenomanian-Turonian boundary stratotype. Geology 34, 125-128.

Schlager, W., Schöllnberger, W. (1973). Das Prinzip stratigraphischer Wenden in der Schichtfolge der Nördlichen Kalkalpen. Mitt. Geol. Ges. Wien 66, 166-193.

Schlanger, S.O., Jenkyns, H.C. (1976). Cretaceous oceanic anoxic events: Causes and consequences, Geol. Mijnbouw 55, 179-184.

Schlanger, S.O., Arthur, M.A., Jenkyns, H.C., Scholle, P.A. (1987). The Cenomanian–Turonian oceanic anoxic event, I. Stratigraphy and distribution of organic carbon-rich beds and the marine $\delta^{13}C$ excursion. In: Brooks, J., Fleet, A.J. (Eds.), Marine Petroleum Source Rocks. Geological Society London Special Publications 26, 371-399.

Schmid-Röhl, A., Röhl, H.-J., Oschmann, W., Frimmel, A., Schwark, L. (2002). Palaeoenvironmental reconstruction of Lower Toarcian epicontinental black shales (Posidonia Shale, SW Germany): global versus regional control. Geobios 35, 13-20.

Sell, B., Ovtcharova, M., Guex, J., Bartolini, A., Jourdan, F., Spangenberg, J.E., Vicente, J.-C., Schaltegger, U. (2014). Evaluating the temporal link between the Karoo LIP and climatic-biologic events of the Toarcian Stage with high-precision U-Pb geochronology. Earth and Planetary Science Letters 408, 48-56.

Spieler, A., Brandner, R. (1989). Vom jurassischen Pull-Apart Becken zur Westüberschiebung der Achentaler Schubmasse (Tirol, Österreich). Geol. Paläont. Mitt. Innsbruck 16, 191-194.

Suan, G., Pittet, B., Bour, I., Mattioli, E., Duarte, L.V., Mailliot, S. (2008). Duration of the Early Toarcian carbon isotope excursion deduced from spectral analysis: consequence for its possible causes. . Earth and Planetary Science Letters 267, 666-679.

Suan, G., Schlögl, J., Mattioli, E. (2016). Bio- and chemostratigraphy of the Toarcian organic-rich deposits of some key successions of the Alpine Tethys. Newsletters on Stratigraphy, published online.

Svensen, H., Planke, S., Chevalier, L., Malthe-Sørensen, A., Corfu, F., Jamveit, B. (2007). Hydrothermal venting of greenhouse gases triggering Early Jurassic global warming. Earth and Planetary Science Letters 256, 554–566.

Thamdrup, B. (2000). Bacterial manganese and iron reduction in aquatic sediments. Advances in Microbial Ecology 16, 41-84.

Tollmann, A. (1976). Analyse des klassischen nordalpinen Mesozoikums. Stratigraphie, Fauna und Fazies der Nördlichen Kalkalpen. Deuticke, Wien, pp. 580.

Tribovillard, N., Algeo, T.J., Lyons, T., Riboulleau, A. (2006). Trace metals as paleoredox and paleoproductivity proxies: An update. Chemical Geology 232, 12-32.

Tsikos, H., Jenkyns, H.C., Walsworth-Bell, B., Petrizzo, M.R., Forster, A., Kolonic, S., Erba, E., Premoli Silva, I., Baas, M., Wagner, T., Sinninghe Damsté, J.S. (2004). Carbon-isotope stratigraphy recorded by the Cenomanian–Turonian Oceanic Anoxic Event: correlation and implications based on three key localities. J. Geol. Soc. Lond. 161, 711-719

Urov, A., Sumberg, K. (1999). Characteristics of oil shales and shale-like rocks of known deposits and outcrops. Oil Shale. A Scientific-Technical Journal (Estonian Academy Publishers) 16, 1-64.

Voigt, S., Erbacher, J., Mutterlose, J., Weiss, W., Westerhold, T., Wiese, F., Wilmsen, M., Wonik, T. (2008). The Cenomanian–Turonian of the Wunstorf section (north Germany): Global stratigraphic reference section and new orbital time scale for oceanic anoxic event 2. Newsletters on Stratigraphy 43, 65-89.

Vortisch, W. (1982). Clay mineralogical studies of some tills in northern Germany. Geologica et Palaeontologica 15, 167-192.

Wacey, D., Wright, D.T., Boyce, A.J. (2008). A stable isotope study of microbial dolomite formation in the Coorong Region, South Australia. Chemical Geology 244, 155-174.

Wang, C., Hu, X., Jansa, L., et al. (2001). The Cenomanian-Turonian anoxic event in southern Tibet. Cretaceous Research 22, 481-490.

Weissert, H. (2000). Deciphering methane's fingerprint. Nature 406, 356-357.

Weissert, H. (2013). C-isotope geochemistry – tool for chemostratigraphy and carbon cycle history. Ciencias da terra 18.

Whiteside, J.H., Olsen, P.E., Kent, D.V., Fowell, S.J., Et-Touhami, M. (2007). Synchrony between the Central Atlantic magmatic province and the Triassic-Jurassic mass extinction event? Palaeogeography, Palaeoclimatology, Palaeoecology 244, 345-367.

Wright, D.T., Oren, A. (2005). Nonphotosynthetic bacteria and the formation of carbonates and evaporites through time. Geomicrobiology Journal 22, 27-53.

Yarincik, K.M., Murray, R.W., Peterson, L.C. (2000). Climatically sensitive eolian and hemiplegic deposition in the Cariaco Basin, Venezuela, over the past 578,000 years: results from Al/Ti and K/Al. Paleoceanography 15, 210-228.

Yin, L. (2006). Current status of oil shale industry in Fushun, China. International Oil Shale Conference. Amman, Jordan.

PUBLICATIONS

7 Oceanic response to Pliensbachian and Toarcian magmatic events: Implications from an organic-rich basinal succession in the NW Tethys

Published in Global and Planetary Change 126 (2015), 62-83.

S. Neumeister [a,*], R. Gratzer [a], T. J. Algeo [b], A. Bechtel [a], H.-J. Gawlick [a], R. J. Newton [c], R. F. Sachsenhofer [a]

[a] *Department of Applied Geosciences and Geophysics, Montanuniversitaet Leoben, Peter-Tunner-Str. 5, A-8700 Leoben, Austria*

[b] *Department of Geology, University of Cincinnati, Cincinnati, OH 45221, USA*

[c] *The School of Earth and Environment, The University of Leeds, Woodhouse Lane, Leeds, West Yorkshire, LS2 9JT, UK*

* Corresponding author at: Department of Applied Geosciences and Geophysics, Montanuniversitaet Leoben, Peter-Tunner-Str. 5, A-8700 Leoben, Austria.
Tel.: +43 664 5049925.
E-Mail address: st.neumeister@hotmail.com (Stefan Neumeister).

Abstract

The Bächental bituminous marls (Bächentaler Bitumenmergel) belonging to the Sachrang Member of the Lower Jurassic Middle Allgäu Formation were investigated using a multidisciplinary approach to determine environmental controls on the formation of organic-rich deposits in a semi-restricted basin of the NW Tethys during the Early Jurassic. The marls are subdivided into three units on the basis of mineralogical composition, source-rock parameters, redox conditions, salinity variations, and diagenetic processes. Redox proxies (e.g., pristane/phytane ratio; aryl isoprenoids; bioturbation; ternary plot of iron, total organic carbon, and sulphur) indicate varying suboxic to euxinic conditions during deposition of the Bächental section. Redox variations were mainly controlled by sea-level fluctuations with the tectonically complex bathymetry of the Bächental basin determining watermass exchange with the Tethys Ocean. Accordingly, strongest anoxia and highest total organic carbon

content (up to 13%) occur in the middle part of the profile (upper *tenuicostatum* and lower *falciferum* zones), coincident with an increase in surface-water productivity during a period of relative sea-level lowstand that induced salinity stratification in a stagnant basin setting. This level corresponds to the time interval of the lower Toarcian oceanic anoxic event (T-OAE). However, the absence of the widely observed lower Toarcian negative carbon isotope excursion in the study section questions its unrestricted use as a global chemostratigraphic marker. Stratigraphic correlation of the thermally immature Bächental bituminous marls with the Posidonia Shale of SW Germany on the basis of C_{27}/C_{29} sterane ratio profiles and ammonite data suggests that deposition of organic matter-rich sediments in isolated basins in the Alpine realm commenced earlier (late Pliensbachian *margaritatus* Zone) than in regionally proximal epicontinental seas (early Toarcian *tenuicostatum* Zone). The late Pliensbachian onset of reducing conditions in the Bächental basin coincided with an influx of volcaniclastic detritus that was possibly connected to complex rifting processes of the Alpine Tethys and with a globally observed eruption-induced extinction event. The level of maximum organic matter accumulation in the Bächental basin corresponds to the main eruptive phase of the Karoo-Ferrar large igneous province (LIP), confirming its massive impact on global climate and oceanic conditions during the Early Jurassic. The Bächental marl succession is thus a record of the complex interaction of global (i.e., LIP) and local (e.g., redox and salinity variations, basin morphology) factors that caused reducing conditions and organic matter enrichment in the Bächental basin. These developments resulted in highly inhomogeneous environmental conditions in semi-restricted basins of the NW Tethyan domain during late Pliensbachian and early Toarcian time.

Keywords: Bächental marl; Sachrang Member; Allgäu Formation; oceanic anoxic event; anoxia; sea level; carbon isotopes; Northern Calcareous Alps; Karoo-Ferrar; Alpine Tethys

7.1 Introduction

The early Toarcian was characterized by the deposition of organic-rich sediments in marine systems globally (e.g., Jenkyns, 1985, 1988; Jenkyns et al., 2002; Pearce et al., 2008), although the main controls on organic matter (OM) production and preservation at that time remain controversial. Widespread anoxia in epicontinental areas of the western Tethyan region (i.e., depositional area of the Posidonia Shale) has been attributed to a surface-water layer with reduced salinity that caused intensified water-column stratification (Praus and

Riegel, 1989; Littke et al., 1991; Sælen et al., 1996). Other possible influences include minor sea-level fluctuations that controlled watermass exchange and, hence, dissolved oxygen levels in semi-restricted basins within the western European epicontinental sea (Röhl et al., 2001; Schmid-Röhl et al., 2002; Frimmel et al., 2004). In contrast, Jenkyns (1985, 1988; a summary is given by Jenkyns, 2010) postulated upwelling connected with the T-OAE of global scale for causing the high rates of organic carbon accumulation in lower Toarcian strata. Tsikos et al. (2004a) found that the definition of Toarcian organic-rich sediments on the basis of their stratigraphic distribution is problematic as preservation and dilution of OM was affected by local variations in depositional and diagenetic conditions.

Changes in global climate during the Early Jurassic created oceanic conditions that were generally conducive to development of anoxia. Significant climatic warming had begun with release of large quantities of greenhouse gases during the CAMP eruptions at ~201 Ma (Marzoli et al., 1999; Whiteside et al., 2007). An interval of relative global cooling during the late Pliensbachian (Price, 1999; Morard et al., 2003; Dera et al., 2010) was followed by eruption of two large igneous provinces in the Early Jurassic: (1) the Karoo LIP at ~183 Ma (Svensen et al., 2007, 2012; Sell et al., 2014), and (2) the Ferrar LIP at ~184-183 Ma (Encarnación et al., 1996; Minor and Mukasa, 1997). These eruptions served to induce further climatic warming from the Pliensbachian/Toarcian boundary onwards, leading to "greenhouse Earth" conditions (Palfy and Smith, 2000; Weissert, 2000; Jenkyns, 2003). The prevailing subtropical climate was accompanied by an accelerated hydrological cycle with heavy monsoonal rainfalls and intense continental weathering that triggered an extensive supply of nutrients for ocean-surface waters, enhancing primary productivity (Parrish and Curtis, 1982; Parrish, 1993; Cohen et al., 2004). In addition, rifting of the Alpine Tethys was associated with several regional magmatic pulses during late Triassic to middle Jurassic time (Mohn et al., 2010; Decarlis et al., 2013). Oceanic break-up in the Penninic realm occurred in the Pliensbachian-Toarcian (Ratschbacher et al., 2004). These environmental changes operated in concert to produce conditions favourable to marine anoxia and black shale accumulation variably at global to local scales during the Early Jurassic.

Several studies have documented significant variation in total organic carbon (TOC) levels within lower Toarcian deposits of northern and southern Europe (see Jenkyns, 2010, for references). Whereas black shales deposited in epicontinental settings in Britain, France, and Germany reach peak TOC contents of up to 20% (e.g., Küspert, 1982; Jenkyns and Clayton,

1997; Röhl et al., 2001), coeval sediments of the pelagic Tethyan realm generally contain smaller amounts of OM (<5 %; e.g., Jenkyns, 1985; 1988; Sabatino et al., 2009, 2013). Bituminous marls of Early Jurassic age (Bächentaler Bitumenmergel) are found in the Bächental valley of the Northern Calcareous Alps (Fig. 7.1A). The Bächental basin was located in the NW part of the Tethys Ocean during the Toarcian (Figs. 7.1B, C). A detailed investigation of the depositional environment of the Bächental bituminous marls as well as exact data regarding the onset and duration of its accumulation are lacking. However, exceptionally high TOC contents (13 %) and an onset of OM accumulation during the Pliensbachian were reported by Kodina et al. (1988).

A multidisciplinary approach with high sample resolution was applied to the investigation of the Bächental bituminous marls. The use of a variety of proxies yielded information on source and thermal maturity of OM, redox conditions, salinity, water-column stratification, sea-level fluctuations, diagenetic processes, and volcanic influences. A comprehensive interpretation of these data permits the establishment of an overall model for the deposition of the Bächental bituminous marls. In addition, new findings regarding the age of marl accumulation facilitate stratigraphic correlation of lower Toarcian deposits from Alpine and epicontinental settings. The present study provides insights concerning the role of global events (e.g., Karoo and Ferrar LIP magmatism, opening of the Atlantic Ocean) as well as the influence of local basinal factors (e.g., redox and salinity variations) on OM accumulation in semi-restricted basins (e.g., Bächental basin) of the northwestern Tethyan domain during the late Pliensbachian and early Toarcian.

7.2 Geological setting and samples

The investigated section is situated in the Bächental valley, which is part of the Karwendel Mountains of northern Tyrol (Fig. 7.1A; GPS: 47°30'31.38"N; 11°37'46.00"E). In this area, lithostratigraphic units of Triassic to Jurassic age belonging to the Lechtal nappe of the Bavaric Unit, a tectonic domain of the Northern Calcareous Alps, are exposed.

The paleogeography of the depositional area of the Bächental bituminous marls (Figs. 7.1B-C) was controlled by extensional tectonics, related to late Hettangian rifting and Toarcian oceanic break-up in the Penninic realm (e.g., Ratschbacher et al., 2004). During late Hettangian to Sinemurian time (Schlager and Schöllnberger, 1973) the final configuration of the roughly north-south trending Bächental basin with half-graben geometry, a depocenter

located in the northern part of the basin, tilt block tectonics and antithetic step faults were established (Spieler and Brandner, 1989; Fig. 7.1D). The distribution of bituminous marls (Fig. 7.1E) deposited during the early Toarcian was limited to the poorly ventilated deepest part of the Bächental basin (Spieler and Brandner, 1989).

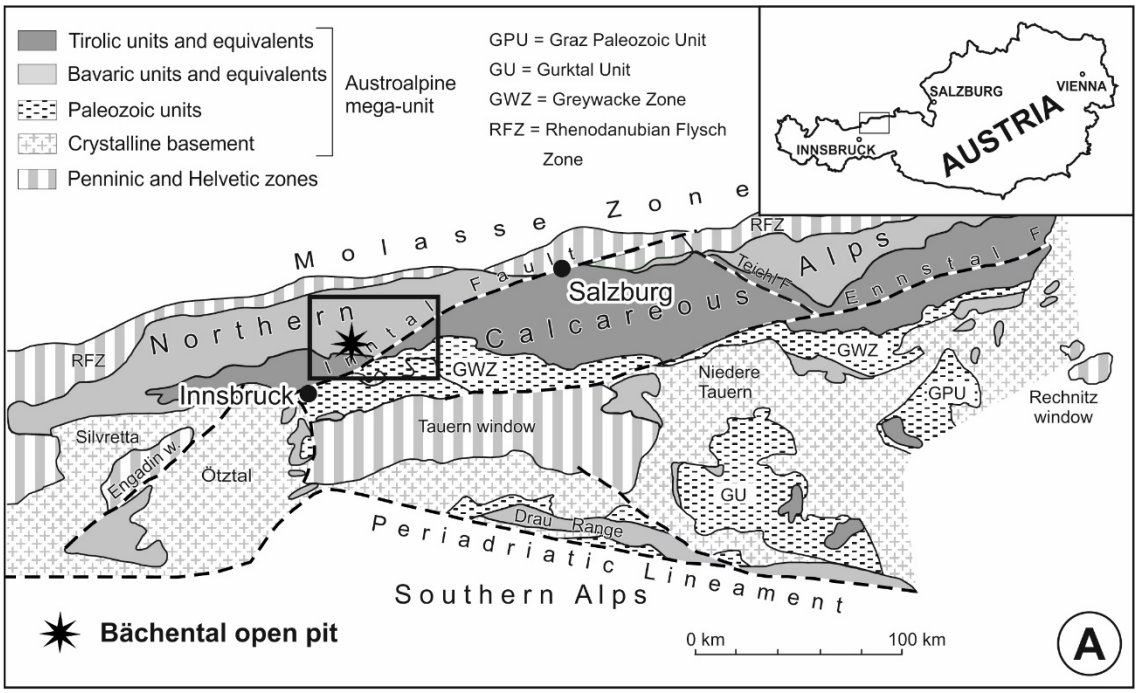

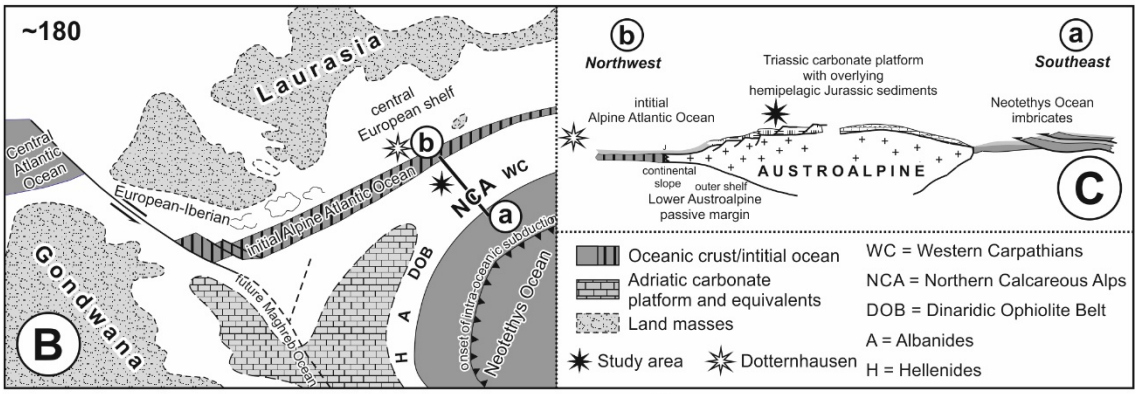

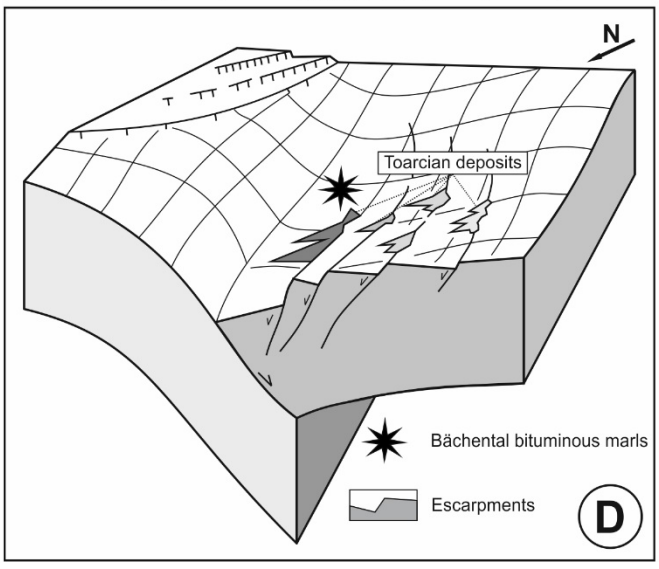

Fig. 7.1: (A) Schematic tectonic map of the Eastern Alps after Frisch and Gawlick (2003). The position of the studied section in the Bächental valley is indicated. (B) Palaeogeographic position of the study section as part of the Northern Calcareous Alps within the Austroalpine domain in late Early Jurassic time (after Frisch, 1979; Golonka, 2002; Vlahović et al., 2005; Gawlick et al., 2008; Bernoulli and Jenkyns, 2009; Missoni and Gawlick, 2011). The Northern Calcareous Alps are part of a continent between the Alpine Atlantic Ocean to the northwest and the Neotethys Ocean to the east/southeast. Formation of oceanic crust started in the late Early Jurassic (Ratschbacher et al., 2004). (C) Schematic cross section (for position, see line a-b in Fig. 7.1B) showing the passive continental margin of the Lower Austroalpine domain (e.g., Frisch, 1979; Tollmann, 1985, Faupl & Wagreich, 2000; Gawlick et al., 2009; Frisch et al., 2011). Rifting and spreading of the Alpine Atlantic commencing in the late Early Jurassic affected the Austroalpine domain by the formation of extensional basins (horst-and-graben structure, asymmetric basins; cf. Bernoulli and Jenkyns, 1974). (D) Paleogeography of the depositional area of Bächental bituminous marl in the Lower Jurassic (Spieler and Brandner, 1989; Brandner, 2011). The accumulation of organic-rich rocks was restricted to the deepest parts of a basin with half-graben geometry. (E) Photograph of the outcropping Bächental bituminous marl in the open pit.

The study section has an overall thickness of 35.54 m (Fig. 7.2) and is well exposed in large parts due to its position in an open-pit mine. At its base, limestone beds with a total thickness of 4.00 m occur. These strata are assigned to the Scheibelberg Formation (Sinemurian to Pliensbachian) and were deposited in water depths of several hundred meters at the transition of distal slope to basin (Spieler and Brandner, 1989). Directly above a 0.25-m-thick weathered mudstone, the Bächental bituminous marls of the upper Pliensbachian to lower Toarcian Sachrang Member of the Middle Allgäu Formation (Tollmann, 1976a; Ebli, 1991; Ebli et al., 1998; Gawlick et al., 2009; this study) are exposed with a total thickness of 23.70 m. The alternating sequence of limestone and marl with a thickness of 4.69 m forming the top of the succession belongs to the Upper Allgäu Formation (upper Toarcian to early Middle Jurassic; Spieler and Brandner, 1989). The dating of the Bächental bituminous marls to the Toarcian was originally based on the occurrence of *Harpoceras* sp. (Klebelsberg, 1935). Kodina et al. (1988) inferred that bituminous marl sedimentation began during the late Pliensbachian based on the occurrence of *Arieticeras* sp. and *Arieticeras* sp. or *Leptaleoceras* sp. near the base of the marls. This is consistent with the presence of *Cleviceras exaratum* in the middle part of the section (13.40 m; Fig. 7.2), a taxon associated with the early Toarcian

falciferum Zone. A late Pliensbachian age (*margaritatus* Zone) for the base of the Sachrang Member in the Bächental basin is further supported by correlations based on C_{27}/C_{29} sterane ratios (Fig. 7.2; see Section 7.5.3.1 for discussion). At its type locality in Bavaria, deposition of the Sachrang Member commenced at the base of the *tenuicostatum* Zone and continued through the entire early Toarcian (Ebli et al., 1998).

Samples were collected from fresh exposures in a trench that was dug up to 4 m deep. A total of 68 samples was collected for geochemical analyses (Fig. 7.2). The Scheibelberg Formation at the base of the study succession is represented by six samples. The Sachrang Member, including a basal mudstone, bituminous marls, and a 1-meter-thick debrite layer (Fig. 7.2), is represented by 52 samples resulting in an average sampling interval of ca. 0.50 m. Ten samples at intervals of 0.10 to 0.90 m were collected from the Upper Allgäu Formation at the top of the section.

7.3 Analytical methods

A total of 28 thin sections were made for analyses via transmitted light microscopy. Polished blocks of 12 samples were prepared for maceral analyses that were performed with a Leica MPV microscope.

Total carbon (TC) and sulphur (S) contents were measured with a Leco 300 CSTM analyser. For the determination of total organic carbon (TOC) sample material was pre-treated with concentrated hydrochloric acid to remove the carbonate-bound carbon. Total inorganic carbon (TIC = TC – TOC) was used to calculate calcite equivalent percentages (Cc_{eq} = TIC x 8.33). Rock Eval pyrolysis was carried out using a Delsi Rock Eval RE II+ instrument. By means of this method the amount of free hydrocarbons (S_1; mg HC/g rock) released at a constant temperature as well as the amount of pyrolysate (S_2; mg HC/g rock) generated from non-volatile OM during subsequent gradual heating of the rock powder in a helium stream can be measured. These values are used to calculate the production index [$PI = S_1/(S_1 + S_2)$] and the hydrogen index [$HI = (S_2/TOC) \times 100$]. The temperature of maximum hydrocarbon generation (T_{max}) can be used as maturity indicator.

X-ray diffraction (XRD) was carried out using Philips X-pert equipment with the following measuring conditions: [i] bulk samples, 2 to 65° 2θ, random powder mount (29 samples); [ii] clay mineral analysis of clay-rich samples, oriented powder mounts (smear on

glass; Vortisch, 1982), 2 to 38° 2θ, untreated, ethylene glycol-treated, heat-treated, 350 °C/2 h, 550 °C/2 h (2 samples); [iii] bulk samples, 25 to 35° 2θ, random powder mount (21 samples). A rough quantification of the amount of diagenetic carbonate (unit: peak area) was established using the carbonate peaks between 30.0 and 31.2° 2θ in XRD diffractograms.

Inorganic carbon ($\delta^{13}C_{carb}$) and oxygen isotope ($\delta^{18}O_{carb}$) measurements were carried out for all samples. Measurements were performed by adding 100 % H_3PO_4 to samples heated at 70 °C in an online system (Gasbench II with carbonate option). Analysis was carried out with a ThermoFisher DELTA V isotope ratio mass spectrometer (Delta V IRMS). The results are reported relative to the Vienna Pee Dee Belemnite (VPDB) standard. Reproducibility was better than 0.2‰. All samples were analysed for their organic carbon isotope composition at the University of Leeds using an Elementar Pyrocube coupled to an Isoprime IRMS. Samples were weighed into tin capsules in sufficient quantity to produce peaks of between 1 and 10nA and combusted at 1150 °C in a helium stream (CP grade) enriched with pure oxygen (N5.0). The resulting gases were passed over tungstic oxide (also at 1150 °C) and excess oxygen and water removed using copper wires held at 850 °C and Sicapent respectively. All solid reagents were sourced from Elemental Microanalysis, UK, and all gases were sourced from BOC, UK. CO_2 was separated from other gases using a temperature controlled adsorption/desorption column. The $\delta^{13}C$ of the sample is derived from the integrated mass 44, 45 and 46 signals from the pulse of sample CO_2, compared to those in an independently introduced pulse of CO_2 reference gas (CP grade). Samples were run in batches of 12-16 bracketed by in-house C4 sucrose and urea standards. These were assigned values of -11.93 ± 0.24 and -46.83 ± 0.22‰ respectively based on 10 replicate analyses and calibration using LSVEC lithium carbonate (-46.479‰), IAEA-CH7 polyethylene (-31.83‰), IAEA-CH6 sucrose (-10.45‰) and IAEA-CO1 Carrara marble (2.48‰). Samples were batch corrected using a simple linear equation. Analysis of the C-isotopic composition of acyclic isoprenoids was performed using a Trace GC Ultra attached to a Delta V IRMS via a combustion interface (GC IsoLink) and an autodilution unit (ConFlow IV), all from Thermo-Fisher. For calibration, a CO_2 standard was injected at the beginning and end of each analysis. The GC coupled to the IRMS was equipped with the column described above and the temperature program was the same as for conventional GC-MS analysis. Isotopic compositions are reported in the δ notation relative to the VPDB standard.

Major- and trace-element concentrations were determined on whole-rock samples using a wavelength-dispersive Rigaku 3040 X-ray fluorescence (XRF) spectrometer at the University of Cincinnati. Raw intensities were calibrated using a set of 65 standards from the USGS, the National Bureau of Standards, and internal lab standards that were analyzed by XRAL Incorporated using XRF and INAA. Analytical precision based on replicate analyses was better than ±2 % for major and minor elements and ±5 % for trace elements, and detection limits were 1 to 2 ppm for most trace elements.

For organic geochemical analyses, samples were extracted using dichloromethane in a Dionex ASE 200 accelerated solvent extractor (temperature: 75 °C; pressure: 50 bar). After separation of asphaltenes, the hexane soluble fractions were separated into NSO compounds, saturated hydrocarbons and aromatic hydrocarbons using medium pressure liquid chromatography with a Köhnen-Willsch instrument (Radke et al., 1980). The saturated and aromatic hydrocarbon fractions were analysed with a GC equipped with a 30 m DB-1 fused-silica capillary column (i.d. 0.25 mm; 0.25 µm film thickness) coupled to a Finnigan MAT GCQ ion trap mass spectrometer. The oven temperature was programmed from 70 to 300 °C at 4 °C/min, followed by an isothermal period of 15 min. Helium was used as carrier gas. The spectrometer was operated in the electron ionization mode over a scan range from m/z 50 to 650. Relative percentages and absolute concentrations of different compound groups in the saturated and aromatic hydrocarbon fractions were calculated using peak areas in the total ion current chromatograms in relation to those of internal standards (deuterated n-tetracosane and 1,1´-binaphthyl, resp.), or by integration of peak areas in appropriate mass chromatograms using response factors to correct for the intensities of the fragment ion used for quantification of the total ion abundance. The concentrations were normalized to TOC.

7.4 Results

7.4.1 Lithology, microfacies, and mineralogy

At the base of the studied section, massive and thick-bedded grey limestones of the Scheibelberg Fm. (0.50-4.50 m; Fig. 7.2) are exposed. These rocks are hemipelagic to pelagic, bioturbated wackestones containing radiolarians, echinoderms, foraminifera, and ostracods. The top is formed by a breccia horizon containing carbonate lithoclasts.

The Sachrang Member (4.50-29.45 m; Fig. 7.2) comprises a 25-cm-thick basal mudstone (4.50-4.75 m), the Bächental bituminous marls (4.75-21.55 m and 22.55-29.45 m) and a debrite (21.55-22.55 m). The carbonate-free basal mudstone consists of black OM-enriched layers that are frequently interrupted by continental-derived OM-free lithoclasts. Quartz and smectite are the main minerals, whereas illite, chlorite, and plagioclase occur in minor amounts. The Bächental bituminous marls can be subdivided based on differing colour reflecting variations in OM richness. The lower part of the section (subsequently Unit 1: 4.75-11.00 m) and its upper part (Unit 3: 22.55-29.45 m) consist of greyish marls, whereas the OM-rich middle part is black-coloured (Unit 2: 11.00-21.55 m). Rocks of Units 1 and 3 are laminated to bioturbated wackestones containing mainly radiolarians and subordinated filaments (Bositra), ostracods, sponge spicules, and some foraminifera (Figs. 7.2A, E). Samples from Unit 2 show varying microfacies. In the lower part (Subunit 2a: 11.00-19.35 m) finely laminated mudstones with mainly radiolarians and additionally Bositra, sponge spicules, ostracods, and foraminifera occur (Fig. 7.2B). Small channels, onlap structures as well as low energetic, fine-grained turbidites with carbonate detritus are present. The occasional occurrence of radiolarian wackestones in the middle and upper parts of Subunit 2a indicate episodic blooms of radiolarians as well as a significant contribution of these organisms to the planktonic biomass of the sediment (Fig. 7.2C; cf. Sabatino et al., 2009). The most striking characteristic in Subunit 2b (19.35-21.55 m) is the presence of re-deposited carbonate detritus layers containing abundant pyrite (Fig. 7.2D). These layers become thicker and more frequent towards the top of Unit 2, which is formed by a 1-m-thick bioturbated wackestone with reworked carbonate intraclasts, interpreted as debris flow deposit. Bioturbation is generally weak, except for samples at the base of Unit 3.

Apart from OM, the Bächental bituminous marls consist mainly of quartz and carbonate minerals. The latter appear as [i] detrital calcite, [ii] secondary calcite, and [iii] typically Mn-rich diagenetic carbonate phases (subsequently referred to as diagenetic Mn-rich carbonates) featuring varying incorporation of Mn, Ca, Mg, and Fe. Pyrite is abundant in all samples. The rock matrix consists of clay and carbonate minerals; muscovite and feldspar occur in subordinate amounts. Diagenetic Mn-rich carbonates are the most abundant carbonate minerals in the majority of samples from Units 1 and 3 showing significant vertical variations in peak area from 2200 to 21300 (Fig. 7.3A; Table 7.9.1 in the Appendix). In contrast, diagenetic Mn-rich carbonates are generally rare in Unit 2 (260-7800 in peak area; Fig. 7.3A; Table 7.9.1 in the Appendix), which contains larger amounts of secondary calcite

instead. Diagenetic Mn-rich carbonates appear with broad, irregular peaks in the diffractograms, suggesting a low degree of crystallinity.

The Upper Allgäu Fm. (30.85-35.54 m) at the top of the section is formed by an alternating sequence of bioturbated light grey limestones and dark grey marls. Both contain radiolarians, Bositra, and some ostracods. The contact of the Sachrang Member and the overlying Upper Allgäu Fm. is not exposed (29.45-30.85 m).

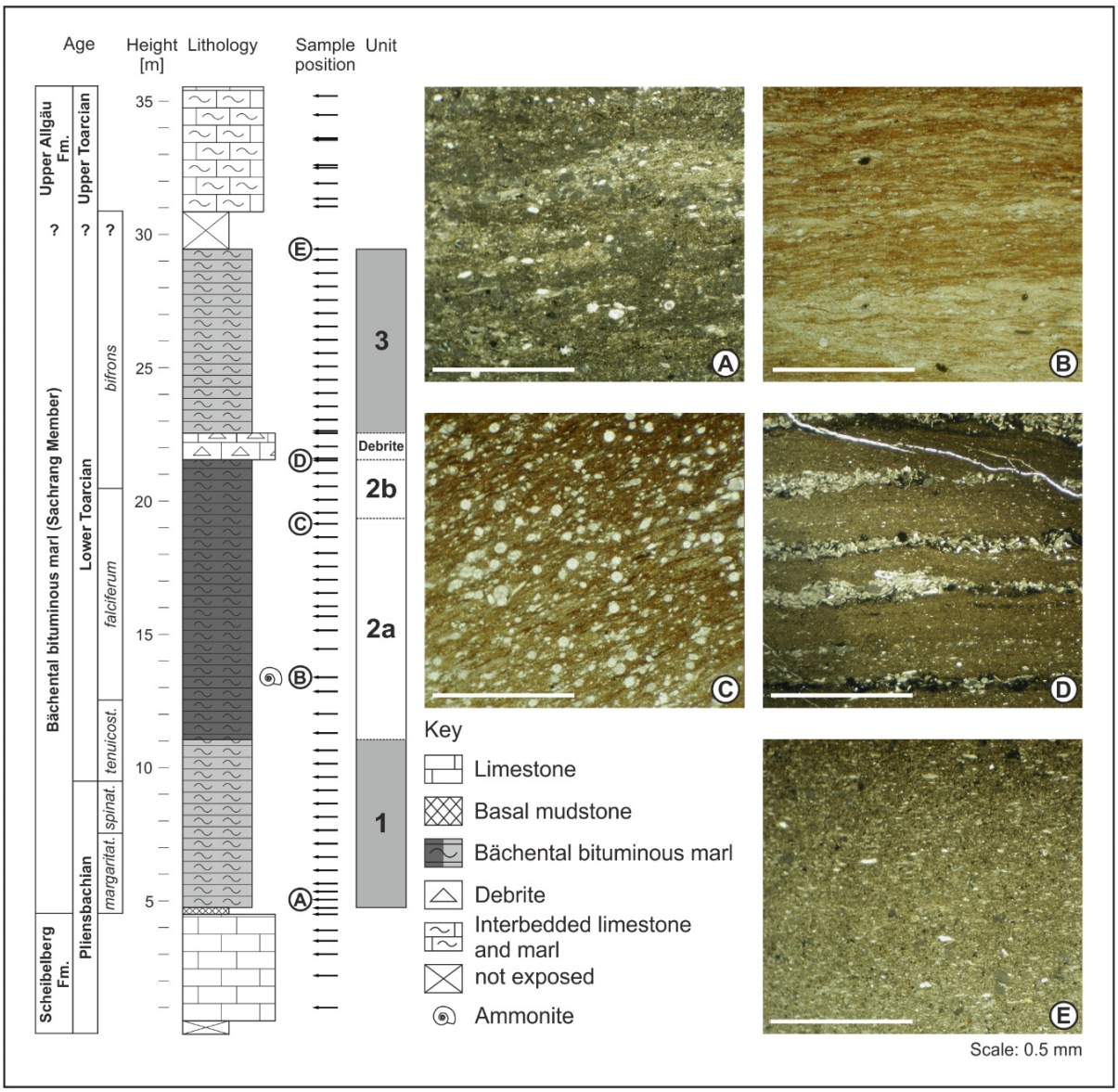

Fig. 7.2: Left: Lithological profile of the investigated Bächental section containing rocks of the Scheibelberg Fm., the Sachrang Member (Middle Allgäu Fm.) and the Upper Allgäu Fm. Stratigraphy follows the new data gained within this study premised on the occurrence of *Cleviceras exaratum* and the comparison of C_{27}/C_{29} steranes ratios. Positions of the 68 investigated samples and the differentiated units are indicated (see text for explanations).

Right: Photographs of thin sections: (A) Greyish wackestone with mainly radiolarians and subordinated *Bositra*, sponge spicules, ostracods and some foraminifera; secondary carbonates are abundant (Unit 1; 5.05 m). (B) Finely laminated mudstone containing some low-energy carbonatic turbidites (Subunit 2a; 13.39 m). (C) Radiolarian wackestone (Subunit 2a; 19.15 m). (D) Mudstone with frequent carbonate turbidites directly below the debrite (Subunit 2b; 21.55 m). (E) Wackestone (Unit 3; 29.45 m) with similar features as (A). Positions of the samples are displayed next to the lithological profile.

7.4.2 Bulk geochemical parameters

The vertical variation of bulk geochemical parameters is shown in Figs. 7.3B-E and 7.4A. The full dataset is presented in the Appendix (Table 7.9.1). T_{max} (416-427 °C) and PI values (<0.1) indicate that the bituminous marls are thermally immature. Higher T_{max} values (~ 444 °C) are restricted to the basal mudstone. Limestones and marls from the Scheibelberg Fm. and the Upper Allgäu Fm. show very low TOC contents (<0.2 and 0.4%, resp.).

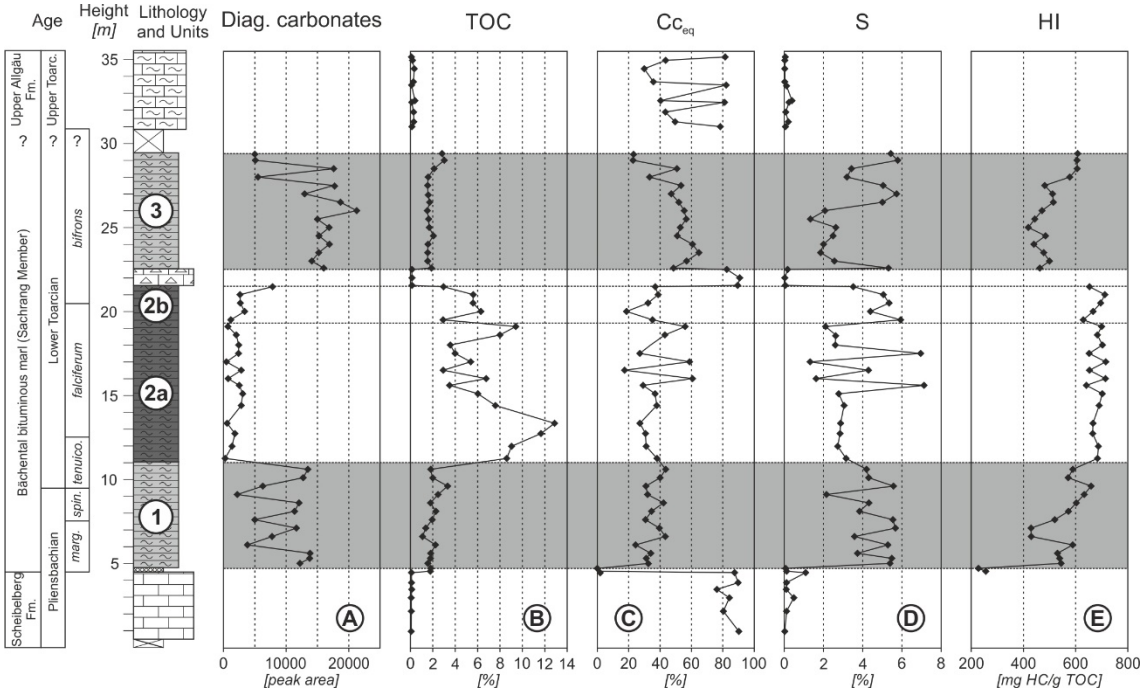

Fig. 7.3: Vertical variation of (A) protodolomite (peak area), (B) total organic carbon (TOC, %), (C) calcite equivalent (Cceq, %), (D) sulfur content (S, %), (E) hydrogen index (HI, mg HC/g TOC) for samples of the study section. The distinguished units within the Bächental bituminous marl are highlighted. See text for explanations.

The basal mudstone of the Sachrang Member contains very low S contents (ca. 0.1%), but significant amounts of OM (TOC: 1.8%). Low HI values (74 and 37 mg HC/g TOC) indicate a high proportion of inert OM. Unit 1 of the Bächental bituminous marls is characterized by moderate TOC (1.1-3.3%) and high S contents (2.2-5.7%). Cc_{eq} range between 24.4 and 43.6%. HI varies between 306 and 612 mg HC/g TOC. Fe contents are rather uniform (3.3-5.2%), but reach 9.2% in a sample at 6.65 m. Samples from Subunit 2a show a wide variety of TOC contents (2.9-12.9%). Two positive TOC excursions are visible from 11.00 to 15.65 m and from 18.05 to 19.55 m. Despite strong TOC variations, HI values are quite uniform (588-687 mg HC/g TOC). The S curve does not mirror the TOC trend but stays constant at relatively low levels (2.1-3.2%). Between 15.15 and 18.05 m S contents show strong fluctuations (1.3-7.1%) and an inverse correlation with both TOC and Cc_{eq} (17.4-58.8%). Marls in Subunit 2b (18.6-38.8% Cc_{eq}) exhibit TOC contents from 2.9 to 6.3% and high HI values (572-683 mg HC/g TOC) and S contents (3.5-5.9%). Fe concentrations in Unit 2 vary strongly from 0.1 to 6.1%. The carbonate debrite, poor in OM and S, marks a significant change in bulk source-rock parameters. TOC contents in Unit 3 are rather uniform (~1.5-2.0%) and are slightly higher (up to 3.0%) only near its top. Cc_{eq} (22.8-64.8%) and S contents (1.3-5.8%) show significant vertical variations. In general, Cc_{eq} is decreasing towards the top, whereas S contents are higher in the upper half of Unit 3. HI values in the lower part of Unit 3 are significantly lower (300-400 mg HC/g TOC) than in the underlying Unit 2 (>600 mg HC/g TOC), but show an upward increase (up to 550 mg HC/g TOC). Fe contents are rather uniform (3.2-6.1%). A single sample with only 1.4% Fe occurs at 27.55 m.

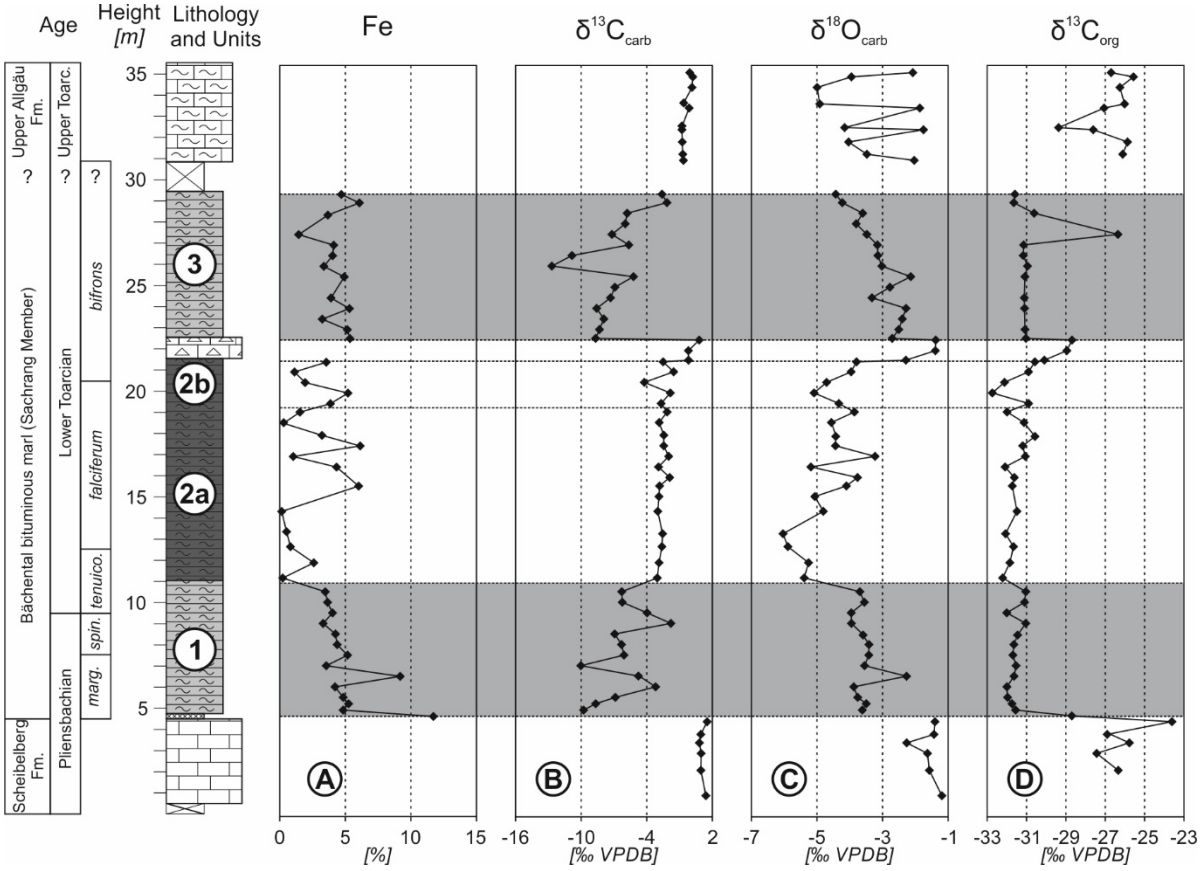

Fig. 7.4: Vertical variation of (A) iron concentration (Fe, %), (B) inorganic carbon isotope composition ($\delta^{13}C_{carb}$, ‰ VPDB), (C) oxygen isotope composition of carbonate ($\delta^{18}O_{carb}$, ‰ VPDB), (D) organic carbon isotope composition ($\delta^{13}C_{org}$, ‰ VPDB) for samples of the study section. The distinguished units within the Bächental bituminous marl are highlighted. See text for explanations.

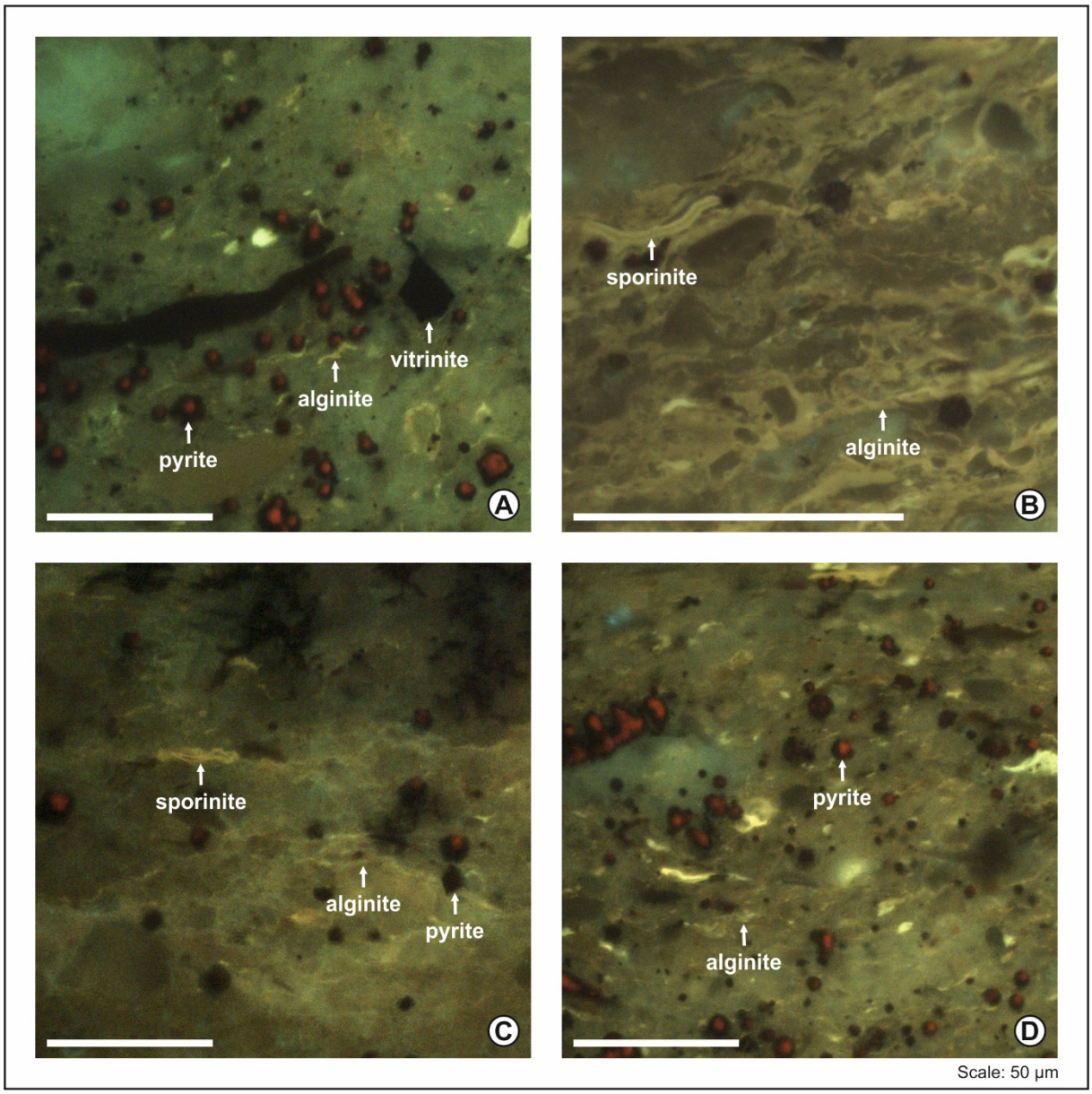

Fig. 7.5: Microphotographs of Bächental bituminous marls (A) Sample BT 15 (Unit 1, 7.65 m), (B) sample BT 25 (Subunit 2a, 13.39 m), (C) BT 44 (Unit 3, 22.60 m), and (D) BT 58 (Unit 3, 29.45 m). All photos under UV light.

7.4.3 Organic petrology

The basal mudstone contains mainly amorphous OM. High reflectivity suggests the presence of charred land-plant material. In addition, inertinite occurs together with traces of liptinite. The OM of the Bächental bituminous marls is dominated by lamalginite (Figs. 7.5A-D). Telalginite, sporinite and fish remains are present with slightly varying, but always low amounts (Figs. 7.5A-D). The sporinite content is slightly increasing upsection. Terrestrial

inertinite and vitrinite occur rarely with tiny irregularly shaped particles. Consequently vitrinite reflectance could not be measured. Pyrite is frequent in Units 1 and 3, whereas most rocks of Unit 2 contain lower pyrite percentages. Pyrite appears disseminated with crystals of framboidal as well as subhedral to euhedral shape; pyritization of organism fragments (especially radiolarians) is also common. In Subunit 2b the bulk of pyrite present is bound to carbonate turbidite layers.

7.4.4 Stable isotope composition of carbonate minerals and organic matter

Bulk carbonate and organic carbon isotope values are shown in Figs. 7.4B-D. The full dataset is presented in the Appendix (Table 7.9.1). Limestones and marls from the Scheibelberg Fm. and the Upper Allgäu Fm. show rather constant $\delta^{13}C_{carb}$ isotope values (0.8 to 1.5‰ VPDB and -0.8 to 0.2‰ VPDB). The same is true for $\delta^{18}O_{carb}$ isotope values for limestone samples from the Scheibelberg Fm. (-2.3 to -1.2‰ VPDB) and the Upper Allgäu Fm. (-2.1 to -1.8‰ VPDB). In contrast, marls from the Upper Allgäu Fm. show significant lower $\delta^{18}O_{carb}$ isotope values (-5.0 to -3.5‰ VPDB). Isotope data from the Sachrang Member are more inhomogeneous. $\delta^{13}C_{carb}$ isotope values vary strongly in Unit 1 (-10.0 to -1.8‰ VPDB). In contrast, $\delta^{13}C_{carb}$ isotopes are rather constant in Unit 2 (-4.2 to -1.5‰ VPDB). While bulk carbonate isotope values of the debrite ($\delta^{13}C_{carb}$: -0.2 to 0.8‰ VPDB; $\delta^{18}O_{carb}$: -2.3 to -1.4‰ VPDB) are in the range of the Scheibelberg Fm., $\delta^{13}C_{carb}$ isotopes from Unit 3 demonstrate a wide range (-12.7 to -2.2‰ VPDB). $\delta^{18}O_{carb}$ isotope values of the bituminous marls vary from -6.0 to -2.1‰ VPDB.

Organic carbon isotope values of the OM-poor Scheibelberg Fm. and Upper Allgäu Fm. are in a similar range (-28.7 to -23.6‰ VPDB and -29.4 to -25.6‰ VPDB). $\delta^{13}C_{org}$ isotope values oscillate in a narrow range in the bituminous marls (-32.7 to -30.6‰ VPDB) and the debrite (-30.1 to -28.7‰ VPDB), showing the strongest fluctuations in Unit 2. Carbon isotope compositions of pristane (Pr) and phytane (Ph) are in a similar range (Pr: -34.6 to -33.0‰ VPDB; Ph: -34.4 to -33.1‰ VPDB) for all samples.

7.4.5 Molecular composition of hydrocarbons

The samples show relative uniform n-alkane distributions characterized by high relative proportions of short- and mid-chain n-alkanes (n-C_{15-19}/Σn-alkanes: 0.23-0.56; n-C_{21-25}/Σn-alkanes: 0.26-0.43, resp.; Figs. 7.6, 7.7A). Short-chain n-alkanes dominate over mid-

chain n-alkanes in all but five samples. Long-chain n-alkanes (n-C_{27-31}/Σn-alkanes) are present with proportions from 0.05 to 0.32 (Figs. 7.6, 7.7A). The carbon preference index (CPI; after Bray and Evans, 1961) varies between 0.85 and 3.20 with lowest values in Unit 2. The vertical variation of the acyclic isoprenoid ratio (Pr/Ph) is shown in Fig. 7.7B. The Pr/Ph ratio is moderately high in Units 1 and 3 (0.88-1.76) and generally lower in Subunits 2a (0.70-1.01) and 2b (0.89-1.30).

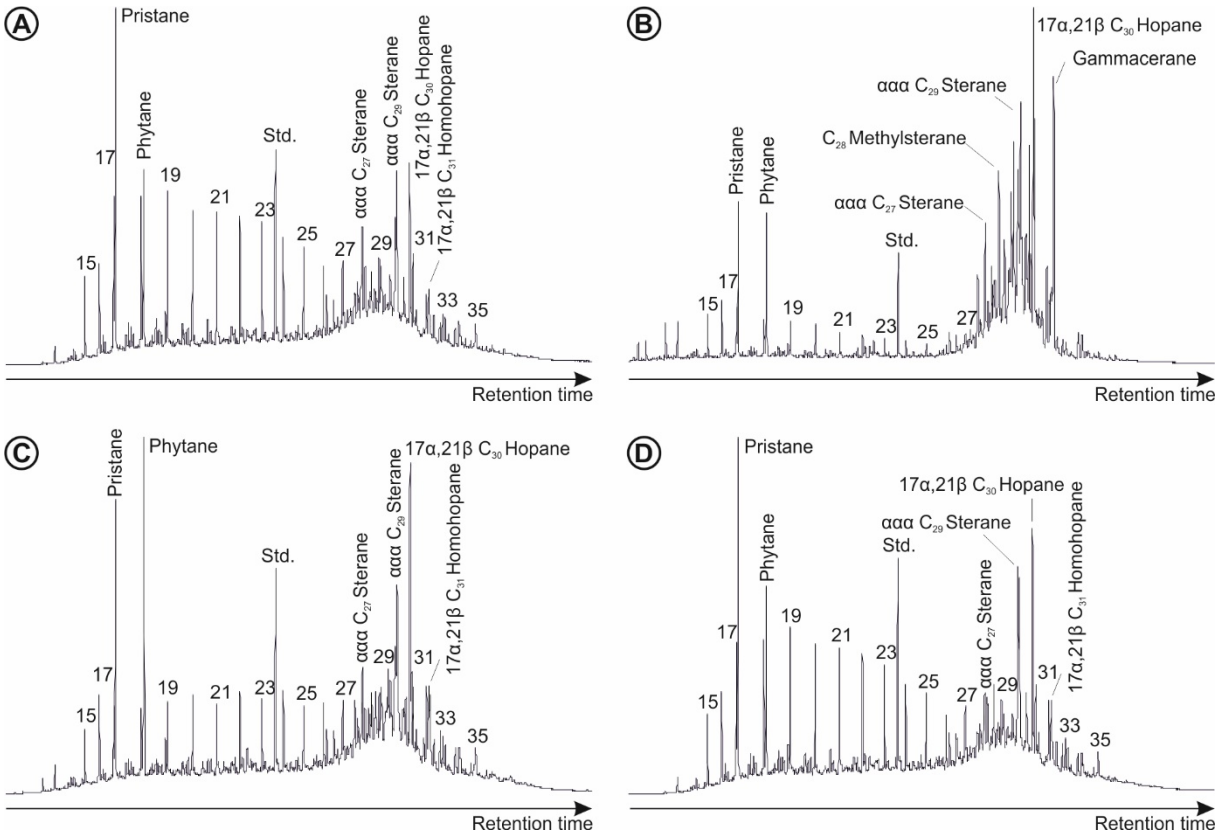

Fig. 7.6: Total ion current gas chromatograms of saturated hydrocarbon fractions: (A) sample BT 15 (Unit 1; 7.65 m), (B) sample BT 25 (Subunit 2a; 13.39 m), (C) sample BT 30 (Subunit 2a; 16.55 m), (D) sample BT 50 (Unit 3; 25.55 m). *n*-alkanes are labelled according to carbon number [Std., standard (deuterated n-tetracosane)].

Among steroids, the ααα-steranes are present in the range of C_{27} to C_{29} and predominate over βαα-isomers (Fig. 7.8). The ratio of C_{27} vs. C_{29} steranes (Fig. 7.7C) increases upwards from 0.70 to 1.24 in the lower part of Unit 1 and decreases in the upper part. The ratio is very low (~0.60) in the lowermost 3 m of Subunit 2a and increases upwards to reach a maximum of 1.10 in Subunit 2b. In Unit 3 the ratio varies from 0.59 to 1.03. The ratio of C_{27}/C_{29} αααR steranes displays a similar vertical trend (Fig. 7.7C). Diasteranes occur

with low concentrations and are represented by their C_{27} homologues in all units. C_{29} diasteranes are restricted to Unit 1. The ratio of 4-methylsteranes vs. ΣC_{29} steranes is relatively high in the lower part of the section and decreases sharply from 3.10 to 1.04 at the boundary between Subunits 2a and 2b (Fig. 7.7D). The ratio of 20S/(20S + 20R) isomers calculated from ααα C_{29} steranes is generally between 0.11 and 0.18 in Units 1, 2b and 3 (Fig. 7.7E). Two outliers occur at 6.15 m (0.27) and 22.60 m (0.32). The ratio in Subunit 2a is higher (0.25-0.33). The vertical trend of mono- vs. triaromatic steroids is shown in Fig. 7.7D. It displays a reversed image to the sterane isomerization ratio, with low values for Unit 2 (1.25-2.17) and high ratios for the rest of the succession (up to 3.81).

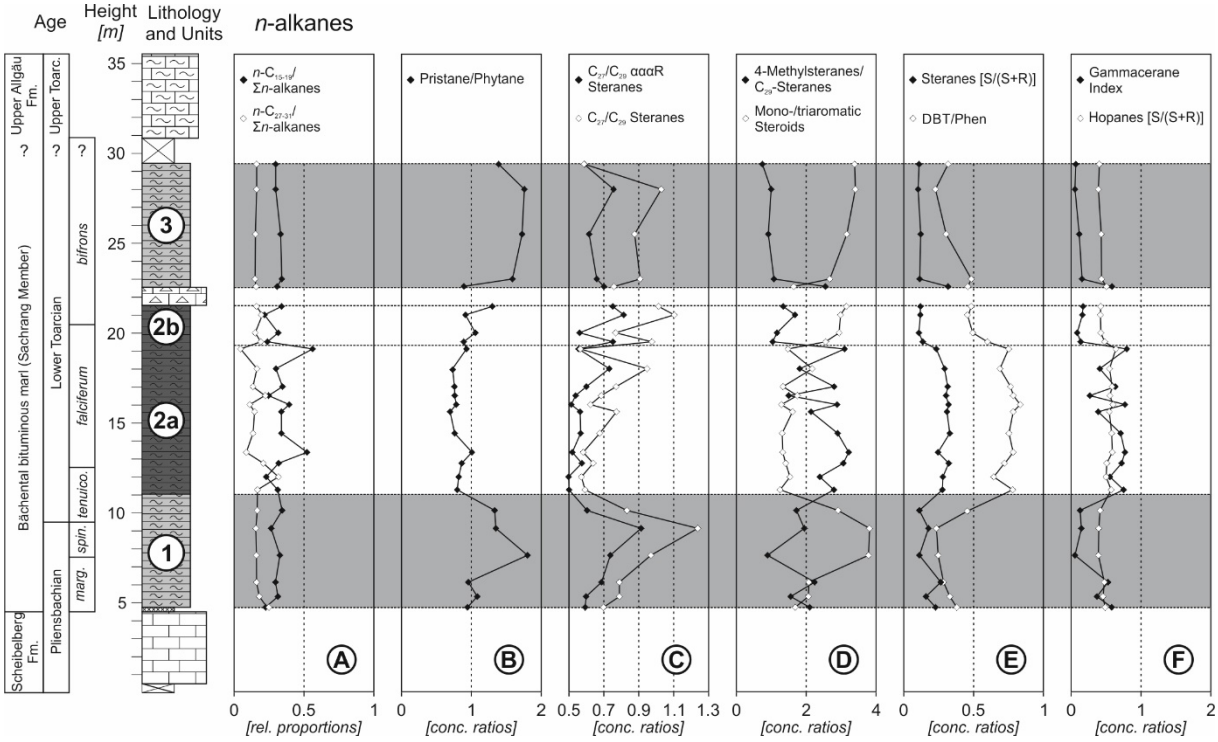

Fig. 7.7: Vertical variation of (A) *n*-alkane proportions of low (*n*-C_{15-19}) and high (*n*-C_{27-31}) molecular weight relative to the concentration of total *n*-alkanes (Σ*n*-alkanes), (B) concentration ratio of pristane vs. phytane, (C) concentration ratios of C_{27}/C_{29} ααα R steranes and C_{27}/C_{29} steranes, (D) concentration ratios of 4-methylsteranes/ΣC_{29} steranes and mono- vs. triaromatic steroids, (E) concentration ratios of [20S/(20S + 20R)] C_{29} steranes and dibenzothiophene vs. phenantrene (DBT/Phen), (F) concentration ratios of gammacerane index and [22S/(22S + 22R)] isomers of C_{31} hopane for bituminous marl samples. The distinguished units within the Bächental bituminous marl are highlighted. See text for explanations.

The hopane distribution is characterized by the predominance of αβ homologues from C_{27} to C_{35}; additionally βα hopanes and bisnorhopane could be detected (Fig. 7.9). Bisnorhopane is enriched in Subunit 2a (25.7-124.7 µg/g TOC) compared to the remaining units (2.5-56.3 µg/g TOC). The ratio of 22S/(22S + 22R) isomers of the αβ C_{31} hopane varies from 0.39 to 0.64 (Fig 7.7F). The vertical trend with high values in Subunit 2a (0.50-0.64; Fig. 7.7F) is identical to the sterane isomerization. Gammacerane could be detected in all samples. The gammacerane index [GI = gammacerane/(gammacerane + αβ C_{30} hopane)] reaches maximum values (0.80) in Subunit 2a and is lower in the other units (0.05-0.59; Fig. 7.7F).

Aryl isoprenoids occur in all samples, but their concentrations vary significantly (3.2-112.1 µg/g TOC). The median values of different units suggest a general upward increase from ca. 15 µg/g TOC (Units 1, 2a) to values exceeding 50 µg/g TOC (Units 2b, 3). Dibenzothiophene (DBT) and phenantrenes (Phen) are present with variable amounts in all samples. The DBT/Phen ratio is low in Units 1 and 3 (0.23-0.48) and higher in Subunits 2a (0.64-0.83) and 2b (0.46-0.60; Fig. 7.7E). The full dataset of organic geochemical analyses is presented in the Appendix (Tables 7.9.2, 7.9.3).

7.5 Discussion

7.5.1 Organic matter sources and preservation

7.5.1.1 Thermal Maturity

The degree of thermal maturity can be estimated using vitrinite reflectance (VR), Rock Eval parameters (T_{max}, PI), and biomarker ratios. However, some biomarker ratios can be inaccurate as maturity indices when applied to the study units. The measurement of VR was impossible because of the low amount and small size of vitrinite particles in the study samples. Low thermal maturity is indicated by low T_{max} and PI values. The equation VR = 0.018 x T_{max} – 7.16, proposed for type I and II kerogen (Peters et al., 2005) suggests a maturity corresponding to a VR of ca. 0.45% R_o. The occurrence of charred organic material in the basal mudstone suggest that its elevated T_{max} values, corresponding to a VR of ca. 0.80% R_o (equation after Peters et al., 2005), are due to the change in organic matter type.

Isomerization ratios of hopanes and steranes in samples from Units 1, 2b, and 3 as well as aromatization of steroids are consistent with a maturity in the range of 0.40 to 0.50% R_o (cf. Mackenzie and Maxwell, 1981; Mackenzie et al., 1982). However, biomarker ratios suggest a slightly higher thermal maturity (~0.60% R_o) for Subunit 2a, which is located in the middle part of an undisturbed and continuous succession. A thermal overprint as the reason for the apparent higher maturity can be excluded. Salinity and/or lithotype variations are regarded as possible triggers of sterane ratio variations (ten Haven et al., 1986; Peters et al., 1990). Bitumen from immature source rocks deposited under hypersaline conditions tends to show more mature hopane patterns owing to unusual diagenetic pathways (ten Haven et al., 1987). For this reason, isomerization ratios are not reliable as a maturity parameter in Subunit 2a (see Section 7.5.2.2), and the Bächental bituminous marls are inferred to have a low maturity corresponding to a VR of 0.40 to 0.50% R_o. These results confirm the questionability of applying isomerization ratios as maturity proxies to sections deposited under hypersaline conditions or strongly variable salinities.

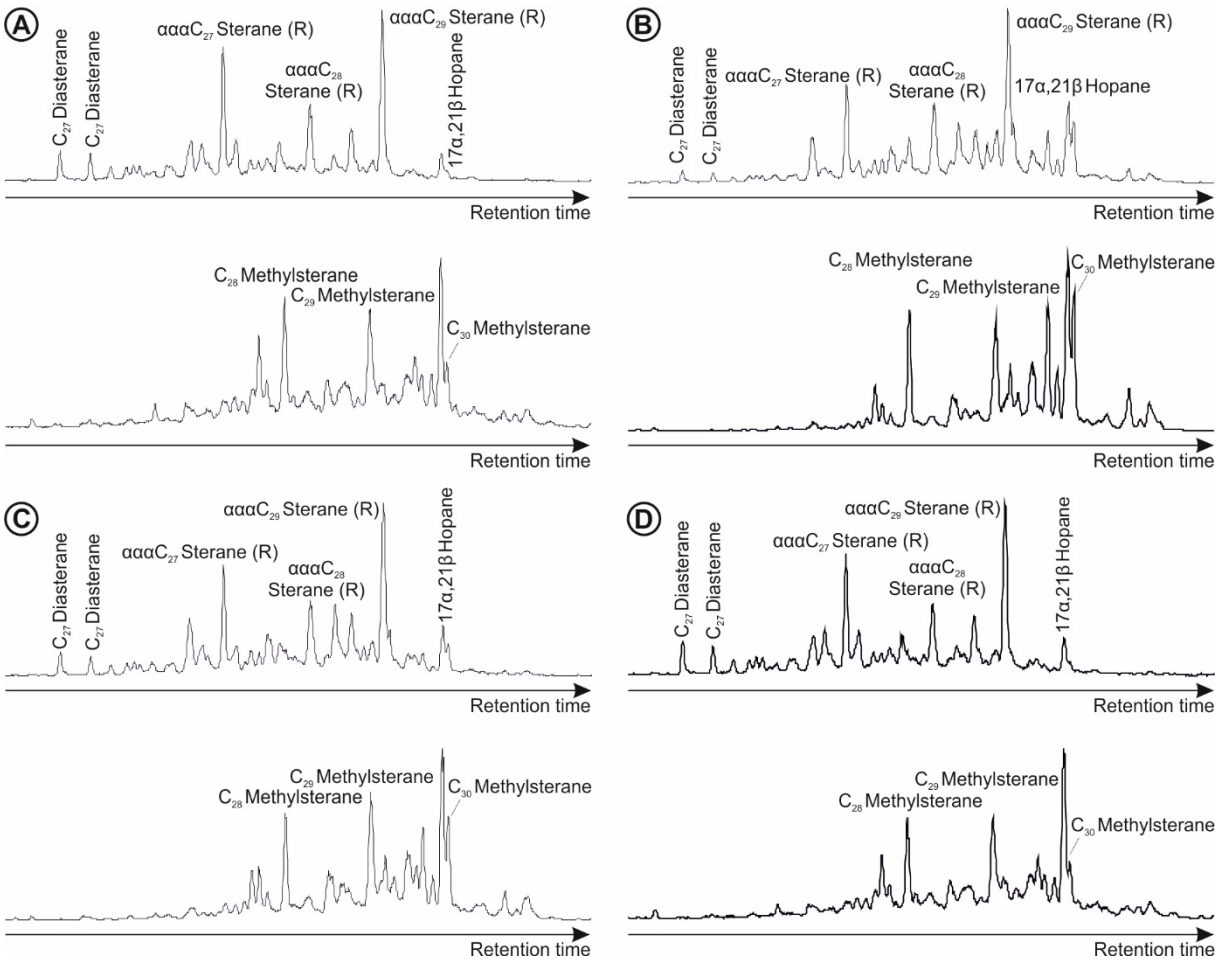

Fig. 7.8: Partial mass chromatograms of steranes (m/z 217) and 4-methylsteranes (m/z 231) in saturated hydrocarbon fractions of (A) sample BT 15 (Unit 1; 7.65 m), (B) sample BT 25 (Subunit 2a; 13.39 m), (C) sample BT 30 (Subunit 2a; 16.55 m), (D) sample BT 50 (Unit 3; 25.55 m).

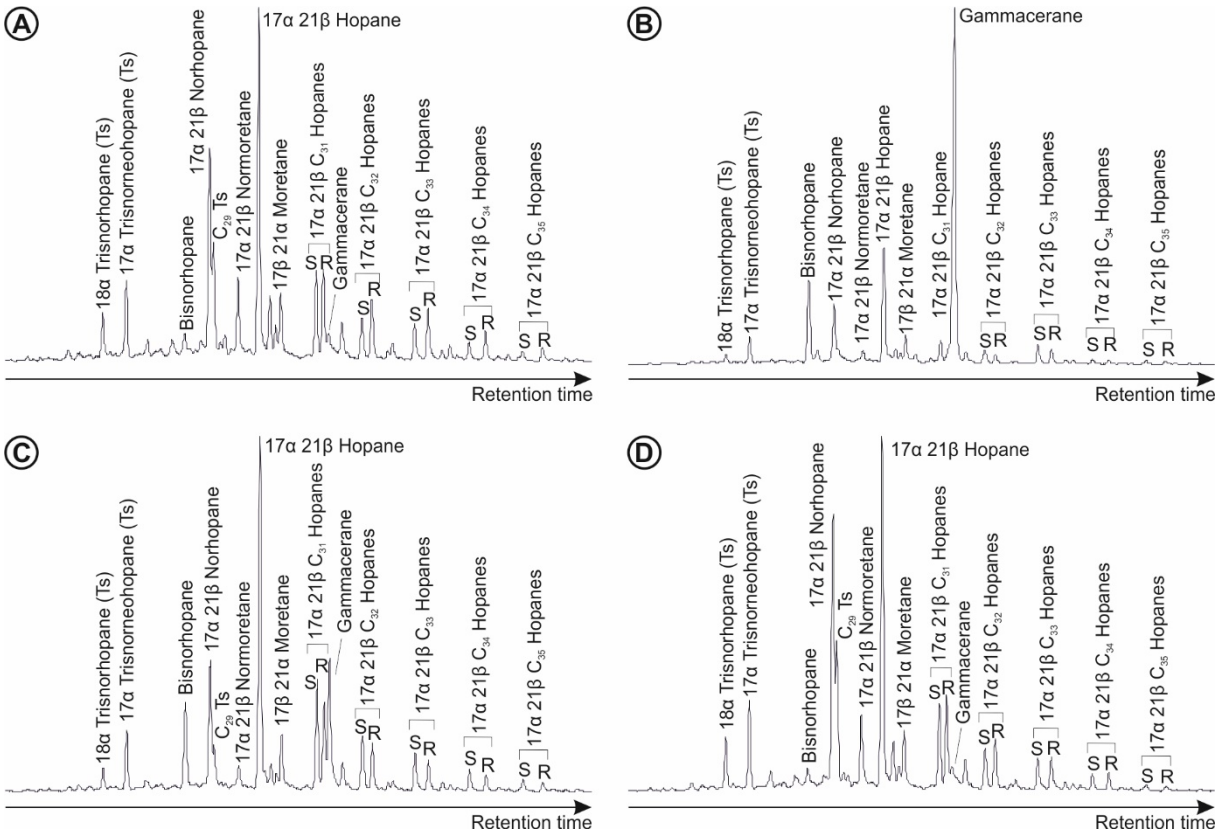

Fig. 7.9: Partial mass chromatograms of hopanes (m/z 191) in saturated hydrocarbon fractions of (A) sample BT 15 (Unit 1; 7.65 m), (B) sample BT 25 (Subunit 2a; 13.39 m), (C) sample BT 30 (Subunit 2a; 16.55 m), (D) sample BT 50 (Unit 3; 25.55 m). Variations of gammacerane and hopane isomerization are remarkable.

7.5.1.2 Organic matter sources

The relative proportions of marine and terrestrial OM determine the kerogen type and provide information about OM source, productivity, and preservation, as well as basin setting and water depth. OM of the basal mudstone mainly consists of charred material indicating terrestrial sources. The occurrence of charred OM is commonly connected to wildfire activity (e.g., Brown et al., 2012). In contrast, the dominant maceral group in Bächental bituminous marls is alginite, which suggests a mainly marine algal source of OM (Taylor et al., 1998).

The most abundant maceral is lamalginite, which may derive from thin-walled planktonic and benthic organisms, including green algae, cyanobacteria, and bacterial mats (Oschmann, 2000). Telalginite originates from algae such as *Botryococcus*, *Tasmanites*, and *Gloeocapsomorpha* that occur as thick-walled unicellular organisms with some internal structure (Hutton, 1987). The low frequency of vitrinite and inertinite suggests terrestrial inputs of OM to be of subordinate importance. The occurrence of radiolarian wackestones in the middle and upper part of Subunit 2a indicates episodic blooms of radiolarians and, hence, significant input of OM from planktonic heterotrophs as well as autotrophs.

HI values vary considerably within the study section, suggesting a mixture of kerogen types II and III. However, relatively invariant maceral compositions imply that OM is derived dominantly from marine algae and bacterioplankton, an inference also supported by the predominance of low molecular weight *n*-alkanes (<*n*-C_{20}; Cranwell, 1977). Variations in HI values therefore reflect an early diagenetic overprint rather than multiple OM sources (see Section 7.5.1.3). Unit 2 has been less affected by this diagenetic overprint than Units 1 and 3, and its HI of 600 to 700 mg HC/g TOC, which is indicative of type II kerogen, is taken as representative of primary OM in the entire section. The primary (i.e., pre-diagenetic) HI of diagenetically altered OM can be estimated from a plot of TOC vs. S_2 (Langford and Blanc-Valleron, 1990), which yields values of ~770 mg HC/g TOC for Units 1 and 3 of the study section (correlation coefficient $r^2 = 0.99$). This is consistent with little variation in kerogen type through the entire profile and a dominantly marine source of OM. The varying HI values are therefore not reflecting the primary source of OM but are rather caused by the mineral matrix effect (Langford and Blanc-Valleron, 1990). However, an influence of early diagenetic OM oxidation on reduced HI values is also likely (cf. Röhl et al., 2001).

Biomarkers provide additional insights regarding OM sources. Algae are the predominant producers of C_{27} sterols; C_{29} sterols are more typically associated with land plants (Volkman and Maxwell, 1986). However, results from biomarker studies add to the growing list of microalgae that contain high amounts of 24-ethylcholesterol (Volkman et al., 1999; Peters et al., 2005). 4-methylsteroids with a C_{30} dinosterol structure are considered as biomarkers of dinoflagellates (Robinson et al., 1984), while others are related to marine and lacustrine precursors (Mackenzie et al., 1982; Volkman et al., 1990; Peters et al., 2005; Auras and Püttmann, 2004). Thus, the relative abundance of non-aromatic steroids in the Bächental bituminous marls indicate the contribution of biomass from marine phytoplankton and a

minor input of terrestrial OM. The 4-methylsteranes most probably originate from dinoflagellates (see also Köster et al., 1995). The most probable biological precursors of the hopane derivatives found in the samples are bacteriohopanepolyols (Ourrison et al., 1979; Rohmer et al., 1992). These compounds have been identified in bacteria as well as in some cryptogames (e.g., mosses and ferns) and in sulphate-reducing bacteria (Blumenberg et al., 2006). The predominance of homohopanes up to C_{35} and the occurrence of benzohopanes from C_{22} to C_{35} in the aromatic hydrocarbon fraction suggest that bacteriohopaneols were a significant constituent of the biomass. In summary, we infer that algal and bacterial biomass of marine origin are the predominant OM sources for Bächental bituminous marls whereas OM input from terrestrial sources is of minor importance. In contrast, the bulk of OM contained in the basal mudstone, including charred material, was derived from terrestrial sources.

7.5.1.3 Influence on organic matter by diagenetic processes

Varying environmental conditions in the Bächental basin also affected diagenetic processes. Different degrees of bacterial degradation of OM and concurrent formation of diagenetic Mn-rich carbonates had a significant impact on bulk source-rock parameters. Early diagenetic degradation mainly controlled OM preservation in Units 1 and 3. This is supported by low TOC contents and HI values, which show a correlation with the amount of diagenetic Mn-rich carbonates. In Units 1 and 3, labile algal OM primarily present in the samples was degraded to a rather constant residual TOC level of ca. 2% during early diagenesis. The generated ^{12}C-enriched carbon was fixed in diagenetic Mn-rich carbonates.

The carbonate C-isotope profile of the study section has been strongly influenced by these diagenetic processes, resulting in a mixed signal derived from primary and secondary carbonate phases. The vertical trends of $\delta^{13}C_{carb}$ isotope values and diagenetic Mn-rich carbonate contents show a significant negative correlation (compare Figs. 7.3A and 7.4B). Isotope ratios get more negative with increasing amounts of diagenetic Mn-rich carbonates, especially where high contents are observed in Units 1 and 3. The carbonate C-isotope compositions of the diagenetic Mn-rich carbonates in those units were determined by the relative proportions of isotopically light carbon from early diagenetic degradation of OM on the one hand and isotopically heavy seawater-sourced dissolved inorganic carbon in sediment pore waters on the other. A minor input of organic-derived carbon into calcite is also possible

but not important compared to the strength of the effect on diagenetic Mn-rich carbonates. Very low $\delta^{13}C_{carb}$ values (-11‰ VPDB) in limestone beds of the Posidonia Shale are also attributed to early diagenetic carbonate precipitation and incorporation of ^{12}C-rich carbon derived from organic matter degradation via sulphate reduction (Röhl et al., 2001).

Unit 2 exhibits anomalously heavy $\delta^{13}C_{carb}$ values (-2 to -3‰ VPDB) compared to Units 1 and 3, but values that are nonetheless lighter than those of other lower Toarcian sections (~0‰ VPDB; e.g. Röhl et al., 2001; Hesselbo et al., 2007; Sabatino et al., 2009). These relatively heavy $\delta^{13}C_{carb}$ values are interpreted to be least altered (i.e., relative to primary marine carbonate phases). In Unit 2, the bulk of carbonate present is secondary calcite whereas the quantity of diagenetic Mn-rich carbonates is typically low (Fig. 7.3A). The lack of the latter also implies smaller amounts of organically sourced carbon that were fixed in secondary carbonates of Unit 2. The precipitation of diagenetic Mn-rich carbonates was inhibited because anoxic bottom waters existed during deposition of Unit 2 (cf. Calvert and Pedersen, 1996; see Section 7.5.2.1). Overall, it is clear that the measured $\delta^{13}C_{carb}$ values reflect the nature and extent of diagenetic processes rather than the primary isotopic signal.

The carbonate O-isotope composition of the study section is also dominated by diagenetic effects. The heaviest values (~-1.0‰ VPDB) are found in the limestones underlying the Bächental bituminous marls (Fig. 7.4C). These values are consistent with a primary normal-marine isotopic composition (~-1.0‰ VPDB, ice-free; e.g., Röhl et al., 2001). All $\delta^{18}O_{carb}$ isotope ratios for the bituminous marls record shifts toward lighter isotopic compositions that are a function of precipitation of diagenetic carbonate at burial temperatures exceeding contemporaneous sea-surface temperatures (cf. Algeo et al., 1992). The more ^{18}O-depleted values are likely to represent precipitation of secondary phases at later diagenetic stages and, hence, higher burial temperatures (cf. Algeo et al., 1992). For this reason, diagenetic carbonate in Units 1 and 3 appears to have formed earlier on average than that in Unit 2. This inference indicates an earlier formation of diagenetic Mn-rich carbonates in Units 1 and 3 compared to the secondary calcite of Unit 2. $\delta^{18}O_{carb}$ isotope ratios for the epicontinental Posidonia Shale of Dotternhausen plot within a narrower range (~-5.0 to -7.0‰ VPDB) compared to those of the Alpine Bächental bituminous marls (~-2.0 to -6.0‰ VPDB). However, whereas the former represents a primary depositional signal derived from carbonate of well-preserved coccoliths and schizosphaerelles (Röhl et al., 2001), the $\delta^{18}O_{carb}$ signal of the latter was controlled by diagenetic processes.

7.5.2 Depositional environmental conditions

7.5.2.1 Redox conditions and iron availability

The Latest Triassic and the Early Jurassic were characterized by global perturbations caused by the activity of LIPs (CAMP, Karoo-Ferrar; Marzoli et al., 1999; Svensen et al., 2007, 2013; Jourdan et al., 2008; Caruthers et al., 2013; Sell et al., 2014) and the rifting of the Alpine Tethys in the Penninic realm with oceanic break-up in the Pliensbachian/Toarcian (Ratschbacher et al., 2004; Mohn et al., 2010; Decarlis et al., 2013) that induced major environmental changes and climate warming ("greenhouse Earth" conditions; Palfy and Smith, 2000; Weissert, 2000; Jenkyns, 2003) resulting in oceanic conditions generally conducive to development of anoxia. The prevailing redox conditions in a depositional basin commonly vary with time and are sensitive to changes in environmental conditions as reflected in the stratigraphic trends of various proxies (e.g., Pr/Ph ratio, arylisoprenoids, bioturbation, and Fe-TOC-S) in the sedimentological record.

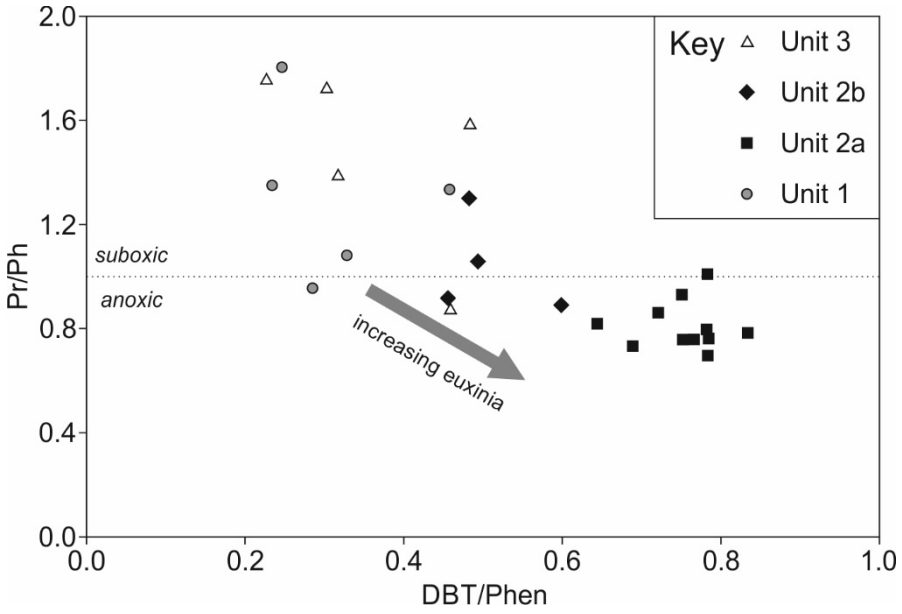

Fig. 7.10: The plot of pristane/phytane vs. dibenzothiophene/phenantrene (Pr/Ph vs. DBT/Phen) suggests the predominance of anoxic conditions during deposition of Subunit 2a and a shift to less reducing conditions in Subunit 2b. In contrast, suboxic conditions prevailed during deposition of Units 1 and 3. Modified after Didyk et al. (1978) and Hughes et al. (1995).

In the study section, extensive bioturbation and relatively low TOC contents are indicative of normal-marine conditions without major perturbations of the carbon cycle during deposition of the Scheibelberg Fm. and the Upper Allgäu Fm. In contrast, redox conditions varied significantly during deposition of the Bächental bituminous marls, as shown by the multiple redox proxies discussed below.

The Pr/Ph ratio is commonly used as a redox indicator during early diagenesis. According to Didyk et al. (1978), Pr/Ph ratios <1.0 indicate anaerobic conditions whereas values >1.0 speak for suboxic to oxic environments. However, Pr/Ph ratios are also known to be affected by maturation (Tissot and Welte, 1984) and different precursors for isoprenoids (Goosens et al., 1984; Volkman and Maxwell, 1986; ten Haven et al., 1987). Both influences can be ruled out in the case of the Bächental section, because of its limited thickness and the similar isotopic compositions of Pr and Ph, which indicates a common precursor. Hence, Pr/Ph ratios suggest generally suboxic conditions for Units 1 and 3; however, short-term anoxia cannot be completely excluded. In contrast, an environment with strictly anoxic bottom waters is suggested for Subunit 2a. Subunit 2b features a shift to less reducing (i.e. suboxic to anoxic) conditions. The postulated paleoredox trend is also visible in a plot of Pr/Ph vs. DBT/Phen (Fig. 7.10). The vertical redox trend suggested by Pr/Ph ratios is confirmed by bioturbation patterns. Small-scale bioturbation is visible in sections from Units 1 and 3, but totally missing in Unit 2. In addition, the occurrence of larger amounts of bisnorhopane argues for an elevated input of anaerobic bacteria typical of predominantly anoxic conditions in Unit 2 (Grantham et al., 1983; Rullkötter and Wendisch, 1982; Watson et al., 2009). Aryl isoprenoids derive from special green sulphur bacteria (Chlorobiaceae) that perform anoxygenic photosynthesis which requires light penetration into H_2S saturated waters (Schwark and Frimmel, 2004). Therefore, aryl isoprenoids can be used to estimate whether the anoxic water column extended into the photic zone (Summons and Powell, 1986; Grice et al., 1996a; Koopmans et al., 1996). Aryl isoprenoids occur in all samples, although in variable amounts, suggesting frequent but transient episodes of photic-zone anoxia.

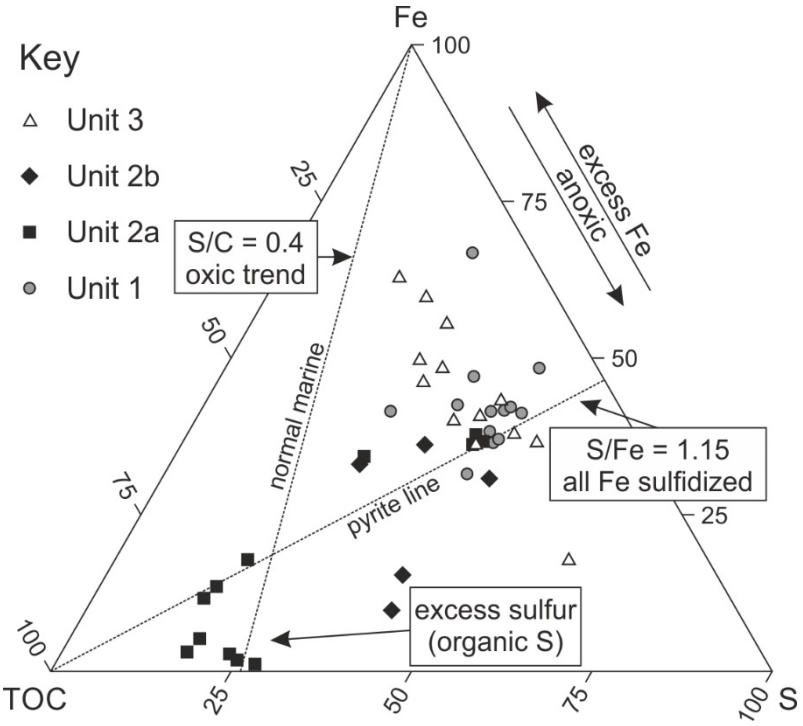

Fig. 7.11: Ternary diagram (Fe-TOC-S) after Dean and Arthur (1989). Samples of Units 1 and 3 plot along the pyrite line and in the field of excess Fe availability suggesting suboxic to anoxic conditions during deposition. In contrast, the plot indicates Fe limitation and persistent anoxia in Unit 2.

Several authors used TOC/S ratios for determining paleoredox conditions (e.g. Berner, 1970, 1984; Leventhal, 1983; Berner and Raiswell, 1983). However, this approach is problematic when Fe is limiting, as is often observed in carbonate environments (cf. Berner and Raiswell, 1983; Raiswell and Berner, 1985). The ternary plot of Dean and Arthur (1989) additionally includes Fe contents and consequently all phases relevant for pyrite formation. Therefore, this approach is used for the Bächental section. Most samples of Units 1 and 3 plot either along the pyrite line or in the field of excess Fe availability (Fig. 7.11). The former indicates anoxic conditions and a sulfidization of all the available Fe; the latter suggests the presence of non-pyritized Fe and suboxic conditions during deposition (Dean and Arthur, 1989; Hofmann et al., 2000; Rimmer et al., 2004). Hence, varying suboxic and anoxic conditions with intense sulphate reduction rates are reflected by the Fe-TOC-S diagram for Unit 1 and the upper part of Unit 3, whereas less reducing conditions prevailed during deposition of the lower part of Unit 3. The large amounts of available Fe in Units 1 and 3 triggered enhanced pyritization during diagenesis. In contrast, the Fe-TOC-S diagram confirms Fe limitation in TOC-rich samples of Unit 2 (Fig. 7.11) consistent with a postulated

anoxic to euxinic environment. The presence of excess S in Subunit 2a is reflected by elevated DBT/Phen ratios due to the incorporation of S in the aromatic fraction of OM during early diagenesis ("natural sulphurization"; Kohnen et al., 1991).

The negative correlation of S contents with both TOC and Cc_{eq} in the interval from 15.15 to 18.05 m (Subunit 2a; Figs. 7.3B-D) suggests changing Fe availability and alkalinity. The large amounts of H_2S produced in the OM-rich layers by sulphate reduction could not be fixed as pyrite because of an insufficient amount of reactive Fe, resulting in significant amounts of free H_2S. Only a small portion of this H_2S was incorporated in OM, producing elevated DBT/Phen ratios in the high-TOC/low-S layers, whereas the excess free H_2S diffused upward until it was fixed as pyrite in layers with relatively low TOC contents but large amounts of reactive Fe, resulting in low-TOC/high-S intervals (cf. Jaminski et al., 1998). The high alkalinity generated by sulphate reduction (e.g., Thomas et al., 2008) triggered the enhanced precipitation of secondary calcite in the high-TOC/low-S intervals. Iron-limiting conditions are directly connected to the available pool of Fe oxides (Raiswell et al., 1994). Several studies confirm a direct relationship between bulk sedimentation rates and variable organic input and clastic flux, respectively (cf. Mangini and Dominik, 1979; Kuehl et al., 1993; Arthur et al., 1994; Jaminski et al., 1998). The mudstone samples of Subunit 2a were deposited in a low-energy environment characterized by the rareness of detrital carbonate layers. We interpret the absence of turbiditic input to have caused Fe limitation in those samples. In contrast, infrequent carbonate turbidites within Subunit 2b provided sufficient reactive Fe to fix H_2S as pyrite in an otherwise Fe-limited environment (e.g., Fig. 7.2D). Consequently, the bulk of pyrite present in Subunit 2b is bound to fine-grained carbonate turbidites. Therefore, detrital influx controlled Fe availability and the degree of pyritization in Unit 2.

Summing up, several redox changes affected the depositional environment of the Bächental bituminous marls. Suboxic to possibly short-term anoxic conditions prevailed during deposition of Units 1 and 3. Intense sulphate reduction and oxidation of OM in the sediment during diagenesis generated H_2S that reacted with available Fe in the basin to produce large amounts of pyrite in Units 1 and 3. In contrast, all redox parameters suggest anoxia for Unit 2. Strongly reducing Subunit 2a is Fe-limited in large part, whereas carbonate turbidites triggered pyritization and, in addition, induced a shift to less reducing (i.e. suboxic to anoxic) conditions during deposition of Subunit 2b.

7.5.2.2 Salinity and water-column stratification

Several authors suggested salinity stratification caused by basin restriction resulting from minor sea-level fluctuations to be the trigger of black shale deposition in the European Toarcian (e.g. Röhl et al., 2001; Frimmel et al., 2004; van de Schootbrugge et al., 2005). Salinity stratification may have resulted from an accelerated hydrological cycle due to a monsoonal climate reducing the salinity of ocean-surface waters (e.g., Sælen et al., 1996). The reconstruction of salinity changes during deposition of the Bächental bituminous marls is based on GI and a plot of GI vs. 4-methylsteranes/ΣC_{29} steranes (Fig. 7.12). High values for GI indicate a stratified water column in marine and non-marine source-rock depositional environments, commonly resulting from a deep hypersaline water body (Fu et al., 1986). Alternatively, gammacerane may also originate from bacterivorous ciliates floating at the chemocline within the water column (Sinninghe Damsté et al., 1996; Schwark et al., 1998). According to these studies, elevated amounts of gammacerane might reflect a well-stratified water column, even in the absence of high-salinity bottom waters. However, the occurrence of bottom waters with elevated salinity in the Bächental basin is also confirmed by increased hopane isomerization ratios, which result from diagenetic processes specific for hypersaline conditions (ten Haven et al., 1987; see also Section 7.5.1.1), as well as by large amounts of 4-methylsteranes, which are frequently related to halophilic microorganisms (e.g., ten Haven et al., 1985). A well-defined positive correlation exists between GI and 4-methylsteranes (Fig. 7.12). The profiles of both GI and 4-methylsteranes indicate normal-marine salinity conditions during deposition of Units 1, 2b and 3. In contrast, generally enhanced salinity of bottom waters and a stratified water column is suggested for samples from Subunit 2a.

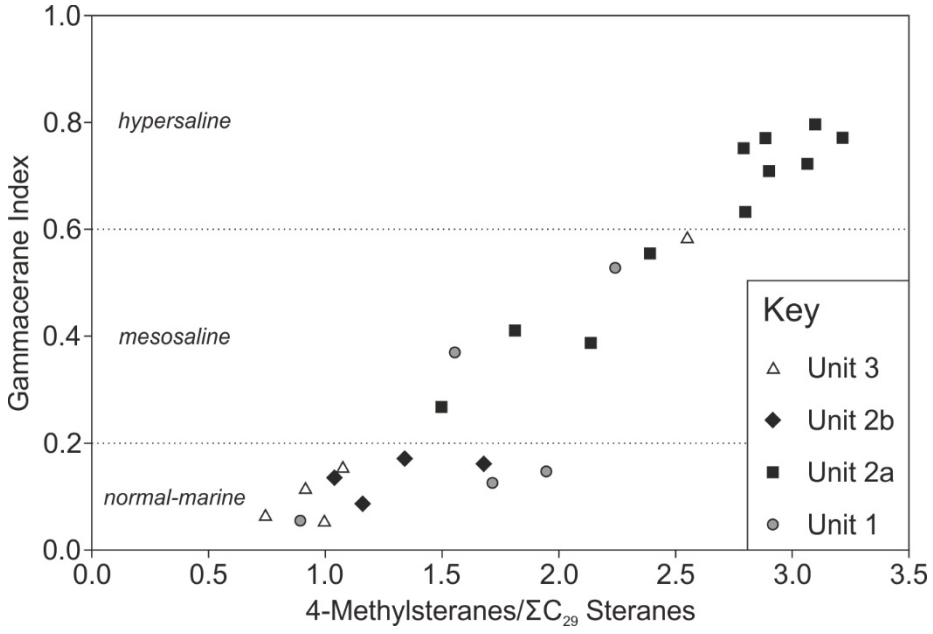

Fig. 7.12: The plot of gammacerane indices vs. 4-methylsteranes/ΣC_{29} steranes (GI vs. 4-methylsteranes/ΣC_{29} steranes) indicates enhanced salinity of bottom waters and a stratified water column during deposition of samples from Subunit 2a whereas normal-marine salinity was prevailing during deposition of the remaining parts of the section. The well-defined positive correlation between GI and 4-methylsteranes suggest a flourishing of halophilic organisms during phases of enhanced salinity. Modified after Schwark et al. (1998) and Bechtel et al. (2012).

During deposition of Unit 1, frequent mixing and ventilation of the water column of the Bächental basin prevented the establishment of a stratified water mass and permanent anoxic conditions. The transition to OM-rich Subunit 2a was associated with a distinct increase of bottom water salinity and a concomitant flourishing of halophilic microorganisms. This interval is assigned to the lower *falciferum* Zone on the basis of occurrences of *Cleviceras exaratum*. Samples of Subunit 2a are also characterized by Pr/Ph ratios <1.0. Hence anoxic conditions in Subunit 2a were typically connected to a stratified water column. Elevated inputs of freshwater due to an accelerated hydrological cycle resulted in a surface-water layer with reduced salinity that caused intensified water-column stratification (Praus and Riegel, 1989; Littke et al., 1991; Sælen et al., 1996) and also may have contributed to salinity variation within the Bächental basin. Transient small-scale mixing of the watermass caused by turbidites triggered an episodic decrease of bottom water salinity reflected by lower GI values for a few samples from the middle and upper parts of Subunit 2a (e.g., 15.65 and 16.55 m; Figs. 7.7F, 7.12). Those samples are additionally characterized by comparatively low TOC and peak S contents (Figs. 7.3B, D). Whereas a stagnant basin setting prevailed during deposition of Subunit 2a, the episodic occurrence of fine-grained carbonate turbidites caused salinity stratification to break down, resulting in less intensely reducing conditions in Subunit 2b (see Section 7.5.2.1). During deposition of Unit 3 a water column with uniform normal salinity went along with suboxic conditions. The observed salinity variations suggest that global climate processes as described for instance by Sælen et al. (1996) were overprinted by local factors within the Bächental basin, e.g., mixing of water bodies by turbidites, which also influenced the intensity of water-column anoxia.

7.5.2.3 Influence of sea-level variation

Variation in sea-level elevations exerted a pronounced influence on deposition of both the Alpine Bächental bituminous marls and the epicontinental Posidonia Shale (e.g., Röhl et al., 2001; Frimmel et al., 2004). The long-term eustatic record shows a sea-level fall from the Pliensbachian into the early Toarcian, a subsequent sea-level rise culminating in a middle Toarcian highstand, and another fall extending into the Aalenian (Haq et al., 1988; Hallam, 1992). However, the short-term trend exhibits several additional sea-level fluctuations in Pliensbachian and Toarcian time (Fig. 7.13). Frimmel et al. (2004) found a remarkable correlation between the trend of C_{27}/C_{29} sterane ratios and the proposed sea-level trend of Haq et al. (1988) for the Posidonia Shale of Dotternhausen. Although sea-level estimations based on biomarker ratios are a rather untested technique, the sterane data for the Alpine Bächental bituminous marls also show a strong correlation with the 3rd order sea-level curve for the upper Pliensbachian-lower Toarcian interval (Haq et al., 1988; Fig. 7.13). These similar relationships thus provide a basis for correlation of the Bächental bituminous marls with the Dotternhausen section (Fig. 7.13; Frimmel et al., 2004; see Section 7.5.3.1). According to sterane ratios of the study section, the sea-level rise from the base of Unit 1 reached a highstand around 9 m, followed by an abrupt sea-level fall. The deposition of Subunit 2a, recording the highest TOC contents, coincided with a sea-level lowstand dated to the lower *falciferum* Zone based on the occurrence of *Cleviceras exaratum*, and a subsequent minor sea-level rise. Another highstand was reached close to the debrite overlying Subunit 2b, followed by minor sea-level fluctuations during deposition of Unit 3.

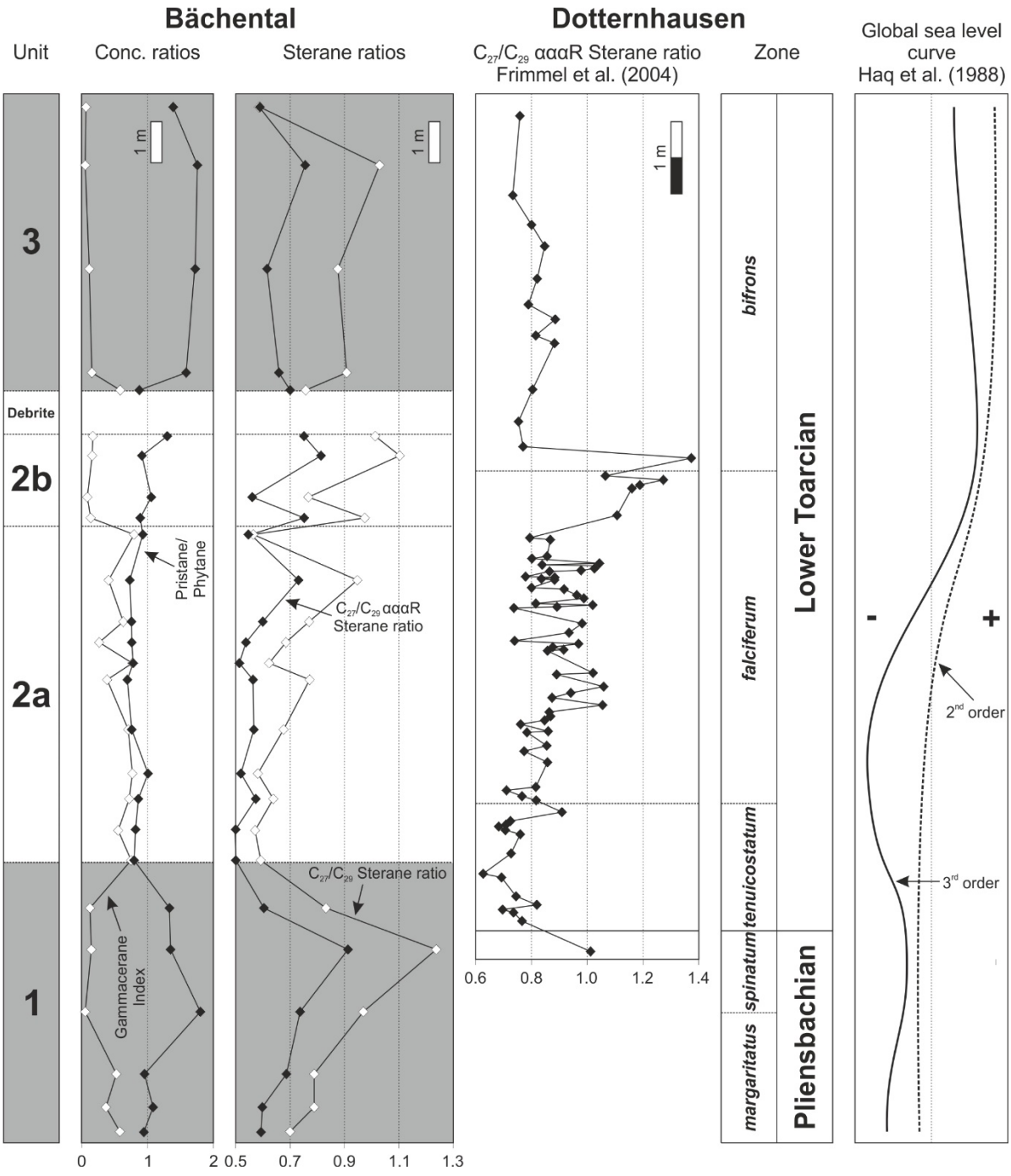

Fig. 7.13: Influence of sea-level changes on depositional environment and correlation of Pliensbachian to Toarcian OM-rich sediments of Alpine (Bächental) and epicontinental (Dotternhausen; Frimmel et al., 2004) settings with global sea-level curve (Haq et al., 1988) using sterane ratios. See text for explanations.

Sea-level fluctuations strongly influenced watermass exchange and hence ventilation of the Bächental basin (Fig. 7.14). Agreement between the sea-level curve and inferred variations in redox conditions and salinity demonstrate this influence. During the sea-level lowstand (Subunit 2a), watermass exchange and consequently oxygenation of basinal bottom

waters were sharply reduced. Consequently, strongly anoxic conditions were established within the stratified watermass. High surface-water productivity and subsequent degradation of OM additionally poisoned the depositional environment. Hence, Subunit 2a is generally characterized by strongly anoxic conditions and high OM preservation reflected by high TOC and HI values. The same correlation between stagnant basin conditions, strongest anoxia and best OM preservation during a sea-level lowstand and a subsequent sea-level rise has been postulated for the epicontinental Posidonia Shale of SW Germany (e.g. Röhl et al., 2001; Schmid-Röhl et al., 2002; Frimmel et al., 2004; see Section 7.5.3.1). In addition, a flourishing of surface-water productivity during the uppermost *tenuicostatum* to lower *falciferum* zones (e.g., Ikeda and Hori, 2014) contributed to elevated OM accumulation in Subunit 2a (see Section 7.5.2.4). During intervals of higher sea level (e.g., Units 1 and 3), better watermass exchange with surrounding epicontinental seas and, possibly, the open Tethys Ocean resulted in improved ventilation of the Bächental basin and in mainly suboxic conditions, reflected by sediments with lower TOC concentrations. Therefore, we suggest that minor sea-level fluctuations in combination with the complex bathymetry of the Bächental basin were among the controlling factors on deposition of the Bächental bituminous marls (Fig. 7.14). Consequently, the local basin setting had a strong influence on the establishment of salinity stratification and anoxic conditions.

7.5.2.4 Marine primary productivity

Marine primary productivity is likely to have been influenced by major changes in global climate, atmospheric composition, and oceanographic conditions during the Early Jurassic. Eruption of the Karoo and Ferrar large igneous provinces (Encarnación et al., 1996; Svensen et al., 2007; Sell et al., 2014) triggered massive perturbations of the global carbon cycle, leading to strong global warming through volcanic CO_2 emissions (McElwain et al., 2005), possible methane release from gas hydrates (Hesselbo et al., 2000), and metamorphism of Paleozoic OM-rich shales (Svensen et al., 2007; Suan et al., 2008). The prevailing subtropical climate during the early Toarcian induced an acceleration of the hydrological cycle, modulated by astronomical forcing (Kemp et al., 2005), and an intensification of continental weathering (Palfy and Smith, 2000; Weissert, 2000; Cohen et al., 2004). These processes resulted in an elevated supply of nutrients to ocean-surface waters, stimulating marine primary productivity (Parrish and Curtis, 1982; Parrish, 1993; Cohen et al., 2004). Jenkyns (2010) hypothesized that there was a globally synchronous increase in organic

productivity in the early Toarcian (upper *tenuicostatum*-lower *falciferum* zones) triggered by high levels of nutrient availability in surface waters. Orbital-scale productivity cycles are suggested to have triggered onset and termination of the T-OAE (Ikeda and Hori, 2014).

Intermediate sea-level: Subunit 2b

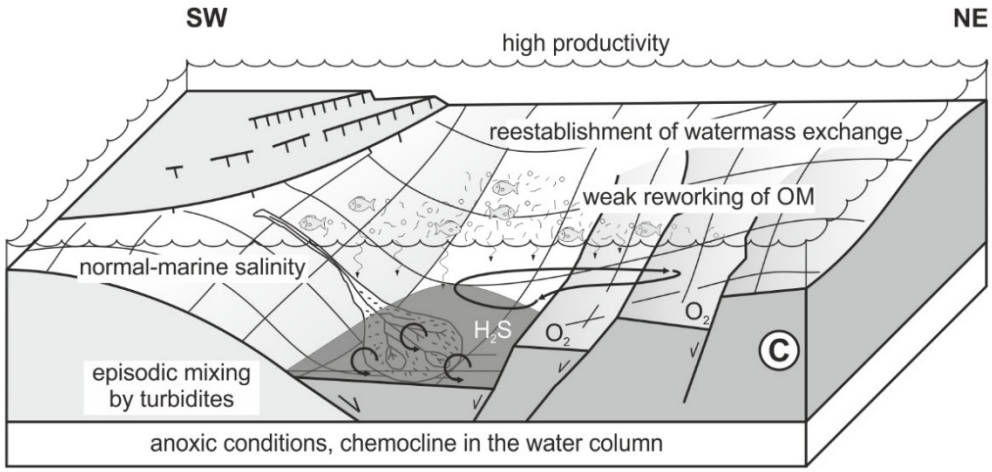

Sea-level lowstand/minor transgression: Subunit 2a

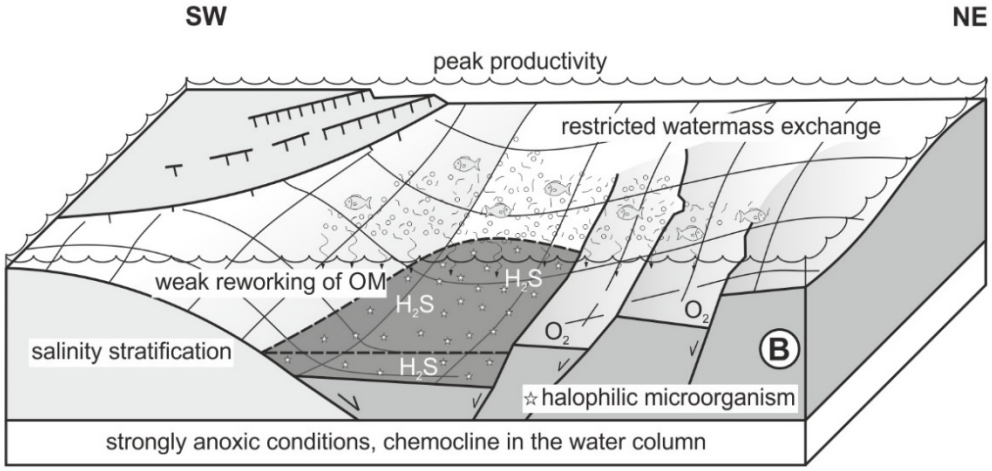

Sea-level highstand: Units 1 and 3

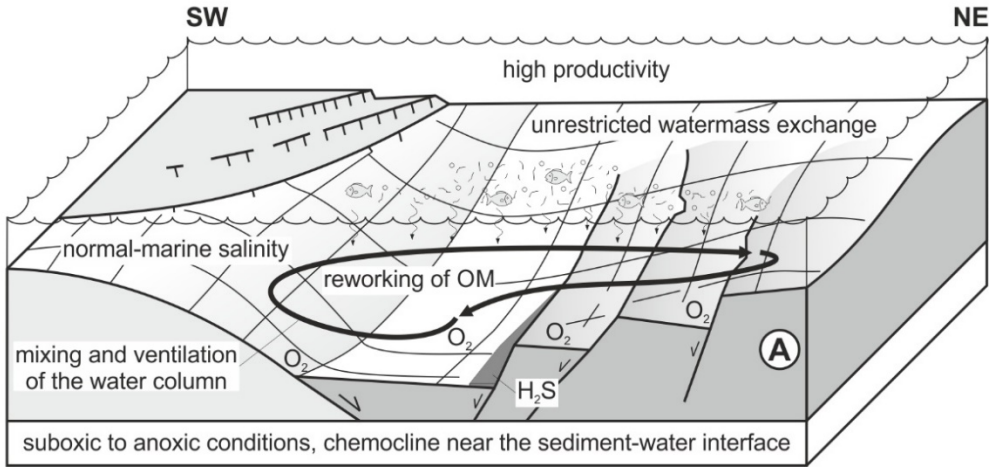

Fig. 7.14: Sketches showing factors controlling the depositional environment of the Bächental bituminous marl. Paleogeographical setting modified after Brandner (2011). (A) Units 1 and 3, (B) Subunit 2a, (C) Subunit 2b. See text for explanations.

A detailed interpretation of stratigraphic variations of primary productivity is not possible for the Bächental section owing to intense bacterial degradation of OM in Units 1 and 3 (see Section 7.5.1.3). However, the remarkable amounts of S in those units suggest a high amount of OM originally present in rocks. Therefore, it is suggested that, on average, high primary production of OM in surface waters prevailed throughout the interval of deposition of the Bächental bituminous marls. Relatively high and uniform HI values suggest a lesser degree of OM degradation in Unit 2. For this reason, TOC variations in Unit 2 are inferred to reflect changes in surface-water primary productivity. This interval is also characterized by a significant TOC increase in the study section (Fig. 7.3A) and in several age-equivalent sections in the European and Mediterranean domains (Jenkyns, 1988; Hesselbo et al., 2000; Röhl et al., 2001; Kemp et al., 2005; Pearce et al., 2008; Sabatino et al., 2009; Kafousia et al., 2014). The two samples that exhibit peak TOC contents after steady increases (at 13.39 m and 19.15 m) are also significantly enriched in short-chained *n*-alkanes (Fig 7.7A). Hence, a flourishing of marine algae and bacterioplankton in surface waters contributed to elevated OM accumulation at least in parts of Subunit 2a.

There is an ongoing discussion whether enhanced organic productivity or increased preservation was the main controlling factor behind the accumulation of OM-rich deposits in the lower Toarcian (e.g., Demaison and Moore, 1980; Pedersen and Calvert, 1990; Ikeda and Hori, 2014). Increased bioproductivity results in larger amounts of OM in bottom sediments that subsequently can accelerate the establishment of reducing conditions due to oxygen depletion by enhanced OM degradation (e.g., Röhl et al., 2001; Ikeda and Hori, 2014). The intervals exhibiting productivity maxima in Subunit 2a are also characterized by a salinity-stratified watermass and intense anoxia during a period of relative sea-level lowstand (see Sections 7.5.3.1-3). Hence, it cannot be fully resolved whether increased productivity or enhanced preservation controlled OM accumulation in those units. However, as strictly reducing conditions and high-salinity bottom waters typically dominated during deposition of Subunit 2a, we suggest that the TOC cycles culminating at 13.39 m and 19.15 m reflect primary productivity cycles during periods of rather constant depositional conditions.

7.5.3 Broader implications

7.5.3.1 Correlation and dating of Bächental bituminous marls

C-isotope chemostratigraphy has been widely used to correlate and date sections with poor biostratigraphic control (see Weissert, 2013 for summary). The early Toarcian is characterized by a distinct negative carbon isotope excursion (CIE) that is commonly recorded by both marine carbonates and marine and terrestrial OM, and that has been used as a global chemostratigraphic marker (e.g., Sabatino et al., 2009; Al-Suwaidi et al., 2010; Mazzini et al., 2010; Gröcke et al., 2011; Caruthers et al., 2011; Sell et al., 2014). As discussed in Section 7.5.1.3, the carbonate C-isotope profile of the Bächental bituminous marls records a mixed signal derived from primary and secondary carbonate phases. The diagenetic overprint especially in Units 1 and 3 is sufficiently strong that it is not possible to extract the primary isotopic signal, and, hence, correlation with age-equivalent sections on the basis of $\delta^{13}C_{carb}$ chemostratigraphy is not possible.

An alternative for correlation of the poorly dated Bächental bituminous marls with the biostratigraphically well-dated epicontinental German Posidonia Shale is provided by sterane ratio profiles. The Posidonia Shale includes three ammonite biozones (from base to top): *tenuicostatum*, *falciferum*, and *bifrons* (Riegraf et al., 1984, 1985; see also Röhl et al., 2001; Frimmel et al., 2004). Frimmel et al. (2004) documented systematic stratigraphic variation in sterane ratios (C_{27}/C_{29}; C_{27}/C_{29} ααα R) at Dotternhausen in SW Germany. The onset of Posidonia Shale deposition is characterized by a shift to lower ratios, from 1.0 in the underlying strata to 0.6 to 0.8 in the lower *tenuicostatum* Zone (Fig.7.13). Sterane ratios increase progressively through the *falciferum* Zone and peak at ~1.4 in the lowermost *bifrons* Zone before declining abruptly to constant values of 0.7-0.9 upsection. It has to be mentioned that stratigraphic correlation based on biomarker data is a rather untested and unconventional technique. Nevertheless, the Bächental bituminous marls exhibit an almost identical pattern of stratigraphic variation in sterane ratios, although absolute values are about 20% lower relative to the Dotternhausen section (Fig. 7.13). According to this correlation, accumulation of the Bächental bituminous marls in the Alpine realm commenced during Pliensbachian time (*margaritatus* Zone), which is consistent with reports of the presence of *Arieticeras* sp. and *Arieticeras* sp. or *Leptaleoceras* sp. from Unit 1 (Kodina et al., 1988). This correlation demonstrates that the base of the Bächental bituminous marls is distinctly older than the base

of the Posidonia Shale deposited in epicontinental areas of SW Germany (*tenuicostatum* Zone; Riegraf et al., 1984, 1985; Frimmel, 2004). Units 2 and 3 at Bächental are correlative with the Posidonia Shale, with Subunit 2a dating to the mid-*tenuicostatum* to upper *falciferum* zones, Subunit 2b to the uppermost *falciferum* and lowermost *bifrons* zones, and Unit 3 to the *bifrons* Zone. This correlation is supported by the occurrence of *Cleviceras exaratum*, which suggests a stratigraphic age for the base of Subunit 2a (13.40 m) equivalent to the lower *falciferum* Zone, as well as by common patterns of sea-level variation in the Bächental and Dotternhausen sections (Fig. 7.13; see Section 7.5.2.3). On the basis of these considerations, we infer that the onset of black marl deposition in the Alpine and epicontinental realm was not coeval (Fig. 7.13). Global forces were overprinted by local factors regarding timing of initiation of OM-accumulation in different basin settings in Pliensbachian and Toarcian times.

7.5.3.2 Applicability of the lower Toarcian CIE as stratigraphic marker

A pronounced negative CIE is widely regarded as a defining characteristic of the T-OAE and a global chemostratigraphic marker for the uppermost *tenuicostatum* and lower *falciferum* zones. This negative CIE has been reported from sections in NW Europe and the Mediterranean (e.g., Röhl et al., 2001; Jenkyns et al., 2001; Kemp et al., 2005; Hesselbo et al., 2007; Sabatino et al., 2009; Kafousia et al., 2014), the NE paleo-Pacific ocean (Caruthers et al., 2011), South America (Al-Suwaidi et al., 2010; Mazzini et al., 2010; Sell et al., 2014), and northwestern Panthalassa (Izumi et al., 2012). The negative CIE has been related to a rapid release of biogenic methane by dissociation of methane hydrates (e.g., Hesselbo et al., 2000, 2007; Jenkyns et al., 2002; Kemp et al., 2005), release of large volumes of CO_2 due to the emplacement of the Karoo-Ferrar LIP (e.g., Palfy and Smith, 2000; Mazzini et al., 2010), thermogenic methane resulting from the intrusion of igneous rocks into Gondwanan coals (McElwain et al., 2005; Svensen et al., 2007), recycling of OM ("recycling model"; Küspert, 1982, 1983; Röhl et al., 2001), and to the contribution of OM deriving either from calcareous or organic-walled plankton (Jenkyns and Clayton, 1986). Caruthers et al. (2011) inferred that the early Toarcian negative CIE was a global signal that had been imprinted on all active global reservoirs of the exchangeable carbon cycle. However, both the organic and inorganic carbon isotope profiles of the Bächental section do not show the typical early Toarcian negative CIE (Figs. 7.4B, D).

Whereas carbonate C-isotope values of Units 1 and 3 reflect a strong diagenetic overprint, $\delta^{13}C_{carb}$ values of Unit 2 are interpreted to be less altered (see Section 7.5.1.3). Age correlation based on sterane data (see Section 7.5.3.1) as well as the occurrence of *Cleviceras exaratum* suggests an upper *tenuicostatum* to lower *falciferum* Zone assignment for the lower half of Subunit 2a, i.e., equivalent in time to the early Toarcian negative CIE. However, neither the organic $\delta^{13}C$ nor the carbonate $\delta^{13}C$ profile of the study section exhibits the early Toarcian negative CIE for reasons that remains unclear.

$\delta^{13}C_{org}$ compositions for the Bächental bituminous marls are considerably lighter (-32.7 to -30.6‰ VPDB) than typical values for modern marine plankton (-24 to -18‰ VPDB; e.g., Lewan, 1986; Tyson, 1995). They are also significantly lighter than average values of other lower Toarcian profiles as the $\delta^{13}C_{org}$ values of the entire Bächental bituminous marls succession are in the range of the lower Toarcian negative organic CIE (Hesselbo et al., 2000; Kemp et al., 2005; Röhl et al., 2001; Sabatino et al., 2009; Al-Suwaidi et al., 2010; Caruthers et al., 2011; Gröcke et al., 2011). The origin of the generally light $\delta^{13}C_{org}$ values in the Bächental bituminous marls is not yet clear, and several mechanisms are possible. [i] ^{13}C-depleted OM produced by means of carbon recycling processes mediated by chemoautotrophic and methanotrophic microbes within an anoxic, stratified water column (e.g., Küspert, 1982, 1983; Hollander and Smith, 2001). Biogenic methane oxidation at the oxic/anoxic interface during periods of highest nutrient concentrations in the water column may have reinforced this signal; hence, the level of eutrophication controls the biogeochemical processes that influence $\delta^{13}C_{org}$ compositions (Hollander and Smith, 2001). [ii] Varying contributions of OM from eukaryotic algae, anaerobic chemoautotrophs, and other microbial plankton (e.g., Luo et al., 2014). In that study, chemoautotrophic bacteria were suggested to be the source of strongly ^{13}C-depleted OM in deepwater environments. [iii] Expandable smectite possibly derived from alteration of volcanic ash is abundant in all samples; hence a contribution of isotopically light CO_2 from volcanic emissions is possible.

On the other hand, OM-poor rocks of Scheibelberg Fm. and Upper Allgäu Fm. show heavier $\delta^{13}C_{org}$ isotope values (-29.4 to -23.6‰ VPDB) that are similar to correlative strata in other Toarcian sections (see above for references) and, hence, were not affected by processes described above. In the case of the lower Toarcian Bächental bituminous marls, the $\delta^{13}C_{carb}$, $\delta^{18}O_{carb}$, and $\delta^{13}C_{org}$ isotopes do not show any correlation. Furthermore, the pronounced negative CIE ($\delta^{13}C_{carb}$ and $\delta^{13}C_{org}$) that characterizes the lower Toarcian globally is missing,

questioning its unrestricted applicability as a ubiquitous chemostratigraphic marker for this time interval. The reason for its absence is not yet clear but may be due to overprinting of the global signal by local controls.

7.5.3.3 OM accumulation in Pliensbachian-Toarcian: Oceanic response to magmatic events

Significant relationships exist between emplacement of LIPs, long-term environmental changes, global climate warming, and extinction events reflected by major geochemical perturbations and increased OM accumulation ("volcanic greenhouse scenario"; Wignall et al., 2005; Caruthers et al., 2013). The end-Triassic release of large quantities of greenhouse gases during the CAMP eruptions (~201 Ma) initiated a significant global warming process during Early Jurassic times (McElwain et al., 1999; McHone, 2003; Cohen and Coe, 2007). Global warming intensified further as a consequence of volcanic activity associated with the rift-related Karoo and Ferrar LIPs (Caruthers et al., 2013) during the Early Jurassic (Encarnación et al., 1996; Minor and Mukasa, 1997; Svensen et al., 2007, 2012; Sell et al., 2014), resulting in peak "greenhouse Earth" conditions in the Toarcian (Jenkyns and Clayton, 1997; Pálfy and Smith, 2000; Weissert, 2000; Jenkyns, 2003). In addition, several volcanic pulses were associated with complex rifting of the Alpine Tethys ranging from the Late Triassic to the Middle Jurassic (Decarlis et al., 2013). The establishment and intensification of greenhouse climate at that time was possibly supported by the release of methane hydrates (Jenkyns and Clayton, 1997; Hesselbo et al., 2000). In addition, the Karoo-Ferrar volcanism intensified continental weathering and the hydrological cycle (Cohen et al., 2004). The marine ecosystem was affected by alterations of seawater chemistry (Martin and Macdougall, 1995) and development of oceanic anoxia (Harnik et al., 2012). The late Pliensbachian and early Toarcian were characterized by several marine extinction events that were probably triggered by eruptions of the Karoo and Ferrar LIPs (Dera et al., 2010; Caruthers et al., 2013). Although the main phase of extinction occurred within an interval ranging from the Pliensbachian-Toarcian boundary to the lowermost *falciferum* Zone, a significant global extinction pulse is also reported for the late Pliensbachian *margaritatus* Zone, indicating a rapid biotic response to LIP activity (Dera et al., 2010; Caruthers at al., 2013). The combination of these global changes provided conditions favourable to OM accumulation during upper Pliensbachian and lower Toarcian in oceanic settings.

The apparent onset of OM accumulation in the tectonically complex Bächental basin during the late Pliensbachian *margaritatus* Zone (Fig. 7.13) is consistent with data from other age-equivalent sections in semi-restricted depositional settings, e.g., Cleveland Basin in NW Europe (McArthur et al., 2008) and the Neuquén Basin in Argentina (Al-Suwaidi et al., 2010). This suggests a rapid oceanic response of semi-restricted basins to greenhouse gas emissions, elevated atmospheric CO_2 levels, and global climate warming triggered by the Karoo and Ferrar LIPs (cf. Mazzini et al., 2010). Whereas high precision U-Pb data suggest a stratigraphic age of ~183 Ma (equivalent to early Toarcian) for the onset of Karoo volcanism (Svensen et al., 2007, 2012; Sell et al., 2014), the Ferrar LIP was active already at ~184 Ma (equivalent to late Pliensbachian; Encarnación et al., 1996; Minor and Mukasa, 1997). Thus, the early stages of Early Jurassic LIP magmatism may have coincided with the onset of OM accumulation for the above-mentioned sections. In the Alpine Tethyan domain, the establishment of anoxia in Pliensbachian to Toarcian times was linked to local basin geometry, with reducing conditions commencing earlier than the Toarcian in basins that were prone to restriction and water-column stratification (Fig. 7.14).

The carbonate-free mudstone at the base of the Bächental bituminous marls contains charred organic material typically connected to wildfires (e.g., Brown et al., 2012) and large amounts of expandable smectite possibly derived from alteration of volcanic ash. In contrast, the underlying Scheibelberg Formation contains only illite in its clay fraction. This suggests that onset of OM accumulation and establishment of reducing conditions in the Bächental basin were associated with a volcanic event of possibly regional scale in the NW Tethyan domain. Significant amounts of smectite present in all marl samples indicate a pronounced contribution of volcanic-derived detritus during deposition of the Bächental bituminous marls. This is consistent with the occurrence of volcanic ashes and lava flows in the Pliensbachian and Toarcian of the Tethyan domain (Decarlis et al., 2013), the complex rift history of the Valais, Briançonnais and Piemonte-Liguria domains at the proximal European and Adriatic margins between late Sinemurian and Callovian time (Mohn et al., 2010), and the contemporaneous break-up of the Ligurian-Penninic oceanic realm (Ratschbacher et al., 2004).

The main pulses of Karoo and Ferrar LIP magmatism during the upper *tenuicostatum*-lower *falciferum* zones are thought to have triggered the T-OAE on a global scale (e.g., Svensen et al., 2007; Dera et al., 2010; Mazzini et al., 2010; Ikeda and Hori, 2014). The main

eruption stage of these LIPs correlates approximately with the base of Subunit 2a (Figs. 7.2, 7.13). Subunit 2a accumulated in a restricted basinal setting characterized by strictly anoxic conditions, a salinity-stratified watermass, and a concurrent flourishing of surface-water productivity during a period of relative sea-level lowstand. Hence, local factors (i.e., basin restriction due to eustatic controls) can sufficiently explain environmental conditions controlling bituminous marl sedimentation in the Bächental basin. However, LIP-related perturbations of the carbon cycle triggered global conditions favoring widespread development of marine anoxia that potentially reinforced the local controlling factors in the Bächental basin and triggered rapid OM accumulation in Subunit 2a of the study section.

7.6 Conclusions

The Bächental bituminous marls provide insights into global and local factors controlling the onset and duration of OM accumulation in semi-restricted basins during late Pliensbachian and early Toarcian times.

- A stagnant basin setting during a period of relative sea-level lowstand in Subunit 2a corresponding to the upper *tenuicostatum* and lower *falciferum* zones triggered the establishment of strong anoxia, a salinity-stratified watermass, and a flourishing of surface-water productivity that jointly enhanced OM accumulation. Hence, redox and salinity changes in the tectonically complex Bächental basin were controlled mainly by minor sea-level fluctuations that resulted in varying watermass exchange and bottom water oxygenation.

- Stratigraphic correlation of the Bächental bituminous marls with the time-equivalent SW German Posidonia Shale suggests that deposition of OM-rich sediments in the Alpine realm commenced earlier (late Pliensbachian *margaritatus* Zone) than in proximal epicontinental areas (early Toarcian *tenuicostatum* Zone) indicating a rapid oceanic response to the major environmental perturbations caused by the activity of Karoo and Ferrar LIPs and complex rifting of the Alpine Tethys in local basins that were prone to the development of water-column stratification and deepwater anoxia because of their geometry or paleogeographic setting. Charred material at the base of the study section suggests that a possibly regional volcanic event was the trigger for onset of OM accumulation. Continued inputs of volcanic detritus during marl deposition confirms volcanic activity during late Pliensbachian and early Toarcian

times in the NW Tethyan domain. Intervals with peak TOC contents in the study section probably correspond to the main magmatic stage of the Karoo and Ferrar LIPs, suggesting a massive effect on coeval marine productivity.

- The early Toarcian negative CIE that is observed in age-equivalent sections worldwide is not visible in either the carbonate or organic carbon $\delta^{13}C$ profiles of the study section. Thus, this chemostratigraphic marker cannot be used in correlation of the Bächental bituminous marls. The global CIE appears to have been overprinted owing to local factors in the study section. Consequently, the unrestricted applicability of the early Toarcian negative CIE as a ubiquitous chemostratigraphic marker for the early Toarcian has to be questioned.

7.7 Acknowledgments

We gratefully thank family Albrecht (Tiroler Steinöl ®) who operate the Bächental open pit for their technical support during sampling and Joachim Blau (Giessen) for identification of the ammonite *Cleviceras exaratum*. Research by TJA is supported by the Sedimentary Geology and Paleobiology program of the U.S. National Science Foundation, the NASA Exobiology program, and the State Key Laboratory of Geological Processes and Mineral Resources, China University of Geosciences, Wuhan (Program GPMR201301).

7.8 References

Algeo, T.J., Wilkinson, B.H., Lohmann, K.C. (1992). Meteoric-burial diagenesis of Pennsylvanian carbonate: water/rock interactions and basin geothermics. Journal of Sedimentary Petrology 62, 652-670.

Al-Suwaidi, A.H., Angelozzi, G.N., Baudin, F., Damborenea, S.E., Hesselbo, S.P., Jenkyns, H.C., Manceñido, M.O., Riccardi, A.C. (2010). First record of the Early Toarcian Oceanic Anoxic Event from the Southern Hemisphere, Neuquén Basin, Argentina. Journal of the Geological Society, London 167, 633-636.

Arthur, M.A., Sageman, B.B. (1994). Marine black shales: Depositional mechanisms and environments of ancient deposits. Annual Review of Earth and Planetary Sciences 2, 126-166.

Auras, S., Püttmann, W. (2004). Zusammensetzung und Herkunft der 4-Methylsteroide im Messeler Ölschiefer. Cour. Forsch.-Inst. Senckenberg 252, 139-149.

Barakat, A.O., Rullkötter, J. (1997). A comparative study of molecular paleosalinity indicators: chromans, tocopherols and C_{20} isoprenoid thiophenes in Miocene lake sediments (Nördlinger Ries, Southern Germany). Aquatic Geochemistry 3, 169-190.

Bechtel, A., Jia, J., Strobl, S.A.I., Sachsenhofer, R.F., Liu, Z., Gratzer, R., Püttmann, W. (2012). Palaeoenvironmental conditions during deposition of the Upper Cretaceous oil shale sequences on the Songliao Basin (NE China): Implications from geochemical analysis. Organic Geochemistry 46, 76-95.

Berner, R.A. (1970). Sedimentary pyrite formation. Am. J. Sci. 268, 1-23.

Berner, R.A. (1984). Sedimentary pyrite formation: An update. Geochimica et Cosmochimica Acta 48, 605-615.

Berner, R.A., Raiswell, R. (1983). Burial of organic carbon and pyrite sulfur in sediments over Phanerozoic time: A new theory. Geochimica et Cosmochimica Acta 47, 862-885.

Bernoulli, D., Jenkyns, H.C. (1974). Alpine, Mediterranean and Central Atlantic Mesozoic facies in relation to the early evolution of the Tethys. In: Dott, R.H., Shaver, R.H. (Eds.), Modern and Ancient Geosynclinal Sedimentation, a Symposium. Special Publication of the Society of economic Paleontologists and Mineralogists 19, pp. 129-160.

Bernoulli, D., Jenkyns, H.C. (2009). Ancient oceans and continental margins of the Alpine-Mediterranean Tethys: deciphering clues from Mesozoic pelagic sediments and ophiolites. Sedimentology 56,149-190.

Blumenberg, M., Krüger, M., Nauhaus, K., Talbot, H.M., Oppermann, B., Seifert, R., Pape, T., Michaelis, W. (2006). Biosynthesis of hopanoids by sulfate-reducing bacteria (genus *Desulfovibrio*). Environ. Microbiol. 8, 1220-1227.

Bray, E.E., Evans, E.D. (1961). Distribution of n-paraffins as a clue to recognition of source beds. Geochimica et Cosmochimica Acta 22, 2-15.

Brandner, R. (2011). In: Geologie des Achenseegebiets. Tagungsband der Arbeitstagung der Geologischen Bundesanstalt, Wien: 220-224.

Brown, S.A.E., Scott, A.C., Glasspool, I.J., Collinson; M.E. (2012). Cretaceous wildfires and their impact on the Earth system. Cretaceous Research 36, 162-190.

Calvert, S.E., Pedersen, T.F. (1996). Sedimentary Geochemistry of Manganese: Implications for the Environment of Formation of Manganiferous Black Shales. Economic Geology 91, 36-47.

Caruthers, A.H., Gröcke, D.R., Smith, P.L. (2011). The significance of an Early Jurassic (Toarcian) carbon-isotope excursion in Haida Gwaii (Queen Charlotte Islands), British Columbia, Canada. Earth and Planetary Science Letters 307, 19-26.

Caruthers, A.H., Smith, P.L., Gröcke, D.R. (2013). The Pliensbachian-Toarcian (Early Jurassic) extinction, a global multi-phased event. Palaeogeography, Palaeoclimatology, Palaeoecology 386, 104-118.

Cohen, A.S., Coe, A.L. (2007). The impact of the Central Magmatic province on climate and on the Sr- and Os-isotope evolution of seawater. Palaeogeography, Palaeoclimatology, Palaeoecology 244, 374-390.

Cohen, A.S., Coe, A.L., Harding, S.M., Schwark, L. (2004). Osmium isotope evidence for the regulation of atmospheric CO_2 by continental weathering. Geology 32, 157-160.

Cranwell, P.A. (1977). Organic geochemistry of CamLoch (Sutherland) sediments. Chemical Geology 20, 205-221.

Dean, W.E., Arthur, M.A. (1989). Iron-sulfur-carbon relationships in organic-rich sequences. In: Cretaceous Western Interior Seaway. American Journal of Science 289, 708-743.

Decarlis, A., Dallagiovanna, G., Lualdi, A., Maino, M., Seno, S. (2013). Stratigraphic evolution in the Ligurian Alps between Variscian heritages and the Alpine Tethys opening: A review. Earth-Science Reviews 125, 43-68

Demaison, G.J., Moore, G.T. (1980). Anoxic environments and oil source bed genesis. AAPG Bulletin 64, 1179-1209.

Dera, G., Neige, P., Dommergues, J.-L., Fara, E., Laffont, R., Pellenard, P. (2010). High-resolution dynamics of Early Jurassic marine extinctions: the case of Pliensbachian–Toarcian ammonites (Cephalopoda). J. Geol. Soc. (Lond.) 167, 21–33.

Didyk, B.M., Simoneit, B.R.T., Brassell, S.C., Eglinton, G. (1978). Organic geochemical indicators of palaeoenvironmental conditions of sedimentation. Nature 272, 216-222.

Ebli, O. (1991). Beiträge von Draxler, I., Klein, P., Kodina, L.A., Lobitzer, H., Schwaighofer, B. Fazies, Paläontologie und organische Geochemie der Sachranger Schiefer (Untertoarcium) im Mittelabschnitt der Nördlichen Kalkalpen zwischen Isar und Saalach. Jahrbuch der Geologischen Bundesanstalt 134/1, 5-14.

Ebli, O., Vetö, I., Lobitzer, H., Sajgò, C., Demény, A., Hetényi, M. (1998). Primary productivity and early diagenesis in the Toarcian Tethys on the example of the Mn rich black shales of the Sachrang Formation, Northern Calcareous Alps. Organic Geochemistry 29, 1635-47.

Encarnación, J., Fleming, T.H., Elliot, D.H., Eales, H.V. (1996). Synchronous emplacement of Ferrar and Karoo dolerites and the early breakup of Gondwana. Geology 24, 535-538.

Espitalié, J., Marquis, F., Barsoni, I. (1984). Geochemical logging. In: Voorhess, K.J. (Eds.), Analytical Pyrolysis. Butterworth, Boston, pp. 53-79.

Fabricus, F. (1966). Beckensedimentation und Riffbildung an der Wende Trias/Jura in den Bayrisch-Tiroler Kalkalpen. Internat. Sedim. Petrogr. Series 9, 143 S.

Faupl, P., Wagreich, M. (2000). Late Jurassic to eocene palaeogeography and geodynamic evolution of the Eastern Alps. Mitteilungen der Österreichischen Geologischen Gesellschaft 92, 79-94.

Frimmel, A., Oschmann, W., Schwark, L. (2004). Chemostratigraphy of the Posidonia Shale, SW Germany I. Influence of sea-level variation on organic facies evolution. Chemical Geology 206, 199-230.

Frisch, W. (1979). Tectonic Progradation on plate tectonic evolution of the Alps. Tectonophysics 60, 121-139.

Frisch, W., Gawlick, H.-J. (2003). The nappe structure of the central Northern Calcareous Alps and its disintegration during Miocene tectonic extrusion – a contribution to understanding the orogenic evolution of the Eastern Alps. International Journal of Earth Sciences 92, 712-727.

Frisch, W., Meschede, M., Blakey, R. (2011). Plate Tectonics. Springer, pp. 112.

Fu, J.G., Sheng, P., Peng, S.C., Brassell, S.C., Eglington, G. (1986). Pecularities of salt lake sediments as potential source rocks in China. Organic Geochemistry 10, 119-127.

Gawlick, H.-J., Frisch, W., Hoxha, L., Dumitrica, P., Krystyn, L., Lein, R., Missoni, S., Schlagintweit, F. (2008). Mirdita Zone ophiolites and associated sediments in Albania reveal Neotethys Ocean origin. International Journal of Earth Sciences 97, 865-881.Gawlick, H-J., Missoni, S., Schlagintweit, F., Suzuki, H., Frisch, W., Krystyn, L., Blau, J., Lein, R., 2009. Jurassic Tectonostratigraphy of the Austroalpine Domain. Journal of Alpine Geology 50, 1-152.

Gawlick, H.-J., Missoni, S., Schlagintweit, F., Suzuki, H., Frisch, W., Krystyn, L., Blau, J., Lein, R. (2009). Jurassic Tectonostratigraphy of the Austroalpine Domain. Journal of Alpine Geology 50, 1-152.

Golonka, J. (2002). Plate-tectonic Maps of the Phanerozoic. In: Kiessling, W., Flügel, E., Golonka, J. (Eds.), Phanerozoic Reef Patterns. SEPM Special Publication 72, pp. 21-75.

Goossens, H., de Leeuw, J.W., Schenck, P.A., Brassell, S.C. (1984). Tocopherols as likely precursors of pristane in ancient sediments and crude oils. Nature 312, 440-442.

Gradstein, F.M., Ogg, J.G., Schmitz, M.D., et al. (2012). The Geologic Time Scale 2012. Elsevier, Boston.

Grantham, P.J., Posthuma, J., Baak, A. (1983). Triterpanes in a number Far Eastern crude oils. In: Bjoroy, M., et al. (Eds.), Advances in Organic Geochemistry. Wiley, Chichester, pp. 675-683.

Grice, K., Gibbison, R., Atkinson, J.E., Schwark, L., Eckardt, C.B.E., Maxwell, J.R. (1996). Maleimides (1H-pyrrole-2,5-diones) as indicators of anoxygenic photo-synthesis in ancient water columns. Geochim. Cosmochim. Acta 60, 3913-3924.

Gröcke, D.R., Hori, R.S., Trabucho-Alexandre, J., Kemp, D.B., Schwark, L. (2011). An open ocean record of the Toarcian oceanic anoxic event. Solid Earth 2, 245-57.

Hallam, A. (1992). Phanerozoic Sea-level Changes. Columbia University Press, New York. pp. 266.

Harnik, P.G., Lotze, H.K., Anderson, S.C., Finkel, Z.V., Finnegan, S., Lindberg, D.R., Liow, L.H., Lockwood, R., McClain, C.R., McGuire, J.L., O`Dea, A., Pandolfi, J.M., Simpson, C., Tittensor, D.P. (2012). Extinctions in ancient and modern seas. Trends in Ecology and Evolution 27, 608-617.

Haq, B.U., Hardenbol, J., Vail, P.R. (1988). Mesozoic and Cenozoic chronostratigraphy and cycles of sea-level change. In: Wilgus, C.K., Hastings, B.S., Posamentier, H., Wagoner, J.V., Ross, C.A., Kendall, C.G.S.C. (Eds.), Sea-Level Changes - An Integrated Approach. SEPM Special Publications 42, pp. 71-108.

Hesselbo, S.P., Gröcke, D.R., Jenkyns, H.C., Bjerrum, C.J., Farrimond, P., Morgans Bell, H.S., Green, O.R. (2000). Massive dissociation of gas hydrate during a Jurassic oceanic anoxic event. Nature 406, 392-395.

Hesselbo, S.P., Jenkyns, H.C., Duarte, L.V., Oliviera, L.C.V. (2007). Carbon-isotope record of the Early Jurassic (Toarcian) Oceanic Anoxic Event from fossil wood and marine carbonate (Lusitanian Basin, Portugal). Earth and Planetary Science Letters 253, 455-470.

Hofmann, P., Ricken, W., Schwark, L., Leythaeuser, D. (2000). Carbon–sulfur–iron relationships and $\delta^{13}C$ of organic matter for Late Albian sedimentary rocks from the North Atlantic Ocean: Palaeoceanographic implications. Palaeogeography, Palaeoclimatology, Palaeoecology 163, 97-113.

Hollander, D.J., Smith, M.A. (2001). Microbially mediated carbon cycling as a control on the d13C of sedimentary carbon in eutrophic Lake Mendota (USA): new models for interpreting isotopic excursions in the sedimentary record. Geochimica et Cosmochimica Acta 65, 4321-4337.

Hughes, W.B., Holba, A.G., Dzou, L.I.P. (1995). The ratios of dibenzothiophene to phenanthrene and pristane to phytane as indicators of depositional environment and lithology of petroleum source rocks. Geochimica et Cosmochimica Acta 59, 3581-3598.

Hutton, A.C. (1987). Petrographic classification of oil shales. Internat. J. Coal Geol. 8, 203-231.

Ikeda, M., Hori, R.S. (2014). Effects of Karoo-Ferrar volcanism and astronomical cycles on the Toarcian Anoxic Events (Early Jurassic). Palaeogeography, Palaeoclimatology, Palaeoecology 410, 134-142.

Irwin, H., Curtis, C.D., Coleman, M. (1977). Isotopic evidence for source of diagenetic carbonates formed during burial of organic-rich sediments. Nature 269, 209-213.

Izumi, K., Miyaji, T., Tanabe, K. (2012). Early Toarcian (Early Jurassic) oceanic anoxic event recorded in the shelf deposits in the northwestern Panthalassa: Evidence from the Nishinakayama Formation in the Toyora area, west Japan. Palaeogeography, Palaeoclimatology, Palaeoecology 315-316, 100-108.

Jaminski, J., Algeo, T.J., Maynard, J.B., Hower, J.C. (1998). Climatic origin of dm-scale compositional cyclicity in the Cleveland Member of the Ohio Shale (Upper Devonian), Central Appalachian Basin, U.S.A. In: Schieber, J., Zimmerle, W., Sethi, P.S. (Eds.), Shales and Mudstones. I.E. Schweizerbart'sche Verlagsbuchhandlung, Stuttgart, pp. 217-242.

Jenkyns H. C. (1985). The Early Toarcian and Cenomanian–Turonian anoxic events in Europe: comparisons and contrasts. Geologische Rundschau 74, 505-518.

Jenkyns, H.C. (1988). The Early Toarcian (Jurassic) anoxic event: stratigraphic, sedimentary, and geochemical evidence. American Journal of Science 288, 101-151.

Jenkyns, H.C. (2003). Evidence for rapid climate change in the Mesozoic–Palaeogene greenhouse world. Philosophical Transactions of the Royal Society of London 361 A, 1885-1916.

Jenkyns, H.C. (2010). The geochemistry of oceanic anoxic events. Geochemistry Geophysics Geosystems 11, Q03004, doi: 10.1029/2009GC002788.

Jenkyns, H.C., Clayton, C.J. (1986). Black shales and carbon isotopes in pelagic sediments from the Tethyan Lower Jurassic. Sedimentology 33, 87-106.

Jenkyns, H.C., Clayton, C.J. (1997). Lower Jurassic epicontinental carbonates and mudstones from England and Wales: chemostratigraphic signals and the early Toarcian anoxic event. Sedimentology 44, 687-706.

Jenkyns, H.C., Gröcke, D.R., Hesselbo, S.P. (2001). Nitrogen isotope evidence for water mass denitrification during the early Toarcian (Jurassic) ocean anoxic event. Paleoceanography 16, 593–603.

Jenkyns, H.C., Jones, C.E., Gröcke, D.R., Hesselbo, S.P., Parkinson, D.N. (2002). Chemostratigraphy of the Jurassic System: applications, limitations and implications for palaeoceanography. Journal of the Geological Society of London 159, 351-378.

Jourdan, F., Féraud, G., Bertrand, H., Watkeys, M.K., Renne, P.R. (2008). The $^{40}Ar/^{39}Ar$ ages of the sill complex of the Karoo large igneous province: implications for the Pliensbachian-Toarcian climate change. Geochemistry, Geophysics, Geosystems 9, 1-20.

Kafousia, N., Karakitsios, V., Mattioli, E., Kenjo, S., Jenkyns, H.C. (2014). The Toarcian Oceanic Anoxic Event in the Ionian Zone, Greece. Palaeogeography, Palaeoclimatology, Palaeoecology 393, 135-145.

Kemp, D.B., Coe, A.L., Cohen, A.S., Schwark, L. (2005). Astronomical pacing of methane release in the early Jurassic period. Nature 437, 396-399.

Klebelsberg, R.v. (1935). Geologie von Tirol. Gebr. Borntraeger, Berlin.

Kodina, L.A., Bogatecheva, M.P., Lobitzer, H. (1988). An anorganic geochemical study of Austrian bituminous rocks. Jb. Geol. B.-A. 131, 291-300, Wien.

Kohnen, M.E.L., Sinninghe Damsté, J.S., de Leeuw, J.W. (1991). Biases from natural sulphurization in palaeoenvironmental reconstruction based on hydrocarbon biomarker distributions. Nature 349, 775-778.

Koopmans, M.P., Köster, J., van Kaam-Peters, H.M.E., Kenig, F., Schouten, S., Hartgers, W.A., de Leeuw, J.W., Sinninghe Damsté, J.S. (1996). Diagenetic and catagenetic products of isorenieratene: molecular indicators for photic zone anoxia. Geochim. Cosmochim. Acta 60, 4467-4496.

Köster, J., Schouten, S., Sinninghe Damsté, J.S.de Leeuw, J.W. (1995). Reconstruction of the depositional environment of Toarcian marlstones (Allgäu Formation, Tyrol/Austria) using biomarkers and compound specific carbon isotope analysis. In: Grimalt, J.O., Dorronsoro, C. (Eds.), Organic Geochemistry: Developments and applications to energy, climate, environment and human history. A.I.G.O.A., San Sebastian, pp. 76-78.

Kuehl, S.A., Fuglseth, T.J., Thunell, R.C. (1993). Sediment mixing and accumulation rates in the Sulu and South China Seas: Implications for organic carbon preservation in deep-water environments. Mar. Geol. 111, 15-35.

Küspert, W. (1982). Environmental changes during oil shale deposition as deduced from stable isotope ratios. In: Einsele, G., Seilacher, A. (Eds.), Cyclic and Event Stratification. Springer, Berlin, pp. 482-501.

Küspert, W. (1983). Faziestypen des Posidonienschiefers (Toarcium, Süddeutschland): Eine isotopen-geologische, organisch-chemische und petrographische Studie. Ph.D. Thesis, Tübingen University.

Langford, F.F., Blanc-Valleron, M.-M. (1990). Interpreting Rock-Eval pyrolysis data using graphs of pyrolyzable hydrocarbons vs. total organic carbon. American Association of Petroleum Geologists Bulletin 74, 799-804.

Leventhal, J.S. (1983). An interpretation of carbon and sulfur relationships in Black Sea sediments as indicators of environments of deposition. Geochimi. Cosmochimi. Acta 47, 133-137.

Lewan, M.D. (1986). Stable carbon isotopes of amorphous kerogens from Phanerozoic sedimentary rocks. Geochim. Cosmochim. Acta 50, 1583-1591.

Littke, R., Rotzal, H., Leythaeuser, D., Baker, D.R. (1991). Organic facies and maturity of Lower Toarcian Posidonia Shale in Southern Germany (Schwäbische Alb). Erdöl & Kohle Erdgas Petrochemie/Hydrocarbon Technology 44, 407-414.

Luo, G.M., Algeo, T.J., Zhou, W.F., Wang, Y.B., Yang, H., Huang, J.H., Richoz, S., Xie, S.C. (2014). Vertical $\delta^{13}C_{org}$ gradients record changes in planktonic microbial community composition during the end-Permian mass extinction. Palaeogeography Palaeoclimatology Palaeoecology 396, 119-131.

Mackenzie, A.S., Maxwell, J.R. (1981). Assessment of thermal maturation in sedimentary rocks by molecular measurements. In: Brooks, J. (Eds.), Organic Maturation Studies and Fossil Fuel Exploration. Academic Press, London, pp. 239-254.

Mackenzie, A.S., Brassell, SC., Eglinton, G., Maxwell, J.R. (1982). Chemical fossils: the geological fate of steroids. Science 217, 491-504.

Mangini, A., Dominik, J. (1979). Late Quaternary sapropel on the Mediterranean ridge: U-budget and evidence for low sedimentation rates. Sedim. Geol. 23, 113-125.

Martin, E.E., Macdougall, J.D. (1995). Sr and Nd isotopes at the Permian Triassic Boundary – a record of climate change. Chemical Geology 125, 73-99.

Marzoli, A., Renne, P.R., Piccirillo, E.M., Ernesto, M., Bellieni, G., De Min, A. (1999). Extensive 200 million-year-old continental flood basalts of the central Atlantic magmatic province. Science 284, 616-618.

Mazzini, A., Svensen, H., Leanza, H.A., Corfu, F., Planke, S. (2010). Early Jurassic shale chemostratigraphy and U–Pb ages from the Neuquén Basin (Argentina): implications for the Toarcian Oceanic Anoxic Event. Earth Planet. Sci. Lett. 297, 633–645.

McArthur, J.M., Algeo, T.J., van de Schootbrugge, B., Li, Q., Howarth, R.J. (2008). Basinal restriction, black shales, Re–Os dating, and the Early Toarcian (Jurassic) oceanic anoxic event. Paleoceanography 23, 1–22.

McElwain, J.C., Beerling, D.J., Woodward, F.I. (1999). Fossil plants and global warming at the Triassic-Jurassic boundary. Science 285, 1386-1390.

McElwain, J.C., Murphy, J.W., Hesselbo, S.P. (2005). Changes in carbon dioxide during an oceanic anoxic event linked to intrusion of Gondwana coals. Nature 435, 479-483.

McHone, J.G. (2003). Volatile Emissions from Central Atlantic Magmatic Province Basalts: Mass Assumptions and Environmental Consequences. In: Hames, W.E., McHone, J.G., Ruppel, C., Renne, P. (Eds.), The Central Atlantic Magmatic Province. American Geophysical Union Monograph, pp 136: 267.

Minor, D.R., Mukasa, S.B. (1997). Zircon U-Pb and hornblende ^{40}Ar-^{39}Ar ages for the Dufek layered mafic intrusion, Antarctica: Implications for the age of the Ferrar large igneous province. Geochimica and Cosmochimica Acta 61, 2497-2504.

Missoni, S., Gawlick, H.-J. (2011). Evidence for Jurassic subduction from the Northern Calcareous Alps (Berchtesgaden; Austroalpine, Germany). International Journal of Earth Sciences 100, 1605-1631.

Mohn, G., Manatschal, G., Müntener, O., Beltrando, M., Masini, E. (2010). Unravelling the interaction between tectonic and sedimentary processes during lithospheric thinning in the Alpine Tethys margins. Int. J. Earth Sci. (Geol. Rundsch.) 99, 75-101.

Morard, A., Guex, J., Bartolini, A., Morettini, E., De Wever, P. (2003). A new scenario for the Domerian-Toarcian transition. Bulletin de la Société géoloique France 174, 351-356.

O'Neil, J.R., Clayton, R.N., Mayeda, T.K. (1969). Oxygen isotope fractionation in divalent metal carbonates. J. Chem. Phys. 51, 5547-5558.

Oschmann, W. (2000). Microbes and black shales. In: Riding, R.E., Awramik, S.M. (Eds.), Microbial Sediments. Springer, Berlin, pp. 137-148.

Ourrison, G, Albrecht, P, Rohmer, M. (1979). The hopanoids: palaeo-chemistry and biochemistry of a group of natural products. Pure and Applied Chemistry 51: 709-729.

Pálfy, J., Smith, P.L. (2000). Synchrony between Early Jurassic extinction, oceanic anoxic event, and the Karoo–Ferrar flood basalt volcanism. Geology 28, 747-750.

Parrish, J.T. (1993). Climate of the supercontinent Pangaea. Journal of Geology 101, 215-233.

Parrish, J.T., Curtis, R.L. (1982). Atmospheric circulation, upwelling, and organic-rich rocks in the Mesozoic and Cenozoic areas. Palaeogeography, Palaeoclimatology, Palaeoecology 40, 31-66.

Pearce, C.R., Cohen, A.S., Coe, A.L., Burton, K.W. (2008). Molybdenum isotope evidence for global ocean anoxia coupled with perturbations to the carbon cycle during the Early Jurassic. Geology 36, 231-234.

Pedersen, T.F., Calvert, S.E. (1990). Anoxia vs. productivity: What controls the formation of organic-carbon-rich sediments and sedimentary rocks? AAPG Bulletin 74, 454-472.

Peters, K.E., Moldowan, J.M., Sundararaman, P. (1990). Effects of hydrous pyrolysis on biomarker thermal maturity parameters: Monterey Phosphatic and Siliceous Members. Organic Geochemistry 15, 249-265.

Peters, K.E., Walters, C.C., Moldowan, J.M. (2005). The Biomarker Guide, Biomarkers and Isotopes in Petroleum Exploration and Earth History, Vol. 1 & 2. Cambridge University Press, New York, NY.

Praus, M., Riegel, W. (1989). Evidence from phytoplanktonic associations for causes of black shale formation in epicontinental seas. N. Jb. Geol. Paläontol. Mh. 11, 671-682.

Price, G.D. (1999). The evidence and implications of polar ice during the Mesozoic. Earth Science Reviews 48, 183-210.

Radke, M., Willsch, H., Welte, D.H. (1980). Preparative hydrocarbon group type determination by automated medium pressure liquid chromatography. Analytical Chemistry 52, 406-411.

Raiswell, R., Berner, R.A. (1985). Pyrite formation in euxinic and semi-euxinic sediments. Am. J. Sci. 285, 710-724.

Raiswell, R., Canfield, D.E., Berner, R.A. (1994). A comparison of iron extraction methods for the determination of degree of pyritisation and the recognition of iron-limited pyrite formation. Chem. Geol. 111, 101-110.

Ratschbacher, L., Dingeldey, C., Miller, C., Hacker, B.R., McWilliams, M.O. (2004). Formation, subduction, and exhumation of Penninic oceanic crust in the Eastern Alps: time constraints from $^{40}Ar/^{39}Ar$ geochronology. Tectonophysics 394, 155-170.

Riegraf, W., Werner, G., Lörcher, F. (1984). Der Posidonienschiefer: Biostratigraphie, Fauna und Fazies des südwestdeutschen Untertoarciums (Lias ε). Enke. pp. 195.

Riegraf, W. (1985). Mikrofauna, Biostratigraphie und Fazies im Unteren Toarcium Südwestdeutschlands und Vergleiche mit benachbarten Gebieten. Tübinger Mikropaläontologische Mitteilungen 3, pp. 232.

Rimmer, S.M., Thompson, J.A., Goodnight, S.A., Robl, T.L. (2004). Multiple controls on the preservation of organic matter in Devonian-Mississippian marine black shales: geochemical and petrographic evidence. Palaeogeography, Palaeoclimatology, Palaeoecology 215, 125-154.

Robinson, N., Eglinton, G., Brassell, S.C., Cranwell, P.A. (1984). Dinoflagellate origin for sedimentary 4α-methylsteroids and 5α(H)-stanols. Nature 308, 439-442.

Röhl, H.J., Schmid-Röhl, A., Oschmann, W., Frimmel, A., Schwark, L. (2001). The Posidonia Shale (Lower Toarcian) of SW-Germany: an oxygen-depleted ecosystem controlled by sea level and palaeoclimate. Palaeogeography, Palaeoclimatology, Palaeoecology 165, 27-52.

Rohmer, M., Bisseret, P., Neunlist, S. (1992). The hopanoids, prokaryotic triterpenoids and precursors of ubiquitous molecular fossils. In: Moldowan, J.M., Albrecht, P., Philp, R.P. (Eds.), Biological Markers in Sediments and Petroleum. Prentice Hall, Englewood Cliffs, N.J, pp. 1-17.

Rullkötter, J., Wendisch, D. (1982). Microbial alteration of 17α(H) hopanes in Madagascar asphalts: removal of C-10 methyl group and ring opening. Geochim. Cosmochim. Acta 41, 1341-1353.

Sabatino, N., Neri, R., Bellanca, A., Jenkyns, H.C., Baudin, F., Parisi, G., Masetti, D. (2009). Carbon-isotope records of the Early Jurassic (Toarcian) Oceanic Anoxic Event from the Valdorbia (Umbria-Marche Apennines) and Monte Mangart (Julian Alps) sections: palaeoceanographic and stratigraphic implications. Sedimentology 56, 1307-1328.

Sabatino, N., Vlahović, I., Jenkyns, H.C., Scopelliti, G., Neri, R., Prtoljan, B., Velić, I. (2013). Carbon-isotope record and palaeoenvironmental changes during the early Toarcian oceanic anoxic event in shallow-marine carbonates of the Adriatic Carbonate Platform in Croatia. Geological Magazine 150, Issue 6, 1085-1102.

Sælen, G., Doyle, P., Talbot, M.R. (1996). Stable-isotope analysis of belemnite rostra from the Whitby Mudstone Fm., England: Surface water conditions during deposition of a marine black shale. Palaios 11, 97-117.

Schlager, W., Schöllnberger, W. (1973). Das Prinzip stratigraphischer Wenden in der Schichtfolge der Nördlichen Kalkalpen. Mitt. Geol. Ges. Wien 66, 166-193.

Schmid-Röhl, A., Röhl, H.-J., Oschmann, W., Frimmel, A., Schwark, L. (2002). Palaeoenvironmental reconstruction of Lower Toarcian epicontinental black shales (Posidonia Shale, SW Germany): global versus regional control. Geobios 35, 13-20.

Schwark L., Vliex, M., Schaeffer, P. (1998). Geochemical characterization of Malm Zeta laminated carbonates from the Franconian Alb, SW Germany (II). Organic geochemistry 29, No. 8, 1921-1952.

Schwark, L., Frimmel, A. (2004). Chemostratigraphy of the Posidonia Black Shale, SW Germany II. Assessment of extent and persistence of photic-zone anoxia using aryl isoprenoids distributions. Chem. Geol. 206, 231-248.

Sell, B., Ovtcharova, M., Guex, J., Bartolini, A., Jourdan, F., Spangenberg, J.E., Vicente, J.-C., Schaltegger, U. (2014). Evaluating the temporal link between the Karoo LIP and climatic-biologic events of the Toarcian Stage with high-precision U-Pb geochronology. Earth and Planetary Science Letters 408, 48-56.

Sinninghe Damsté, J.S., Kock-Van Dalen, A.C., de Leeuw, J.W., Schenk, P.A., Guoying, S., Brassell, S.C. (1987). The identification of mono-, di-, and trimethyl 2-methyl-2-(4,8,12-trimethyltridecyl)chromans and their occurrence in geosphere. Geochimica et Cosmochimica Acta 51, 2393-2400.

Sinninghe Damsté, J.S., van Duin, A.C.T., Hollander, D., Kohnen, M.E.L., de Leeuw, J.W. (1995). Early diagenesis of bacteriohopanepolyol derivatives: Formation of fossil homohopanoids. Geochimica et Cosmochimica Acta 59, 5141-5156.

Spieler, A., Brandner, R. (1989). Vom jurassischen Pull-Apart Becken zur Westüberschiebung der Achentaler Schubmasse (Tirol, Österreich). Geol. Paläont. Mitt. Innsbruck 16, 191-194.

Suan, G., Pittet, B., Bour, I., Mattioli, E., Duarte, L.V., Mailliot, S. (2008). Duration of the Early Toarcian carbon isotope excursion deduced from spectral analysis: consequence for its possible causes. Earth Planet. Sci. Lett. 267, 666-679.

Summons, R.E., Powell, T.G. (1986). Chlorobiaceae in Palaeozoic seas revealed by biological markers, isotopes and geology. Nature 319, 763-765.

Svensen, H., Planke, S., Chevalier, L., Malthe-Sørensen, A., Corfu, F., Jamveit, B. (2007). Hydrothermal venting of greenhouse gases triggering Early Jurassic global warming. Earth and Planetary Science Letters 256, 554-566.

Svensen, H., Corfu, F., Polteau, S., Hammer, Ø., Planke, S. (2012). Rapid magma emplacement in the Karoo Large Igneous Province. Earth Planet. Sci. Lett. 325–326, 1–9.

Taylor, G.H., Teichmüller, M., Davis, A., Diessel, C.F.K., Littke, R., Robert, P. (1998). Organic Petrology, Gebr. Borntraeger, Berlin & Stuttgart, 704 p.

ten Haven, H.L., de Leeuw, J.W., Peakman, T.M., Maxwell, J.R. (1986). Anomalies in steroid and hopanoid maturity indices. Geochimica et Chosmochimica Acta 50, 853-855.

ten Haven, H.L., de Leeuw, J.W., Rullkötter, J., Sinninghe Damsté, J.S. (1987). Restricted utility of the pristane / phytane ratio as a palaeoenvironmental indicator. Nature 330, 641-643.

ten Haven, H.L., de Leeuw, J.W., Schenk, P.A. (1985). Organic geochemical studies of a Messinian evaporitic basin, northern Appenines (Italy): Hydrocarbon biological markers for a hypersaline environment. Geochim. Cosmochim. Acta 49, 2181-2191.

Thomas, H., Schiettecatte, L.-S., Suykens, K., Kone, Y.J.M., Shadwick, E.H., Prowe, A.E.F., Bozec, Y., de Baar, H.J.W., Borges, A.V. (2008). Enhanced ocean carbon storage from anaerobic alkalinity generation in coastal sediments. Biogeosciences Discuss. 5, 3575-3591.

Tissot, B.T., Welte, D.H. (1984). Petroleum Formation and Occurrences, Second Ed. Springer-Verlag, Berlin. pp. 699.

Tollmann, A. (1976). Analyse des klassischen nordalpinen Mesozoikums. Stratigraphie, Fauna und Fazies der Nördlichen Kalkalpen. Deuticke, Wien, pp. 580.

Tollmann, A. (1985). Geologie von Österreich, Band 2. Deuticke, Wien, pp. 718.

Tsikos, H., Jenkyns, H.C., Walsworth-Bell, B., Petrizzo, M.R., Forster, A., Kolonic, S., Erba, E., Premoli Silva, I., Baas, M., Wagner, T., Sinninghe Damsté, J.S. (2004). Carbon-isotope stratigraphy recorded by the Cenomanian–Turonian Oceanic Anoxic Event: correlation and implications based on three key localities. J. Geol. Soc. Lond. 161, 711-719

Tyson, R.V. (1995). Sedimentary Organic Matter - Organic Facies and Palynofacies. Chapman and Hall, London.

van de Schootbrugge, B., McArthur, J.M., Bailey, T.R., Rosenthal, Y., Wright, J.D., Miller, K.G. (2005). Toarcian anoxic event: An assessment of global using belemnite C isotope records. Paleoceanography 20, PA3008, doi:10.1029/2004PA001102.

Vlahović, I., Tišljar, J., Velić, I., Matičec, D. (2005). Evolution of the Adriatic Carbonate Platform: Palaeogeography, main events and depositional dynamics. Palaeogeography, Palaeoclimatology, Palaeoecology 220, 333-360.

Volkman, J.K., Maxwell, J.R. (1986). Acyclic isoprenoids as biological markers. In: Johns, R.B. (Eds.), Biological Markers in the Sedimentary Record. Elsevier, Amsterdam, pp. 1-42.

Volkman, J.K., Kearney, P., Jeffrey, S.W. (1990). A new source of 4-methyl steroids and 5α(H)-stanols in sediments: prymnesiophyte microalgae of the genus Pavlova. Organic Geochemistry 15, 489-497.

Volkman, J.K., Barrett, S.M., Blackburn, S.I. (1999). Eustigmatophyte microalgae are potential sources of C_{29} sterols, C_{22}-C_{28} n-alcohols and C_{28}-C_{32} n-alkyl diols in freshwater environments. Organic Geochemistry 30, 307-318.

Vortisch, W. (1982). Clay mineralogical studies of some tills in northern Germany. Geologica et Palaeontologica 15, 167-192.

Watson, J.S., Jolley, D.W., Kelly, S.P. (2009). High concentration of 28,30-bisnorhopane and 25,28,30-trisnorhopane at the PETM in the Faroe-Shetland basin. In: 24th International Meeting on Organic Geochemistry, 6-11 September 2009. Bremen, Germany.

Weissert, H. (2000). Deciphering methane's fingerprint. Nature 406, 356-357.

Weissert, H. (2013). C-isotope geochemistry – tool for chemostratigraphy and carbon cycle history. Ciencias da terra 18.

Whiteside, J.H., Olsen, P.E., Kent, D.V., Fowell, S.J., Et-Touhami, M. (2007). Synchrony between the Central Atlantic magmatic province and the Triassic-Jurassic mass extinction event? Palaeogeography, Palaeoclimatology, Palaeoecology 244, 345-367.

Wignall, P.B., Newton, R.J., Little, C.T.S. (2005). The timing of paleoenvironmental change and cause-and-effect relationships during the Early Jurassic mass extinction. Europ. American Journal of Science 305, 1014-1032.

7.9 Appendix: Full data set for samples of the Bächental section

Table 7.9.1: Bulk geochemical data for samples of Bächental section.

Sample	Diag. carb. *[peak area]*	TOC *[%]*	Cc_e^q *[%]*	S *[%]*	HI *[mg HC/g TOC]*	Fe *[%]*	$\delta^{13}C_{carb}$ *[‰ VPDB]*	$\delta^{18}O_{carb}$ *[‰ VPDB]*	$\delta^{13}C_{org}$ *[‰ VPDB]*
BT 68	-	0.1	81.5	0.1	-	0.2	-0.1	-2.1	-26.7
BT 67	-	0.2	43.6	0.0	-	0.8	0.2	-3.9	-25.6
BT 66	-	0.3	29.9	0.0	-	2.6	0.1	-5.0	-26.3
BT 65	-	0.3	35.8	0.0	-	1.5	-0.7	-4.9	-26.0
BT 64	-	0.1	82.2	0.1	-	0.	-0.1	-1.9	-27.1
BT 63	-	0.4	40.4	0.4	-	0.6	-0.8	-4.2	-29.4
BT 62	-	0.1	71.1	0.2	-	-	-0.8	-1.8	-27.6
BT 61	-	0.3	43.4	0.1	-	0.6	-0.8	-4.0	-25.9
BT 60	-	0.3	49.6	0.2	-	0.4	-0.7	-3.5	-26.1
BT 59	-	0.1	78.4	0.1	-	-	-0.6	-2.0	-
BT 58	4990	2.8	23.2	5.4	544	4.7	-2.6	-4.4	-31.6
BT 57	5080	3.0	22.8	5.8	541	6.1	-2.2	-4.2	-31.6
BT 56	17590	2.1	50.8	3.4	541	3.7	-5.8	-3.6	-30.6
BT 55	6250	1.6	33.3	3.2	503	-	-6.0	-3.8	-
BT 54	17560	1.5	53.3	5.0	375	1.4	-7.2	-3.5	-26.4
BT 53	14040	1.6	47.1	5.7	415	4.	-5.6	-3.2	-31.1
BT 52	18680	1.7	52.0	5.0	419	4.0	-10.8	-3.1	-31.2
BT 51	21260	1.5	55.4	2.1	362	3.4	-12.7	-3.0	-30.9
BT 50	14960	1.6	56.7	1.3	325	4.9	-5.2	-2.1	-31.1
BT 49	16860	1.7	52.9	2.6	292	-	-6.9	-2.8	-
BT 48	16510	2.1	51.0	2.5	379	3.9	-7.3	-3.3	-31.1
BT 47	16900	1.6	60.7	2.0	320	5.3	-8.6	-2.3	-31.1
BT 46	15200	1.5	64.8	1.9	370	3.2	-7.9	-2.4	-
BT 45	14100	1.5	56.9	2.6	400	5.2	-8.3	-2.5	-31.1
BT 44	15990	1.9	48.6	5.3	350	5.4	-8.7	-2.7	-31.0
BT 43	-	0.1	82.6	0.2	-	0.9	0.8	-1.4	-28.7
BT 42	-	0.1	90.8	0.0	-	0.6	-0.2	-1.4	-29.0
BT 41	-	0.1	89.5	0.1	-	0.8	-0.2	-2.3	-30.1
BT 40	7830	3.0	36.9	3.5	604	3.5	-2.5	-3.8	-30.6
BT 39	2630	5.6	38.8	5.1	683	1.1	-1.5	-4.0	-30.9
BT 38	2690	5.6	32.3	5.3	661	1.9	-4.2	-4.7	-32.1
BT 37	3370	6.3	18.6	4.4	622	5.2	-1.8	-5.1	-32.7
BT 36	1170	2.9	35.2	5.9	572	3.9	-2.7	-4.3	-30.9
BT 35	710	9.4	56.0	2.1	666	1.5	-2.1	-3.9	-32.0
BT 34	2040	8.0	43.1	2.6	644	0.3	-2.9	-4.6	-31.1
BT 33	2430	3.6	33.9	2.6	670	3.2	-2.4	-4.4	-30.6
BT 32	2400	4.0	27.1	7.0	602	6.1	-2.4	-4.4	-31.2

BT 31	470	5.4	58.8	1.3	687	1.0	-2.0	-3.2	-31.1

Sample	**Diag. carb.** *[peak area]*	**TOC** *[%]*	**Cc_e** ^{q} *[%]*	**S** *[%]*	**HI** *[mg HC/g TOC]*	**Fe** *[%]*	**$\delta^{13}C_{carb}$** *[‰ VPDB]*	**$\delta^{18}O_{carb}$** *[‰ VPDB]*	**$\delta^{13}C_{org}$** *[‰ VPDB]*
BT 30	2840	2.9	17.4	4.3	604	4.3	-2.9	-5.2	-32.1
BT 29	740	6.8	60.7	1.6	686	1.2	-1.9	-3.8	-31.6
BT 28	2520	3.5	29.2	7.1	588	6.0	-2.8	-4.1	-31.7
BT 27	3070	6.0	36.8	2.8	670	-	-2.9	-5.1	-
BT 26	2830	7.6	37.9	3.0	653	0.1	-3.0	-4.8	-31.5
BT 25	580	12.9	27.2	2.9	622	0.5	-2.6	-6.0	-32.1
BT 24	1830	11.7	30.7	2.8	621	0.5	-2.6	-5.9	-31.7
BT 23	1360	9.0	31.1	2.7	649	2.6	-2.9	-5.3	-31.8
BT 22	260	8.6	38.0	3.2	645	0.2	-3.0	-5.4	-32.2
BT 21	13460	1.8	43.6	4.2	519	3.5	-6.3	-3.7	-31.0
BT 20	12720	2.0	40.0	4.3	495	3.6	-6.2	-3.6	-31.1
BT 19	4280	3.3	31.0	5.6	612	4.0	-4.0	-4.0	-32.0
BT 18	2200	2.5	32.1	2.2	577	3.3	-1.8	-3.9	-31.0
BT 17	12060	1.8	42.2	4.3	537	4.2	-6.9	-3.6	-31.5
BT 16	11350	2.3	34.6	3.8	497	4.4	-6.3	-3.4	-31.6
BT 15	4940	1.9	30.7	5.5	427	5.2	-6.1	-3.4	-31.7
BT 14	11630	1.4	39.6	5.7	306	3.5	-10.0	-3.5	-31.5
BT 13	7750	1.1	43.4	3.6	307	9.2	-4.7	-2.3	-31.6
BT 12	3820	2.2	24.4	5.3	518	4.2	-3.2	-3.9	-32.0
BT 11	13820	1.8	34.1	3.7	441	4.8	-6.9	-3.8	-32.0
BT 10	13750	1.8	31.2	5.5	452	5.2	-8.7	-3.5	-31.7
BT 9	12200	1.6	32.9	5.4	459	4.8	-9.8	-3.6	-31.6
BT 8	-	1.8	0.6	0.1	37	11.7	-26.0	-24.3	-
BT 7	-	1.8	1.0	0.1	74	21.9	-23.5	-22.9	-28.7
BT 6	-	0.1	87.5	1.1	-	0.3	1.5	-1.4	-23.6
BT 5	-	0.1	89.8	0.1	-	0.0	0.9	-1.4	-26.9
BT 4	-	0.1	76.2	0.1	-	0.0	0.8	-2.3	-25.8
BT 3	-	0.1	84.2	0.5	-	0.0	1.0	-1.6	-27.4
BT 2	-	0.1	80.4	0.1	-	0.0	1.0	-1.6	-26.3
BT 1	-	0.1	90.2	0.0	-	-	1.4	-1.2	-

Table 7.9.2: Organic geochemical data for investigated bituminous marls of Bächental section.

Sample	*n*-C_{15-19}/ Σ*n*-alkanes *[rel. prop.]*	*n*-C_{27-31}/ Σ*n*-alkanes *[rel. prop.]*	Pr/Ph *[conc. ratios]*	C_{27}/C_{29} ααα*R* Steranes *[conc. ratios]*	C_{27}/C_{29} Steranes *[conc. ratios]*	4-Methylsteranes/ C_{29} Steranes *[conc. ratios]*
BT58	0.30	0.16	1.39	0.59	0.59	0.74
BT 55	0.30	0.16	1.76	0.76	1.03	1.00
BT 50	0.33	0.15	1.73	0.62	0.88	0.92
BT 45	0.34	0.15	1.59	0.66	0.91	1.08
BT 44	0.31	0.16	0.88	0.70	0.76	2.55
BT 40	0.34	0.16	1.30	0.75	1.01	1.34
BT 39	0.22	0.20	0.92	0.81	1.10	1.68
BT 37	0.32	0.15	1.06	0.56	0.77	1.16
BT 36	0.24	0.19	0.89	0.75	0.97	1.04
BT 35	0.56	0.02	0.93	0.56	0.57	3.10
BT 33	0.30	0.16	0.73	0.73	0.95	1.81
BT 31	0.35	0.13	0.76	0.60	0.77	2.80
BT 30	0.25	0.22	0.76	0.54	0.68	1.50
BT 29	0.39	0.11	0.78	0.51	0.62	2.89
BT 28	0.34	0.15	0.70	0.56	0.77	2.14
BT 26	0.34	0.13	0.76	0.57	0.68	2.90
BT 25	0.52	0.09	1.01	0.52	0.58	3.22
BT 24	0.32	0.21	0.86	0.57	0.64	3.06
BT 23	0.23	0.32	0.82	0.50	0.57	2.39
BT 22	0.31	0.17	0.80	0.50	0.59	2.79
BT 20	0.34	0.17	1.33	0.60	0.83	1.72
BT 18	0.27	0.16	1.35	0.91	1.24	1.95
BT 15	0.33	0.16	1.80	0.74	0.97	0.89
BT 12	0.30	0.16	0.96	0.69	0.79	2.24
BT 10	0.31	0.18	1.08	0.60	0.79	1.56
BT 8	0.23	0.24	0.94	0.59	0.70	2.10

Table 7.9.3: Organic geochemical data for investigated bituminous marls of Bächental section.

Sample	Mono-/triaromatic Steroids *[conc. ratios]*	Steranes [S/(S+R)] *[conc. ratios]*	DBT/Phen *[conc. ratios]*	Gammacerane Index *[conc. ratios]*	Hopanes [S/(S+R)] *[conc. ratios]*	Aryl-Isoprenoids *[µg/g TOC]*
BT 58	3.39	0.11	0.32	0.07	0.80	107.65
BT 55	3.41	0.10	0.23	0.05	0.73	52.76
BT 50	3.16	0.12	0.30	0.12	0.92	37.93
BT 45	2.68	0.11	0.48	0.16	0.93	25.00
BT 44	1.64	0.32	0.46	0.59	1.16	112.14
BT 40	3.15	0.12	0.48	0.17	0.80	52.61
BT 39	2.98	0.12	0.46	0.16	0.77	62.17
BT 37	2.94	0.11	0.49	0.09	0.78	5.76
BT 36	2.55	0.14	0.60	0.14	0.91	69.93
BT 35	1.48	0.23	0.75	0.80	1.33	33.65
BT 33	2.17	0.29	0.69	0.41	1.0	54.14
BT 31	1.34	0.31	0.76	0.63	1.43	15.54
BT 30	1.74	0.30	0.78	0.27	1.27	28.82
BT 29	1.29	0.32	0.83	0.77	1.72	10.92
BT 28	1.61	0.31	0.78	0.39	1.35	10.03
BT 26	1.31	0.33	0.75	0.71	1.42	9.31
BT 25	1.33	0.25	0.78	0.77	1.28	84.01
BT 24	1.41	0.32	0.72	0.72	1.25	21.20
BT 23	1.54	0.28	0.64	0.55	1.21	15.59
BT 22	1.25	0.28	0.78	0.75	1.46	9.63
BT 20	2.91	0.11	0.46	0.13	0.79	27.82
BT 18	3.81	0.18	0.23	0.15	0.81	8.01
BT 15	3.78	0.11	0.25	0.05	0.77	3.15
BT 12	2.07	0.27	0.29	0.53	1.01	22.88
BT 10	2.06	0.16	0.33	0.37	0.99	13.31
BT 8	1.68	0.23	0.38	0.58	1.11	1.26

8 Redox conditions and depositional environment of the Lower Jurassic Bächental bituminous marls (Tyrol, Austria)

Accepted for publication in the Austrian Journal of Earth Science, issue December 2016.

S. Neumeister [a,*], T. J. Algeo [b], A. Bechtel [a], H.-J. Gawlick [a], R. Gratzer [a], R. F. Sachsenhofer [a]

[a] *Department of Applied Geosciences and Geophysics, Montanuniversitaet Leoben, Peter-Tunner-Str. 5, A-8700 Leoben, Austria*

[b] *Department of Geology, University of Cincinnati, Cincinnati, OH 45221, USA*

* Corresponding author.

E-mail address: st.neumeister@hotmail.com (Stefan Neumeister)

Abstract

A suite of trace elements (TEs) characterized by an affinity to reducing environments, including molybdenum (Mo), uranium (U), vanadium (V), copper (Cu), and nickel (Ni), were used to investigate secular variations in environmental redox conditions during deposition of the Bächental bituminous marls (Bächentaler Bitumenmergel). These marls, which belong to the Sachrang Member of the Lower Jurassic Middle Allgäu Formation in the Northern Calcareous Alps, are subdivided on the basis of Al-normalized TE concentrations and concentration ratios into three units that correspond to major shifts in depositional redox conditions. The lower and upper units (Units 1 and 3, respectively) were deposited under suboxic to transiently anoxic conditions. The removal of TEs to the sediment was connected to siliciclastic input, diagenetic processes, and organic-matter accumulation in the sediment. In contrast, the middle unit (Unit 2) was characterized by intense anoxia as reflected in strong TE enrichments and peak total organic carbon (TOC) contents up to 13 %. Enrichment of TEs was linked mainly to adsorption onto organic matter in Unit 2, reflecting control of TE enrichment by the availability of an organic substrate. Comparison of inorganic and organic (e.g., pristane/phytane ratio, gammacerane index) geochemical proxies for environmental

conditions permits detection of periods with elevated surface-water bioproductivity. A flourishing of algal and planktonic organisms contributed to the significant increase of TOC content at the base of Unit 2. This increase corresponds to the time-equivalent early Toarcian oceanic anoxic event characterized by the global occurrence of organic-rich sediments.

Eine Auswahl an Spurenelementen (Mo, U, V, Cu, Ni), charakterisiert durch ihre Affinität zu reduzierenden Milieus, wurde verwendet um Variationen der vorherrschenden Redoxbedingungen während der Ablagerung der unterjurassischen Bächentaler Bitumenmergel (Sachrang-Member der Mittleren Allgäu-Formation in den Nördlichen Kalkalpen) zu untersuchen. Die Bitumenmergelabfolge wurde auf Basis dieser Spurenelementdaten in drei Einheiten unterteilt. Anorganisch-geochemische Parameter reflektieren wechselnde Umweltbedingungen während der Ablagerung der Bitumenmergel. Der untere und der obere Bereich (Units 1 und 3) der Bächental Bitumenmergel wurden unter suboxischen bis teils anoxischen Bedingungen abgelagert. Die Anreicherung der Spurenelemente im Sediment erfolgte durch siliziklastischen Eintrag, diagenetische Prozesse und Akkumulation von organischem Material. Maximalgehalte an Spurenelementen und von organischem Detritus (bis zu 13 %) bestätigen durchgehend anoxische Bedingungen während der Ablagerung des Mittelteils des Profils (Unit 2). Die Fixierung der Spurenelemente im Sediment erfolgte in diesem Bereich ausschließlich durch Adsorption an organischem Material. Folglich war die Verfügbarkeit von organischem Material der limitierende Faktor für die Spurenelementanreicherung. Der Vergleich der anorganisch-geochemischen und organisch-geochemischen (Pristan/Phytan-Verhältnis, Gammaceran Index) Parameter ermöglicht die Identifizierung von Perioden mit erhöhter Bioproduktivität. Demnach hat ein Aufblühen von algalen und planktonischen Organismen zu den signifikant hohen Gehalten an organischem Material an der Basis von Unit 2 beigetragen. Dieses Intervall entspricht dem Zeitraum des ozeanischen anoxischen Ereignisses des Unteren Toarciums, welches durch weltweites Auftreten von organisch-reichen Sedimenten charakterisiert wird.

Keywords: Sachrang Member; Northern Calcareous Alps; oceanic anoxic event; trace elements; bioproductivity

8.1 Introduction

The Lower Toarcian is characterized by the global occurrence of marine deposits containing elevated contents of organic matter (OM; e.g., Jenkyns, 1985, 1988; Jenkyns et al., 2002; Pearce et al., 2008). However, the main factors controlling the production and the preservation of OM in these units remain controversial. The Early Jurassic was an interval of climatic warming and major perturbations of the global carbon cycle triggered by massive volcanic eruptions of the Central Atlantic Magmatic Province (CAMP; Marzoli et al., 1999; Whiteside et al., 2007) and the Karroo-Ferrar large igneous province (Encarnación et al., 1996; Minor and Mukasa, 1997; Svensen et al., 2007, 2012; Sell et al., 2014). Emission of greenhouse gases during these eruptions resulted in "greenhouse Earth" conditions by the early Toarcian (Pálfy and Smith, 2000; Weissert, 2000; Jenkyns, 2003). Attendant climate changes included an acceleration of the hydrological cycle and an increase of continental weathering. These global perturbations induced a flourishing of oceanic bioproductivity caused by an increased supply of nutrients to surface waters as well as the establishment of conditions favoring the development of anoxia and deposition of black shales (Parrish and Curtis, 1982; Parrish, 1993; Cohen et al., 2004). The accumulation of OM-rich deposits has been attributed to (1) upwelling connected with an oceanic anoxic event (T-OAE; Jenkyns, 1985, 1988; see summary in Jenkyns, 2010), (2) a surface-water layer with reduced salinity that caused intensified water-column stratification in epicontinental areas of the western Tethyan realm (Praus and Riegel, 1989; Littke et al., 1991; Sælen et al., 1996), and (3) minor sea-level fluctuations that controlled watermass exchange and, hence, dissolved oxygen levels in semi-restricted basins within the western European epicontinental sea located on the northern side of the Alpine Atlantic (Röhl et al., 2001; Schmid-Röhl et al., 2002; Frimmel et al., 2004). The latter model can also be adapted to the southern side of the Alpine Atlantic, i.e., the "Lower Austroalpine margin" (Fig. 8.1). For any of these mechanisms, short-term variation in OM accumulation may have been modulated by orbital forcings (Ikeda and Hori, 2014).

Redox variation is a key feature of any depositional system that influences the accumulation/formation of OM, TEs, and diagenetic phases. There are several methods for assessing paleoredox variation including organic geochemistry [e.g., pristane/phytane ratio (Pr/Ph), aryl isoprenoids], microscopy (e.g., bioturbation, benthic biofacies), bulk parameters [e.g., relationships between total organic carbon and sulfur (TOC/S), ternary diagram of TOC,

iron (Fe), and S], and inorganic geochemical data [e.g., trace element (TE) concentrations, TE ratios]. TEs show low background concentrations only under oxic to weakly suboxic conditions, with authigenic enrichment associated with more reducing conditions (e.g., Piper and Calvert, 2009). This provides the basis for utilization of TE enrichment patterns for paleoredox analysis (e.g., Dean et al., 1999; Tribovillard et al., 2006; Algeo and Tribovillard, 2009). Several of these redox-sensitive elements (including Mo, U, V, Cu, and Ni) show an affinity to anoxic to euxinic paleoenvironments ("euxinic affinity"; e.g., Algeo and Maynard, 2004; Brumsack, 2006; Tribovillard et al., 2006; Piper and Calvert, 2009), as confirmed by TE data from modern euxinic environments (e.g., Dean et al., 1999; Yarincik et al., 2000; Morford et al., 2001).

The Bächentaler Bitumenmergel consists of a 24-m-thick succession of bituminous marls in the Bächental valley of Tyrol in the Northern Calcareous Alps (Figs. 8.1A, 8.2). Neumeister et al. (2015) investigated controls on OM accumulation in the semi-restricted Bächental basin using a multidisciplinary approach based on microscopy, X-ray diffraction (XRD), bulk geochemistry, stable isotopy, and organic geochemistry. They identified influences on OM accumulation operating on both global (e.g., magmatism, opening of the Alpine Atlantic Ocean) and local scales (e.g., basin morphology, salinity variations). Significant secular variation in TOC (1.1-12.9 %) was induced by paleoenvironmental changes within the Bächental basin, including watermass redox state. Redox variations are clearly reflected by activity of sedimentologic (lamination-bioturbation) and organic geochemical proxies (e.g., Pr/Ph ratios, gammacerane index) in the study section. Neumeister et al. (2015) also established a stratigraphic correlation of time-equivalent OM-enriched sediments between the Alpine realm (i.e., Bächental basin) and western European epicontinental settings.

The Bächentaler Bitumenmergel succession provides an excellent opportunity to compare other proxies such as redox-sensitive TEs with the redox interpretations previously generated on the basis of sedimentologic and organic geochemical data (Neumeister et al., 2015). The goal of the present study, therefore, is to evaluate the utility of multiple redox-sensitive TEs as proxies for watermass redox conditions in a carbonate-dominated basinal setting subjected to a complex set of environmental, depositional, and diagenetic factors. In this study, we focus on the elements Mo, U, V, Cu, and Ni, which are commonly strongly enriched under reducing conditions and generally little affected by post-depositional

remobilization (e.g., Tribovillard et al., 2006). Moreover, the application of a suite of TEs provides the possibility for identification of common trends and of irregularities and perturbations possibly related to authigenic uptake of a single TE.

8.2 Geological setting

The geological setting of the Bächental section, which is well exposed in an open-pit mine, was recently described by Neumeister et al. (2015) and is briefly summarized here. The investigated section is situated in the Bächental valley, which is part of the Karwendel Mountains in western Austria (Fig. 8.1A; GPS: 47°30'31.38"N; 11°37'46.00"E). In this area, lithostratigraphic units of Triassic to Jurassic age belonging to the Lechtal nappe of the Bavaric Unit, a tectonic domain of the Northern Calcareous Alps, are exposed.

In the late Early Jurassic, the study area was situated on the northwestern continental margin of the Neotethys Ocean and the southeastern newly formed passive margin of the Alpine Atlantic (Figs. 8.1B, C). This area was affected by extensional tectonics, related to late Hettangian rifting and Toarcian oceanic break-up in the Alpine Atlantic (Penninic) realm (e.g., Ratschbacher et al., 2004), which resulted in formation of synrift basins such as the Bächental basin. The final configuration of the roughly north-south-trending Bächental basin developed during late Hettangian to Sinemurian time (Schlager and Schöllnberger, 1973). The basin exhibits tilt-block tectonics and antithetic step faults, producing a half-graben geometry with a depocenter in its northern part (Spieler and Brandner, 1989). Deposition of bituminous marls during the early Jurassic was limited to the poorly ventilated deepest part (depocenter) of the Bächental basin (Spieler and Brandner, 1989).

The study section has an overall thickness of ~35 m (Fig. 8.2A). It includes at its base the uppermost 4 m of cherty limestones belonging to the Scheibelberg Formation (Sinemurian to Pliensbachian), which were deposited in water depths of several hundred meters at the transition of distal slope to basin. Overlying the bituminous Middle Allgäu Formation (which includes the Bächentaler Bitumenmergel) is an alternating ~6-m-thick succession of limestone and marl beds belonging to the Upper Allgäu Formation (Spieler and Brandner, 1989).

The Middle Allgäu Formation consists of the 24.90-m-thick Sachrang Member (?late Pliensbachian to early Toarcian; Tollmann, 1976; Ebli, 1991; Ebli et al., 1998; Gawlick et al., 2009; Neumeister et al., 2015; Suan et al., 2016). The Sachrang Member is dominated by the

Bächental bituminous marls although it also contains a 0.25-m-thick basal mudstone and a 1.00-m-thick debrite layer ~17 m above the base of the unit. The basal mudstone, which consists mainly of quartz and clay minerals of terrigenous origin, marks an abrupt change from nearly pure carbonates to OM-rich marls (Neumeister et al., 2015). The presence of charred organic material and expandable smectite minerals argues for a volcaniclastic contribution to the sediment, which potentially may have triggered the onset of OM accumulation in the Bächental basin (Neumeister et al., 2015). Considerable amounts of smectite are present throughout the Sachrang Member, suggesting continued influx of volcaniclastic material.

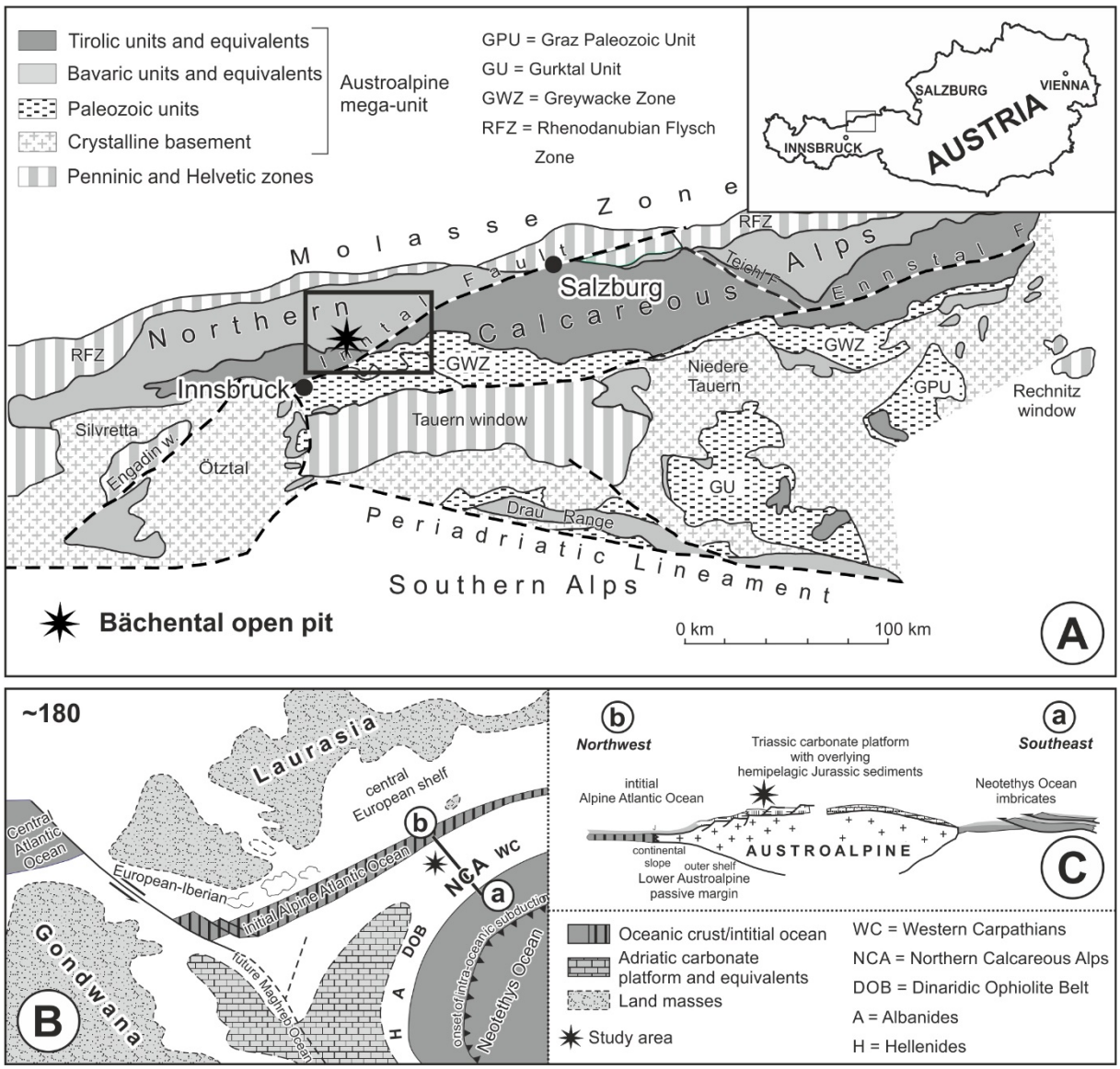

Fig. 8.1: (A) Schematic tectonic map of the Eastern Alps (after Frisch and Gawlick, 2003) with the position of the studied Bächental section. (B) Palaeogeographic position of the study section as part of the Northern Calcareous Alps within the Austroalpine domain in late Early Jurassic time (modified after Gawlick et al., 2009). (C) Schematic cross section (line a-b in B) showing the passive continental margin of the Lower Austroalpine domain (modified after Gawlick et al., 2009). Rifting and spreading of the Alpine Atlantic commencing in the late Early Jurassic affected the Austroalpine domain by the formation of extensional, asymmetric basins exhibiting horst-and-graben structure (cf. Bernoulli and Jenkyns, 1974).

The bituminous marl succession was subdivided into three units on the basis of lithology and bulk geochemical data (Figs. 8.2A, B; Neumeister et al., 2015). According to that study, sedimentologic and geochemical proxies indicate mainly suboxic conditions, although with brief periods of anoxia, during deposition of the lowermost unit (Unit 1). This pattern suggests that the chemocline was generally located at shallow depths below the sediment-water interface. The transition to Subunit 2a was characterized by an abrupt shift to strongly anoxic conditions with the chemocline positioned at or above the sediment-water interface. These conditions developed as a consequence of a sea-level lowstand and a subsequent minor sea-level rise, producing a salinity-stratified water column within a stagnant, low-energy basin in which the deep waters became intensely reducing (Neumeister et al., 2015). In this setting, halophilic microorganisms flourished as a consequence of enhanced salinity, and elevated bioproductivity in the surface waters triggered a high sinking flux of OM that supported the establishment and maintenance of anoxic deep-water conditions. A subsequent sea-level rise re-established ventilation of the deep basin and initiated the frequent influx of carbonate turbidites, gradually weakening deep-water anoxia during deposition of Subunit 2b. Finally, a large debris flow effectively ventilated the basin depocenter and permanently re-established suboxic conditions during deposition of Unit 3. Thus, redox and salinity changes in the Bächental basin were determined mainly by sea-level fluctuations that controlled marginal sill depths and the degree of bottom-water ventilation.

The dating of the Bächental bituminous marls to the Toarcian was originally based on the occurrence of *Harpoceras* sp. (Klebelsberg, 1935). This is consistent with the presence of *Cleviceras exaratum* in the middle part of the section, a taxon associated with the early Toarcian *falciferum* Zone (Neumeister et al., 2015). Kodina et al. (1988) and Lobitzer et al. (1988) inferred that bituminous marl sedimentation began during the late Pliensbachian based

on the occurrence of *Arieticeras* sp. and, possibly, *Leptaleoceras* sp. Neumeister et al. (2015) proposed that the deposition of the Sachrang Member in the Bächental basin lasted from late Pliensbachian (*margaritatus* Zone) to early Toarcian (*bifrons* Zone) based on correlation of C_{27}/C_{29} sterane data from Bächental and Dotternhausen (epicontinental Posidonia Shale) sections with sea level. However, new biostratigraphic data – including the re-examination of the ammonites published by Kodina et al. (1988) – indicate that Units 2 and 3 solely belong to the Lower Toarcian *falciferum*-Zone, whereas data for the basal part of the section is missing (Suan et al., 2016). At its type locality in Bavaria, deposition of the Sachrang Member commenced at the base of the *tenuicostatum* Zone and continued through the entire early Toarcian (Ebli et al., 1998).

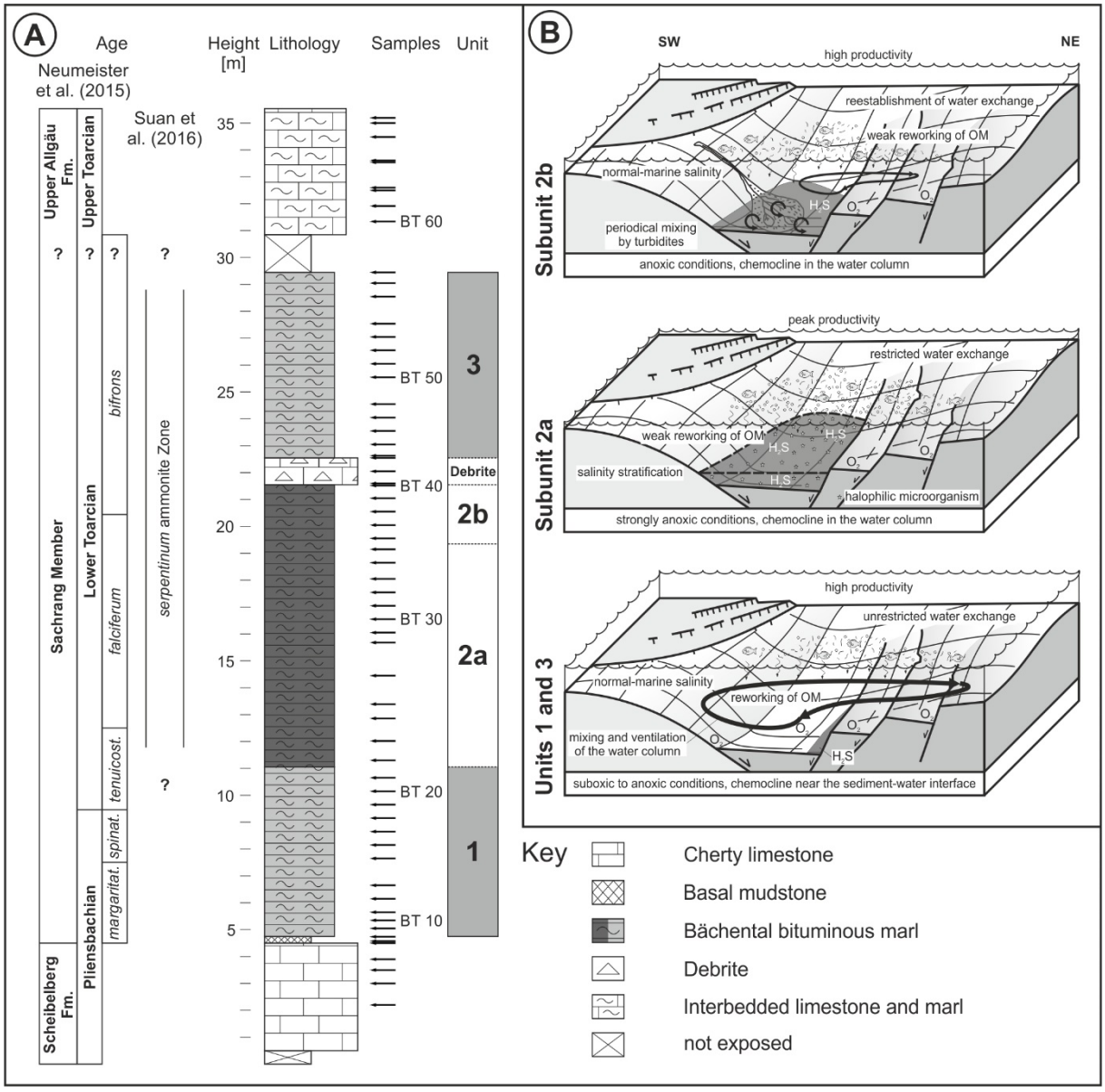

Fig. 8.2: (A) Lithological profile of the investigated Bächental section with positions of samples. Subdivision of the Sachrang Member follows Neumeister et al. (2015). Stratigraphy after Neumeister et al. (2015) and Suan et al. (2016). (B) Depositional environments of the units of the Bächental bituminous marl (after Neumeister et al., 2015). Paleogeographical setting modified after Brandner (2011).

8.3 Samples and analytical methods

A total of 62 samples was collected from fresh exposures in a trench that was excavated up to 4 m deep (Fig. 8.2A). This suite includes five samples from the Scheibelberg Formation (BT 2-6), forty-nine samples from the Sachrang Member (BT 7-13, BT 15-26, BT 28-48, BT 50-54, BT 56-58), and nine samples from the lowermost 5 m of the Upper Allgäu Formation (BT 60-68). Note: discontinuous sample numbers owing to a lack of sample material for XRD measurements for samples BT 1, BT 14, BT 27, BT 49, BT 55, and BT 59.

Major- and trace-element concentrations were determined on whole-rock samples using a wavelength-dispersive Rigaku 3040 X-ray fluorescence (XRF) spectrometer in the University of Cincinnati Department of Geology. Raw intensities were calibrated using a set of 65 standards from the USGS, the National Bureau of Standards, and internal lab standards that were analysed by XRAL Incorporated using XRF and INAA. Analytical precision based on replicate analyses was better than ±2 % for major and minor elements and ±5 % for TEs, and detection limits were 1 to 2 ppm for most TEs.

XRD analysis were carried out on bulk samples using Philips X-pert equipment and CuKα-radiation (1.54 Å, 35 kV, 35 mA). The single scans were operated in spin-mode with a goniometer velocity of ½ °/min in the range from 2 to 65° 2θ in the air-dry state (random powder mount). The individual peaks were identified by the use of standardized tables and by comparison with reference samples.

8.4 Results

In general, all measured TEs (Mo, U, V, Cu, and Ni) show comparable vertical trends (Table 8.1). TE concentrations are typically low in the TOC-poor samples from the Scheibelberg Formation, the Upper Allgäu Formation, and the debrite layer of the Sachrang Member (Mo: 0.0-2.1 ppm; U: 0.0-1.7 ppm; V: 31-75 ppm; Cu: 0.0-29 ppm; Ni: 0.0-48 ppm).

Whereas samples from Units 1 and 3, the basal mudstone, and Subunit 2b feature intermediate TE concentrations (Mo: 0.0-5.5 ppm; U: 0.0-3.5 ppm; V: 43-215 ppm; Cu: 5.9-74 ppm; Ni: 8.3-116 ppm), Subunit 2a is characterized by the highest measured concentrations for all TEs (Mo: 1.1-28 ppm; U: 0.2-3.6 ppm; V: 82-440 ppm; Cu: 28-124 ppm; Ni: 24-64 ppm) except for Ni, which reaches maximum concentrations in the basal mudstone (up to 116 ppm). Peak TE concentrations are generally associated with the TOC-rich lower part of Subunit 2a.

Aluminium (Al) concentrations range between 0.6 % and 6.0 % (Table 8.1). Carbonate-rich samples from the Scheibelberg Formation, the debrite layer (Sachrang Member) and the Upper Allgäu Formation show the lowest concentrations on average (0.6-2.7 %). In contrast, marls from the Upper Allgäu Formation exhibit high Al concentrations (4.0-5.5 %). Whereas samples from the basal mudstone, Unit 1, and Unit 2 of the Sachrang Member feature Al concentrations in a similar range (2.2-6.0 %), Unit 3 is characterized by low and relatively uniform values (2.0-3.5 %), with elevated values occurring only near its top (up to 5.8 %).

Fe data for the Bächental section, based on a multiple-regression method for intensity-concentration correlation commonly used for shales, was previously published by Neumeister et al. (2015). However, re-assessment of the XRF dataset showed that this standard method is inappropriate for carbonate-rich rock samples containing high amounts of manganese (Mn), such as Bächental bituminous marls, resulting in erroneous absolute elemental concentrations although the vertical trends remain the same. Consequently, the revised Fe data is quoted in Table 8.1 even though it is not part of the discussion of the present paper.

Results for TOC, Mn-carbonate content, Pr/Ph ratios, and gammacerane index [GI = gammacerane/(gammacerane + αβ C30 hopane)] were previously reported by Neumeister et al. (2015). The full geochemical dataset is presented in Table 8.1.

Sample	Mo [ppm]	U [ppm]	V [ppm]	Cu [ppm]	Ni [ppm]	Al [%]	Fe [%]	TOC [%]	Mn-rich carbonates [p. a.]	Pr/Ph [conc. ratios]	GI [conc. ratios]
BT 68	1.1	0.7	40.6	4.5	6.2	1.4	0.5	0.1	-	-	-
BT 67	2.1	0.4	65.2	24.0	24.5	4.0	0.9	0.2	-	-	-
BT 66	0.7	1.7	71.5	29.5	48.4	4.9	1.5	0.3	-	-	-
BT 65	B.D.L.	0.9	74.9	28.1	39.5	5.5	1.4	0.3	-	-	-
BT 64	1.5	0.3	31.6	4.8	5.9	1.4	0.4	0.1	-	-	-
BT 63	1.0	0.6	34.2	B.D.L.	B.D.L.	0.6	0.2	0.4	-	-	-
BT 62	1.4	B.D.L.	39.8	5.1	4.2	1.4	0.4	0.1	-	-	-
BT 61	0.8	1.4	64.3	20.9	24.4	4.2	0.9	0.3	-	-	-
BT 60	0.6	1.3	65.9	16.2	25.6	4.3	0.9	0.3	-	-	-
BT 58	3.3	0.4	153.5	73.7	48.4	5.0	4.5	2.8	4990	1.4	0.1
BT 57	3.9	1.8	178.4	73.5	37.3	5.8	4.9	3.0	5080	-	-
BT 56	0.8	0.4	102.1	22.8	12.1	3.0	2.3	2.1	17590	-	-
BT 54	1.8	0.2	43.5	5.9	8.3	2.0	0.5	1.5	17560	-	-
BT 53	0.3	1.5	86.3	13.9	16.1	3.3	3.8	1.6	14040	-	-
BT 52	0.9	0.9	115.7	17.4	16.5	3.4	3.3	1.7	18680	-	-
BT 51	0.4	0.5	84.7	11.1	14.6	2.2	1.7	1.5	21260	-	-
BT 50	0.3	1.5	111.9	12.9	11.8	2.4	2.6	1.6	14960	1.7	0.1
BT 48	0.8	1.8	100.5	21.3	29.6	3.7	2.5	2.1	16510	-	-
BT 47	0.1	1.0	113.2	12.3	14.5	2.6	3.3	1.6	16900	-	-
BT 46	0.3	0.8	101.7	8.6	9.6	2.3	2.5	1.5	15200	-	-
BT 45	0.5	0.7	100.2	13.1	17.5	2.9	3.3	1.5	14100	1.6	0.2
BT 44	0.8	0.1	113.9	15.6	52.2	3.5	4.0	1.9	15990	0.9	0.6
BT 43	0.3	0.7	36.1	3.4	2.4	1.3	0.3	0.1	-	-	-
BT 42	0.8	0.2	31.1	B.D.L.	0.3	0.6	0.2	0.1	-	-	-
BT 41	1.1	0.5	42.2	2.0	3.4	1.2	0.2	0.1	-	-	-
BT 40	1.6	0.3	85.4	30.5	24.5	5.4	2.6	3.0	7830	1.3	0.2
BT 39	1.2	3.5	81.5	35.3	32.3	4.3	3.3	5.6	2630	0.9	0.2
BT 38	4.1	2.5	142.5	45.9	39.4	4.8	3.7	5.6	2690	-	-
BT 37	5.5	2.3	160.2	62.8	45.3	6.0	4.1	6.3	3370	1.1	0.1
BT 36	4.6	0.7	90.6	25.8	20.3	3.2	3.6	2.9	1170	0.9	0.1
BT 35	11.6	3.2	177.6	33.3	38.2	2.7	1.2	9.4	710	0.9	0.8
BT 34	11.1	2.9	217.5	61.3	49.6	3.7	1.6	8.0	2040	-	-
BT 33	1.1	1.4	82.5	40.7	28.8	3.8	1.8	3.6	2430	0.7	0.4
BT 32	4.1	0.7	114.4	37.7	28.5	4.0	5.3	4.0	2400	-	-
BT 31	7.6	2.6	138.2	32.8	29.1	2.6	0.8	5.4	470	0.8	0.6
BT 30	5.1	1.7	172.3	37.3	33.3	3.6	3.1	2.9	2840	0.8	0.3
BT 29	9.5	3.1	187.1	41.7	35.7	2.8	0.9	6.8	740	0.8	0.8
BT 28	3.6	0.2	120.3	27.6	24.2	3.5	4.8	3.5	2520	0.7	0.4
BT 26	9.6	3.6	186.4	53.4	43.9	3.6	1.9	7.6	2830	0.8	0.7
BT 25	27.7	3.6	439.9	123.7	64.1	3.9	2.1	12.9	580	1.0	0.8
BT 24	25.0	3.3	348.2	91.3	56.7	3.3	1.6	11.7	1830	0.9	0.7
BT 23	22.1	1.5	325.1	97.2	50.8	4.1	2.0	9.0	1360	0.8	0.6
BT 22	17.3	1.6	317.4	57.6	52.0	3.6	2.1	8.6	260	0.8	0.8
BT 21	2.9	1.1	174.6	21.7	18.8	3.0	2.4	1.8	13460	-	-
BT 20	1.6	1.1	124.0	22.3	16.1	3.2	2.4	2.0	12720	1.3	0.1
BT 19	2.0	0.8	136.6	48.3	31.6	5.2	4.1	3.3	4280	-	-
BT 18	0.1	1.2	81.1	33.8	28.1	5.6	2.2	2.5	2200	1.4	0.1
BT 17	1.6	0.5	110.8	39.2	26.3	3.4	3.0	1.8	12060	-	-
BT 16	1.1	0.9	128.4	46.9	21.7	4.1	3.0	2.3	11350	-	-
BT 15	B.D.L.	1.2	109.4	36.5	27.4	4.6	3.9	1.9	4940	1.8	0.1
BT 13	0.5	1.4	114.8	14.4	13.2	2.2	6.4	1.1	7750	-	-
BT 12	2.5	3.0	152.6	66.6	34.4	5.3	4.3	2.2	3820	1.0	0.5
BT 11	0.8	0.2	121.1	41.5	28.9	3.9	3.3	1.8	13820	-	-
BT 10	1.6	0.6	120.0	38.9	34.7	4.4	4.0	1.8	13750	1.1	0.4
BT 9	1.0	0.4	120.1	39.5	28.4	4.4	3.7	1.6	12200	-	-
BT 8	2.9	1.0	215.6	66.9	57.2	5.9	8.5	1.6	-	0.9	0.6
BT 7	2.7	B.D.L.	173.5	51.4	115.8	4.4	20.5	1.8	-	-	-
BT 6	0.4	0.4	36.6	0.6	7.9	0.8	0.8	0.1	-	-	-
BT 5	0.7	1.3	37.5	2.2	6.8	0.7	0.2	0.1	-	-	-
BT 4	0.3	0.1	54.1	8.6	15.1	2.7	0.6	0.1	-	-	-
BT 3	0.6	0.5	38.4	5.1	11.2	1.4	0.4	0.1	-	-	-
BT 2	1.4	0.1	42.3	7.4	7.8	1.0	0.3	0.1	-	-	-

Table 8.1: Geochemical data for samples from the Bächental section. Notes: Data original to this study except TOC contents, amount of diagenetic Mn-rich carbonates, pristane/phytane ratios (Pr/Ph), and gammacerane index (GI), which are from Neumeister et al. (2015). Stratigraphic units: Scheibelberg Formation, BT 2-6; basal mudstone, BT 7-8; Unit 1, BT 9-21; Subunit 2a, BT 21-35; Subunit 2b, BT 36-40; debrite layer, BT 41-43; Unit 3, BT 44-58; Upper Allgäu Formation, BT 60-68. p.a. = peak area, B.D.L. = below detection limit.

8.5. Definitions and models

8.5.1 Oxygen availability and redox conditions in marine environments

Marine environments show different oxygenation levels depending on setting and water depth. The level of dissolved oxygen in seawater is the basis for classification of environmental redox conditions as oxic (>2 ml O_2 L^{-1}), suboxic (>0 to ~2 ml O_2 L^{-1}), and anoxic (~0 ml O_2 L^{-1}), with measurable quantities of H_2S representing euxinic conditions (Savrda and Bottjer, 1991; Wignall, 1994). These redox states determine the activity of microbially-driven oxidation reactions degrading the OM present in seawater and marine sediments (Breck, 1974).

Oxygen is the dominant electron acceptor that controls the degradation of OM under oxic conditions (Berner, 1981). Under suboxic conditions any remaining oxygen, nitrate, Mn(IV), and Fe(III) serve as electron acceptors (e.g., Tribovillard et al., 2006; Piper and Calvert, 2009). In contrast, sulfate is the dominant electron acceptor under euxinic conditions.

8.5.2 TEs in marine systems

TEs in oceanic systems derive from two sources: (1) Weathering and erosion of continental crust and subsequent fluvial or atmospheric transport of the products to the global oceans (e.g., Rex and Goldberg, 1958; Martin and Meybeck, 1979) and (2) hydrothermal activity (e.g., Lyle, 1976; Von Damm, 1990). The transport of TEs through the water column as well as their removal to the sediment and their subsequent preservation are mediated by various biogenic and chemical processes in the depositional and diagenetic environments:

(1) TEs transferred with the detrital fraction to the sediment may result in significant concentrations of lithogenously derived TEs (e.g., Dean et al., 1999; Adelson et al., 2001).

This process of TE enrichment is especially important for sediments with TOC contents <2.5 % deposited under oxic to suboxic conditions (Algeo and Maynard, 2004; Tribovillard et al., 2006).

(2) Certain dissolved TEs referred to as bio-sensitive (Cu, Ni) are removed from the water column as they participate in marine biogeochemical cycling through assimilatory uptake by planktonic organisms (e.g., Collier and Edmond, 1983; Tribovillard et al., 2006; Piper and Calvert, 2009). The subsequent accumulation of the TE-enriched OM in the sediment contributes to their removal to marine deposits (Ho et al., 2003; Piper and Perkins, 2004; Nameroff et al., 2004; Naimo et al., 2005). The OM-bound fractions of Cu and Ni are liberated by degradation processes and can subsequently be fixed in the sediment through precipitation as Cu- or Ni-sulfide phases or uptake by Fe sulfides provided that anoxic conditions prevail in the burial environment (Huerta-Diaz and Morse, 1992; Achterberg et al., 1997; Morse and Luther, 1999). Hence, high primary productivity is favorable for elevated Cu and Ni concentrations in the sediment (Lewan and Maynard, 1982; Brumsack, 1986; Algeo and Maynard, 2004).

(3) Besides the bio-sensitive Cu and Ni, several other TEs (including Mo, U and V) show an affinity to reducing environments (e.g., Wignall, 1994; Algeo and Maynard, 2004). The accumulation of TEs in the sediment under reducing conditions mainly occurs via chemically-controlled, non-biogenic processes including adsorption onto organic or lithogenic substrates (Mo, V, Ni; e.g., Brumsack, 1989; Morford and Emerson, 1999; Algeo and Maynard, 2004), formation of organometallic ligands (U, V, Cu; e.g., Emerson and Huested, 1991; Morford and Emerson, 1999; Algeo and Maynard, 2004), uptake by authigenic Fe sulfides in solid solution (Mo, Cu, Ni; e.g., Huerta-Diaz and Morse, 1992; Morse and Luther, 1999; Adelson et al., 2001), precipitation as individual solid oxide, hydroxide or sulfide phases (U, V, Cu; e.g., Achterberg et al., 1997; Morse and Luther, 1999; Zheng et al., 2002), and adsorption onto particulate Mn/Fe oxyhydroxides that promote the delivery of TEs to the sediment via redox cycling of Mn and Fe in the water column (Mo, V, Cu, Ni; Adelson et al., 2001; Algeo and Maynard, 2004; Algeo and Tribovillard, 2009). In contrast to the bio-sensitive TEs, enrichment of Mo, U, and V exclusively reflects the prevailing redox conditions during deposition (e.g., Tribovillard et al., 2006).

(4) Remobilization and translocation of TEs during diagenesis can influence TE concentrations in the sediment resulting in TE compositions that do not reflect primary depositional controls (e.g., Breit and Wanty, 1991; Thomson et al., 1993).

8.5.3 TE-based paleoredox proxies

The classification of TEs in terms of their origin is commonly established via model approaches based on bulk parameters providing estimates of the TE fractions that are derived from either lithogenous or seawater sources (e.g., Calvert and Pedersen, 2007; Perkins et al., 2008; Piper and Calvert, 2009). In this process, the concentration of the TE in question is normalized to a lithogenic element in the sediment (Calvert and Pedersen, 2007; Piper and Calvert, 2009). The use of Al as a normalizing element is common owing to its high concentration in many sediments and its relative immobility in the diagenetic environment (e.g., Wedepohl, 1995; Taylor and McLennan, 1985). The lithogenous fraction of a given TE is commonly estimated based on its relationship to Al: a line is drawn from the origin of the TE-Al crossplot through the sample points with lowest TE concentrations to represent the approximate TE/Al ratio of the lithogenous fraction (e.g., Piper and Calvert, 2009). TE concentrations plotting above this line represent the fractions originating from either biogenous or hydrogenous sources (Piper et al., 2007; Piper and Calvert, 2009).

However, the classification of TE sources by means of this approach entails some limitations and uncertainties:

(1) The removal of TEs by post-depositional alteration processes (e.g., Breit and Wanty, 1991; Thomson et al., 1993) induces a shift to lower TE concentrations that depends on the magnitude of depletion. As a result, this procedure may result in underestimation of lithogenously derived TEs and overestimation of TEs derived from other sources.

(2) Different types of clay minerals can be characterized by varying amounts of mineral-bound TEs (e.g., Wedepohl, 1971; Kogel and Lewis, 2001). Hence, the use of a single detrital TE-Al regression for all samples may produce biased results, if the mineralogical composition of the clay fraction changes during deposition of a section.

(3) This approach presupposes that all non-seawater-derived TEs are bound to the detrital siliciclastic fraction (e.g., Piper and Calvert, 2009). However, lithogenously derived TEs (e.g., Mo, V) can also be incorporated into diagenetic carbonates (see Section 8.6.2).

(4) Relative amounts of TEs linked to siliciclastics and organics cannot be resolved in sections where Al concentrations and TOC contents show a positive correlation (see Section 8.6.2).

Despite these limitations, TE-Al diagrams provide a simple method to approximately differentiate TE sources and, therefore, are used in this study (Figs. 8.3A-E).

Plots of TE vs. TOC content (Figs. 8.3F-J) provide additional information about environmental redox conditions and TE removal to the sediment. Linear TE-TOC correlations have been reported from numerous black shale formations (e.g., Holland, 1984; Robl and Barron, 1987; Algeo and Maynard, 2004). According to Algeo and Maynard (2004), TE/TOC relationships depend on redox conditions and TOC thresholds:

(1) There is only little covariation visible in black shales with relatively low TOC contents (<2.5 %) deposited under dysoxic conditions as in that case TEs are mainly connected with the detrital fraction of the sediment.

(2) TEs are mainly present in organometallic complexes under non-sulfidic anoxic conditions (Pratt and Davis, 1992) and, hence, show a significant covariation with TOC content. OM is the limiting factor for TE accumulation in the sediment.

(3) Under euxinic conditions (free H_2S in the water column) the accumulation of TEs is linked to the precipitation of authigenic solid TE phases (e.g., Morse and Luther, 1999) or conversion of reduced TEs to particle-active phases (e.g., Helz et al., 1996), resulting in strong TE enrichment and weak TE-TOC covariation.

However, in stagnant and anoxic settings, TE/TOC ratios may also be affected by the degree of restriction of the subchemoclinal watermass and temporal changes thereof related to deepwater renewal in anoxic basins (Algeo and Lyons, 2006; Algeo and Maynard, 2008; Algeo and Rowe, 2012). In such systems, increasing restriction is reflected by a systematic decrease of TE/TOC ratios in silled basins. This relationship is caused by the continuous depletion of a given TE due to the removal of the element to the sediment without adequate

resupply by deepwater renewal ("basin-reservoir effect"; Algeo and Lyons, 2006). Hence, low sedimentary TE concentrations and TE/TOC ratios may reflect significant restriction of silled marine basins. However, it is also possible that, in deep-time systems, low TE concentrations in the sediment reflect low TE concentrations in contemporaneous global seawater (Scott et al., 2008).

The concentrations of authigenic (auth) Mo and U in the sediment can be used to differentiate depositional redox conditions and processes (Algeo and Tribovillard, 2009). According to this study, $(Mo/U)_{auth}$ ratios less than the Mo/U molar ratio of seawater (~7.5-7.9; Chen et al., 1986) typically occur in oceanic systems under suboxic conditions, whereas increasingly reducing and at least occasionally euxinic conditions are reflected by $(Mo/U)_{auth}$ ratios equaling or even exceeding that of seawater. The use of this approach requires the calculation of "enrichment factors" (EF; $X_{EF} = [(X/Al)_{sample}/(X/Al)_{UCC}]$), where X is the element of interest (Tribovillard et al., 2006). For the present study, samples were normalized to the upper continental crust (UCC) compositions of McLennan (2001). The results for Mo_{EF}/U_{EF} ratios for Bächental bituminous marls were plotted in Figure 8.5 (see Section 8.6 for discussion).

8.5.4 Organic geochemical-based paleoredox and -salinity proxies

Stratigraphic variations in redox and salinity conditions during deposition of the Bächental section were determined on the basis of the pristane/phytane (Pr/Ph) ratio and the gammacerane index (GI, hopane isomerization ratio, 4-methylsteranes), respectively (Neumeister et al., 2015). The Pr/Ph ratio is commonly used as a redox indicator during early diagenesis, with values <1.0 indicating anoxic conditions and values >1.0 indicating suboxic to oxic conditions (Didyk et al., 1978). High values for GI indicate a stratified water column in marine and non-marine source-rock depositional environments, commonly resulting from a deep hypersaline water body (Fu et al., 1986). Alternatively, gammacerane may also originate from bacterivorous ciliates floating at the chemocline within the water column (Sinninghe Damsté et al., 1995; Schwark et al., 1998). According to these studies, elevated amounts of gammacerane might reflect a well-stratified water column, even in the absence of high-salinity bottom waters. Furthermore, increased hopane isomerization ratios, which result from diagenetic processes specific for hypersaline conditions (ten Haven et al., 1987), as well as large amounts of 4-methylsteranes, which are frequently related to halophilic microorganisms

(e.g., ten Haven et al., 1985), are indicators for an elevated salinity of bottom-waters in the Bächental basin.

8.6 Discussion

Interpretation of TE concentrations and concentration ratios (TE/Al, TE/TOC) provides information about siliciclastic input, biogenic supply to the basin floor, prevailing redox conditions, and the impact of diagenetic processes. In the following, each stratigraphic unit of the Bächental section is discussed separately.

8.6.1 TE redox proxies in the Scheibelberg and Upper Allgäu formations

Low TOC contents (<0.5 %) and substantial bioturbation suggest oxic conditions during deposition of limestones and marls of the Scheibelberg and Upper Allgäu formations (Neumeister et al., 2015). This is confirmed by generally low concentrations of Mo, U, V, Cu, and Ni (Figs. 8.4A-E) as well as pronounced positive covariation of all TEs with Al indicating solely lithogenous TE sources for those units. All samples display nearly equal values for Mo/Al, U/Al, Cu/Al, and Ni/Al ratios suggesting a similar siliciclastic source (Table 8.2). In contrast, the fraction of Al-bound V is significantly higher in the Scheibelberg Formation compared to the Upper Allgäu Formation (Table 8.2). Comparison of TE/Al ratios for the Upper Allgäu Formation with those for average upper continental crust (McLennan, 2001; Table 8.2) shows that TE concentrations are close to crustal values. In contrast, samples from the Scheibelberg Formation feature relative enrichment of V and Ni, whereas Mo, U, and Cu concentrations are close to crustal values. Because strong positive TE-Al covariation in both units confirms a dominantly lithogenous source, the differences in TE patterns between the Scheibelberg and Upper Allgäu formations indicate somewhat different sources of detrital material.

8.6.2 TE redox proxies in the basal mudstone, Unit 1, and Unit 3 of the Sachrang Member

The lower (basal mudstone and Unit 1) and the upper (Unit 3) intervals of the OM-enriched Sachrang Member were deposited under similar environmental conditions. According to geochemical proxies (Pr/Ph, TOC-Fe-S, GI, hopane isomerization ratio, 4-methylsteranes), suboxic conditions and a watermass of normal salinity existed during deposition of these units (Neumeister et al., 2015).

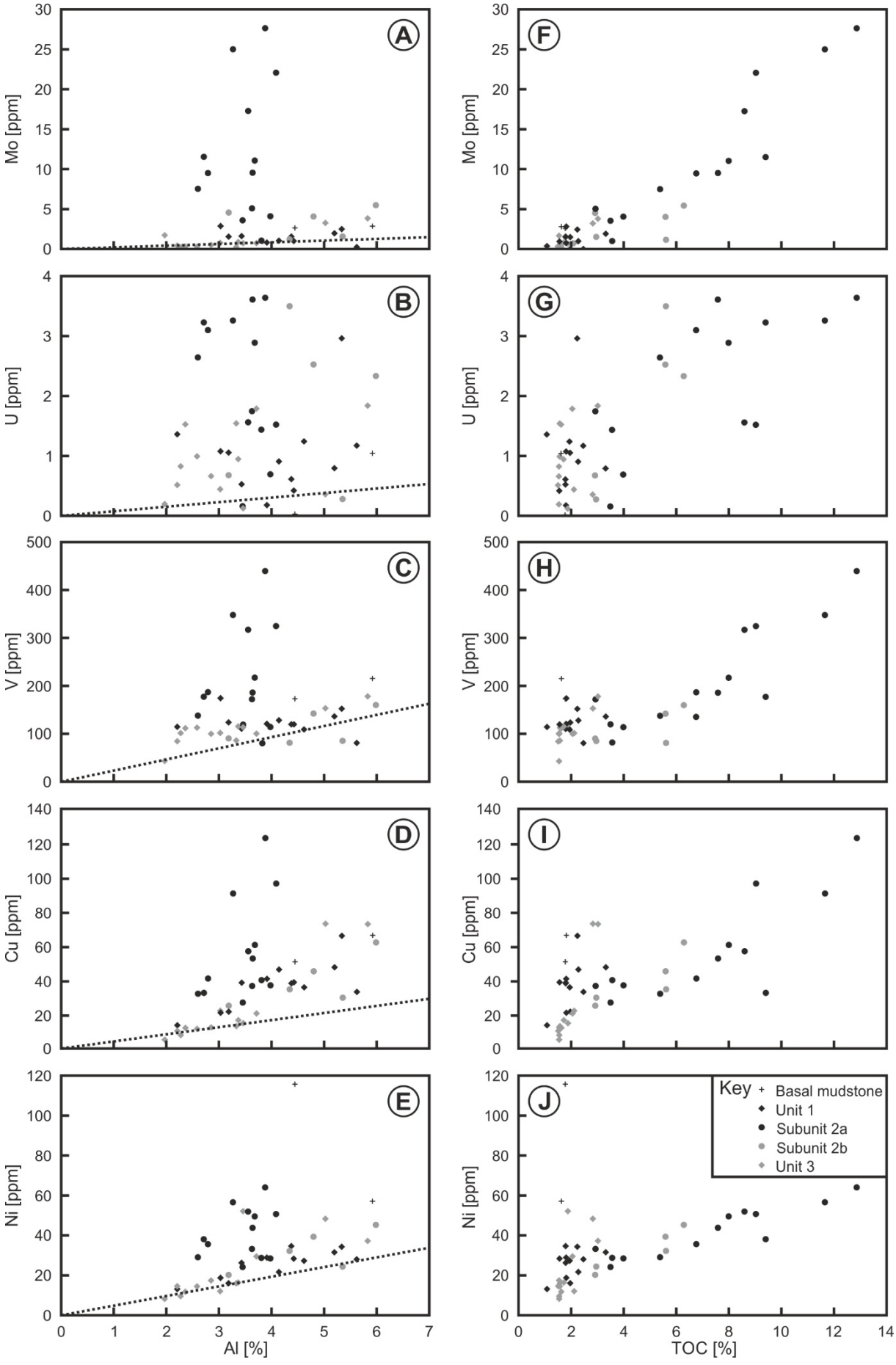
A
B
C
D
E
F
G
H
I
J
Mo [ppm]
U [ppm]
V [ppm]
Cu [ppm]
Ni [ppm]
Al [%]
TOC [%]
Key
Basal mudstone
Unit 1
Subunit 2a
Subunit 2b
Unit 3

Fig. 8.3: Left: Aluminum (Al) vs. trace element (TE) concentrations: (A) molybdenum (Mo), (B) uranium (U), (C) vanadium (V), (D) copper (Cu), and (E) nickel (Ni). Dotted lines indicate the lithogenous TE fractions, and excess TE concentrations above these lines represent the biogenic and authigenic fractions. Right: Total organic carbon (TOC) vs. TE concentrations: (F) molybdenum (Mo), (G) uranium (U), (H) vanadium (V), (I) copper (Cu), and (J) nickel (Ni). Positive covariation reveals the dependence of TE uptake on organic-matter accumulation.

		Mo/Al	U/Al	V/Al	Cu/Al	Ni/Al
Upper Allgäu Formation		0.5	0.3	16.5	3.8	5.9
Sachrang Member	**Unit 3**	0.2	0.3	33.7	5.0	5.6
	Debrite layer	0.9	0.5	36.5	1.7	1.8
	Subunit 2b	0.9	0.4	26.7	8.1	7.4
	Subunit 2a	3.0	0.8	59.0	14.7	12.4
	Unit 1	0.3	0.2	29.8	8.9	6.1
	Basal mudstone	0.5	0.1	37.7	11.4	17.9
Scheibelberg Formation		0.5	0.3	40.6	3.2	8.1
Average upper continental crust		0.2	0.3	13.3	3.1	5.5

Table 8.2: Median TE/Al ratios for stratigraphic units of the Bächental section. Notes: Values for average upper continental crust are from McLennan (2001).

TEs show similar characteristics in the basal mudstone as well as in Units 1 and 3 (Figs. 8.3A-J, 8.4A-E, 8.5, 8.6). Median values for TE/Al ratios are typically in the same range for Units 1 and 3 (Table 8.2). Mo, U, and Ni show concentrations similar to average upper continental crust, V and Cu concentrations are elevated in both units with higher values occurring in Unit 1 (McLennan, 2001; Table 8.2). In contrast to the Scheibelberg and Upper Allgäu formations, in which the clay fractions contain only illite, significant amounts of smectite are present in the Bächental bituminous marls. These large amounts of smectite are likely to have been derived from alteration of volcanic ash, indicating a pronounced contribution of volcanic detritus during marl deposition (Neumeister et al., 2015). Thus, it seems likely that the lithogenous TE fractions were related to volcaniclastic inputs to the Sachrang Member. However, differences in clay mineral composition do not markedly influence the fractions of lithogenous-derived TEs in the study section. This is indicated by the similar ranges of TE/Al ratios for samples from the transition zones (i.e., Scheibelberg Formation - basal mudstone and Unit 1 of the Sachrang Member; Unit 3 of the Sachrang Member - Upper Allgäu Formation; Table 8.2).

The different TEs show varying affinities to siliciclastics, carbonates, and OM in Units 1 and 3 (Figs. 8.4A-J, 8.6). Positive U-Al covariation suggests that U concentrations were mainly linked to lithogenous inputs. In contrast, Mo and V concentrations show correlations to both Al content and the amount of diagenetic Mn-rich carbonates. Cu and, in part, Ni show vertical trends that are similar to those of Al and TOC (Fig. 8.6). Because samples of Units 1 and 3 are characterized by positive covariation between Al and TOC (Fig. 8.6), it is impossible to determine conclusively whether Cu and Ni enrichment was mainly connected to detrital input or OM accumulation (see Section 8.5.3). Generally, the removal of Cu and Ni to the sediment is typically controlled by similar processes (e.g., Tribovillard et al., 2006). Besides lithogenous inputs, the main source of the bio-sensitive TEs Cu and Ni to the sediment is adsorption onto OM (Tribovillard et al., 2006). Whereas the latter process is significant in anoxic environments, Cu and Ni is typically connected with the detrital fraction in sediments with moderate TOC content (<2-3 %) deposited under oxic to dysoxic conditions, such as in Units 1 and 3 (TOC: 1.1-3.3 %). However, both bulk geochemical and organic geochemical parameters indicate transient shifts to more reducing conditions during deposition of these units (Neumeister et al., 2015), suggesting that Cu and Ni concentrations were at least partly controlled by adsorption onto OM.

Al concentrations and amount of Mn-rich carbonates show a negative correlation caused by the interrelation of siliciclastic input and carbonate dilution in Units 1 and 3 (Fig. 8.6). In those units, rather constant values for absolute concentrations and TE/Al ratios as well as prevailing suboxic conditions indicate a common source and an accumulation linked to lithogenous inputs for both Mo and V (Figs. 8.4A, C, 8.6, Table 8.2). However, Mo and V are characterized by a varying correlation with Al concentrations and amount of Mn-rich carbonates in Units 1 and 3 (Fig. 8.6), indicating that, the uptake of those TEs was related, in different stratigraphic intervals, to either siliciclastics or formation of diagenetic Mn-rich carbonates. Mo and V concentrations reflect primarily detrital inputs in the lower part of Unit 1 (up to sample BT 13, 6.65 m). In contrast, the covariation of Mo and V concentrations with amount of Mn-rich carbonates implies that their enrichment was mainly associated with precipitation of diagenetic Mn-rich carbonates in the upper part of Unit 1 and in parts of Unit 3 (Mo: BT 52-54, 26.55-27.55 m; V: BT 44-50, 22.60-25.55 m; Fig. 8.6). Hence, although Mo and V probably derived from a common lithogenous source, their enrichment in the sediment potentially was controlled by different processes. The occurrence of diagenetic Mn-rich carbonates implies that the sediment accumulated in oxygenated bottom waters (e.g.,

Calvert and Pedersen, 1996). Apart from the lithogenous contribution, the fixation of the redox-sensitive TEs Mo and V in the sediment requires reducing depositional conditions (e.g., Tribovillard et al., 2006; Piper and Calvert, 2009). Mo and V enrichment under oxic conditions is effected by adsorption onto the surfaces of Mn oxides rather than by reduction (e.g., Algeo and Maynard, 2004; Morford et al., 2005; Tribovillard et al., 2006). However, the absence of corresponding peaks in XRD diffractograms excludes the presence of Mn oxides in bituminous marls of Units 1 and 3 (Neumeister et al., 2015). Dissolution of Mn oxides in sediment layers below the chemocline releases ^{12}C-enriched carbon, Mn, Mo, and V to porewaters (e.g., Morford et al., 2005). Elevated concentrations of Mo und V in porewaters of recent bottom sediments are commonly due to complexation of those elements with dissolved organic carbon (e.g., Emerson and Huested, 1991; Morford et al., 2005). Diagenetic Mn-rich carbonates in samples from Units 1 and 3 contain high amounts of ^{12}C-enriched carbon (Neumeister et al., 2015). Hence, we speculate that the positive covariation among diagenetic Mn-rich carbonates, Mo, and V concentrations in parts of Units 1 and 3 was caused by the incorporation of organic-derived carbon and also its absorbed Mo and V, into the lattice of Mn-rich carbonates during their early diagenetic formation at the chemocline in the sediment.

Bituminous marls from Units 1 and 3 generally feature lower values for Mo_{EF}/U_{EF} ratios (median: 2.2; Fig. 8.5A) relative to the typical Mo/U molar ratio of seawater (~7.8; Chen et al., 1986), which is consistent with suboxic depositional conditions (cf. Algeo and Tribovillard, 2009). However, elevated values, equaling or even exceeding that of seawater, suggest the occurrence of more intensely reducing conditions at the top of Unit 3. Prevailing suboxic conditions and unrestricted deepwater exchange during deposition of Units 1 and 3 (Neumeister et al., 2015) exclude the use of Mo/TOC ratios for interpretation of environmental conditions in those intervals (cf. Algeo and Lyons, 2006).

The debrite at the base of Unit 3 represents a rapidly deposited sediment layer that interrupted bituminous marl sedimentation in the Bächental basin. The low TE concentrations of these OM-poor carbonates are indicative of oxic depositional conditions.

To sum up, the onset of OM accumulation in the Bächental basin was accompanied by a mineralogical change of the clay fraction potentially linked to the onset of volcaniclastic inputs to the sediment. In contrast to U, which was solely derived from lithogenous sources, Mo and V concentrations are characterized by varying relationships to siliciclastic inputs and

potentially to precipitation of diagenetic Mn-rich carbonates. Removal of the bio-sensitive elements Cu and Ni to the sediment was established by means of adsorption onto OM and siliciclastic input. Based on TE redox proxies, the paleoenvironment in the Bächental basin during deposition of Units 1 and 3 was characterized by mainly suboxic conditions interrupted by short-term episodes of more intensely reducing conditions. This corresponds well to redox interpretations based on sedimentologic and organic geochemical parameters.

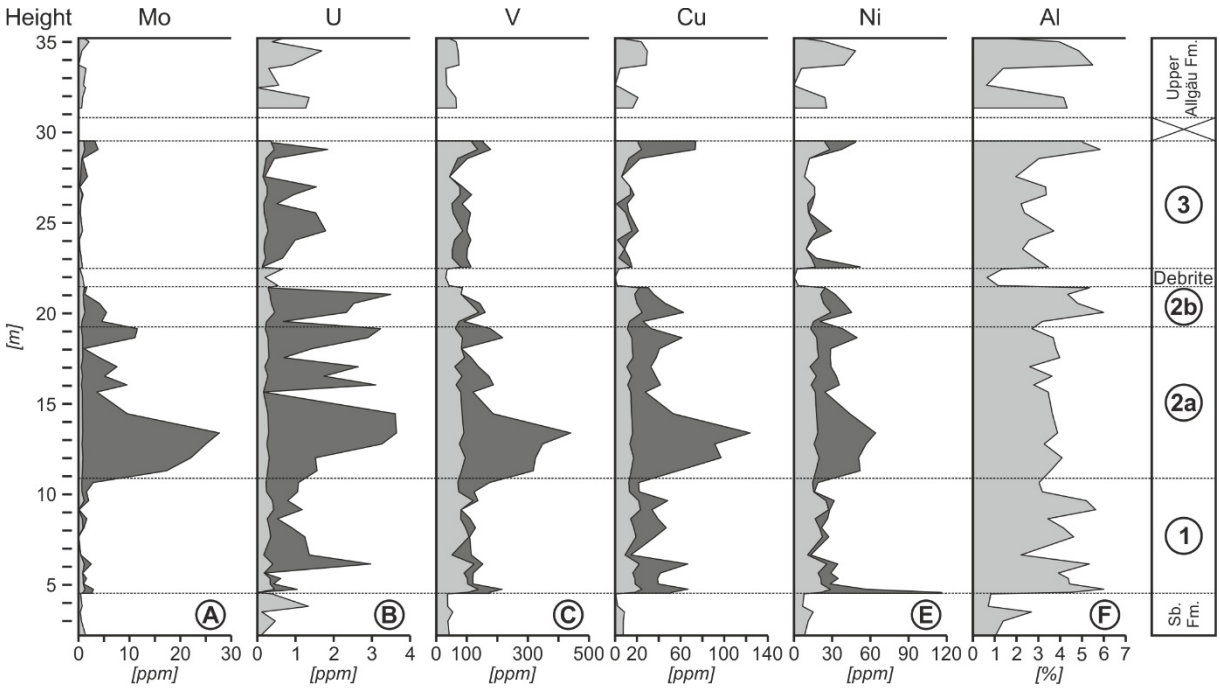

Fig. 8.4: Stratigraphic variation of lithogenous (light grey) and authigenic (dark grey) trace element fractions in the study section: (A) molybdenum (Mo), (B) uranium (U), (C) vanadium (V), (D) copper (Cu), (E) nickel (Ni), and (F) aluminum (Al). Sb. Fm. = Scheibelberg Formation.

8.6.3 TE redox proxies in Unit 2 of the Sachrang Member

Black and finely laminated strata of Unit 2 comprising the middle part of the Sachrang Member show high TOC (up to 12.9 %) and HI values (ca. 580-690 mg HC/g TOC; Neumeister et al., 2015). According to organic geochemical (Pr/Ph, GI, hopane isomerization ratio, 4-methylsteranes) and bulk geochemical (TOC-Fe-S) proxies, Subunit 2a accumulated in a strongly reducing, mainly Fe-limited stagnant basinal setting. Intense anoxia was reinforced by a salinity-stratified water column during a period of relative sea-level lowstand. During deposition of Subunit 2b, infrequently occurring turbidity currents served to

transiently mix bottom waters and disrupt water-column stratification, although anoxic conditions continued to prevail in the sediment (Fig. 8.2; Neumeister et al., 2015).

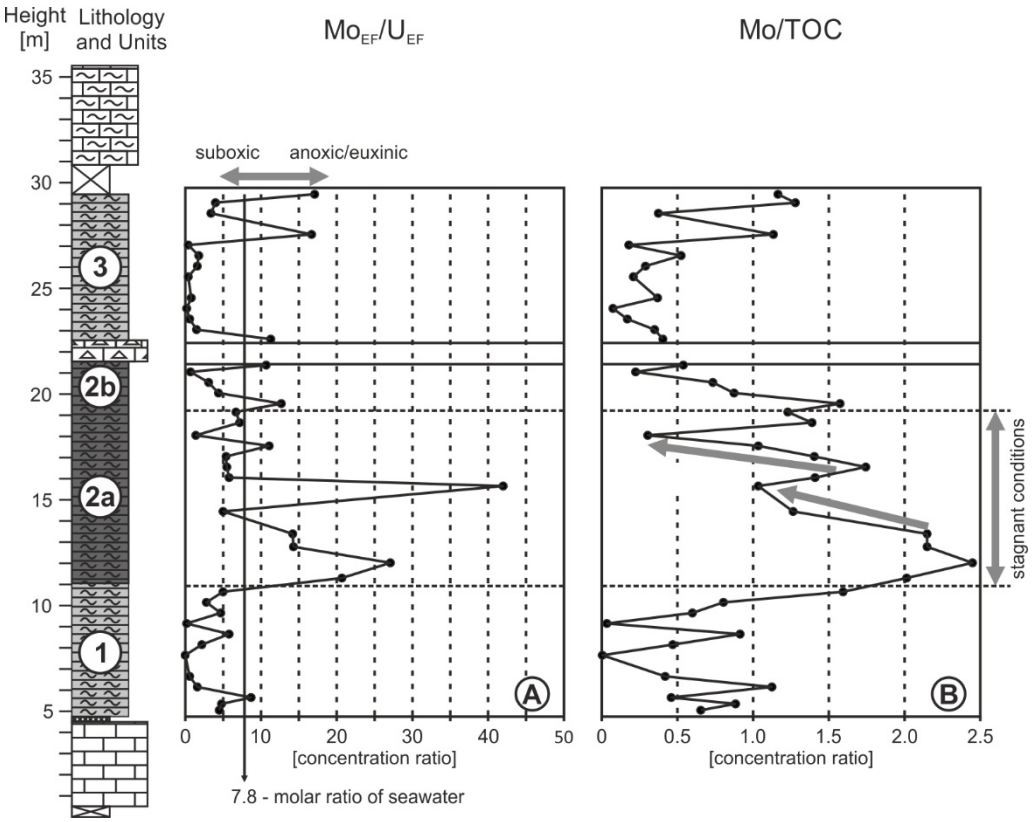

Fig. 8.5: Stratigraphic variation of (A) molybdenum vs. uranium enrichment factor (Mo_{EF}/U_{EF}) and (B) molybdenum vs. total organic carbon (Mo/TOC) ratio. Comparison of Mo/U ratio with that of seawater (~7.8; Chen et al., 1986) provides information about prevailing redox conditions during deposition (Algeo and Tribovillard, 2009). Accordingly, low values of samples from Units 1 and 3 indicate suboxic conditions, whereas elevated values of samples from Unit 2 imply predominating anoxia. Given anoxic conditions, Mo/TOC ratios reflect paleohydrographic restriction (Algeo and Lyons, 2006), with ratios of <3 as for Subunit 2a implying strongly reducing conditions.

Redox-sensitive (Mo, U, and V) as well as bio-sensitive (Cu and Ni) TEs show peak concentrations in Unit 2 (Figs. 8.4A-E, 8.6). None of the investigated TEs display significant covariation with Al concentrations, and most samples are enriched in TEs distinctly above lithogenous values, suggesting a dominant seawater source (Figs. 8.3A-E, 8.4A-E). This is confirmed by positive TE-TOC covariation, indicating a chemically controlled TE enrichment process connected to OM accumulation (Figs. 8.3F-J, 8.6). Hence, availability and

preservation of OM were the limiting factors for TE removal to the sediment. The observed TE-TOC correlations are commonly associated with depositional environments characterized by anoxic, but non-euxinic, conditions (Algeo and Maynard, 2004; Tribovillard et al., 2006). The existence of anoxia during deposition of Unit 2 is also suggested by Mo_{EF}/U_{EF} ratios in the lower part of Subunit 2a (Fig. 8.5A; cf. Algeo and Tribovillard, 2009). Low amounts of diagenetic Mn-rich carbonates in Unit 2 (Fig. 8.6; Neumeister et al., 2015) additionally confirm the dominance of strongly reducing conditions as the precipitation of Mn-carbonates is inhibited in fully anoxic environments (Calvert and Pedersen, 1996). Although water-column stratification collapsed during deposition of Subunit 2b due to the episodic occurrence of fine-grained carbonate turbidites (Neumeister et al., 2015), the concurrent trends of TE concentrations and TOC content confirm the persistence of anoxic conditions within the sediment. These redox interpretations are supported by the excellent correspondence of inorganic and organic geochemical proxies (Fig. 8.6; cf. Neumeister et al., 2015).

The occurrence of a salinity-stratified water column induced stagnant and continuously anoxic conditions during deposition of Subunit 2a (Neumeister et al., 2015). In such basinal settings, the ratio of Mo vs. TOC (Mo/TOC) is applicable as a proxy for paleohydrographic restriction (Algeo and Lyons, 2006). The utility of this proxy is based on the continuous removal of Mo to the sediment without adequate resupply by deepwater renewal, causing Mo depletion in the water column. This condition results in low authigenic Mo uptake rates and, hence, low sediment Mo/TOC ratios, despite intensely reducing deepwater conditions (Algeo and Lyons, 2006). In Subunit 2a, low Mo/TOC ratios (<2.4) confirm strong deepwater restriction during its deposition. Furthermore, Mo/TOC ratios show a gradual decline upsection from relative peak values at two stratigraphic levels (grey arrows in Fig. 8.5B), implying multiple intervals of progressive depletion of Mo in stagnant bottom waters (cf. Algeo and Lyons, 2006).

The detailed comparison of vertical trends of organic geochemical proxies (Pr/Ph, GI) and TE concentrations reveals that Pr/Ph ratios of samples with maximum TOC contents show an exceptional behavior. Generally Pr/Ph ratios and GI values are expected to display opposing vertical trends, as seen in Units 1 and 3, because elevated salinity of bottom waters (higher GI) is commonly associated with a stratified water column and more intense reducing conditions (lower Pr/Ph ratio). However, Pr/Ph ratios exhibit significant positive covariation with GI, TE concentrations, and TOC contents in Unit 2 (Fig. 8.6). Pr/Ph values typically <1

confirm the predominance of anoxic conditions during deposition of Subunit 2a. However, the samples characterized by peak values for TOC and GI (e.g., BT 25, 13.39 m) also show slightly elevated Pr/Ph ratios, suggesting a shift to less reducing conditions. We propose that increased values for Pr/Ph ratios were caused by elevated productivity of planktonic and algal organisms in surface waters and/or different pathways of OM transport to the sediment that resulted in a relative increase of Pr. This is consistent with a suggested flourishing of marine algae and bacterioplankton during deposition of the lower part of Subunit 2a (incl. BT 25, 13.39 m) comprising the time interval of the T-OAE (Neumeister et al., 2015). Hence, Pr/Ph ratios signal a flourishing of bioproductivity in parts of Unit 2.

To summarize, TE uptake during deposition of Unit 2 was exclusively associated with OM accumulation, a relationship characteristic of anoxic facies. This is consistent with a stagnant basinal setting as confirmed by bulk geochemical and organic geochemical proxies. Abnormally high Pr/Ph ratios that are found in intervals characterized by high TE concentrations, peak OM preservation, and elevated bottom-water salinity reflect time periods with enhanced bioproductivity.

Fig. 8.6: Left: Stratigraphic variation of trace element concentrations: molybdenum (Mo), uranium (U), vanadium (V), copper (Cu), and nickel (Ni). Right: Stratigraphic variation of total organic carbon (TOC), aluminum (Al), amount of diagenetic Mn-rich carbonates, pristane/phytane (Pr/Ph) ratios, and gammacerane index (GI). Note the different scales for the individual units. Relationship between oxic/suboxic and anoxic conditions for Pr/Ph ratios after Didyk et al. (1978). Relationship between salinity conditions and GI after Schwark et al. (1998). Samples characterized by specific attributes are highlighted. See text for explanations.

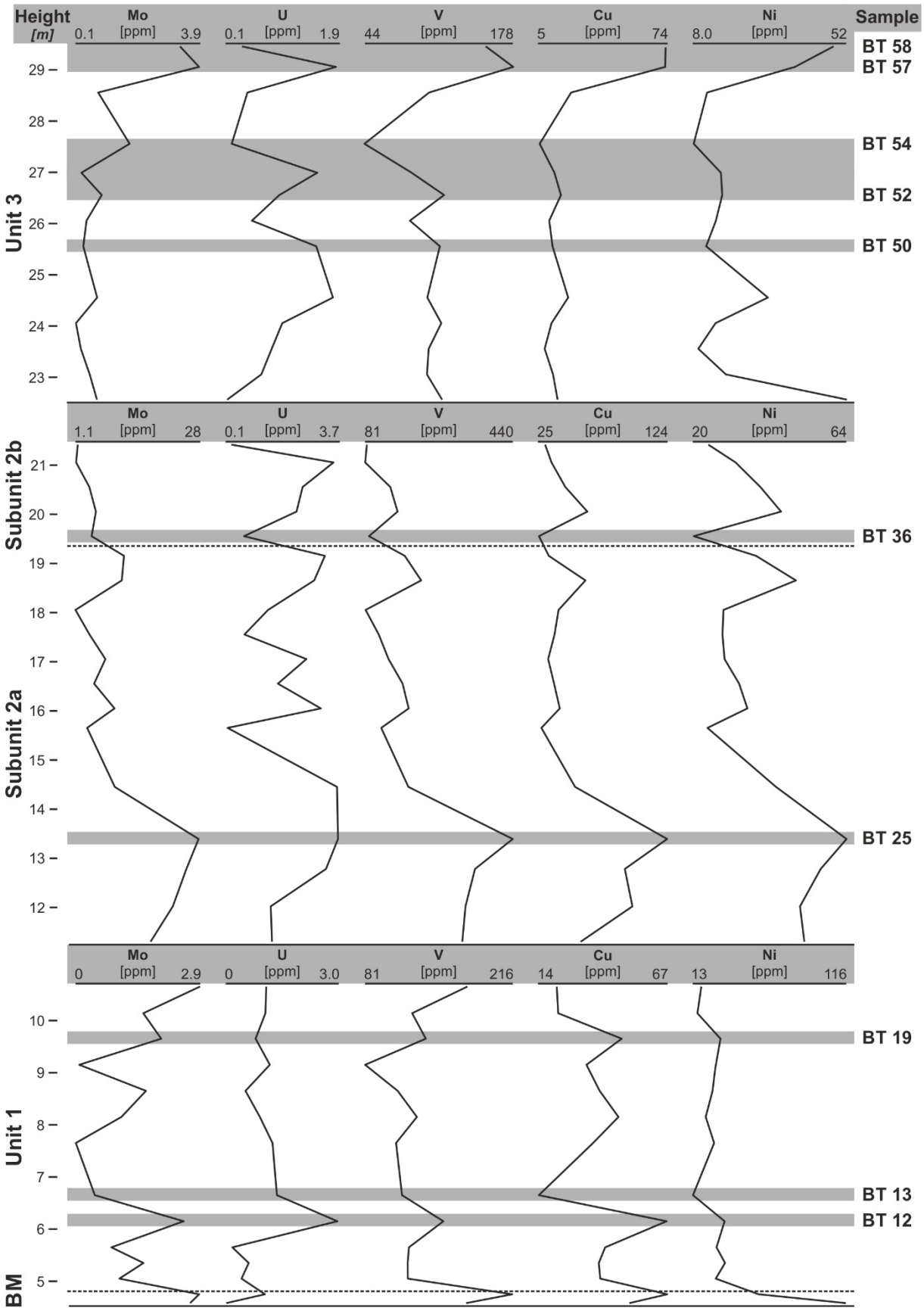
Height
[m]
Sample
Mo
0.1 [ppm] 3.9
U
0.1 [ppm] 1.9
V
44 [ppm] 178
Cu
5 [ppm] 74
Ni
8.0 [ppm] 52
BT 58
BT 57
BT 54
BT 52
BT 50
Unit 3
29
28
27
26
25
24
23
Mo
1.1 [ppm] 28
U
0.1 [ppm] 3.7
V
81 [ppm] 440
Cu
25 [ppm] 124
Ni
20 [ppm] 64
Subunit 2b
21
20
BT 36
Subunit 2a
19
18
17
16
15
14
13
12
BT 25
Mo
0 [ppm] 2.9
U
0 [ppm] 3.0
V
81 [ppm] 216
Cu
14 [ppm] 67
Ni
13 [ppm] 116
10
BT 19
9
Unit 1
8
7
BT 13
6
BT 12
BM
5

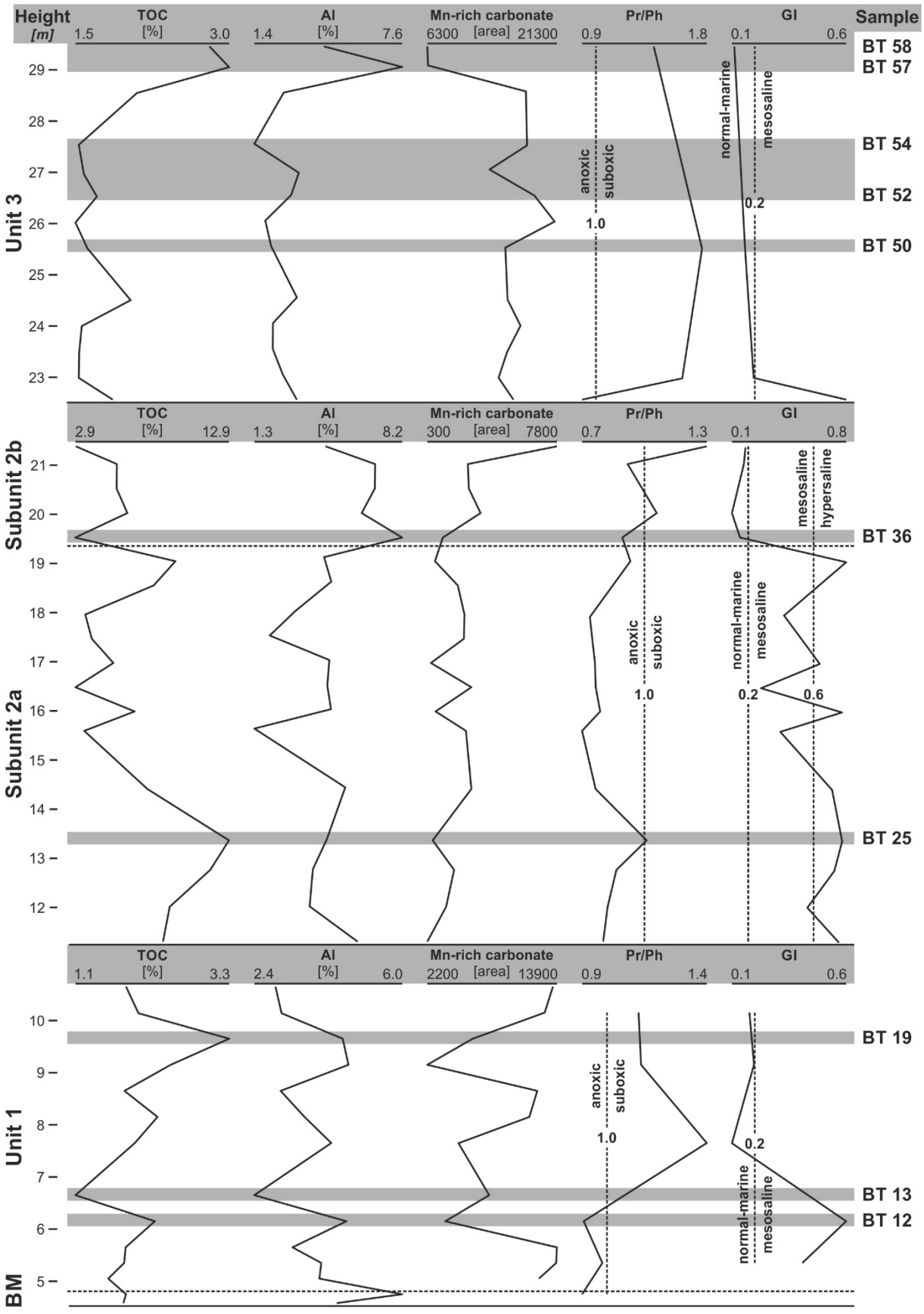
Height
[m]
TOC
[%]
1.5
3.0
Al
[%]
1.4
7.6
Mn-rich carbonate
[area]
6300
21300
Pr/Ph
0.9
1.8
GI
0.1
0.6
Sample
BT 58
BT 57
BT 54
BT 52
BT 50
Unit 3
anoxic
suboxic
1.0
normal-marine
mesosaline
0.2
TOC
[%]
2.9
12.9
Al
[%]
1.3
8.2
Mn-rich carbonate
[area]
300
7800
Pr/Ph
0.7
1.3
GI
0.1
0.8
Subunit 2b
Subunit 2a
BT 36
BT 25
anoxic
suboxic
1.0
normal-marine
mesosaline
0.2
mesosaline
hypersaline
0.6
TOC
[%]
1.1
3.3
Al
[%]
2.4
6.0
Mn-rich carbonate
[area]
2200
13900
Pr/Ph
0.9
1.4
GI
0.1
0.6
Unit 1
BM
BT 19
BT 13
BT 12
anoxic
suboxic
1.0
normal-marine
mesosaline
0.2

8.7 Conclusions

The interpretation of redox proxies based on bulk geochemical parameters, biomarker data as well as TE concentrations and concentration ratios results in a consistent stratigraphic redox trend for Bächental section. TE compositions of OM-poor samples from the Scheibelberg Formation, the Upper Allgäu Formation and the debrite layer (Sachrang Member) solely derive from lithogenous sources consistent with oxic depositional conditions.

Whereas illite is the only clay mineral in OM-poor rocks of the Scheibelberg and Upper Allgäu formations, smectite, potentially connected with intense volcanic activity in the course of LIP eruptions and/or the breakup of the Alpine Atlantic Ocean, is the dominant clay mineral during the time period of OM accumulation in the Bächental basin. However, the abrupt changes in clay mineralogy at the base and top of the Sachrang Member, respectively, are largely unrelated to TE concentrations in the siliciclastic fraction of the samples. Inorganic geochemical proxies suggest suboxic conditions during deposition of Units 1 and 3. Enrichment of TEs was connected to siliciclastic input (Mo, U, V, Cu, Ni) and potentially to precipitation of diagenetic Mn-rich carbonates (Mo, V) and adsorption onto OM (Cu, Ni).

The occurrence of linear TE-TOC covariations and elevated values for Mo_{EF}/U_{EF} ratio suggest the predominance of anoxic to euxinic conditions during deposition of Subunits 2a and 2b, with OM representing the limiting factor for TE accumulation. In Subunit 2a, low Mo/TOC ratios correspond to strong deepwater restriction and intense anoxia. Pr/Ph ratios are controlled by prevailing redox conditions and bioproductivity. Thus, the comparison of vertical trends of geochemical redox proxies provides a means to detect intervals characterized by elevated surface-water productivity. Accordingly, a flourishing of marine algae and bacterioplankton contributed to the significant TOC increase at the base of Subunit 2a corresponding to the time-equivalent occurrence of OM-rich deposits worldwide connected to the T-OAE.

8.8 Acknowledgments

We gratefully thank family Albrecht (Tiroler Steinöl ®) who operate the Bächental open pit for their technical support during sampling. Research by TJA is supported by the Sedimentary Geology and Paleobiology program of the U.S. National Science Foundation, the

NASA Exobiology program, and the China University of Geosciences-Wuhan (SKL-GPMR program GPMR201301, and SKL-BGEG program BGL201407).

8.9 References

Achterberg, E.P., Van Den Berg, C.M.G., Boussemart, M. and Davison, W., 1997. Speciation and cycling of trace metals in Esthwaite Water: a productive English lake with seasonal deep-water anoxia. Geochimica et Cosmochimica Acta, 61, 5233-5253. http://dx.doi.org/10.1016/S0016-7037(97)00316-5

Adelson, J.M., Helz, G.R. and Miller, C.V., 2001. Reconstructing the rise of recent coastal anoxia; molybdenum in Chesapeake Bay sediments. Geochimica et Cosmochimica Acta, 65, 237-252. http://dx.doi.org/10.1016/S0016-7037(00)00539-1

Algeo, T.J. and Maynard, J.B., 2004. Trace-element behaviour and redox facies in core shales of Upper Pennsylvanian Kansas-type cyclothems. Chemical Geology, 206, 289-318. http://dx.doi.org/10.1016/j.chemgeo.2003.12.009

Algeo, T.J. and Maynard, J.B., 2008. Trace-metal covariation as a guide to water-mass conditions in ancient anoxic marine environments. Geosphere, 4(5), 872-887. http://dx.doi.org/10.1130/GES00174.1

Algeo, T. J. and Lyons, T.W., 2006. Mo-total organic carbon covariation in modern anoxic marine environments: Implications for analysis of paleoredox and paleohydrographic conditions. Paleoceanography, 21, PA1016. http://dx.doi.org/10.1029/2004PA001112

Algeo, T. J., and Rowe, H., 2012. Paleoceanographic applications of trace-metal concentration data. Chemical Geology, 324, 6-18. doi:10.1016/j.chemgeo.2011.09.002

Algeo, T.J. and Tribovillard, N., 2009. Environmental analysis of paleoceanographic systems based on molybdenum-uranium covariation. Chemical Geology, 268, 211-225. http://dx.doi.org/10.1016/j.chemgeo.2009.09.001

Berner, R.A., 1981. A new geochemical classification of sedimentary environments. Journal of Sedimentary Petrology, 51, 59-365. http://dx.doi.org/10.1306/212F7C7F-2B24-11D7-8648000102C1865D

Bernoulli, D. and Jenkyns, H.C., 1974. Alpine, Mediterranean and Central Atlantic Mesozoic facies in relation to the early evolution of the Tethys. In: R.H. Dott and R.W. Shaver (eds.), Modern and Ancient Geosynclinal Sedimentation, a Symposium. Special Publication of the Society of economic Paleontologists and Mineralogists, 19, 129-160.

Brandner, R., 2011. In: Geologie des Achenseegebiets. Tagungsband der Arbeitstagung der Geologischen Bundesanstalt, Wien, 220-224.

Breck, W.G., 1974. Redox levels in the sea. In: E.D. Goldberg (eds.), The Sea, vol. 5. Wiley, New York, pp. 153-179.

Breit, G.N. and Wanty, R.B., 1991. Vanadium accumulation in carbonaceous rocks: a review of geochemical controls during deposition and diagenesis. Chemical Geology, 91, 83-97. http://dx.doi.org/10.1016/0009-2541(91)90083-4

Brumsack, H.J., 1986. The inorganic geochemistry of Cretaceous black shales (DSDP Leg 41) in comparison to modern upwelling sediments from the Gulf of California. In: C.P. Summerhayes and N.J. Shackleton (eds.), North Atlantic Palaeoceanography. Geological Society London Special Publications, 21, pp. 447-462. http://dx.doi.org/10.1144/GSL.SP.1986.021.01.30

Brumsack, H.J., 1989. Geochemistry of recent TOC-rich sediments from the Gulf of California and the Black Sea. International Journal of Earth Sciences (formerly Geologische Rundschau), 78, 851-882. http://dx.doi.org/10.1007/BF01829327

Brumsack, H.J., 2006. The trace metal content of recent organic carbon-rich sediments: implications for Cretaceous black shale formation. Palaeogeography Palaeoclimatology Palaeoecology, 232, 344-361. http://dx.doi.org/10.1016/j.palaeo.2005.05.011

Calvert, S.E. and Pedersen, T.F., 1996. Sedimentary geochemistry of manganese: implications for the environment of formation of manganiferous black shales. Economic Geology, 91, 36-47. http://dx.doi.org/10.2113/gsecongeo.91.1.36

Calvert, S.E. and Pedersen, T.F., 2007. Elemental proxies for palaeoclimatic and palaeoceanographic variability in marine sediments: interpretation and application. In: C. Hillaire-Marcel and A. de Vernal (eds.), Paleoceanography of the Late Cenozoic. Part 1. Methods in Late Paleoceanography. Elsevier, New York, pp. 567-644. http://dx.doi.org/10.1016/S1572-5480(07)01019-6

Chen, J.H., Edwards, R.L. and Wasserburg, G.J., 1986. 238U, 234U and 232Th in seawater. Earth and Planetary Science Letters, 80, 241-251. http://dx.doi.org/10.1016/0012-821X(86)90108-1

Cohen, A.S., Coe, A.L., Harding, S.M. and Schwark, L., 2004. Osmium isotope evidence for the regulation of atmospheric CO2 by continental weathering. Geology, 32, 157-160. http://dx.doi.org/10.1130/G20158.1

Collier, R.W. and Edmond, J.M., 1983. Plankton composition and trace element fluxes from the surface ocean. In: C.S. Wong, E. Boyle, K.W. Bruland, J.D. Burton and E.D. Goldberg (eds.), Trace Metals in Seawater, NATO Conference Series IV-9. Plenum Press, New York, pp. 789-809.

Dean, W.E., Piper, D.Z. and Peterson, L.C., 1999. Molybdenum accumulation in Cariaco basin sediment over the past 24 k. y.: A record of water-column anoxia and climate. Geology, 27, 507-510. http://dx.doi.org/10.1130/0091-7613(1999)027<0507:MAICBS>2.3.CO;2

Didyk, B.M., Simoneit, B.R.T., Brassell, S.C. and Eglinton, G., 1978. Organic geochemical indicators of palaeoenvironmental conditions of sedimentation. Nature, 272, 216-222. http://dx.doi.org/10.1038/272216a0

Ebli, O., 1991 mit Beiträgen von I. Draxler, P. Klein, L.A. Kodina, H. Lobitzer and B. Schwaighofer. Fazies, Paläontologie und organische Geochemie der Sachranger Schiefer (Untertoarcium) im Mittelabschnitt der Nördlichen Kalkalpen zwischen Isar und Saalach. Jahrbuch der Geologischen Bundesanstalt, 134/1, 5-14.

Ebli, O., Vetö, I., Lobitzer, H., Sajgò, C., Demény, A. and Hetényi, M., 1998. Primary productivity and early diagenesis in the Toarcian Tethys on the example of the Mn rich black shales of the Sachrang Formation, Northern Calcareous Alps. Organic Geochemistry, 29, 1635-47. http://dx.doi.org/10.1016/S0146-6380(98)00069-2

Emerson, S.R. and Huested, S.S., 1991. Ocean anoxia and the concentration of molybdenum and vanadium in seawater. Marine Chemistry, 34, 177-196. http://dx.doi.org/10.1016/0304-4203(91)90002-E

Encarnación, J., Fleming, T.H., Elliot, D.H. and Eales, H.V., 1996. Synchronous emplacement of Ferrar and Karoo dolerites and the early breakup of Gondwana. Geology, 24, 535-538. http://dx.doi.org/10.1130/0091-7613(1996)024<0535:SEOFAK>2.3.CO;2

Frimmel, A., Oschmann, W. and Schwark, L., 2004. Chemostratigraphy of the Posidonia Shale, SW Germany I. Influence of sea-level variation on organic facies evolution. Chemical Geology, 206, 199-230. http://dx.doi.org/10.1016/j.chemgeo.2003.12.007

Frisch, W. and Gawlick, H.-J., 2003. The nappe structure of the central Northern Calcareous Alps and its disintegration during Miocene tectonic extrusion – a contribution to understanding the orogenic evolution of the Eastern Alps. International Journal of Earth Sciences (formerly Geologische Rundschau), 92, 712-727. http://dx.doi.org/10.1007/s00531-003-0357-4

Fu, J.G., Sheng, P., Peng, S.C., Brassell, S.C. and Eglington, G., 1986. Pecularities of salt lake sediments as potential source rocks in China. Organic Geochemistry 10, 119-127. doi:10.1016/0146-6380(86)90015-X

Gawlick, H.-J., Missoni, S., Schlagintweit, F., Suzuki, H., Frisch, W., Krystyn, L., Blau, J. and Lein, R., 2009. Jurassic Tectonostratigraphy of the Austroalpine Domain. Journal of Alpine Geology, 50, 1-152.

Helz, G.R., Miller, C.V., Charnock, J.M., Mosselmans, J.F.W., Pattrick, R.A.D., Garner, C.D. and Vaughan, D.J., 1996. Mechanism of molybdenum removal from the sea and its concentration in black shales: EXAFS evidence. Geochimica et Cosmochimica Acta, 60, 3631–3642. http://dx.doi.org/10.1016/0016-7037(96)00195-0

Ho, T.Y., Quigg, A., Finkel, Z.V., Milligan, A.J., Wyman, K., Falkowski, P.G. and Morel, F.M., 2003. The elemental composition of some marine phytoplankton. Journal of Phycology, 39, 1145-1159. http://dx.doi.org/10.1111/j.0022-3646.2003.03-090.x

Holland, H.D., 1984. The Chemical Evolution of the Atmosphere an Oceans. Princeton University Press, Princeton, N.Y., 582 pp.

Huerta-Diaz, M.A. and Morse, J.W., 1992. Pyritisation of trace metals in anoxic marine sediments. Geochimica et Cosmochimica Acta, 56, 2681-2702. http://dx.doi.org/10.1016/0016-7037(92)90353-K

Ikeda, M. and Hori, R.S., 2014. Effects of Karoo-Ferrar volcanism and astronomical cycles on the Toarcian Anoxic Events (Early Jurassic). Palaeogeography, Palaeoclimatology, Palaeoecology, 410, 134-142. http://dx.doi.org/10.1016/j.palaeo.2014.05.026

Jenkyns, H.C., 1985. The Early Toarcian and Cenomanian–Turonian anoxic events in Europe: comparisons and contrasts. International Journal of Earth Sciences (formerly Geologische Rundschau), 74, 505-518. http://dx.doi.org/10.1007/BF01821208

Jenkyns, H.C., 1988. The Early Toarcian (Jurassic) anoxic event: stratigraphic, sedimentary, and geochemical evidence. American Journal of Science, 288, 101-151. http://dx.doi.org/10.2475/ajs.288.2.101

Jenkyns, H.C., Jones, C.E., Gröcke, D.R., Hesselbo, S.P. and Parkinson, D.N., 2002. Chemostratigraphy of the Jurassic System: applications, limitations and implications for palaeoceanography. Journal of the Geological Society of London, 159, 351-378. http://dx.doi.org/10.1144/0016-764901-130

Jenkyns, H.C., 2003. Evidence for rapid climate change in the Mesozoic–Palaeogene greenhouse world. Philosophical Transactions of the Royal Society of London, 361 A, 1885-1916. http://dx.doi.org/10.1098/rsta.2003.1240

Jenkyns, H.C., 2010. The geochemistry of oceanic anoxic events. Geochemistry Geophysics Geosystems, 11, Q03004. http://dx.doi.org/10.1029/2009GC002788.

Klebelsberg, R.v., 1935. Geologie von Tirol. Gebrüder Borntraeger, Berlin, 872 pp.

Kodina, L.A., Bogatecheva, M.P. and Lobitzer, H., 1988. An anorganic geochemical study of Austrian bituminous rocks. Jahrbuch der Geologischen Bundesanstalt, 131, 291-300.

Kogel, J.E. and Lewis, S.A., 2001. Baseline studies of the clay minerals society source clays: Chemical analysis by inductively coupled plasma-mass spectroscopy (ICP-MS). Clays and Clay Minerals, 49(5), 387-392.

Lewan, M.D. and Maynard, J.B., 1982. Factors controlling enrichment of vanadium and nickel in the bitumen of organic sedimentary rocks. Geochimica et Cosmochimica Acta, 46, 2547-2560. http://dx.doi.org/10.1016/0016-7037(82)90377-5

Littke, R., Rotzal, H., Leythaeuser, D. and Baker, D.R., 1991. Organic facies and maturity of Lower Toarcian Posidonia Shale in Southern Germany (Schwäbische Alb). Erdöl & Kohle Erdgas Petrochemie/Hydrocarbon Technology, 44, 407-414.

Lyle, M., 1976. Estimation of hydrothermal manganese input to the oceans. Geology, 4, 733-736. http://dx.doi.org/10.1130/0091-7613(1976)4<733:EOHMIT>2.0.CO;2

Martin, J.H. and Meybeck, M., 1979. Elemental mass-balance of material carried by major world rivers. Marine Chemistry, 7, 173-206. http://dx.doi.org/10.1016/0304-4203(79)90039-2

Marzoli, A., Renne, P.R., Piccirillo, E.M., Ernesto, M., Bellieni, G. and De Min, A., 1999. Extensive 200 million-year-old continental flood basalts of the central Atlantic magmatic province. Science, 284, 616-618. http://dx.doi.org/10.1126/science.284.5414.616

McLennan, S.M., 2001. Relationships between the trace element composition of sedimentary rocks and upper continental crust. Geochemistry Geophysics Geosystems, 2, paper # 2000GC000109. http://dx.doi.org/10.1029/2000GC000109

Minor, D.R. and Mukasa, S.B., 1997. Zircon U-Pb and hornblende 40Ar-39Ar ages for the Dufek layered mafic intrusion, Antarctica: Implications for the age of the Ferrar large igneous province. Geochimica et Cosmochimica Acta, 61, 2497-2504. http://dx.doi.org/10.1016/S0016-7037(97)00098-7

Morford, J.L. and Emerson, S., 1999. The geochemistry of redox sensitive trace metals in sediments. Geochimica et Cosmochimica Acta, 63, 1735-1750. http://dx.doi.org/10.1016/S0016-7037(99)00126-X

Morford, J.L., Russell, A.D. and Emerson, S., 2001. Trace metal evidence for changes in the redox environment associated with the transition from terrigenous clay to diatomaceous sediments, Saanich Inlet, BC. Marine Geology, 174, 355-369. http://dx.doi.org/10.1016/S0025-3227(00)00160-2

Morford, J.L., Emerson, S.R., Breckel, E.J. and Kim, S.H., 2005. Diagenesis of oxyanions (V, U, Re, and Mo) in pore waters and sediments from a continental margin. Geochimica et Cosmochimica Acta, 69, 5021-5032. http://dx.doi.org/10.1016/j.gca.2005.05.015

Morse, J.W. and Luther III, G.W., 1999. Chemical influences on trace metal-sulfide interactions in anoxic sediments. Geochimica et Cosmochimica Acta, 63, 3373-3378. http://dx.doi.org/10.1016/S0016-7037(99)00258-6

Naimo, D., Adamo, P., Imperato, M. and Stanzione, D., 2005. Mineralogy and geochemistry of a marine sequence, Gulf of Salerno, Italy. Quaternary International, 140-141, 53-63. http://dx.doi.org/10.1016/j.quaint.2005.05.004

Nameroff, T.J., Calvert, S.E. and Murray, J.W., 2004. Glacial-interglacial variability in the eastern tropical North Pacific oxygen minimum zone recorded by redox-sensitive trace metals. Paleoceanography, 19, PA1010. http://dx.doi.org/10.1029/2003PA000912.

Neumeister, S., Gratzer, R., Algeo, T.J., Bechtel, A., Gawlick, H.-J., Newton, R.J. and Sachsenhofer, R.F., 2015. Oceanic response to Pliensbachian and Toarcian magmatic events: Implications from an organic-rich basinal succession in the NW Tethys. Global and Planetary Change, 126, 62-83. http://dx.doi.org/10.1016/j.gloplacha.2015.01.007

Pálfy, J. and Smith, P.L., 2000. Synchrony between Early Jurassic extinction, oceanic anoxic event, and the Karoo–Ferrar flood basalt volcanism. Geology, 28, 747-750. http://dx.doi.org/10.1130/0091-7613(2000)28<747:SBEJEO>2.0.CO;2

Parrish, J.T., 1993. Climate of the supercontinent Pangaea. Journal of Geology, 101, 215-233.

Parrish, J.T. and Curtis, R.L., 1982. Atmospheric circulation, upwelling, and organic-rich rocks in the Mesozoic and Cenozoic areas. Palaeogeography, Palaeoclimatology, Palaeoecology, 40, 31-66. http://dx.doi.org/10.1016/0031-0182(82)90084-0

Pearce, C.R., Cohen, A.S., Coe, A.L. and Burton, K.W., 2008. Molybdenum isotope evidence for global ocean anoxia coupled with perturbations to the carbon cycle during the Early Jurassic. Geology, 36, 231-234. http://dx.doi.org/10.1130/G24446A.1

Perkins, R.B., Piper, D.Z. and Mason, C.E., 2008. Trace-element budgets in the Ohio-Sunbury shales of Kentucky: constraints on ocean circulation and primary productivity in the Devonian-Mississippian

Appalachian Basin. Palaeogeography Palaeoclimatology Palaeoecology, 265, 14-29. http://dx.doi.org/10.1016/j.palaeo.2008.04.012

Piper, D.Z. and Perkins, R.B., 2004. A modern vs. Permian black shale – the hydrography, primary productivity, and water-column chemistry of deposition. Chemical Geology, 206, 177-197. http://dx.doi.org/10.1016/j.chemgeo.2003.12.006

Piper, D.Z., Perkins, R.B. and Rowe, H.D., 2007. Rare-earth elements in the Permian Phosphoria Formation: paleo proxies of ocean geochemistry. Deep-Sea Research, 54, 1396-1413. http://dx.doi.org/10.1016/j.dsr2.2007.04.012

Piper, D.Z. and Calvert, S.E., 2009. A marine biogeochemical perspective on black shale deposition. Earth Science Reviews, 95, 63-96. http://dx.doi.org/10.1016/j.dsr2.2007.04.012

Pratt, L.M. and Davis, C.L., 1992. Intertwined fates of metals, sulphur, and organic carbon in black shales. In: Pratt et al. (Eds.), Geochemistry of Organic Matter in Sediments and Sedimentary Rocks. SEPM Short Course, 27, 1-27.

Praus, M. and Riegel, W., 1989. Evidence from phytoplanktonic associations for causes of black shale formation in epicontinental seas. Neues Jahrbuch für Geologie und Paläontologie, Monatshefte, 11, 671-682.

Ratschbacher, L., Dingeldey, C., Miller, C., Hacker, B.R. and McWilliams, M.O., 2004. Formation, subduction, and exhumation of Penninic oceanic crust in the Eastern Alps: time constraints from 40Ar/39Ar geochronology. Tectonophysics, 394, 155-170. http://dx.doi.org/10.1016/j.tecto.2004.08.003

Rex, R.W. and Goldberg, E.D., 1958. Quartz contents of pelagic sediments in the Pacific Ocean. Tellus, 10, 153-159.

Robl, T.L. and Barron, L.S., 1987. The geochemistry of Devonian black shales in central Kentucky and its relationship to interbasinal correlation and depositional environment. In: N.J. McMillan et al. (eds.), Devonian of the World, 2, Sedimentation. Mem. of the Canadian Society of Petroleum Geologists, 14, pp. 377-392.

Röhl, H.J., Schmid-Röhl, A., Oschmann, W., Frimmel, A. and Schwark, L., 2001. The Posidonia Shale (Lower Toarcian) of SW-Germany: an oxygen-depleted ecosystem controlled by sea level and palaeoclimate. Palaeogeography, Palaeoclimatology, Palaeoecology, 165, 27-52. http://dx.doi.org/10.1016/S0031-0182(00)00152-8

Sælen, G., Doyle, P. and Talbot, M.R., 1996. Stable-isotope analysis of belemnite rostra from the Whitby Mudstone Fm., England: Surface water conditions during deposition of a marine black shale. Palaios, 11, 97-117. http://dx.doi.org/10.2307/3514466

Savrda, C.E. and Bottjer, D.J., 1991. Oxygen-related biofacies in marine strata: an overview and update. In: R.V. Tyson and T.H. Pearson (eds.), Modern and Ancient Continental Shelf Anoxia. Geological Society London Special Publications, 58, pp. 201-219.

Schlager, W. and Schöllnberger, W., 1973. Das Prinzip stratigraphischer Wenden in der Schichtfolge der Nördlichen -Kalkalpen. Mitteilungen der Geologischen Gesellschaft Wien, 66, 166-193.

Schmid-Röhl, A., Röhl, H.-J., Oschmann, W., Frimmel, A. and Schwark, L., 2002. Palaeoenvironmental reconstruction of Lower Toarcian epicontinental black shales (Posidonia Shale, SW Germany): global versus regional control. Geobios, 35, 13-20. http://dx.doi.org/10.1016/S0016-6995(02)00005-0

Schwark, L., Vliex, M. and Schaeffer, P., 1998. Geochemical characterization of Malm Zeta laminated carbonates from the Franconian Alb, SW Germany (II). Organic Geochemistry, 29, 1921-1952. doi:10.1016/S0146-6380(98)00192-2

Scott, C., Lyons, T. W., Bekker, A., Shen, Y., Poulton, S. W., Chu, X., and Anbar, A. D., 2008. Tracing the stepwise oxygenation of the Proterozoic ocean. Nature, 452(7186), 456-459. doi:10.1038/nature06811

Sell, B., Ovtcharova, M., Guex, J., Bartolini, A., Jourdan, F., Spangenberg, J.E., Vicente, J.-C. and Schaltegger, U., 2014. Evaluating the temporal link between the Karoo LIP and climatic-biologic events of the Toarcian Stage with high-precision U-Pb geochronology. Earth and Planetary Science Letters, 408, 48-56. http://dx.doi.org/10.1016/j.epsl.2014.10.008

Sinninghe Damsté, J.S., van Duin, A.C.T., Hollander, D., Kohnen, M.E.L. and de Leeuw, J.W., 1995. Early diagenesis of bacteriohopanepolyol derivatives: Formation of fossil homohopanoids. Geochimica et Cosmochimica Acta 59, 5141-5156. doi:10.1016/0016-7037(95)00338-X

Spieler, A. and Brandner, R., 1989. Vom jurassischen Pull-Apart Becken zur Westüberschiebung der Achentaler Schubmasse (Tirol, Österreich). Geologisch-Paläontologische Mitteilungen Innsbruck, 16, 191-194.

Suan, G., Schlögl, J. and Mattioli, E., 2016. Bio- and chemostratigraphy of the Toarcian organic-rich deposits of some key successions of the Alpine Tethys. Newsletters on Stratigraphy, published online.

Svensen, H., Planke, S., Chevalier, L., Malthe-Sørensen, A., Corfu, F. and Jamveit, B., 2007. Hydrothermal venting of greenhouse gases triggering Early Jurassic global warming. Earth and Planetary Science Letters, 256, 554-566. http://dx.doi.org/10.1016/j.epsl.2007.02.013

Svensen, H., Corfu, F., Polteau, S., Hammer, Ø. and Planke, S., 2012. Rapid magma emplacement in the Karoo Large Igneous Province. Earth and Planetary Science Letters, 325–326, 1-9. http://dx.doi.org/10.1016/j.epsl.2012.01.015

Taylor, S.R. and McLennan, S.M., 1985. The Continental Crust, its Composition and Evolution. Blackwell Scientific, Oxford. 312 pp.

ten Haven, H.L., de Leeuw, J.W. and Schenk, P.A., 1985. Organic geochemical studies of a Messinian evaporitic basin, northern Appenines (Italy): Hydrocarbon biological markers for a hypersaline environment. Geochimica et Cosmochimica Acta 49, 2181-2191. doi:10.1016/0016-7037(85)90075-4

ten Haven, H.L., de Leeuw, J.W., Rullkötter, J. and Sinninghe Damsté, J.S., 1987. Restricted utility of the pristane/phytane ratio as a palaeoenvironmental indicator. Nature 330, 641-643. doi:10.1038/330641a0

Thomson, J., Higgs, N.C., Croudace, I.W., Colley, S. and Hydes, D.J., 1993. Redox zonation of elements at an oxic/post-oxic boundary in deep-sea sediments. Geochimica et Cosmochimica Acta, 57(3), 579-595. http://dx.doi.org/10.1016/0016-7037(93)90369-8

Tollmann, A., 1976. Analyse des klassischen nordalpinen Mesozoikums. Stratigraphie, Fauna und Fazies der Nördlichen Kalkalpen. Deuticke, Wien, 580 pp.

Tribovillard, N., Algeo, T.J., Lyons, T. and Riboulleau, A., 2006. Trace metals as paleoredox and paleoproductivity proxies: An update. Chemical Geology, 232, 12-32. http://dx.doi.org/10.1016/j.chemgeo.2006.02.012

Von Damm, K.L., 1990. Seafloor hydrothermal activity: Black smoker chemistry and chimneys. Annual Review of Earth and Planetary Sciences, 18, 173-204. http://dx.doi.org/10.1146/annurev.ea.18.050190.001133

Wedepohl, K.H., 1971. Environmental influences on the chemical composition of shales and clays. Physics and Chemistry of the Earth, 8, 305-333. http://dx.doi.org/10.1016/0079-1946(71)90020-6

Wedepohl, K.H., 1995. The composition of the continental crust. Geochimica et Cosmochimica Acta, 59, 1217-1232. http://dx.doi.org/10.1016/0016-7037(95)00038-2

Weissert, H., 2000. Deciphering methane's fingerprint. Nature, 406, 356-357. http://dx.doi.org/10.1038/35019230

Whiteside, J.H., Olsen, P.E., Kent, D.V., Fowell, S.J. and Et-Touhami, M., 2007. Synchrony between the Central Atlantic magmatic province and the Triassic-Jurassic mass extinction event? Palaeogeography, Palaeoclimatology, Palaeoecology, 244, 345-367. http://dx.doi.org/10.1016/j.palaeo.2006.06.035

Wignall, P.B., 1994. Black Shales. Clarendon Press, Oxford, 127 pp.

Yarincik, K.M., Murray, R.W. and Peterson, L.C., 2000. Climatically sensitive eolian and hemiplegic deposition in the Cariaco Basin, Venezuela, over the past 578,000 years: results from Al/Ti and K/Al. Paleoceanography, 15, 210-228. http://dx.doi.org/10.1029/1999PA900048

Zheng, Y., Anderson, R.F., van Geen, A. and Fleisheir, M.Q., 2002. Preservation of non-lithogenic particulate uranium in marine sediment. Geochimica et Cosmochimica Acta, 66, 3085-3092. http://dx.doi.org/10.1016/S0016-7037(01)00632-9

9 Diagenesis of organic-rich marls under shifting suboxic to euxinic conditions

Submitted for publication in the International Journal of Earth Sciences.

S. Neumeister [a,*], T. J. Algeo [b], H.-J. Gawlick [a], R. Gratzer [a], R. F. Sachsenhofer [a]

[a] *Department of Applied Geosciences and Geophysics, Montanuniversitaet Leoben, Peter-Tunner-Str. 5, A-8700 Leoben, Austria*

[b] *Department of Geology, University of Cincinnati, Cincinnati, OH 45221, USA*

* Corresponding author.

E-mail address: st.neumeister@hotmail.com (Stefan Neumeister)

Abstract

The Bächental bituminous marls (Bächentaler Bitumenmergel) belonging to the Sachrang Member of the Middle Allgäu Formation were investigated using a multidisciplinary approach to identify the processes and products of early diagenesis, as well as controls thereon, within a carbonate-dominated semi-restricted basin of the NW Tethys realm. The Bächental basin was subjected to significant environmental variations during the Early Jurassic, including shifts between suboxic and euxinic redox conditions. Redox-dependent organic-matter (OM) oxidation processes are clearly reflected by stratigraphic variation in bulk organic parameters in the study section, allowing recognition of discrete litho-diagenetic units (Units 1-2a-2b-3 from base to top). Suboxic conditions, dominating in Units 1 and 3, enabled the activity of aerobic and denitrifying microbes in sediment surface layers in addition to anaerobic reduction of Mn and Fe oxides and sulfate. The availability of abundant Mn oxides resulted in strong Mn reduction, causing a maximum OM loss in the range of 0.9 to 1.5 % and a lowering of hydrogen index values by up to 400 mg HC/g TOC. In contrast to Units 1 and 3, sulfate reduction was the dominant degradation process in anoxic-euxinic Unit 2. However, natural sulphurization of OM under Fe-limited conditions induced an early termination of sulfate reduction, contributing to enhanced OM preservation in Unit 2, as reflected in a more limited decrease of hydrogen index values (by 100 mg HC/g TOC). Mn

oxides were already reduced within the SH--bearing water column during deposition of Unit 2. In the Bächental basin, OM oxidation processes caused an increase of pH values (up to >9) and alkalinity in pore waters. These changes initiated redox-dependent precipitation of diagenetic carbonate phases in all samples and caused advanced dissolution of biogenic silica and incipient alteration of pyrite exclusively in the anoxic-euxinic and radiolarian-silica-rich Unit 2. Dolomite formation, occurring in the sediment surface layers, was favored by suboxic conditions and mediated by aerobic and denitrifying bacteria. Whereas low-temperature dolomite precipitation was not influenced by sulfate concentrations in pore waters and anaerobic reduction processes, it was distinctly impeded during periods of anoxia. Anaerobic Mn reduction triggered the release of isotopically light carbon and Mn supersaturation of pore waters, which was especially significant in suboxic Units 1 and 3. This caused a transition from dolomite to kutnohorite (Mn carbonate) precipitation. Kutnohorite was precipitated at the chemocline during maximum OM degradation and, hence, features abnormally negative carbonate-C isotope values derived from Mn reduction. Mn-bearing siderite occurs solely within a 3-m-thick interval at the base of suboxic Unit 3 characterized by the predominance of Fe over sulfate reduction. In Unit 2, anoxia inhibited kutnohorite precipitation, and Mn-bearing calcite is the dominant secondary carbonate phase instead. This mineral contains small amounts of isotopically light C derived from sulfate reduction, and it was formed at later diagenetic stages when OM oxidation rates were lower. Thus, diagenetic carbonates formed rapidly and exclusively above the chemocline under suboxic conditions, whereas carbonate precipitation persisted for longer periods and occurred mainly below the chemocline under anoxic conditions. The study section provides detailed insights into the processes and products of early diagenesis of OM-rich marls under a range of redox conditions.

Keywords: Bächental bituminous marl; Sachrang Member; Northern Calcareous Alps; organic-matter oxidation; manganese reduction; sequenced precipitation of carbonate phases

9.1 Introduction

Organic-rich marine deposits are subjected to a variety of early diagenetic processes affecting organic matter (OM) preservation and authigenic mineral precipitation. In such environments, early diagenetic OM degradation is controlled by a sequence of redox-dependent, microbially mediated aerobic and anaerobic processes using inorganic electron

acceptors (e.g., Froelich et al., 1979; Thamdrup, 2000; Jørgensen, 2000). These oxidation processes can create pore-water conditions that are favorable for precipitation of a variety of authigenic mineral phases (Wright and Oren, 2005; Wacey et al., 2008) including dolomite and manganese (Mn)-bearing carbonates, which are common in both modern and ancient OM-rich successions (e.g., Compton, 1988; Jenkyns, 1988; Middelburg et al., 1990; Mazzullo, 2000; Heiser et al., 2001; Polgári et al., 2004; Sabatino et al., 2011; Meister et al., 2013). The formation of dolomite, which can occur anywhere from synsedimentary surface to deep burial environments has received especial attention (e.g., Mazzullo, 2000; Warren, 2000; Machel, 2004; Meister et al., 2007). Furthermore, Mn-sources and environmental factors causing the significant Mn enrichment in several Lower Jurassic black shale deposits of the Tethyan realm (e.g., Jenkyns, 1988; Polgári et al., 2012 and references therein) are still controversially discussed. However, despite intensive research, the nature and sequence of the reactions governing the formation of authigenic carbonates during diagenesis of OM-rich sediments remain incompletely known.

A 24-m-thick succession of bituminous marls (the Lower Jurassic Bächentaler Bitumenmergel) with up to 13 % TOC is found in the Bächental valley of Tyrol in the Northern Calcareous Alps (Fig. 9.1A). The study units accumulated in the Bächental basin, which was located at the NW continental margin of the Tethys Ocean and the SW continental margin of the Alpine Atlantic, respectively (Figs. 9.1A, B). Neumeister et al. (2015, 2016) used a multi-analytical approach based on microscopy, X-ray diffraction (XRD) analysis, bulk geochemistry, stable isotopy, and organic geochemistry to determine environmental conditions effective on global (e.g., magmatism, opening of the Alpine Atlantic Ocean, sea level fluctuations) and local (e.g., redox state, salinity variations, basin morphology) scales that controlled OM accumulation in the semi-restricted Bächental basin. Strong environmental changes within this basin during the Early Jurassic resulted in pronounced stratigraphic variation that provides the basis for subdivision of the section into three units (Units 1-3; Neumeister et al., 2015, 2016). These units represent distinct redox states that were closely linked to the nature and intensity of early diagenetic processes. Hence, the Bächentaler Bitumenmergel provides a valuable opportunity to investigate differences regarding the relative significance of diagenetic processes and products associated with OM oxidation in a marine setting subjected to highly variable depositional conditions.

The aim of this study was to determine the diagenetic response to varying (suboxic to euxinic) redox conditions within the Bächental basin. To this end, we applied a multidisciplinary approach to define the essential processes controlling [i] OM degradation and preservation, [ii] pH and alkalinity conditions in pore waters, [iii] occurrence, time of formation, amount, and mineralogical composition of the individual secondary carbonate phases present, [iv] dissolution of biogenic quartz, and [v] alteration of pyrite in the study section. Thus, the results provide insights into the complex processes occurring during early diagenesis in a carbonate-dominated hemipelagic basin within the NW Tethyan realm.

9.2 Geological setting

The Lower Toarcian is characterized by the global occurrence of marine deposits with elevated organic matter (OM) content (e.g., Jenkyns, 1985, 1988; Jenkyns et al., 2002; Pearce et al., 2008). Their accumulation has been attributed to upwelling connected with an oceanic anoxic event in the Toarcian (T-OAE; see summary in Jenkyns, 2010), as well as with water-column stratification in the western European epicontinental realm, caused by a surface-water layer with reduced salinity (Praus and Riegel, 1989; Littke et al., 1991; Sælen et al., 1996) or by minor sea-level fluctuations (Röhl et al., 2001; Schmid-Röhl et al., 2002; Frimmel et al., 2004; McArthur et al., 2008). For any of these mechanisms, short-term variation in OM accumulation may have been modulated by orbital forcings (Ikeda and Hori, 2014). Beside Karoo-Ferrar magmatism, Neumeister et al. (2015) also pointed to the potential effects of volcanic activity related to the early opening of the Alpine Atlantic commencing in late early Jurassic times.

Lower Toarcian OM-rich deposits of the western Tethyan realm commonly contain high amounts of diagenetic Mn-rich carbonates (Jenkyns, 1988; Vetö et al., 1997; Ebli et al., 1998; Bellanca et al., 1999; Gawlick and Suzuki, 1999; Corbin et al., 2000; Polgári et al., 2004, 2012; Sabatino et al., 2011). Exceptionally high Mn concentrations, partly reaching ore grade, are suggested to have been caused by hydrothermal activity in the course of breakup of the Pangean supercontinent (e.g., Corbin et al., 2000; Jach and Dudek, 2005), greater weathering fluxes of continentally derived Mn (Jenkyns et al., 1991; Sabatino et al., 2011), and microbial activity (Polgári et al., 2015). In addition, several studies propose a linkage between sea-level changes and Mn enrichment as both Mn availability and sea-level variations are affected by mid-oceanic hydrothermal fluxes related to global tectonic activity

(e.g., Pratt et al., 1991, Accarie et al., 1993; Corbin et al., 2000; de Rafélis et al., 2001; Sabatino et al., 2011).

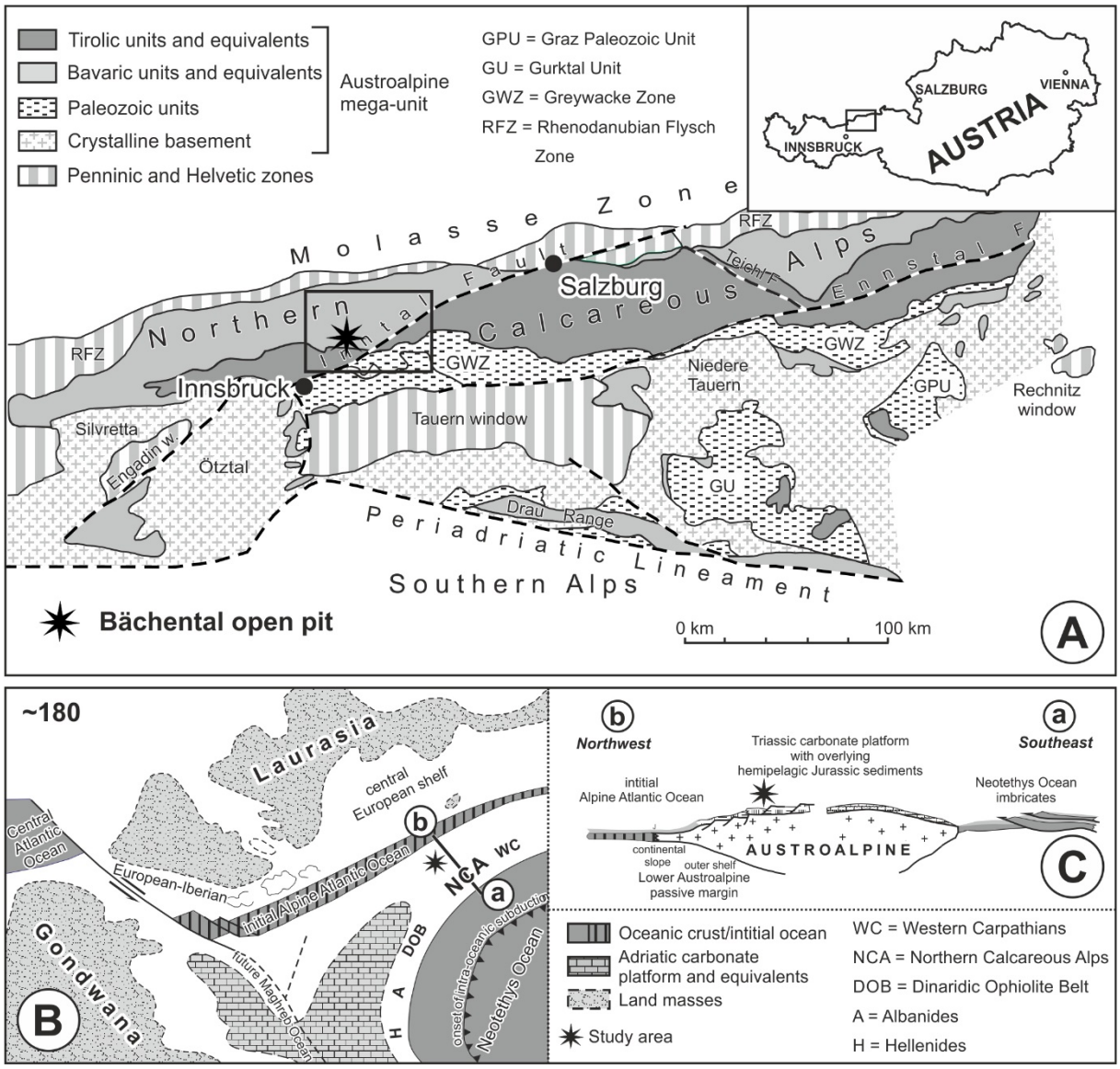

Fig. 9.1: (A) Schematic tectonic map of the Eastern Alps (after Frisch and Gawlick, 2003) showing location of the Bächental study section. (B) Palaeogeographic position of the study section as part of the Northern Calcareous Alps within the Austroalpine domain in Early Jurassic time (modified after Gawlick et al., 2009). Line a-b represents cross-section in c. (C) Schematic cross-section across the passive continental margin of the Lower Austroalpine domain (modified after Missoni and Gawlick, 2011). Rifting and spreading of the Alpine Atlantic commencing in the late Early Jurassic affected the Austroalpine domain through formation of asymmetric extensional basins with horst-and-graben structure (cf. Bernoulli and Jenkyns, 1974).

The geological setting of the Bächental section, which is well exposed in an open-pit mine, was recently described by Neumeister et al. (2015) and is briefly summarized here. The investigated section is situated in the Bächental valley, which is part of the Northern Calcareous Alps in western Austria (Fig. 9.1A; GPS: 47°30'31.38"N; 11°37'46.00"E). In the late Early Jurassic, the study area was situated on a drowned plateau between the NW continental margin of the Neo-Tethys Ocean and the SE of the newly formed passive margin of the Alpine Atlantic (Figs. 9.1B, C; Missoni and Gawlick 2011). This area was affected by extensional tectonics, related to late Hettangian rifting and Toarcian oceanic break-up in the Alpine Atlantic (Penninic) realm (e.g., Ratschbacher et al., 2004), that resulted in formation of synrift basins such as the Bächental basin. The basin exhibits tilt block tectonics and antithetic step faults, producing a half-graben geometry with a depocenter in its northern part (Spieler and Brandner, 1989). Deposition of bituminous marls during the early Jurassic was limited to the poorly ventilated deepest part (depocenter) of the Bächental basin (Spieler and Brandner, 1989).

The dating of the Bächental bituminous marls to the Toarcian was originally based on the occurrence of *Harpoceras* sp. (Klebelsberg, 1935). This is consistent with the presence of *Cleviceras exaratum* in the middle part of the section, a taxon associated with the early Toarcian *falciferum* Zone (Neumeister et al., 2015). Kodina et al. (1988) and Lobitzer et al. (1988) inferred that bituminous marl sedimentation began during the late Pliensbachian based on the occurrence of *Arieticeras* sp. and, possibly, *Leptaleoceras* sp. Neumeister et al. (2015) proposed that the deposition of the Sachrang Member in the Bächental basin lasted from late Pliensbachian (*margaritatus* Zone) to early Toarcian (*bifrons* Zone) based on correlation of C_{27}/C_{29} sterane data from Bächental and Dotternhausen (epicontinental Posidonia Shale) sections with sea level. However, new biostratigraphic data – including the reexamination of the ammonites published by Kodina et al. (1988) – indicate that Units 2 and 3 solely belong to the Lower Toarcian *falciferum*-Zone, whereas data for the basal part of the section is missing (Suan et al., 2016). At its type locality in Bavaria, deposition of the Sachrang Member commenced at the base of the *tenuicostatum* Zone and continued through the entire early Toarcian (Ebli et al., 1998).

In the study section, Bächental bituminous marls of the Sachrang Member (Middle Allgäu Formation) overlie pure carbonates of the Scheibelberg Formation (Sinemurian to Pliensbachian) with a sharp contact. The top of the Sachrang Member is formed by an

alternating sequence of limestone and marl (Upper Allgäu Formation; Spieler and Brandner, 1989). Beside bituminous marls, the Sachrang Member comprises a basal mudstone and a carbonate debrite layer. The basal mudstone consists exclusively of quartz and clay minerals reflecting terrigenous origin. Charred OM material and smectite in this layer reflect volcaniclastic inputs, which potentially triggered the onset of OM accumulation in the Bächental basin (Neumeister et al., 2015). The occurrence of considerable amounts of smectite through the entire Sachrang Member suggests continuing inputs from volcanic sources.

Bächental bituminous marls were subdivided into three units on the basis of lithology and bulk geochemical data (Fig. 9.2; Neumeister et al., 2015, 2016). Organic and inorganic redox proxies indicate suboxic conditions during deposition of Units 1 and 3, but strictly anoxic-euxinic conditions and a salinity-stratified water column during deposition of Unit 2. Redox and salinity changes in the Bächental basin, which was characterized by a complex bathymetry, were determined mainly by minor sea-level fluctuations that controlled patterns of bottom-water ventilation. The depocenter of the basin was subjected to episodic sediment gravity flows as well as to intense bioproductivity in surface waters especially during deposition of Subunit 2a.

9.3 Samples and analytical methods

A total of 47 samples (BT 9-40, BT 44-58) of the Bächental bituminous marls of the Sachrang Member of the Middle Allgäu Formation were analyzed in this study. The samples were collected from fresh exposures on an active mine face located in the Bächental valley, which is part of the Karwendel Mountains of northern Tyrol (Fig. 9.1A).

Major- and trace-element (TE) concentrations were determined on whole-rock samples using a wavelength-dispersive Rigaku 3040 X-ray fluorescence (XRF) spectrometer at the University of Cincinnati. Raw intensities were calibrated using a set of 65 standards from the USGS, the National Bureau of Standards, and internal lab standards that were analyzed by XRAL Incorporated using XRF and INAA. Analytical precision based on replicate analyses was better than ±2 % for major and minor elements and ±5 % for TEs, and detection limits were 1 to 2 ppm for most TEs.

XRD analysis were carried out on bulk samples using Philips X-pert equipment and CuKα-radiation (1.54 Å, 35 kV, 35 mA) at the University of Leoben, Austria. The single scans were operated in spin-mode with a goniometer velocity of 0.5° min-1 in the range from 25 to 35° 2θ for identification of carbonate phases in the air-dry state (random powder mount). The individual peaks were identified by the use of standardized tables and by comparison with reference samples.

Quantitative analyses of carbonates were performed on selected samples by using an electron microprobe (Superprobe Jeol JXA 8200) installed at the Eugen F. Stumpfl Laboratory at the University of Leoben, Austria, operated in WDS mode and applying 15 kV accelerating voltage and 10 nA beam current. The counting times for peak and both backgrounds (left and right) were 20 s and 10 s, respectively. The beam diameter was ~1 μm. Natural diopside, apatite, magnetite, rhodochrosite, and strontianite were used as standards for magnesium (Mg), calcium (Ca), iron (Fe), manganese (Mn), and strontium (Sr). The X-ray lines used were: Kα for Mg, Ca, Fe, and Mn and Lα for Sr. The following diffracting crystals were selected: TAP for Mg, PETJ for Ca, LIFH for Fe and Mn, and PETH for Sr. The subsequently quoted detection limits (all in ppm) are automatically calculated by the microprobe software: Mg = 100, Ca = 150, Fe = 200, Mn = 150, and Sr = 200.

9.4 Results

The concentrations of silicon (Si), Ca, Mg, and Mn for Bächental bituminous marls are shown in Fig. 9.2 and Table 9.10.1 (note: all data tables are shown in the Appendix). Si concentrations of samples from Unit 1 exhibit rather constant values (16.6-20.6 %), contrasted by varying values for Units 2 and 3 (6.6-26.2 %). Ca is generally enriched in the upper half (8.1-10.9 %) of Unit 1 compared to its lower part (6.6-7.8 %) while samples from Units 2 and 3 display on average higher but strongly fluctuating Ca concentrations (5.3-22.5 %). Samples from Units 1, 2b, and 3 generally show elevated Mg concentrations (1.4-5.5 %) compared to those of Unit 2a (2.1-2.9 %). Whereas Unit 2 is characterized by low Mn concentrations (<1.2 %), the element is commonly enriched in samples from Units 1 and 3 (0.4-11.6 %), reaching peak values in the lower 4 m of Unit 3.

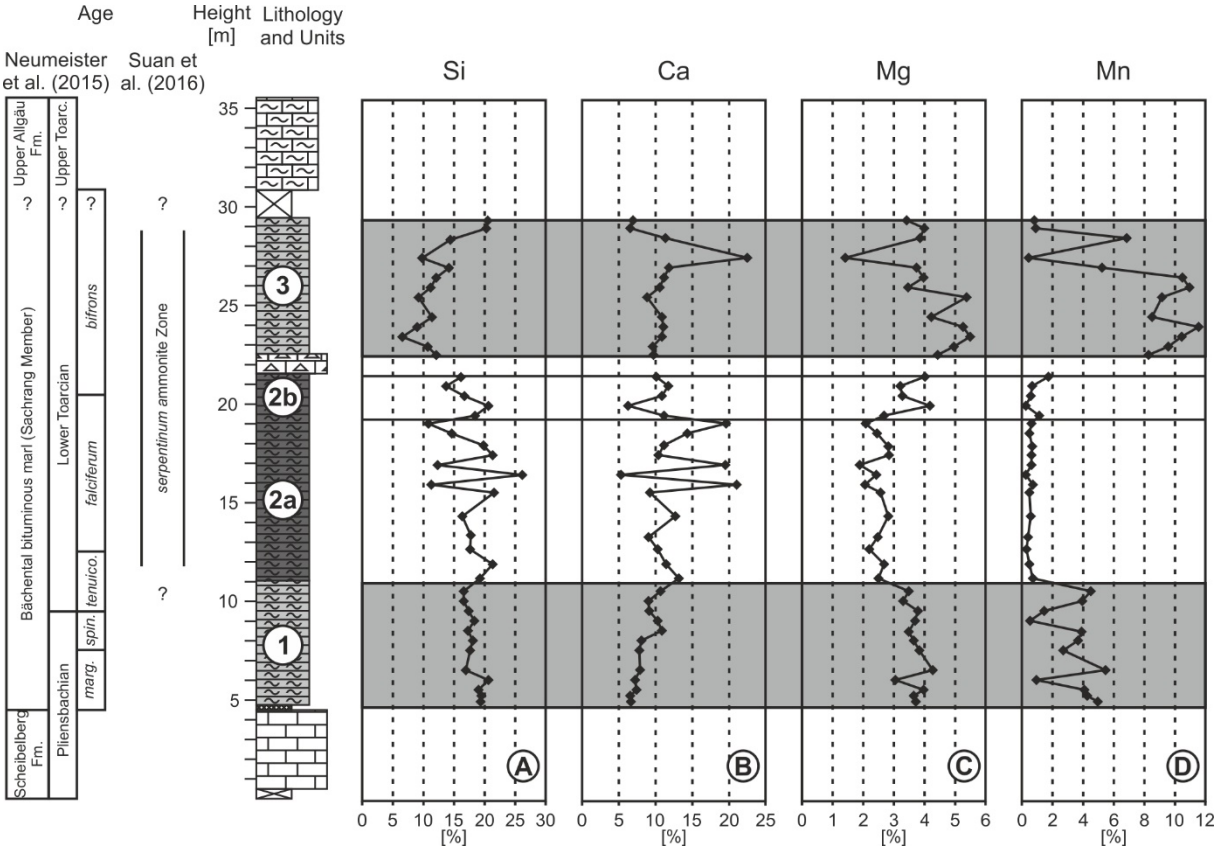

Fig. 9.2: Profiles of bulk geochemical concentrations in the Bächental study section: (A) silicon (Si), (B) calcium (Ca), (C) magnesium (Mg), (D) manganese (Mn). Stratigraphic subdivision of the Bächental bituminous marls follows Neumeister et al. (2015) and Suan et al. (2016); Units 1 and 3 shaded for emphasis.

The Bächental bituminous marls contain several carbonate phases that are distinguishable on the basis of elemental composition, as measured by microprobe (note that all are diagenetic in origin except for phase I). These phases are: [i] detrital calcite (Ca: 35.6-38.3 %), [ii] dolomite (Ca: 21.8-24.1 %; Mg: 10.6-13.1 %), [iii] kutnohorite (Ca: 9.1-21.2 %; Mn: 16.7-32.4 %), [iv] Mn-bearing siderite, and [v] Mn-bearing calcite (Ca: 32.4-40.4 %; Mn: 0.6-4.2 %; Fig. 9.3; Table 9.10.2). Kutnohorite is a Mn-carbonate with the chemical composition $(Ca_xMn_{2-x})(CO_3)_2$, where x ranges from ~0.5 to ~1.5. The individual carbonate phases were approximately quantified by calculating peak areas for their main peaks in XRD diffractograms (Figs. 9.3, 9.5; Table 9.10.1). Although the complete separation of all carbonate phases was impossible because of overlap of their XRD peaks, the shapes and positions of XRD peaks suggest dominance of diagenetic calcite over detrital calcite and of kutnohorite over dolomite (Fig. 9.4). The relative amounts of calcite and kutnohorite/dolomite exhibit strong variation in Units 1 and 3 (16.0-88.4 % and 11.6-81.0 %, respectively). In

contrast, Unit 2 is characterized by high calcite concentrations (66.7-99.0 %) and rather low amounts of kutnohorite and dolomite (1.0-33.3 %). Mn-bearing siderite (5.6-20.3 %) is present solely in the lower 3 m of Unit 3. All carbonates phases are Sr-poor (<0.25 %; Table 9.10.2).

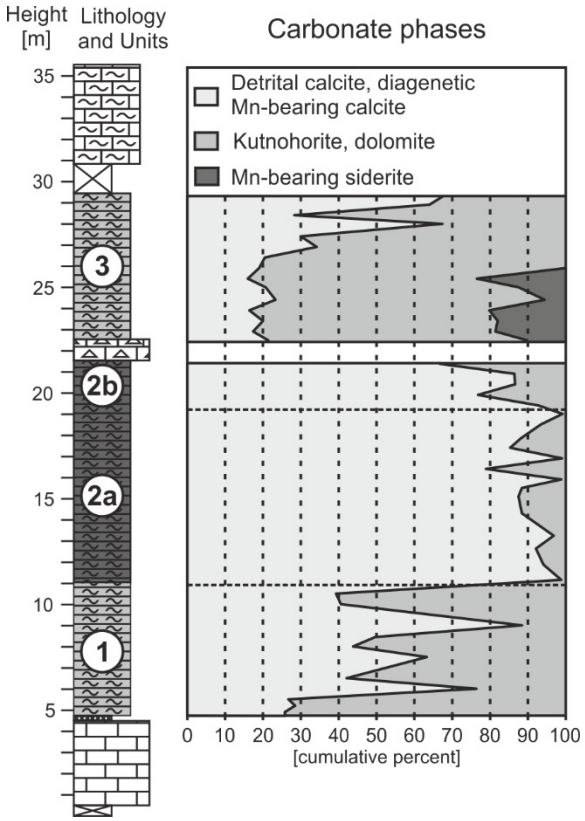

Fig. 9.3: Profiles of carbonate phases: detrital calcite and Mn-bearing calcite (light grey), kutnohorite and dolomite (mid-grey), and Mn-bearing siderite (dark grey).

The detrital calcite derives from marine invertebrate shell and test fragments transported to the depositional basin. Dolomite is present in idiomorphic-rhombohedral to roundish shaped aggregates (Figs. 9.5A-C). The crystals are always surrounded by a rim of kutnohorite. Kutnohorite, Mn-bearing siderite, and Mn-bearing calcite appear as irregularly shaped aggregates in the samples (Figs. 9.5A-C, E, F). The latter also substitutes for biogenic silica in the form of recrystallized radiolarian ghosts (Fig. 9.5E). The elemental compositions of kutnohorite show a significant zonation in some samples from Units 1 and 3. Alternating rims of Ca-poor/Mn-rich (Ca: ~10 %; Mn: ~31 %) and Ca-rich/Mn-poor (Ca: ~27 %; Mn: ~13 %) kutnohorite around a nucleus consisting of either a detrital grain (calcite, clay, quartz) or Mn-rich kutnohorite indicate a polyphase growth history of this carbonate mineral (Figs.

9.5F, G). Mn-rich kutnohorite typically forms the innermost as well as the outermost rim of grains. The removal of S from the pyrite lattice resulted in the conversion of pyrite to Fe(II) oxide in TOC-rich samples of Subunit 2a (Fig. 9.5D). Whereas smaller grains are totally converted, the alteration process did not reach the nucleus of larger pyrite aggregates (>10 µm diam.), which show normal pyrite composition surrounded by a rim of Fe(II) oxide.

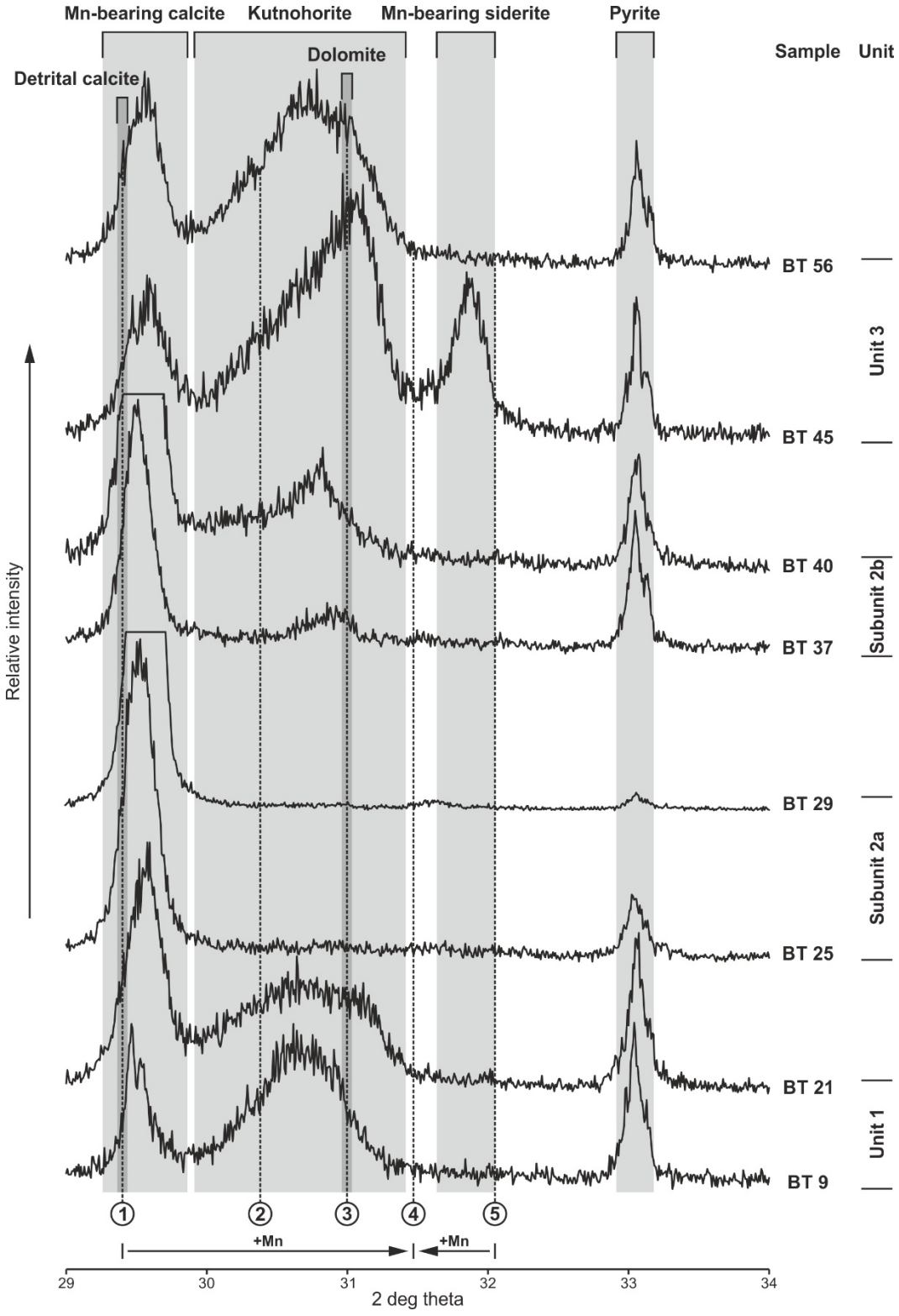

Fig. 9.4: X-ray diffractograms of selected samples: BT 9 and BT 21 (Unit 1), samples BT 25 and BT 29 (Subunit 2a), samples BT 37 and BT 40 (Subunit 2b), and samples BT 45 and BT 56 (Unit 3). Light grey rectangles mark the peak areas of detrital calcite, Mn-bearing calcite, kutnohorite, dolomite, Mn-bearing siderite, and pyrite in the samples. Also shown are the positions of the standard peaks of (1) calcite, (2) kutnohorite, (3) dolomite, (4) rhodochrosite, and (5) siderite. Note that relative intensities of the individual chromatograms are not adjusted to a common scale.

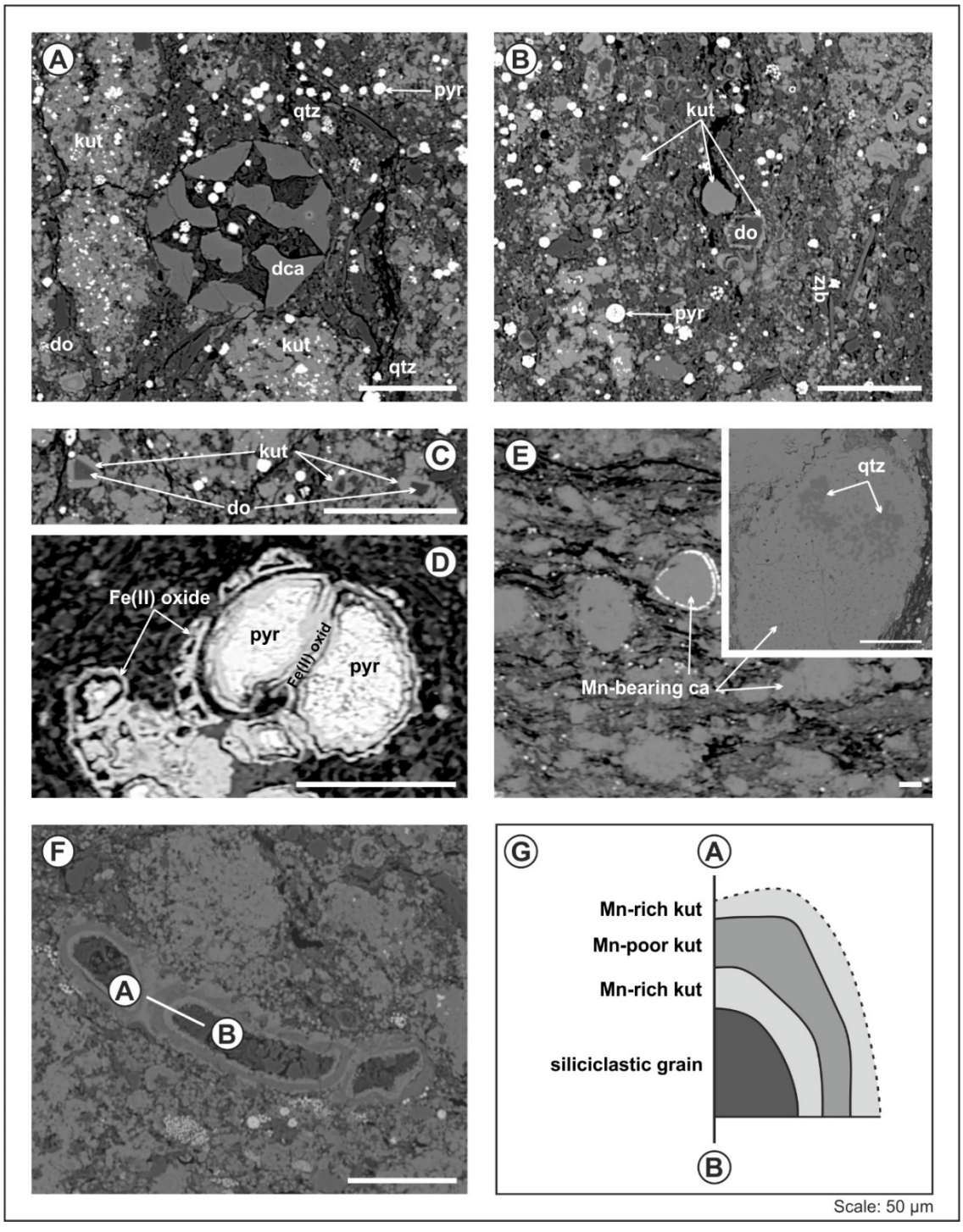

Fig. 9.5: Microphotographs of selected samples using the microprobe: (A-C) BT 9 (Unit 1), (D) BT 25 (Subunit 2a), (E) BT 29 (Subunit 2a), (F) BT 45 (Unit 3), and (G) sketch showing carbonate zonation surrounding a siliciclastic grain (for position, see line a-b in F). Indicated mineral phases: detrital calcite (dca), Mn-bearing calcite (Mn-bearing ca), kutnohorite (kut), dolomite (do), quartz (qtz), pyrite (pyr), and iron (II) oxide (Fe (II) oxide). Scale: 50 µm.

Results for TOC, Fe, S, and aluminium (Al) concentrations, calcite equivalent percentages (Cc_{eq} = total inorganic carbon x 8.33), values for hydrogen index (HI), carbonate isotopes ($\delta^{13}C_{carb}$, $\delta^{18}O_{carb}$), and pristane/phytane ratio (Pr/Ph) as well as the amount of kutnohorite/dolomite were previously reported by Neumeister et al. (2015, 2016). The full dataset is given in Tables 9.10.1 and 9.10.3.

9.5 Early diagenetic processes in organic matter-rich sediments

The obtained mineralogical and geochemical data for Bächental bituminous marls result from various early diagenetic processes (see Section 9.6). To provide a better understanding, a general overview of the processes relevant to the study section is given in the following.

9.5.1 Microbially mediated OM oxidation processes

Early diagenetic microbially mediated OM degradation includes aerobic and anaerobic mineralization processes using inorganic electron acceptors. OM oxidation processes show a well-defined sequence of activity under steady-state conditions in marine environments due to the preferential reaction of electron acceptors providing higher amounts of free energy for respiration, as follows: $O_2 > NO_3^- >$ Mn (IV) > Fe (III) > $SO_4^{2-} > CO_2$ (e.g., Froelich et al., 1979; Thamdrup, 2000; Jørgensen, 2000). Molecular oxygen is the primary electron acceptor under oxic conditions (e.g., Piper and Calvert, 2009). Nitrate and the remaining oxygen serve as electron acceptors under suboxic or denitrifying conditions (e.g., Tribovillard et al., 2006; Piper and Calvert, 2009), and Mn (IV) and Fe (III) undergo reduction prior to sulfate in anoxic environments. However, nitrate, Mn (IV), and Fe (III) are generally present in low concentrations in seawater and sediment pore waters, resulting in a narrow depth range of activity that is commonly overlooked or inadequately considered (Piper and Calvert, 2009).

Although a significant portion of the reaction products of Mn and sulfate reduction (i.e. Mn^{2+} and HS^- ions) are re-oxidized or escape to the water column (e.g., Berner and Westrich, 1985; Middelburg et al., 1987; Cruse and Lyons, 2004), the amounts of Mn and S that are preserved in stable mineral phases can be used to estimate the amount of OM lost during these reduction processes. Vetö et al. (1997) developed equations using Mn and sulfate concentrations and stoichiometric coefficients arising from these reduction processes to calculate OM loss in the sediment due to Mn reduction (Eq. 1) and sulfate reduction (Eq. 2):

$$TOC_{Mn} = [Mn] \times 0.11 \quad (1)$$

$$TOC_{S} = [S] \times 0.75 \times 1.33 \quad (2)$$

9.5.2 Early diagenetic effects of OM oxidation processes

OM-rich marine deposits commonly contain diagenetic carbonate phases (e.g., Mazzullo, 2000; Heiser et al., 2001; Röhl et al., 2001; Sabatino et al., 2011; Polgári et al., 2012). Carbonate precipitation is caused by an increase of both pH and alkalinity in pore waters mediated by microbial OM oxidation processes (Berner, 1980; Burns et al., 1988; Compton, 1988; Slaughter and Hill, 1991; Wright and Oren, 2005; Wacey et al., 2008). These changes in pore water chemistry also favor the dissolution and alteration of mineral phases, such as biogenic quartz and pyrite (e.g., Russell and Hall, 2006; Sabatino et al., 2011).

The exact mechanisms and rates of dolomite formation in marine environments are still controversial (the “dolomite problem”; e.g., Mazzullo, 2000; Warren, 2000; Machel, 2004; Meister et al., 2007). This is reflected in the fact that sulfate concentrations are considered to be both a potential inhibitor (Baker and Kastner, 1981; Kastner, 1984) and a catalyst for dolomite formation (Mirsal and Zankl, 1985; Vasconcelos and McKenzie, 1997; Zhang et al., 2012). However, dominant control of dolomite precipitation by dissolved sulfate concentrations is unlikely. Instead, the key influences on low-temperature dolomite formation are probably microbial activity and environmental changes attributable to microbial sulfate reduction, including alkalinity and large pH changes in pore waters (e.g., Rivadeneyra et al., 2006; Morse et al., 2007; Sánchez-Román et al., 2007, 2009). Such dolomites commonly feature unusually negative carbonate-C isotope values (e.g., Claypool and Kaplan, 1974; Mazzullo, 2000). Ca and Mg cations for dolomite formation mainly derive either from diffusion from overlying seawater and/or dissolution of precursor carbonate sediments (e.g.,

Irwin, 1980; Baker and Burns, 1985). An insufficient supply of those cations may, therefore, be the limiting factor for carbonate precipitation (e.g., Burns et al., 1988).

Mn plays an important role in oxygen-depleted oceanic systems due to its redox-dependent behavior in aquatic environments (Tribovillard et al., 2006; Calvert and Pedersen, 2007; Och et al., 2012). Mn^{2+} cations are released through reductive dissolution of Mn oxides below the redoxcline (e.g., Tribovillard et al., 2006). The high solubility of Mn^{2+} in reducing sediments induces cationic diffusion upward and downward within the sediment (e.g., Brumsack, 1989; Calvert and Pedersen, 1996; O'Sullivan and Reynolds, 2005) as Mn is not incorporated in any organic or sulfidic phase (Algeo and Maynard, 2004). Whereas diffusion of Mn^{2+} may cause precipitation of Mn-bearing carbonates in adjacent oxidized sediments (e.g., Coleman, 1985; Canfield et al., 1993; Calvert and Pedersen, 1993; Morford et al., 2001), the cations commonly escape to the water column in anoxic basins (Cruse and Lyons, 2004) resulting in the occurrence of Mn-depleted deposits (e.g., Hild and Brumsack, 1998).

Microbially-mediated anaerobic reduction of Fe oxides causes the release of Fe^{2+} below the chemocline. In contrast to highly soluble Mn^{2+}, diffusion of Fe^{2+} cations out of the sediment is impeded under anoxic conditions due to the elements reaction kinetics (Stumm and Morgan, 1981; Lovley and Phillips, 1988). Consequently, the bulk of reduced iron is rapidly fixed in authigenic phases, including diagenetic pyrite and Fe-bearing carbonates, under anoxic conditions in the sediment (Berner, 1989; Canfield et al., 1993). Pyrite precipitation can also occur syngenetically in the water column in case of euxinic depositional conditions (i.e. chemocline located in the water column; e.g., Wilkin et al., 1996; Cruse and Lyons, 2004). Fe-bearing carbonates are formed in sediments containing insufficient sulfide to fix the available Fe^{2+} in pyrite and, hence, indicate a minor role of sulfate reduction (cf. Pye et al., 1990).

Microbial-mediated sulfate reduction commonly is the dominant anaerobic OM oxidation process in marine settings and causes the release of H_2S^- to pore waters (e.g., Jørgensen, 1982). This process is especially significant in surficial sediment layers (<10 cm below the seafloor) due to the presence of freshly buried and undegraded OM (Berner, 1978; Jørgensen, 1983). Pyrite, which is rapidly formed by H_2S^- and Fe^{2+}, is the major sink for S in marine sediments under reducing conditions (e.g., Vairavamurthy and Schoonen, 1995). Incorporation of S into the aromatic fraction of OM ("natural sulphurization"; Kohnen et al.,

1991) is especially important for Fe-limited environments such as carbonate systems (e.g., Bosselmann, 2007).

9.6 Discussion

The Bächental basin experienced significant secular redox variations, as reflected in bulk geochemical (trace elements, TOC, HI) and organic geochemical (Pr/Ph ratio) proxies. Stratigraphic variation in these proxies provides the basis for a subdivision of the Bächental bituminous marls into three distinct units. Whereas Units 1 and 3 were deposited under predominantly suboxic conditions, Unit 2 records anoxic-euxinic conditions within a stagnant basin setting (Neumeister et al., 2015, 2016). The individual units show sharply defined stratigraphic transitions. This enables determination of the diagenetic response to shifting, suboxic to euxinic redox conditions within the Bächental basin, as discussed in the following. Furthermore, the results provide general insights into the complex effects of early diagenetic processes on OM-rich marls deposited in hemipelagic, semi-restricted depositional settings.

9.6.1 Early diagenesis under predominantly suboxic conditions (Units 1 and 3)

9.6.1.1 OM oxidation

Since the immature Bächental bituminous marls had uniform marine-algal OM sources (Neumeister et al., 2015), HI variations mainly reflect redox-dependent activity of early diagenetic degradation processes. Intervals with predominantly suboxic depositional conditions in the Bächental basin correspond to greyish, poorly laminated sediments that typically feature low HI and TOC values (HI: ~300-550 mg HC/g TOC; TOC: ~1.5-2.2 %) and elevated Pr/Ph ratios (Figs. 9.6A, B), consistent with less reducing conditions (Didyk et al., 1978). The occurrence of a suboxic sediment surface layer enabled the activity of aerobic and denitrifying bacteria during deposition of Units 1 and 3. However, the effect of denitrification on OM degradation was probably minimal because of low NO_3^- concentrations in seawater (cf. Piper and Calvert, 2009). Below the chemocline, a sequence of anaerobic reduction processes in concert effectively degraded the hydrogen-rich OM to a rather constant amount of residual OM with varying but mostly low HI values. The chemocline probably was located <1 cm below the seafloor as the available oxygen in pore waters was rapidly consumed due to the continuous supply of hydrogen-rich OM to the sediment.

Exceptionally high Mn concentrations in suboxic Units 1 and 3 probably derive from volcanic inputs and from the activity of hydrothermal vents connected to rifting and spreading of the Alpine Atlantic starting in the late early Jurassic (Neumeister et al., 2015, 2016; cf. Sabatino et al., 2011; Polgári et al., 2012). However, Mn fixation in Bächental bituminous marls was governed by prevailing redox conditions as Mn is solely contained in diagenetic carbonates (see Sections 9.6.1.3, 9.6.2.3) indicative of deposition under oxic to suboxic bottom waters (cf. Calvert and Pedersen, 1996). Therefore, Mn enrichment can be used for discrimination of suboxic and anoxic conditions during deposition (Fig. 9.6C). This is confirmed by the agreement of vertical variations of Mn concentrations and organic and inorganic geochemical redox proxies in the study section (Neumeister et al., 2015, 2016). Redox-dependent Mn enrichment is reflected by the occurrence of generally elevated Mn concentrations in suboxic Units 1 and 3. Maximum Mn concentrations (up to 11.6 %) occur in the lower 4 m of Unit 3, deposited directly above anoxic Unit 2 and during an interval of elevated sea level (cf. Neumeister et al., 2015). Thus, peak Mn concentrations potentially result either from a significant enrichment of dissolved Mn in anoxic and stagnant bottom waters during deposition of Unit 2, which finally could be fixed in carbonates under predominating suboxic conditions in the lower part of Unit 3 and/or from an elevated availability of Mn oxides during stages of intense hydrothermal activity at mid-oceanic ridges also affecting relative sea level (cf. Corbin et al., 2000).

The occurrence of negative covariations between organic bulk parameters (TOC, HI) and Mn concentrations suggests that OM degradation was mainly mediated by Mn reduction under the suboxic conditions that prevailed during deposition of Units 1 and 3 (Figs. 9.6C, D). This inference is confirmed by the lack of Mn oxides in all samples reflecting the effectiveness of the Mn reduction process. Although samples from Unit 1 show lower Mn concentrations compared to those of Unit 3, absolute rates of OM degradation were probably similar owing to the additional effect of Fe reduction in Unit 1 (Figs. 9.6E, F). Pyrite is the only S-bearing mineral phase in the study section. The frequency of pyrite in Units 1 and 3 confirms the availability of dissolved Fe and H_2S, both generated by anaerobic reduction processes, for pyritization. However, sulfate reduction, which postdated Mn and Fe reduction, was of only minor importance and did not cause significant oxidation of the organic fraction in these units, as shown by the lack of a relationship of S concentrations to both TOC content and HI values (Figs. 9.6G, H). An additional input of detrital pyrite is likely for samples from Units 1 and 3. Diagenetic carbonates in Bächental bituminous marls typically contain less

than 1.5 % Fe. In contrast, Mn-bearing siderite, occurring only in the lower 3 m of Unit 3 (see Section 9.6.1.3), suggests a particular predominance of Mn and Fe reduction over sulfate reduction in that interval (cf. Pye et al., 1990).

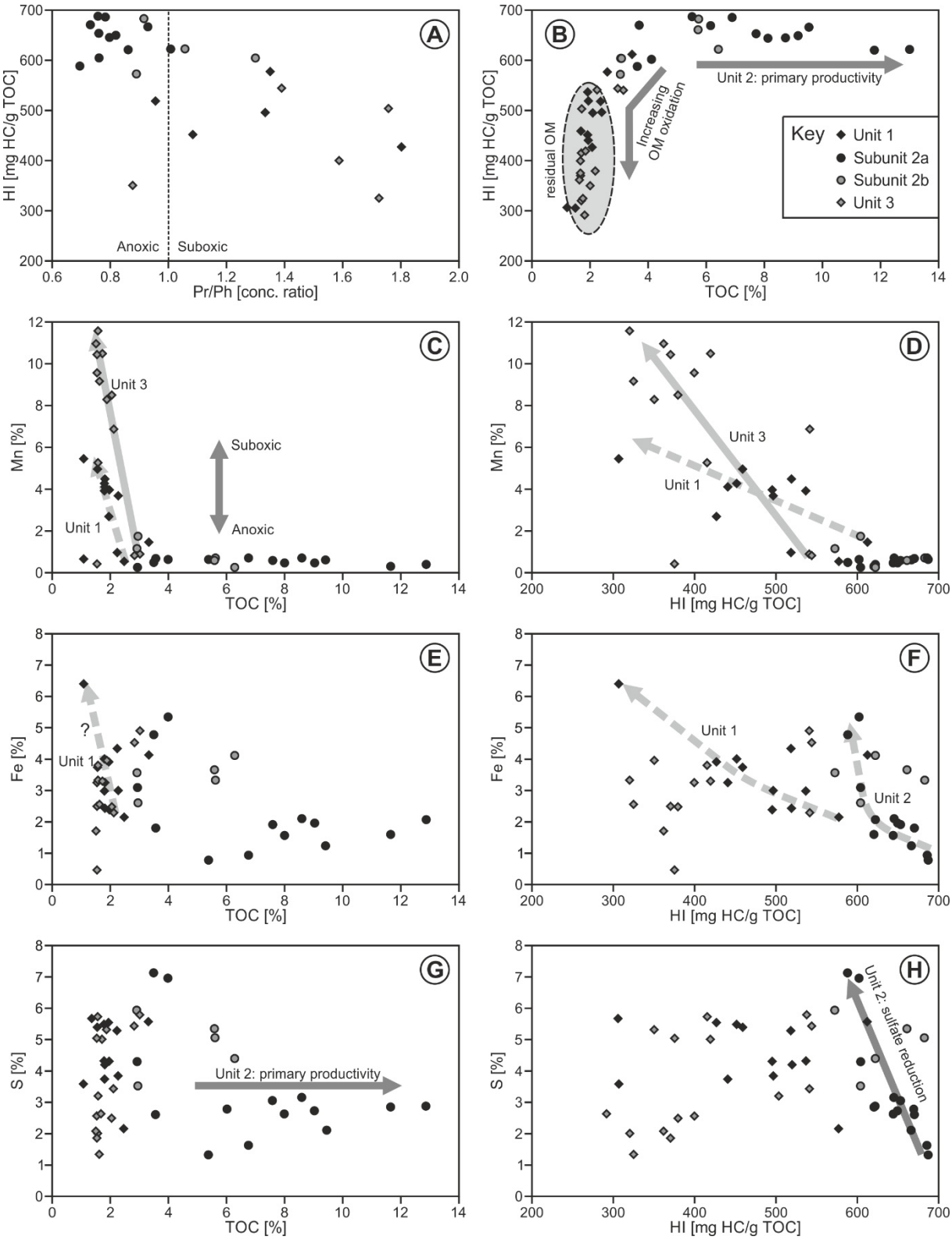

Fig. 9.6: Crossplots showing the relationship of redox conditions and reduction processes to OM degradation. (A) Pristane/phytane ratio (Pr/Ph, concentration ratio) vs. hydrogen index (HI, mg HC/g TOC), (B) total organic carbon content (TOC, %) vs. HI, (C) TOC vs. manganese concentration (Mn, %), (D) HI vs. Mn, (E) TOC vs. iron concentrations (Fe, %), (F) HI vs. Fe, (G) TOC vs sulfur content (S, %), and (H) HI vs. S.

9.6.1.2 Quantification of microbially mediated OM decay

The relationship of TOC content vs. Mn concentration suggests control of OM degradation in suboxic Units 1 and 3 by Mn reduction (Fig. 9.6C). Within these units, samples with the highest TOC contents (~2.5-3.3 %) and HI values (~500-600 mg HC/g TOC) are also characterized by the lowest Mn concentrations (<1.5 %), reflecting minimal early diagenetic decay due to Mn reduction. In contrast, samples with the lowest TOC contents (~1.5-1.6 %) and HI values (~300-450 mg HC/g TOC) have the highest Mn concentrations (up to 11.6 %), reflecting strong OM degradation due to Mn reduction. For these samples, Mn reduction effected a maximum OM loss of ~0.9 % (Unit 1) to ~1.5 % (Unit 3) corresponding to an OM consumption of ca. 0.15 to 0.20 % of OM per 1.0 % of generated Mn (Fig. 9.6C) that was subsequently incorporated into carbonates. During this strong OM decay process, HI values were reduced by up to 400 mg HC/g TOC.

The calculated TOC_{Mn} contents (Fig. 9.7; Table 9.10.3) showing maximum values of roughly 0.6 % (Unit 1) and 1.3 % (Unit 3) are in the same range as the suggested OM loss inferred from Fig. 9.6C, confirming the reliability of the assumptions. However, according to the calculated results for TOC_S (Fig. 9.7; Table 9.10.3), more than 90 % (Units 1 and upper part of Unit 3) and roughly 65 % (lower part of Unit 3), respectively, of OM loss was mediated by sulfate reduction. This result is attributed to the coefficients used in Eqs. 1 and 2, which assume predominance of sulfate reduction over Mn reduction in OM decay (see Section 9.5.1). In the study unit, however, S concentrations lack relationships with TOC contents and HI values in suboxic Units 1 and 3 (Figs. 9.6G, H), whereas the relationship of Mn reduction on OM degradation is evident (Fig. 9.6C). Thus, the importance of sulfate reduction in suboxic Units 1 and 3 is probably overestimated. Therefore, we speculate that less than 0.5 % of TOC was degraded by sulfate reduction and, hence, total OM loss in suboxic Units 1 and 3 was rather in the range of ca. 1.5 to 2.0 %.

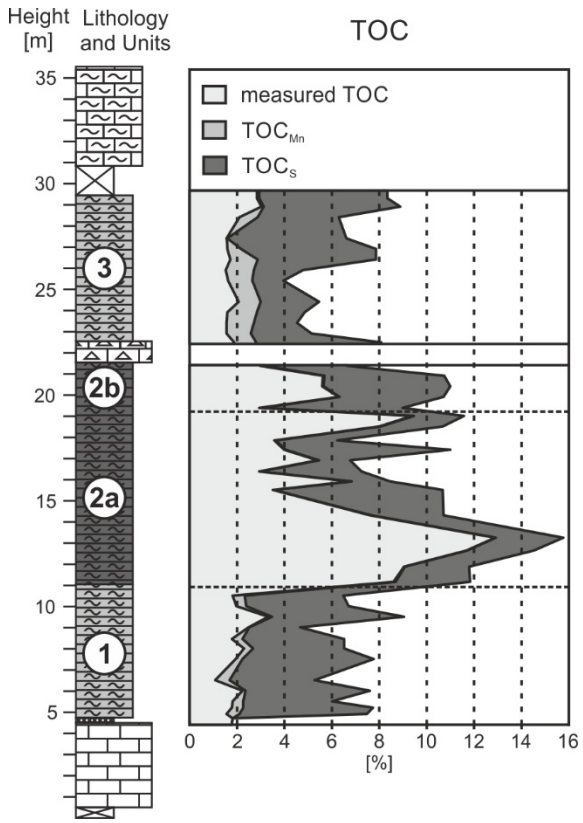

Fig. 9.7: Profile of measured TOC content (light grey) and calculated amounts of OM lost through Mn reduction (TOCMn, mid-grey) and sulfate reduction (TOCS, dark grey) using Eqs. 1 and 2 (from Vetö et al., 1997).

9.6.1.3 Sequential precipitation of carbonate phases

Elevated pH and alkalinity conditions caused by activity of microbially mediated OM oxidation processes favored the diagenetic formation of carbonates in the sediment. Besides small amounts of detrital calcite, Bächental bituminous marls from suboxic Units 1 and 3 contain varying amounts of several diagenetic carbonate phases characterized by a specific sequence of formation.

There exists a commonly accepted relationship between dolomite formation and anoxic conditions in marine environments, in which dolomite precipitation is governed by changes in pH and alkalinity conditions of pore water triggered by activity of sulfate reduction (e.g., Rivadeneyra et al., 2006; Morse et al., 2007; Sánchez-Román et al., 2007, 2009). Moreover, sulfate is suggested to be both a catalyst (Mirsal and Zankl, 1985; Vasconcelos and McKenzie, 1997; Zhang et al., 2012) and an inhibitor (Baker and Kastner, 1981; Kastner, 1984) for low-temperature dolomite formation. However, these suggestions

are not suitable for characterizing dolomite formation in the Bächental basin. Dolomite is the least abundant diagenetic carbonate phase in the Bächental basin, although quantification based on XRD diffractograms is impossible as the dolomite peak overlaps with and is subsumed by the larger kutnohorite signal. According to thin section analysis (Fig. 9.5) and XRD diffractograms (Fig. 9.4), dolomite in the study section [i] is Fe-poor (generally <1 % Fe; Table 9.10.2), [ii] typically forms euhedral to subhedral crystals (Figs. 9.5A-C) suggesting precipitation within the practically un-consolidated soft sediment during earliest diagenesis, [iii] always shows rims of Mn-bearing carbonates (Figs. 9.5A-C) formed below oxygenated bottom waters (cf. Calvert and Pedersen, 1996), and [iv] occurs more frequently in suboxic Units 1 and 3 and less commonly in anoxic-euxinic Unit 2 (see Section 9.6.2.3). These observations imply a redox-dependent origin of dolomite in the Bächental basin.

Dolomite growth occurred very early during sediment diagenesis, as shown by its mostly euhedral form and by overgrowths of Mn-bearing carbonates that formed under suboxic conditions (i.e., prior to the zone of sulfate reduction). The limited amounts of dolomite in the study samples despite its formation in the uppermost sediment layers argue against termination of dolomite precipitation due to depletion of dissolved Mg in pore waters. However, the dolomitization process ceased prior to the formation of Mn-bearing carbonates and, thus, prior to reduction of Mn(IV), as shown by low concentrations of Mn in the dolomite (median value: 0.3 %) and by rims of kutnohorite surrounding all dolomite crystals. Once Mn(IV) reduction began, the intensity of this process yielded large amounts of dissolved Mn at the chemocline (see Section 9.6.1.1), resulting in Mn supersaturation of pore waters. At that point, dolomite formation ceased and precipitation of Mn-bearing carbonate commenced (see below). Consequently, dolomite formation was restricted to the uppermost suboxic sediment layers (slightly below the seafloor during deposition of Units 1 and 3) where the chemical composition of pore waters resembled that of sea water. We therefore infer that dolomite precipitation was mediated by an increase of porewater alkalinity caused by aerobic decay and denitrification, and that high porewater sulfate concentrations in the surficial sediment layers did not inhibit its formation.

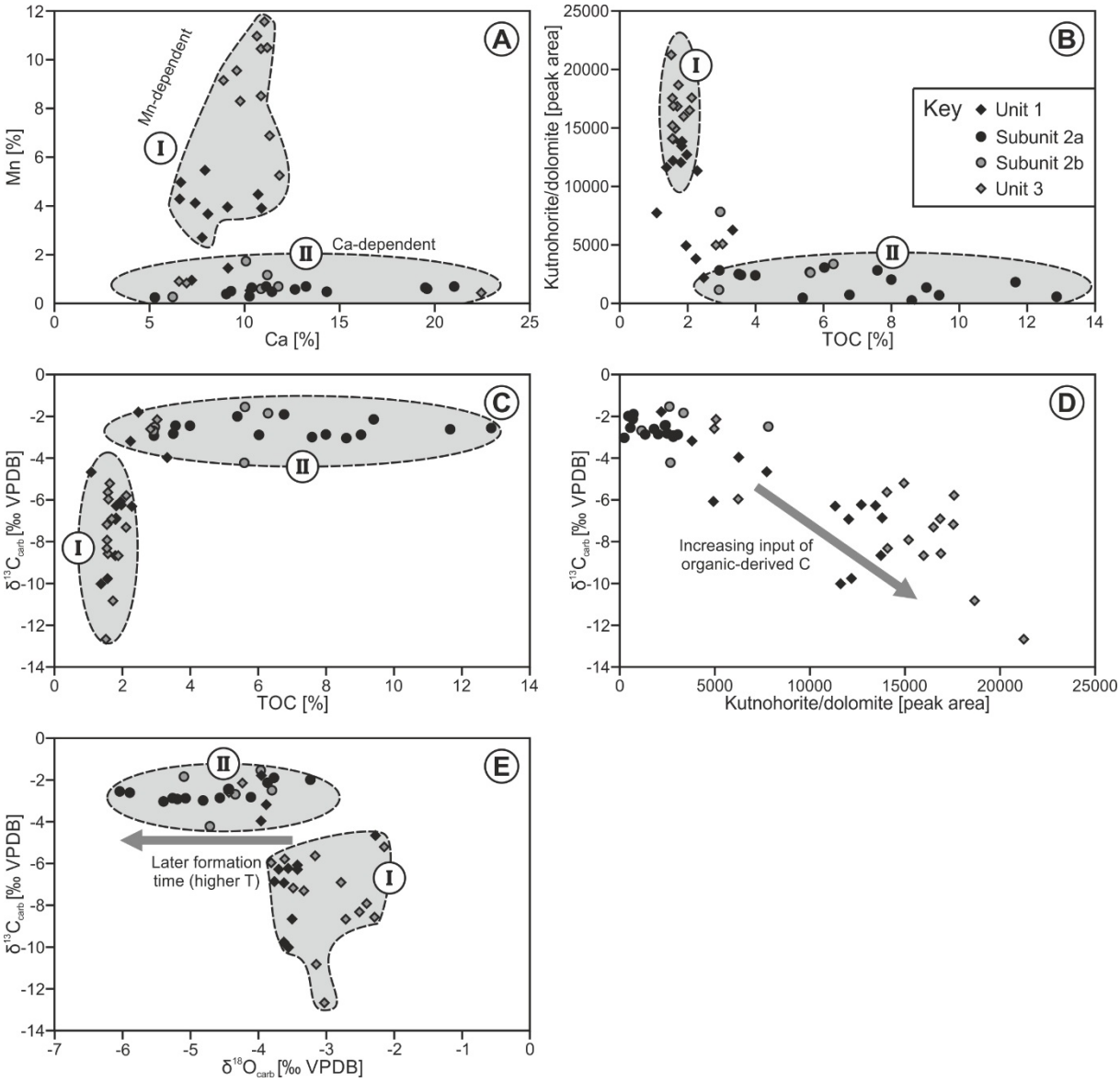

Fig. 9.8: Crossplots showing the relationships of Mn reduction to elemental and isotopic composition of diagenetic carbonate phases (A-D), and the variable timing of carbonate formation as indicated by oxygen isotope composition of carbonate minerals (E). (A) Calcium (Ca, %) vs. manganese (Mn, %) concentrations, (B) total organic carbon content (TOC, %) vs. amount of kutnohorite/dolomite (peak area), (C) TOC vs. inorganic carbon isotope composition ($\delta^{13}C_{carb}$, ‰ VPDB), (D) amount of kutnohorite/dolomite vs. $\delta^{13}C_{carb}$, and (E) oxygen isotope composition of carbonate ($\delta^{18}O_{carb}$, ‰ VPDB) vs. $\delta^{13}C_{carb}$.

The most abundant diagenetic phases in suboxic Units 1 and 3 are Mn-rich carbonates (mainly kutnohorite). The key role of Mn availability in the formation of diagenetic carbonates is shown by the bimodal distribution of Ca and Mn concentrations (Fig. 9.8A). Samples from suboxic Units 1 and 3 show rather constant Ca concentrations and high but

varying Mn concentrations (cluster I). These samples contain abundant kutnohorite (Fig. 9.8B) in the form of carbonate cement. The kutnohorite cement is commonly zoned, with a Mn-rich inner rim (in contact with the host mineral grain), a Mn-poor middle layer, and a Mn-rich outer rim (Figs. 9.5F, G). This zonation reflects fluctuating concentrations of dissolved Mn in the pore water and/or small-scale fluctuations of the chemocline governing the incorporation of Mn into secondary carbonates.

The formation of kutnohorite was linked to the high availability of Mn(IV) oxides in Units 1 and 3. Intense Mn reduction in the upper sediment layers yielded abundant dissolved Mn(II) in pore waters, and upward diffusion of Mn(II) triggered Mn-carbonate supersaturation at the chemocline, resulting in kutnohorite precipitation superseding dolomite formation (see Section 9.6.1.1). The operation of this process is supported by C-isotope variation. Mn reduction was linked to OM oxidation, which liberated large amounts of isotopically light carbon to porewaters. Low-TOC samples from suboxic Units 1 and 3 are characterized by highly negative $\delta^{13}C_{carb}$ values (-12.7 to -4.7 ‰ VPDB; Fig. 9.8C, cluster I) and a moderate negative correlation between $\delta^{13}C_{carb}$ and kutnohorite content (Fig. 9.8D). These patterns suggest that the release of isotopically-light organic-derived C due to OM oxidation and its subsequent incorporation in kutnohorite accounts for much of the shift to lower C-isotope values for bulk carbonate in these samples. Thus, the main phases of diagenetic carbonate formation occurred in conjunction with maximum OM degradation under suboxic conditions in the Bächental basin. Note that dolomite formed in the uppermost suboxic sediment layer is Mn-poor (~0.3 %). This indicates that dissolved Mn was completely fixed at the chemocline and did not diffuse into shallower horizons and, further, confirms that kutnohorite formation succeeded dolomite precipitation.

Mn-bearing siderite is limited to the lower 3 m of suboxic Unit 3, deposited during a period of elevated sea level (cf. Neumeister et al., 2015). The bulk of hydrogen-rich OM was degraded by Mn reduction due to an exceptional high availability of Mn oxides in that interval (see Section 9.6.2.1), reflected by maximum Mn concentrations (9.6C, D). Whereas Fe^{2+} was generated by Fe reduction in the sediment, sulfate reduction was impeded owing to a lack of degradable OM after intense activity of Mn and Fe reduction in that part. Thus, the lack of H_2S^- in pore waters was the limiting factor for pyrite formation, which consequently caused the incorporation of the remaining dissolved Fe into Mn-bearing siderite (cf. Pye et al., 1990; see Section 9.6.1.1). Mn-bearing siderite and kutnohorite cannot be differentiated by means of

visual investigation in the samples. This and the presence of Mn in the lattice of siderite indicates a precipitation of the mineral at or directly above the chemocline, similar to kutnohorite formation.

Bächental bituminous marls mainly contain carbonates of diagenetic origin. Thus, the measured bulk $\delta^{18}O_{carb}$ values rather reflect diagenetic impact than primary isotopic composition of sea water (-1 ‰, ice free; Röhl et al., 2001). In general, a shift to lower $\delta^{18}O_{carb}$ values can be caused by both elevated burial temperatures and/or decreasing salinity of pore waters (e.g., Epstein and Mayeda, 1953). Within Bächental bituminous marls, samples from suboxic Units 1 and 3 show more ^{18}O-enriched carbonate O-isotopes (-4.0 to -2.1 ‰ VPDB; Fig. 9.8E, cluster I) compared to anoxic-euxinic Unit 2 despite the occurrence of a salinity-stratified water column during deposition of the latter unit (see Section 9.6.2.3). Accordingly, $\delta^{18}O_{carb}$ values of the study section were mainly determined by temperature variations and, hence, argue for an on average earlier formation of diagenetic carbonate phases (i.e. at lower burial temperatures) and a rather early termination of carbonate precipitation in Units 1 and 3. This is consistent with the predominance of Mn-rich secondary carbonate phases in suboxic Units 1 and 3 implying that carbonate precipitation did not occur below the chemocline. Extensive carbonate formation potentially caused both the gradual depletion of dissolved Ca and Mn in pore waters and a reduction of porosity and effective permeability through cementation in Units 1 and 3.

9.6.2 Early diagenesis under predominantly anoxic-euxinic conditions (Unit 2)

9.6.2.1 OM oxidation

Laminated samples from Unit 2 are generally characterized by elevated HI and TOC values (HI: ~620-690 mg HC/g TOC; TOC: ~3.5-12.9 %) and Pr/Ph ratios <1, indicating anoxic-euxinic depositional conditions (Didyk et al., 1978). TOC fluctuations in Unit 2 are mainly attributed to primary productivity changes in surface waters of the Bächental basin (cf. Neumeister et al., 2015, 2016). The complete absence of bioturbation in Unit 2 indicates that the chemocline was located at or, at least periodically, above the sediment-water interface. Location of the chemocline in the water column limited the activity of denitrifying bacteria in the sediment, which was entirely within the sulfate reduction zone. Mn concentrations are low in Unit 2 because reduction of Mn(IV) oxides occurred mainly in the water column or at the sediment-water interface (cf. Section 9.6.3.2). Fe concentrations show strong fluctuations

(Figs. 9.6E, F), suggesting that some reduction of Fe(III) continued in the sediment, probably of more refractory Fe phases. However, pyrite formation was minimal owing to the limited availability of reactive Fe in Unit 2. Although inputs of Mn and Fe oxides to the sediment probably continued during deposition of Unit 2, their reduction did not measurably influence bulk organic parameters (Figs. 9.6C-F; cf. Section 9.6.3.2). In contrast, sulfate reduction caused a small decrease of HI values from 700 to 600 mg HC/g TOC (Fig. 9.6H). TOC content was probably controlled by primary productivity variation (Fig. 9.6G). Overall, the magnitude of anaerobic OM degradation was small in anoxic-euxinic Unit 2, and the OM fraction is relatively well-preserved. Preservation was enhanced by sulfurization of OM, which resulted from incorporation of excess sulfide, transforming metabolizable OM into non-metabolizable OM (cf. Sinninghe Damsté et al., 1989; Lückge et al., 1996). Excess sulfide was present in Unit 2 owing to Fe-limitation, which resulted in early depletion of reactive Fe through pyrite formation (Neumeister et al., 2015).

A reliable quantification of early diagenetic OM loss linked to Mn and sulfate reduction (e.g., using Eqs. 1 and 2) is not possible for samples from Unit 2 because anoxic-euxinic conditions inhibited the fixation of Mn in secondary carbonates, and Fe-limited conditions resulted in the diffusive loss of microbially generated sulfide from the sediment (cf. Jørgensen, 1982; Berner and Westrich, 1985). According to the calculated values for TOC_{Mn} and TOC_S (Fig. 9.7; Table 9.10.3), more than 95 % of OM loss in the sediment was caused by sulfate reduction in anoxic-euxinic Unit 2. Despite the mentioned limitations, these results are reasonable due to the importance of microbial sulfate reduction in degradation of OM in Unit 2.

9.6.2.2 Sequential precipitation, dissolution, and alteration of mineral phases

In samples from anoxic-euxinic Unit 2, Mg concentrations are low and dolomite is rare or even missing (Figs. 9.5, 9.6D, E). This confirms the redox-dependent formation of the mineral. Its non-formation during deposition of this unit was probably related to the position of the chemocline at or above the sediment-water interface, which displaced the suboxic zone upward into the water column and severely limited the activity of the aerobic and denitrifying bacteria responsible for dolomite precipitation in the sediment (cf. Section 9.6.1.3). The lack of dolomite in Unit 2 samples, which were deposited entirely within the sulfate reduction zone, indicates the lack of influence of the latter on dolomite formation.

The anoxic-euxinic conditions of Unit 2 also impeded incorporation of Mn into diagenetic carbonate phases, as reflected in the dominance of Ca-rich carbonates (Figs. 9.8A, cluster II) and limited amounts of kutnohorite in Unit 2 samples (Fig. 9.8B). However, Mn-bearing carbonates can potentially form in predominantly anoxic facies during episodes of transient oxygenation (Schaller and Wehrli, 1996; Naeher et al., 2013). Although stagnant anoxic conditions generally prevailed during deposition of Unit 2, the sporadic occurrence of turbidites caused transient, small-scale mixing and deepwater ventilation (cf. Neumeister et al., 2015), resulting in limited formation of kutnohorite in some samples. The dominant diagenetic carbonate phase in Unit 2 is calcite, which contains small quantities of Mn (0.6-4.2 %).

Carbonate C-isotopes suggest that the Mn-bearing calcite of Unit 2 incorporated smaller amounts of organic-derived C than kutnohorite from Units 1 and 3 (see Section 9.6.1.3). This inference is supported by the relatively small negative shifts in $\delta^{13}C_{carb}$ of Unit 2 samples (-4.2 to -1.5 ‰ VPDB; Fig. 9.8C, cluster II). Consequently, mainly seawater-sourced C was used for formation of Mn-bearing calcite in Unit 2. Whereas precipitation of secondary carbonates coincided with the peak stage of OM degradation in Units 1 and 3, formation of Mn-bearing calcite occurred at later diagenetic stages when OM oxidation rates mediated by sulfate reduction were rather low and/or decay of OM was limited due to natural sulphurization (see Section 9.6.2.1). This inferred sequence of formation of secondary carbonate phases is supported by oxygen isotope data. Specifically, ^{18}O-depleted isotope ratios for Mn-bearing calcite of anoxic-euxinic Unit 2 (-6.0 to -3.2 ‰ VPDB; Fig. 9.8E, cluster II) indicate that carbonate precipitation persisted during longer burial intervals and/or proceeded at later diagenetic stages and, hence, higher burial temperatures than in Units 1 and 3 (see Section 9.6.1.3; cf. Algeo et al., 1992; Neumeister et al., 2015). We speculate that the differential timing of secondary carbonate precipitation under suboxic conditions (Units 1 and 3) versus anoxic-euxinic conditions (Unit 2) was mediated mainly by the intensity of Mn(IV) reduction. High rates of Mn reduction in the sediment during deposition of Units 1 and 3 provided abundant Mn(II) cations that led to supersaturation of pore waters with respect to Mn-carbonate minerals such as kutnohorite. Hence, in addition to Ca cations also Mn cations were available for carbonate formation. Secondary carbonate precipitation in Unit 2 was comparatively slower and associated with sulfate reduction. Furthermore, solely Ca cations were in place for carbonate formation. However, bulk carbonate concentrations are similar

throughout the study section, in part because the interval of secondary carbonate formation in Unit 2 was significantly longer than that of Units 1 and 3.

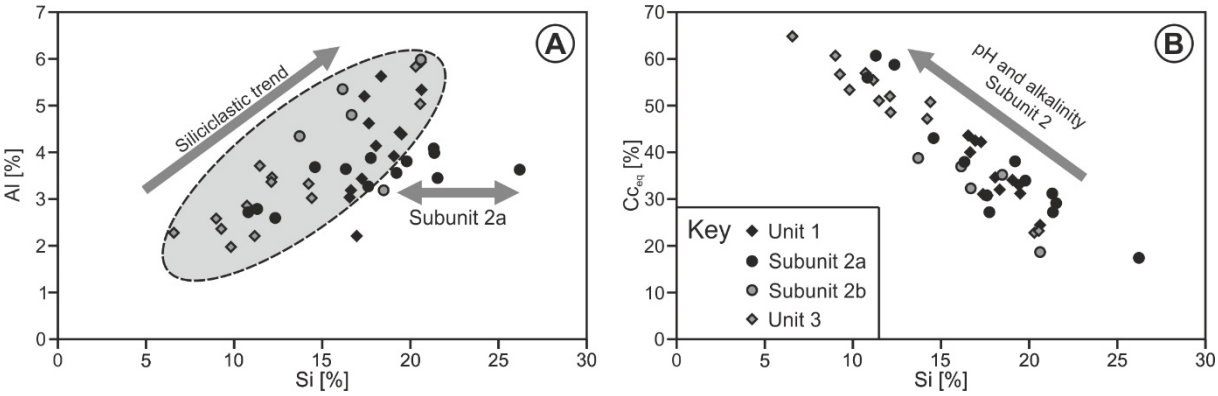

Fig. 9.9: Crossplots showing varying sources of silicon (Si) and the impact of elevated pH and alkalinity conditions on dissolution of biogenic quartz and precipitation of carbonates in Unit 2. (A) Si (%) vs. aluminium (Al, %) concentrations (B) Si concentrations vs. calcite equivalent percentages (Cc_{eq}, %).

During deposition of Unit 2, intense microbially driven anaerobic OM oxidation induced significant increases of pH and alkalinity in pore waters. These changes caused the dissolution and alteration of certain mineral phases in the sediment. Whereas samples from suboxic Units 1 and 3 show a linear relationship of Si vs. Al concentrations, suggesting mainly detrital siliciclastic sources of Si, samples from the radiolarian-rich Unit 2 do not show this relationship, indicating that a significant fraction of Si is of biogenic origin (Fig. 9.9A). However, all units are characterized by a negative relationship between Si concentrations and Cc_{eq} contents, highlighting the linkage between Si accumulation and carbonate precipitation (Fig. 9.9B). For Units 1 and 3, the negative relationship can be attributed to dilution effects, e.g., carbonate dilution of the detrital siliciclastic flux. For Unit 2, in contrast, the negative relationship between Si and Cc_{eq} is the result of varying degrees of replacement of biogenic quartz by Mn-bearing calcite. Petrographic observations for Unit 2 samples support this interpretation: radiolarian tests are mostly dissolved and contain only small remnants of the original biogenic silica (Figs. 9.6D, E).

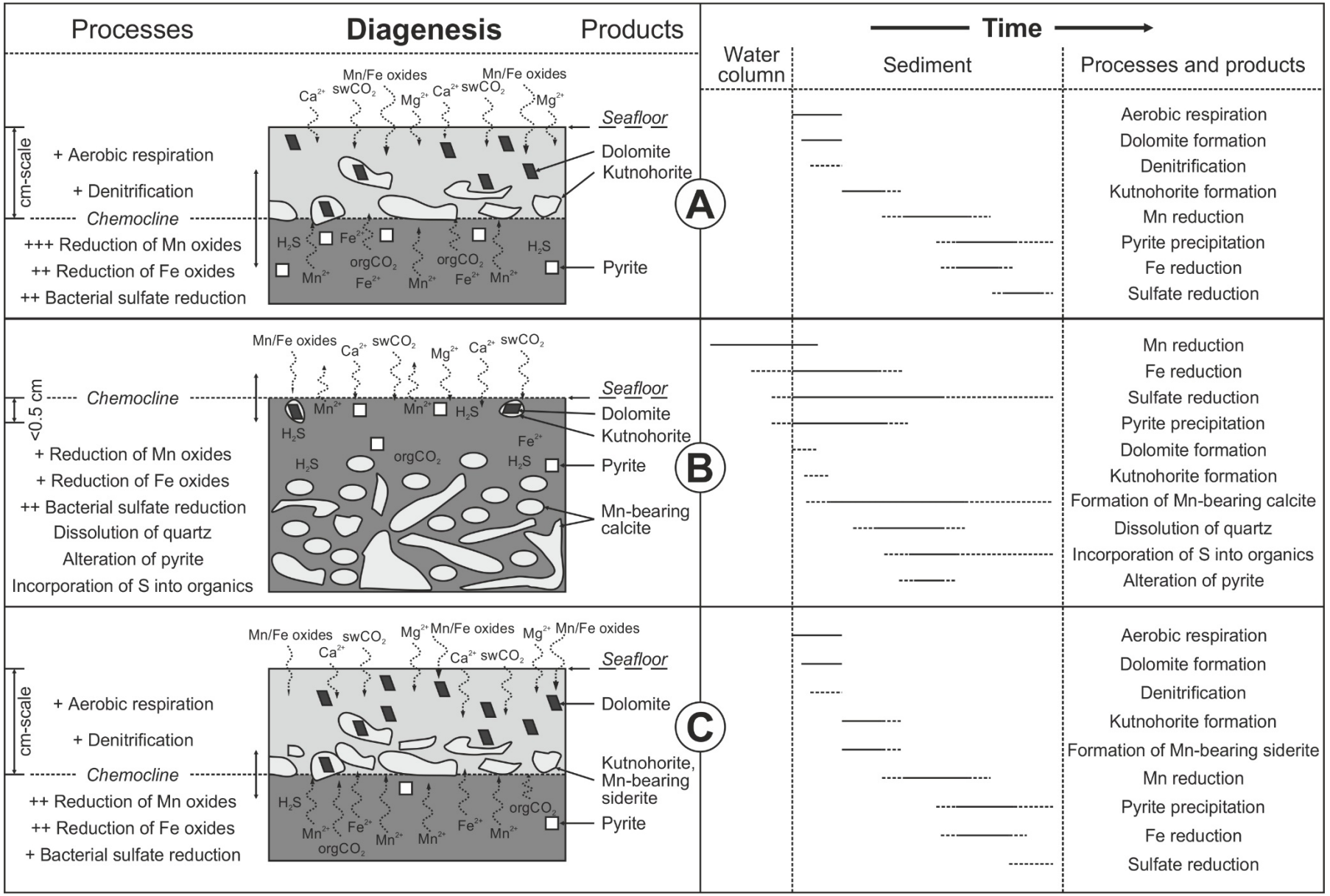
Processes
Diagenesis
Products
Time
Water column
Sediment
Processes and products
Mn/Fe oxides
swCO2
Ca2+
Mg2+
Seafloor
Dolomite
Kutnohorite
Pyrite
cm-scale
+ Aerobic respiration
+ Denitrification
Chemocline
+++ Reduction of Mn oxides
++ Reduction of Fe oxides
++ Bacterial sulfate reduction
H2S
Fe2+
Mn2+
orgCO2
A
Aerobic respiration
Dolomite formation
Denitrification
Kutnohorite formation
Mn reduction
Pyrite precipitation
Fe reduction
Sulfate reduction
<0.5 cm
+ Reduction of Mn oxides
+ Reduction of Fe oxides
++ Bacterial sulfate reduction
Dissolution of quartz
Alteration of pyrite
Incorporation of S into organics
Mn-bearing calcite
B
Mn reduction
Fe reduction
Sulfate reduction
Pyrite precipitation
Dolomite formation
Kutnohorite formation
Formation of Mn-bearing calcite
Dissolution of quartz
Incorporation of S into organics
Alteration of pyrite
++ Reduction of Mn oxides
++ Reduction of Fe oxides
+ Bacterial sulfate reduction
Kutnohorite, Mn-bearing siderite
C
Formation of Mn-bearing siderite

[160]

Fig. 9.10: Cartoons showing processes and products of early diagenesis in the Bächental basin under shifting suboxic to euxinic conditions. (A) Predominantly suboxic conditions (Unit 1 and upper part of Unit 3), (B) anoxic-euxinic conditions (Unit 2), and (C) suboxic conditions with peak availability of manganese and iron (lower 3 m of Unit 3). Left: Depth range of diagenetic processes and products. Right: Relative timing and duration of diagenetic events. See text for discussion.

In contrast to biogenic silica, pyrite in Unit 2 samples shows only incipient alteration. Pyrite grains commonly exhibit development of ~10-µm-thick Fe(II)-oxide rims surrounding a nucleus of unaltered pyrite because the main alteration process (i.e., removal of S) did not penetrate into the interior of the grains. Dissolution of biogenic silica and alteration of pyrite were both controlled by pore water pH and alkalinity conditions. Whereas the dissolution of biogenic silica starts at pH values of ~7.0 (e.g., Van Cappellen and Qiu, 1997; Loucaides et al., 2008), the alteration of pyrite to Fe(II) oxide commences at pH values of ~9.0 (Russell and Hall, 2006). The incipient alteration of pyrite in Units 2 shows that pore water pH values exceeded ~9.0 for at least part of the interval of early diagenesis. Moreover, elevated pH and alkalinity conditions triggered the formation of Mn-bearing calcite (<4.2 % Mn) below the chemocline.

9.7 Conclusions

The Lower Jurassic Bächentaler Bitumenmergel of the Sachrang Member of the Middle Allgäu Formation provides insights into the factors controlling early diagenetic OM oxidation processes and their products in bituminous marl successions. The dominant processes were markedly redox-dependent and varied strongly between sediments that accumulated under suboxic versus anoxic-euxinic conditions. All relevant processes and products associated with early diagenesis in the Bächental basin are shown in Fig. 9.10:

Suboxic conditions (Units 1 and 3):

- The activity of aerobic microbes and denitrifying bacteria within the suboxic sediment surface layer (<1 cm) favored the precipitation of dolomite.

- Mn reduction degraded the original hydrogen-rich OM to a rather constant amount of residual OM (~1.5-2.2 %) with decreased HI values (300-550 mg HC/g TOC). Sulfate

reduction did not further affect the organic fraction. Hence, Mn reduction was the dominant OM oxidation process in suboxic settings given the availability of abundant Mn oxides.

- Dissolved Mn and isotopically light C, both derived from Mn reduction, and seawater-sourced Ca co-reacted at the chemocline to form kutnohorite, which comprises 20 to 65 % of the sediment. This process postdated dolomite formation and occurred during the main stage of OM degradation.

- The formation of Mn-bearing siderite was limited to an interval in which the exceptionally high availability of Mn and Fe oxides triggered Mn and Fe reduction and suppressed sulfate reduction.

- Carbonate precipitation was mainly governed by the activity of Mn reduction and ceased at the chemocline.

Anoxic-euxinic conditions (Unit 2):

- Mn oxides were reduced by SH^- in the water column. Hence the influence of Mn reduction is not visible in the organic fraction of the sediment.

- Sulfate reduction represents the dominant OM oxidation process. However, natural sulfurization of OM induced the early termination of this process, resulting in enhanced OM preservation and only a slight decrease of HI values (up to 100 mg HC/g TOC).

- Sulfate reduction also caused elevated alkalinity and pH (>9) conditions in pore waters, reflected by advanced dissolution of biogenic quartz and incipient alteration of pyrite.

- Dolomite precipitation was significantly impeded under anoxic-euxinic conditions. Its formation was not influenced by anaerobic sulfate reduction.

- Mn-bearing calcite, formed below the chemocline, is the main carbonate phase. The mineral contains small fractions of isotopically light carbon, derived from sulfate reduction, and was formed at late stages of OM decay.

These results highlight the highly complex diagenetic processes occurring in semi-restricted marine environments subjected to shifting redox conditions. Mn was the main factor controlling early diagenesis in oxygen-depleted marine basins located at the NW Tethyan realm during the late early Jurassic.

9.8 Acknowledgments

We gratefully thank family Albrecht (Tiroler Steinöl ®) who operates the Bächental open pit for their technical support during sampling and Federica Zaccarini (University of Leoben) for assistance with the microprobe. Research by TJA is supported by the Sedimentary Geology and Paleobiology program of the U.S. National Science Foundation, the NASA Exobiology program, and the China University of Geosciences-Wuhan (SKL-GPMR program GPMR201301, and SKL-BGEG program BGL21407).

9.9 References

Accarie, H., Renard, M., Jorgensen, N.O., 1993. Le manganèse dans les carbonates pélagiques: un outil d'intérêt stratigraphique et paléogéographique (le Sénonien d'Italie, de Tunisie et du Danemark). Comptes Rendus de l'Académie des Sciences Paris 316, 1-8.

Algeo, T.J., Wilkinson, B.H., Lohmann, K.C., 1992. Meteoric-burial diagenesis of Pennsylvanian carbonate: water/rock interactions and basin geothermics. Journal of Sedimentary Petrology 62, 652-670.

Algeo, T.J., Maynard, J.B., 2004. Trace-element behavior and redox facies in core shales of Upper Pennsylvanian Kansas-type cyclothems. Chemical Geology 206, 289-318.

Baker, P.A., Kastner, M., 1981. Constraints on the formation of sedimentary dolomite. Science 213, 214-216.

Baker, P.A., Burns, S.J., 1985. Occurrence and formation of dolomite in organic-rich continental margin sediments. American Association of Petroleum Geologists Bulletin 69, 1917-1930.

Bellanca, A., Masetti, D., Neri, R., Venezia, F., 1999. Geochemical and sedimentological evidence of productivity cycles recorded in Toarcian black shales from the Belluno Basin, Southern Alps, Northern Italy. Journal of Sedimentary Research 69, 466-476.

Berner, R.A., 1978. Sulfate reduction and the rate of deposition of marine sediments. Earth and Planetary Science Letters 37, 492-498.

Berner, R.A., 1980. Early diagenesis: A Theoretical Approach. Princeton University Press, Princeton

Berner, R.A., 1989. Biogeochemical cycles of carbon and sulphur and their effect on atmospheric oxygen over phanerozoic time. Palaeogeography, Palaeoclimatology, Palaeoecology 75, 97-122.

Berner, R.A., Westrich, J.T., 1985. Bioturbation and the early diagenesis of carbon and sulphur. American Journal of Science 285, 193-206.

Bernoulli, D., Jenkyns, H.C., 1974. Alpine, Mediterranean and Central Atlantic Mesozoic facies in relation to the early evolution of the Tethys. In: Dott, R.H., Shaver, R.W. (Eds.), Modern and Ancient Geosynclinal Sedimentation, a Symposium. Special Publication of the Society of economic Paleontologists and Mineralogists 19, pp. 129-160.

Bosselmann, K. (2007). Sulfate reduction and iron-manganese cycling in intertidal surface sediments of the southern North Sea. PhD Thesis.

Brumsack, H.J., 1989. Geochemistry of recent TOC-rich sediments from the Gulf of California and the Black Sea. International Journal of Earth Sciences 78, 851-882.

Burns, S.J., Baker, P.A., Showers, W.K., 1988. The factors controlling the formation and chemistry of dolomite in organic-rich sediments: Miocene Drakes Bay Formation, California. In: Shukla, V., Baker, P.A., (Eds.), Sedimentology and Geochemistry of Dolostones. SEPM Special Publication 43, 41-52.

Calvert, S.E., Pedersen, T.F., 1993. Geochemistry of recent oxic and anoxic sediments: implications for the geological record. Marine Geology 113, 67-88.

Calvert, S.E., Pedersen, T.F., 1996. Sedimentary geochemistry of manganese: implications for the environment of formation of manganiferous black shales. Economic Geology 91, 36-47.

Calvert, S.E., Pedersen, T.F., 2007. Elemental proxies for palaeoclimatic and palaeoceanographic variability in marine sediments: interpretation and application. In: Hillaire-Marcel, C., de Vernal, A. (Eds.), Paleoceanography of the Late Cenozoic. Part 1. Methods in Late Paleoceanography. Elsevier, New York, pp. 567-644.

Canfield, D.E., Jørgensen, B.B., Fossing, H., Glud, R., Gundersen, J., Ramsing, N.B., Thamdrup, B., Hansen, J.W., Nielsen, L.P., Hall, P.O.J., 1993. Pathways of Organic-Carbon Oxidation in 3 Continental-Margin Sediments: Marine Geology 113, 27-40.

Claypool, G.E., Kaplan, R., 1974. The origin and distribution of methane in marine sediments. In: Kaplan, I.R. (Eds.), Natural Gases in Marine Sediments. Plenum Press, New York, pp. 94-139.

Coleman, M.L., 1985. Geochemistry of diagenetic non-silicate minerals: kinetic considerations. Philosophical Transactions of the Royal Society London A315, 39-56.

Compton, J.S., 1988. Degree of supersaturation and precipitation of organogenic dolomite. Geology 16, 318-321.

Corbin, J.C., Person, A., Iatzoura, A., Ferré, B., Renard, M., 2000. Manganese in pelagic carbonates: indication of major Tectonic events during the geodynamic evolution of a passive continental margin (the Jurassic European margin of the Tethys–Ligurian Sea). Palaeogeography Palaeoclimatology Palaeoecology 156, 123-138.

Cornelius, P., Plöchinger, B., 1952. Der Tennengebirge-N-Rand mit seinen Manganerzen und die Berge im Bereich des Lammertals. Jahrbuch der Geologischen Bundesanstalt 95, 145-225.

Cruse, A.M., Lyons, T.W., 2004. Trace metal records of regional paleoenvironmental variability in Pennsylvanian (Upper Carbonaferous) black shales. Chemical Geology 206, 319-345.

De Rafélis, M., Emmanuel, R., Renard, M., Atrops, F., Du Chene, R.J., 2001. Geochemical characterization (Mn content) of third order eustatic sequences in Upper Jurassic pelagic carbonates of the Vocontian Trough (SE France). Eclogae Geologicae Helvetiae 94, 145-152.

Didyk, B.M., Simoneit, B.R.T., Brassell, S.C., Eglinton, G., 1978. Organic geochemical indicators of palaeoenvironmental conditions of sedimentation. Nature 272, 216-222.

Ebli, O., Vetö, I., Lobitzer, H., Sajgò, C., Demény, A., Hetényi, M., 1998. Primary productivity and early diagenesis in the Toarcian Tethys on the example of the Mn rich black shales of the Sachrang Formation, Northern Calcareous Alps. Organic Geochemistry 29, 1635-1647.

Epstein, S., Mayeda, T.K., 1953. Variations of the 18O/16O ratio in natural waters. Geochimica et Cosmochimica Acta 4, 213-225.

Frimmel, A., Oschmann, W., Schwark, L., 2004. Chemostratigraphy of the Posidonia Shale, SW Germany I. Influence of sea-level variation on organic facies evolution. Chemical Geology 206, 199-230.

Frisch, W., Gawlick, H.-J., 2003. The nappe structure of the central Northern Calcareous Alps and its disintegration during Miocene tectonic extrusion – a contribution to understanding the orogenic evolution of the Eastern Alps. International Journal of Earth Sciences: 92, 712-727.

Froelich, P.N., Klinkhammer, G.P., Bender, M.L., Luedtke, N.A., Heath, G.R., Cullen, D., Dauphin, P., Hammond, D., Hartman, B., Maynard, V., 1979. Early oxidation of organic matter in pelagic sediments of the eastern equatorial Atlantic: suboxic diagenesis. Geochimica et Cosmochimica Acta 43, 1075-1090.

Gawlick, H.-J., Suzuki, H., 1999. Zur stratigraphischen Stellung der Strubbergschichten in den Nördlichen Kalkalpen (Callovium - Oxfordium). N. Jb. Geol. Paläont. Abh. 211, 233-262.

Gawlick, H.-J., Missoni, S., Schlagintweit, F., Suzuki, H., Frisch, W., Krystyn, L., Blau, J., Lein, R., 2009. Jurassic Tectonostratigraphy of the Austroalpine Domain. Journal of Alpine Geology 50, 1-152.

Heiser, U., Neumann, T., Scholten, J., Stüben, D., 2001. Recycling of manganese from anoxic sediments in stagnant basins by seawater inflow: a study of surface sediments from the Gotland Basin, Baltic Sea. Marine Geology 177, 151-166.

Hild, E., Brumsack, H.-J., 1998. Major and minor element geochemistry of Lower Aptian sediments from the NW German Basin (core Hoheneggelsen KB 40). Cretaceous Research 19, 615-633.

Ikeda, M., Hori, R.S., 2014. Effects of Karoo-Ferrar volcanism and astronomical cycles on the Toarcian Anoxic Events (Early Jurassic). Palaeogeography, Palaeoclimatology, Palaeoecology 410, 134-142.

Irwin, H., 1980. Early diagenetic carbonate precipitation and pore fluid migration in the Kimmeridge Clay of Dorset, England. Sedimentology 27, 577-591.

Jach, R., Dudek, T., 2005. Origin of a Toarcian manganese carbonate/silicate deposit from the Krížna unit, Tatra Mountains, Poland. Chemical Geology 224, 136-152.

Jenkyns, H.C., 1985. The Early Toarcian and Cenomanian–Turonian anoxic events in Europe: comparisons and contrasts. Geologische Rundschau 74, 505-518.

Jenkyns, H.C., 1988. The Early Toarcian (Jurassic) anoxic event: stratigraphic, sedimentary, and geochemical evidence. American Journal of Science 288, 101-151.

Jenkyns, H.C., 2010. The geochemistry of oceanic anoxic events. Geochemistry Geophysics Geosystems 11, Q03004, doi: 10.1029/2009GC002788.

Jenkyns, H.C., Géczy, B., Marshall, J.D., 1991. Jurassic manganese carbonates of central Europe and the Early Toarcian anoxic event. The Journal of Geology 99, 137-149.

Jenkyns, H.C., Jones, C.E., Gröcke, D.R., Hesselbo, S.P., Parkinson, D.N., 2002. Chemostratigraphy of the Jurassic System: applications, limitations and implications for palaeoceanography. Journal of the Geological Society of London 159, 351-378.

Jørgensen, B.B., 1982. Mineralization of organic matter in the sea bed-the role of sulphate reduction. Nature 296, 643-645.

Jørgensen, B.B., 1983. The microbial sulfur cycle. In: Krumbein, W.E. (Eds.), Microbial geochemistry. Blackwell, London, pp. 91-124.

Jørgensen, B.B., 2000. Bacteria and marine biogeochemistry. In: Schulz, H.D., Zabel, M. (Eds.), Marine Geochemistry. Springer Verlag, Berlin, pp. 173-207.

Kastner, M., 1984. Control of dolomite formation. Nature 311, 410-411.

Kohnen, M.E.L., Sinninghe Damsté, J.S., de Leeuw, J.W., 1991. Biases from natural sulphurization in palaeoenvironmental reconstruction based on hydrocarbon biomarker distributions. Nature 349, 775-778.

Littke, R., Rotzal, H., Leythaeuser, D., Baker, D.R., 1991. Organic facies and maturity of Lower Toarcian Posidonia Shale in Southern Germany (Schwäbische Alb). Erdöl & Kohle Erdgas Petrochemie/Hydrocarbon Technology 44, 407-414.

Loucaides, S., Van Cappellen, P., Behrends, T., 2008. Dissolution of biogenic silica from land to ocean: The role of salinity and pH. Limnology and Oceanography 53, 1614-1621.

Lovley, D.R., Phillips, E.J.P., 1988. Manganese inhibition of microbial iron reduction in anaerobic sediments: Applied and Environmental Microbiology 53, 145-155.

Lückge, A., Boussafir, M., Lallier-Vergès, E., Littke, R., 1996. Comparative study of organic matter preservation in immature sediments along the continental margins of Peru and Oman. Part I: Results of petrographical and bulk geochemical data. Organic Geochemistry 24, 437-451.

Machel, H.G., 2004. Concepts and models of dolomitization: a critical reappraisal. In: Braithwaite, C.J.R., Rizzi, G., Darke, G. (Eds), The Geometry and Petrogenesis of Dolomite Hydrocarbon Reservoirs. Geological Society, London, Special Publications, 235, 7-63.

Mazzullo, S.J., 2000. Organogenic dolomitization in peritidal to deep-sea sediments. Journal of Sedimentary Research 70, 10-23.

McArthur, J.M., Algeo, T.J., van de Schootbrugge, B., Li, Q., Howarth, R.J., 2008, Basinal restriction, black shales, and the Early Toarcian (Jurassic) oceanic anoxic event. Paleoceanography, v. 23, PA4217, doi:10.1029/2008PA001607.

Meister, P., McKenzie, J.A., Vasconcelos, C., Bernasconi, S., Frank, M., Gutjahr, M., 2007. Dolomite formation in the dynamic deep biosphere: results from the Peru margin. Sedimentology 54, 1007-1031.

Meister, P., McKenzie, J.A., Bernasconi, S.M., Brack, P., 2013. Dolomite formation in the shallow seas of the Alpine Triassic. Sedimentology 60, 270-291.

Middelburg, J.J., De Lange, G.J., van der Weijden, C.H., 1987. Manganese solubility control in marine pore waters. Geochimica et Cosmochimica Acta 51, 759-763.

Middelburg, J.J., de Lange, G.J., Kreulen, R., 1990. Dolomite formation in anoxic sediments of Kau Bay, Indonesia. Geology 18, 399-402.

Mirsal, I.A., Zankl, H., 1985. Some phenomenological aspects of carbonate chemistry. The control effect of transition metals. Geologische Rundschau 74, 367-377.

Missoni, S., Gawlick, H.-J., 2011. Evidence for Jurassic subduction from the Northern Calcareous Alps (Berchtesgaden; Austroalpine; Germany). International Journal of Earth Sciences 100, 1605-1631.

Morford, J.L., Russell, A.D., Emerson, S., 2001. Trace metal evidence for changes in the redox environment associated with the transition from terrigenous clay to diatomaceous sediments, Saanich Inlet, BC. Marine Geology 174, 355-369.

Morse, J.W., Arvidson, R.S., Lüttge, A., 2007. Calcium carbonate formation and dissolution. Chemical Reviews 107, 342-381.

Naeher, S., Gilli, A., North, R.P., Hamann, Y., Schubert, C.J., 2013. Tracing bottom water oxygenation with sedimentary Mn/Fe ratios in Lake Zurich, Switzerland. Chemical Geology 353, 125-133.

Neumeister, S., Gratzer, R., Algeo, T.J., Bechtel, A., Gawlick, H.-J., Newton, R.J., Sachsenhofer, R.F., 2015. Oceanic response to Pliensbachian and Toarcian magmatic events: Implications from an organic-rich basinal succession in the NW Tethys. Global and Planetary Change 126, 62-83.

Neumeister, S., Algeo, T.J., Bechtel, A., Gawlick, H.-J., Gratzer, R., Sachsenhofer, R.F., 2016. Redox conditions and depositional environment of the Lower Jurassic Bächental bituminous marls (Tyrol, Austria). Austrian Journal of Earth Sciences.

Och, L.M., Müller, B., Voegelin, A., Ulrich, A., Göttlicher, J., Steiniger, R., Mangold, S., Vologina, E.G., Sturm, M., 2012. New insights into the formation and burial of Fe/Mn accumulations in Lake Baikal sediments. Chemical Geology 330-331, 244-259.

O'Sullivan, P.E., Reynolds, C.S., 2005. The Lakes Handbook: Lake restoration and rehabilitation. Blackwell Science, Oxford.

Pearce, C.R., Cohen, A.S., Coe, A.L., Burton, K.W., 2008. Molybdenum isotope evidence for global ocean anoxia coupled with perturbations to the carbon cycle during the Early Jurassic. Geology 36, 231-234.

Piper, D.Z., Calvert, S.E., 2009. A marine biogeochemical perspective on black shale deposition. Earth Science Reviews 95, 63-96.

Polgári, M., Szabó-Drubina, M., Szabó, Z., 2004. Theoretical model for Jurassic manganese mineralization in Central Europe, Úrkút, Hungary. Bulletin of Geoscience 79, 53-61.

Polgári, M., Hein, J.R., Vigh, T., Szabó-Drubina, M., Fórizs, I., Bíró, L., Müller, A., Tóth, A.L., 2012. Microbial processes and the origin of the Úrkút manganese deposit, Hungary. Ore Geology Reviews 47, 87-109.

Polgári, M., Németh, T., Pál-Molnár, E., Futó, I., Vighe, T., Mojzsis, S.J., 2016. Correlated chemostratigraphy of Mn-carbonate microbialites (Úrkút, Hungary). Gondwana Research 29, Issue 1: 278–289.

Pratt, L.M., Force, E.R., Pomerol, B., 1991. Coupled manganese and carbon-isotopic events in marine carbonates at the Cenomanian–Turonian boundary. Journal of Sedimentary Petrology 61, 370-383.

Praus, M., Riegel, W., 1989. Evidence from phytoplanktonic associations for causes of black shale formation in epicontinental seas. Neues Jahrbuch für Geologie und Paläontologie Monatshefte 11, 671-682.

Pye, K., Dickson, A.D., Schiavon, N., Coleman, M.L., Cox, M., 1990. Formation of siderite-Mg-calcite-iron sulfide concentrations in intertidal marsh and sandflat sediments, north Norfolk, England. Sedimentology 37, 325-343.

Ratschbacher, L., Dingeldey, C., Miller, C., Hacker, B.R., McWilliams, M.O., 2004. Formation, subduction, and exhumation of Penninic oceanic crust in the Eastern Alps: time constraints from 40Ar/39Ar geochronology. Tectonophysics 394, 155-170.

Rivadeneyra, M.A., Delgado, R., Parraga, J., Ramos-Cormenzana, A., Delgado, G., 2006. Precipitation of minerals by 22 species of moderately halophilic aerobic bacteria in artificial marine salts media: influence of salt concentration. Folia Microbiologica 51, 445-453.

Röhl, H.J., Schmid-Röhl, A., Oschmann, W., Frimmel, A., Schwark, L., 2001. The Posidonia Shale (Lower Toarcian) of SW-Germany: an oxygen-depleted ecosystem controlled by sea level and palaeoclimate. Palaeogeography, Palaeoclimatology, Palaeoecology 165, 27-52.

Russell, M.J., Hall, A.J., 2006. The onset and early evolution of life. In: Kesler, S.E., Ohmoto, H., (Eds.), Evolution of Early Earth's Atmosphere, Hydrosphere, and Bioshpere – Constraints from Ore Deposits. Geological Society of America Memoir, 198, pp. 1-32.

Sabatino, N., Neri, R., Bellanca, A., Jenkyns, H.C., Masetti, D., Scopelliti, G., 2011. Petrography and high-resolution geochemical records of Lower Jurassic manganese-rich deposits from Monte Mangart, Julian Alps. Palaeogeography, Palaeoclimatology, Palaeoecology 299, 97-109.

Sælen, G., Doyle, P., Talbot, M.R., 1996. Stable-isotope analysis of belemnite rostra from the Whitby Mudstone Fm., England: Surface water conditions during deposition of a marine black shale. Palaios 11, 97-117.

Sánchez-Román, M., Rivadeneyra, M.A., McKenzie, J.A., 2007. Carbonate and phosphate precipitation by halophilic bacteria: influence of Ca2+ and Mg2+ ions. FEMS Microbiology Ecology 61, 273-284.

Sánchez-Román, M., McKenzie, J.A., de Luca Rebello Wagener, A., Rivadeneyra, M.A., Vasconcelos, C., 2009. Presence of sulfate does not inhibit low-temperature dolomite precipitation. Earth and Planetary Science Letters 285, 131-139.

Schaller, T., Wehrli, B., 1996. Geochemical focusing of manganese in lake sediments – an indicator of deep-water oxygen conditions. Aquatic Geochemistry 2, 359-378.

Schmid-Röhl, A., Röhl, H.-J., Oschmann, W., Frimmel, A., Schwark, L., 2002. Palaeoenvironmental reconstruction of Lower Toarcian epicontinental black shales (Posidonia Shale, SW Germany): global versus regional control. Geobios 35, 13-20.

Sinninghe Damsté, J.S., Eglinton, T.I., De Leeuw, J.W., Schenck, P.A., 1989. Organic sulphur in macromolecular sedimentary organic matter: 1. Structure and origin of sulphur-containing moieties in kerogen, asphaltenes and coal as revealed by flash pyrolysis. Geochimica et Cosmochimica Acta 53, 389-415.

Slaughter, M., Hill, R.J., 1991. The influence of organic matter in organogenic dolomitization. Journal of Sedimentary Petrology 61, 296-303.

Spieler, A., Brandner, R., 1989. Vom jurassischen Pull-Apart Becken zur Westüberschiebung der Achentaler Schubmasse (Tirol, Österreich). Geologische und Paläontologische Mitteilungen Innsbruck 16, 191-194.

Stumm, W., Morgan, J.J., 1981. Aquatic Chemistry. Wiley & Sons, New York.

Suan, G., Schlögl, J., Mattioli, E., 2016. Bio- and chemostratigraphy of the Toarcian organic-rich deposits of some key successions of the Alpine Tethys. Newsletters on Stratigraphy, published online.

Thamdrup, B., 2000. Bacterial manganese and iron reduction in aquatic sediments. Advances in Microbial Ecology 16, 41-84.

Tribovillard, N., Algeo, T.J., Lyons, T., Riboulleau, A., 2006. Trace metals as paleoredox and paleoproductivity proxies: An update. Chemical Geology 232, 12-32.

Vairavamurthy, M.A., Schoonen, M.A.A., 1995. Geochemical transformation of sedimentary Sulphur. Washington DC, ACS Symposium Series 612, 16-37.

Vasconcelos, C., McKenzie, J.A., 1997. Microbial mediation of modern dolomite precipitation and diagenesis under anoxic conditions (Lagoa Vermelha, Rio de Janeiro, Brazil). Journal of Sedimentary Research 67, 378-390.

Van Cappellen, P., Qiu, L., 1997. Biogenic silica dissolution in sediments of the Southern Ocean. I. Solubility. Deep Sea Research II 44, 1109-1128.

Vetö, I., Demeny, A., Hertelendi, E., Hetenyi, M., 1997. Estimation of primary productivity in the Toarcian Tethys: a novel approach based on TOC, reduced sulphur and manganese contents. Palaeogeography, Palaeoclimatology, Palaeoecology 132, 355-371.

Wacey, D., Wright, D.T., Boyce, A.J., 2008. A stable isotope study of microbial dolomite formation in the Coorong Region, South Australia. Chemical Geology 244, 155-174.

Warren, J., 2000. Dolomite: occurrence, evolution and economically important associations. Earth-Science Reviews 52, 1-81.

Wilkin, R.T., Barnes, H.L., Brantley, S.L., 1996. The size distribution of framboidal pyrite in modern sediments: an indicator of redox conditions. Geochimica et Cosmochimica Acta 60, 3897-3912.

Wright, D.T., Oren, A., 2005. Nonphotosynthetic bacteria and the formation of carbonates and evaporites through time. Geomicrobiology Journal 22, 27-53.

Zhang, F., Xu, H., Konishi, H., Kemp, J.M., Roden, E.E., Shen, Z., 2012. Dissolved sulfide-catalyzed precipitation of disordered dolomite: Implications for the formation mechanism of sedimentary dolomite. Geochimica et Cosmochimica Acta 97, 148-165.

9.10 Appendix: Full data set for samples of the Bächental section

Table 9.10.1: Bulk geochemical and mineralogical data for samples of the Bächental section. Mineral phases are expressed in [peak area; p. a.]. Relative percentages of carbonate phases were calculated based on amount of total carbonate according to XRD analysis. Unit 1: BT 9-21, Subunit 2a: BT 21-35, Subunit 2b: BT 36-40, Unit 3: BT 44-58.

Sample	Si	Ca	Mg	Mn	Detr./diag. calcite		Kutnohorite/dolomite		Mn-bearing siderite	
	[%]	*[%]*	*[%]*	*[%]*	*[p. a.]*	*[relative percentages]*	*[p. a.]*	*[relative percentages]*	*[p. a.]*	*[relative percentages]*
BT 58	20.5	7.0	3.4	0.8	10390	67.5	4990	32.5		
BT 57	20.3	6.6	4.0	0.9	9050	64.0	5080	36.0		
BT 56	14.4	11.3	3.9	6.9	6950	28.3	17590	71.7		
BT 54	9.8	22.5	1.4	0.4	7520	30.0	17560	70.0		
BT 53	14.2	11.8	3.7	5.3	7310	34.2	14060	65.8		
BT 52	12.1	11.2	4.0	10.5	4810	20.5	18680	79.5		
BT 51	11.2	10.6	3.5	11.0	5000	19.0	21260	71.0	5830	23.6
BT 50	9.3	8.9	5.4	9.2	3850	20.9	14960	79.1	3460	12.5
BT 48	11.5	10.9	4.2	8.5	5410	23.3	16510	71.1	1310	5.6
BT 47	9.0	11.0	5.3	11.6	4370	20.6	16900	79.4	5410	20.3
BT 46	6.6	10.9	5.5	10.4	4900	20.0	15200	62.0	4410	18.0
BT 45	10.7	9.6	5.0	9.6	3820	17.3	14100	64.0	4110	18.6
BT 44	12.1	9.8	4.4	8.3	4990	23.8	15990	76.2	2400	10.3
BT 40	16.1	10.1	4.0	0.7	15670	66.7	7830	33.3		
BT 39	13.7	11.8	3.2	0.7	16740	86.4	2630	13.6		
BT 38	16.7	10.8	3.3	0.6	17370	86.6	2690	13.4		
BT 37	20.6	6.2	4.2	0.3	11160	76.8	3370	23.2		
BT 36	18.5	11.2	2.7	1.2	15030	92.8	1170	7.2		
BT 35	10.8	19.6	2.1	0.6	36600	98.1	710	1.		
BT 34	14.6	14.3	2.4	0.5	28750	93.4	2040	6.6		
BT 33	19.8	11.1	2.8	0.7	17960	88.1	2430	11.9		
BT 32	21.4	10.4	2.9	0.6	13870	85.3	2400	14.7		
BT 31	12.3	19.5	1.9	0.6	46400	99.0	470	1.0		
BT 30	26.2	5.3	2.4	0.3	10620	78.9	2840	21.1		
BT 29	11.3	21.0	2.1	0.7	62170	98.8	740	1.2		
BT 28	21.5	9.3	2.6	0.5	19170	88.4	2520	11.6		
BT 26	16.3	12.7	2.8	0.6	21470	88.3	2830	11.7		
BT 25	17.8	9.0	2.5	0.4	17510	96.8	580	3.2		
BT 24	17.6	10.3	2.2	0.3	21150	92.1	1830	7.9		
BT 23	21.3	11.5	2.7	0.5	21790	94.1	1360	5.9		
BT 22	19.2	13.2	2.5	0.7	21280	98.8	260	1.2		
BT 21	16.6	10.7	3.5	4.5	8730	39.3	13460	60.7		
BT 20	16.6	9.1	3.3	4.0	8700	40.6	12720	59.4		
BT 19	17.4	9.1	3.8	1.5	11390	64.5	6280	35.5		
BT 18	18.3	10.3	3.7	0.5	16830	88.4	2200	11.6		
BT 17	17.3	10.9	3.5	3.9	11900	49.7	12060	50.3		
BT 16	18.1	8.1	3.6	3.7	8850	43.8	11350	56.2		
BT 15	17.7	7.8	3.8	2.7	8530	63.3	4940	36.7		
BT 13	16.9	7.9	4.3	5.5	5630	26.4	7750	36.3		
BT 12	20.6	7.2	3.1	1.0	12370	76.4	3820	23.6		
BT 11	19.1	7.4	4.0	4.1	5020	26.6	13820	73.4		
BT 10	19.5	6.6	3.7	4.3	5470	28.5	13750	71.5		
BT 9	19.4	6.6	3.7	5.0	4240	25.8	12200	74.2		

Table 9.10.2: Elemental composition of diagenetic carbonate phases.

Carbonate phase	Sample	Ca *[%]*	Mg *[%]*	Fe *[%]*	Mn *[%]*
Dolomite	**BT 45**	21.8	12.4	0.2	0.3
	BT 45	23.6	12.4	0.3	0.4
	BT 45	22.9	12.4	0.1	0.3
	BT 45	22.5	12.0	0.5	0.6
	BT 45	22.2	13.1	0.4	0.3
	BT 29	21.9	12.2		
	BT 9	22.5	12.5	0.1	0.4
	BT 9	21.9	12.8	0.1	0.2
	BT 9	22.8	12.4	0.1	0.1
	BT 9	21.9	10.6	1.0	0.9
	BT 9	22.7	12.5		0.1
	BT 9	24.1	12.1	0.3	0.2
	BT 9	21.8	12.8	0.1	0.1
Kutnohorite	**BT 45**	9.1	0.8	0.5	32.4
	BT 45	12.8	1.0	1.2	27.2
	BT 45	19.1	1.1	0.2	22.4
	BT 45	13.6	0.8	0.5	22.6
	BT 45	17.6	0.9	0.3	23.7
	BT 45	16.6	0.9	0.3	24.4
	BT 45	16.7	1.1	0.7	23.9
	BT 9	18.7	1.4	0.6	21.2
	BT 9	18.5	1.2	0.5	21.0
	BT 9	15.8	0.9	0.3	24.6
	BT 9	21.2	1.6	0.9	16.7
	BT 9	20.3	1.0	0.1	18.7
Kutnohorite zonation	**BT 45**				
Inner rim		8.8	1.6	1.7	30.8
Middle rim		27.2	1.4	0.5	13.3
Outer rim		10.2	0.9	0.6	30.7
Mn-bearing calcite	**BT 29**	39.4	0.4	0.5	3.9
	BT 29	39.2	0.4	0.3	4.2
	BT 29	39.4	0.4	0.4	4.0
	BT 29	38.8	0.5	0.4	4.1
	BT 29	38.3	0.3	0.3	3.3
	BT 25	32.8	0.9	0.1	0.7
	BT 25	32.4	1.0	0.1	0.6
	BT 25	36.6	0.3	0.5	1.9
	BT 25	40.4	0.5	0.4	2.6

Table 9.10.3: Results for TOC_{Mn} and TOC_S as well as adopted data from Neumeister et al. (2015, 2016). Unit 1: BT 9-21, Subunit 2a: BT 21-35, Subunit 2b: BT 36-40, Unit 3: BT 44-58.

Sample	TOC_{Mn} *[%]*	TOC_S *[%]*	TOC *[%]*	Cc_{eq} *[%]*	S *[%]*	HI *[mg HC/g TOC]*	Fe *[%]*	Al *[%]*	$\delta^{13}C_{carb}$ *[‰ VPDB]*	$\delta^{18}O_{carb}$ *[‰ VPDB]*	Pr/Ph *[conc. ratio]*
BT 58	0.1	5.4	2.8	23.2	5.4	544	4.5	5.0	-2.6	-4.4	1.4
BT 57	0.1	5.8	3.0	22.8	5.8	541	4.9	5.8	-2.2	-4.2	
BT 56	0.8	3.4	2.1	50.8	3.4	541	2.3	3.0	-5.8	-3.6	
BT 54	0.0	5.0	1.5	53.3	5.0	375	0.5	2.0	-7.2	-3.5	
BT 53	0.6	5.7	1.6	47.1	5.7	415	3.8	3.3	-5.6	-3.2	
BT 52	1.2	5.0	1.7	52.0	5.0	419	3.3	3.4	-10.8	-3.1	
BT 51	1.2	2.1	1.5	55.4	2.1	362	1.7	2.2	-12.7	-3.0	
BT 50	1.0	1.3	1.6	56.7	1.3	325	2.6	2.4	-5.2	-2.1	1.7
BT 48	0.9	2.5	2.1	51.0	2.5	379	2.5	3.7	-7.3	-3.3	
BT 47	1.3	2.0	1.6	60.7	2.0	320	3.3	2.6	-8.6	-2.3	
BT 46	1.1	1.8	1.5	64.8	1.9	370	2.5	2.3	-7.9	-2.4	
BT 45	1.1	2.6	1.5	56.9	2.6	400	3.3	2.9	-8.3	-2.5	1.6
BT 44	0.9	5.3	1.9	48.6	5.3	350	4.0	3.5	-8.7	-2.7	0.9
BT 40	0.2	3.5	3.0	36.9	3.5	604	2.6	5.4	-2.5	-3.8	1.3
BT 39	0.1	5.0	5.6	38.8	5.1	683	3.3	4.3	-1.5	-4.0	0.9
BT 38	0.1	5.3	5.6	32.3	5.3	661	3.7	4.8	-4.2	-4.7	
BT 37	0.0	4.4	6.3	18.6	4.4	622	4.1	6.0	-1.8	-5.1	1.1
BT 36	0.1	5.9	2.9	35.2	5.9	572	3.6	3.2	-2.7	-4.3	0.9
BT 35	0.1	2.1	9.4	56.0	2.1	666	1.2	2.7	-2.1	-3.9	0.9
BT 34	0.1	2.6	8.0	43.1	2.6	644	1.6	3.7	-2.9	-4.6	
BT 33	0.1	2.6	3.6	33.9	2.6	670	1.8	3.8	-2.4	-4.4	0.7
BT 32	0.1	6.9	4.0	27.1	7.0	602	5.3	4.0	-2.4	-4.4	
BT 31	0.1	1.	5.4	58.8	1.3	687	0.8	2.6	-2.0	-3.2	0.8
BT 30	0.0	4.3	2.9	17.4	4.3	604	3.1	3.6	-2.9	-5.2	0.8
BT 29	0.1	1.6	6.8	60.7	1.6	686	0.9	2.8	-1.9	-3.8	0.8
BT 28	0.1	7.1	3.5	29.2	7.1	588	4.8	3.5	-2.8	-4.1	0.7
BT 26	0.1	3.0	7.6	37.9	3.0	653	1.9	3.6	-3.0	-4.8	0.8
BT 25	0.0	2.9	12.9	27.2	2.9	622	***2.1***	3.9	-2.6	-6.0	1.0
BT 24	0.0	2.8	11.7	30.7	2.8	621	1.6	3.3	-2.6	-5.9	0.9
BT 23	0.1	2.7	9.0	31.1	2.7	649	2.0	4.1	-2.9	-5.3	0.8
BT 22	0.1	3.1	8.6	38.0	3.2	645	2.1	3.6	-3.0	-5.4	0.8
BT 21	0.5	4.2	1.8	43.6	4.2	519	2.4	3.0	-6.3	-3.7	
BT 20	0.4	4.3	2.0	40.0	4.3	495	2.4	3.2	-6.2	-3.6	1.3
BT 19	0.2	5.6	3.3	31.0	5.6	612	4.1	5.2	-4.0	-4.0	
BT 18	0.1	2.1	2.5	32.1	2.2	577	2.2	5.6	-1.8	-3.9	1.3
BT 17	0.4	4.3	1.8	42.2	4.3	537	3.0	3.4	-6.9	-3.6	
BT 16	0.4	3.8	2.3	34.6	3.8	497	3.0	4.1	-6.3	-3.4	
BT 15	0.3	5.5	1.9	30.7	5.5	427	3.9	4.6	-6.1	-3.4	1.8
BT 13	0.6	3.6	1.1	43.4	3.6	307	6.4	2.2	-4.7	-2.3	
BT 12	0.1	5.3	2.2	24.4	5.3	518	4.3	5.3	-3.2	-3.9	1.0
BT 11	0.5	3.7	1.8	34.1	3.7	441	3.3	3.9	-6.9	-3.8	
BT 10	0.5	5.5	1.8	31.2	5.5	452	4.0	4.4	-8.7	-3.5	1.1
BT 9	0.5	5.4	1.6	32.9	5.4	459	3.7	4.4	-9.8	-3.6	

10 Comment on the recent publication of Suan et al. (2016), published online in Newsletters on Stratigraphy in February 2016

Suan et al. (2016) recently published a paper dealing with bio- and chemostratigraphy of Toarcian organic-rich deposits of some key successions of the Alpine Tethys, including the Bächental section. Two papers, based on data generated in the course of the present thesis, have already been published and accepted for publication, respectively (see Sections 7 and 8). Furthermore, the paper of Suan et al. (2016) has not been published till this thesis was completed for submission. Therefore, the impact of the new stratigraphic data and associated interpretations of Suan et al. (2016) are discussed within this separate section.

10.1 Stratigraphy of Bächental bituminous marls

Neumeister et al. (2015) based their stratigraphy of Bächental bituminous marls on several lines of evidence: [i] published biostratigraphic data (ammonites, radiolaria, nannofossils) suggesting a late Pliensbachian to early Toarcian age of the Bächental bituminous marls of the Sachrang Member (Klebelsberg, 1935; Kodina et al., 1988; Lobitzer et al., 1988), [ii] the finding of *Cleviceras exaratum* in the middle part of the section (13.40 m; lower part of high-TOC Unit 2), a taxon associated with the early Toarcian *falciferum* Zone, and [iii] the chemostratigraphic correlation of the Bächental section with both the epicontinental Posidonia Shale of Dotternhausen (SW Germany) and the global sea level curve for the Lower Jurassic after Haq et al. (1988) based on sterane data and indicating a Upper Pliensbachian to Lower Toarcian age of the study section (*margaritatus* Zone to *bifrons* Zone; Fig. 10.1).

However, Kodina et al. (1988) and Lobitzer et al. (1988) did not provide figures to show the absolute position of the ammonites (*Arieticeras* sp. and, possibly, *Leptaleoceras* sp.) indicating a late Pliensbachian age for the Bächental section. Hence, because of their finding of *Cleviceras exaratum* in the middle part of the section (13.40 m), suggesting an age of *falciferum* Zone for that interval, Neumeister et al. (2015) erroneously assumed, that the ammonites published by Kodina et al. (1988) derived from a lower position (i.e., “near the base of the marls”) in the Bächental section.

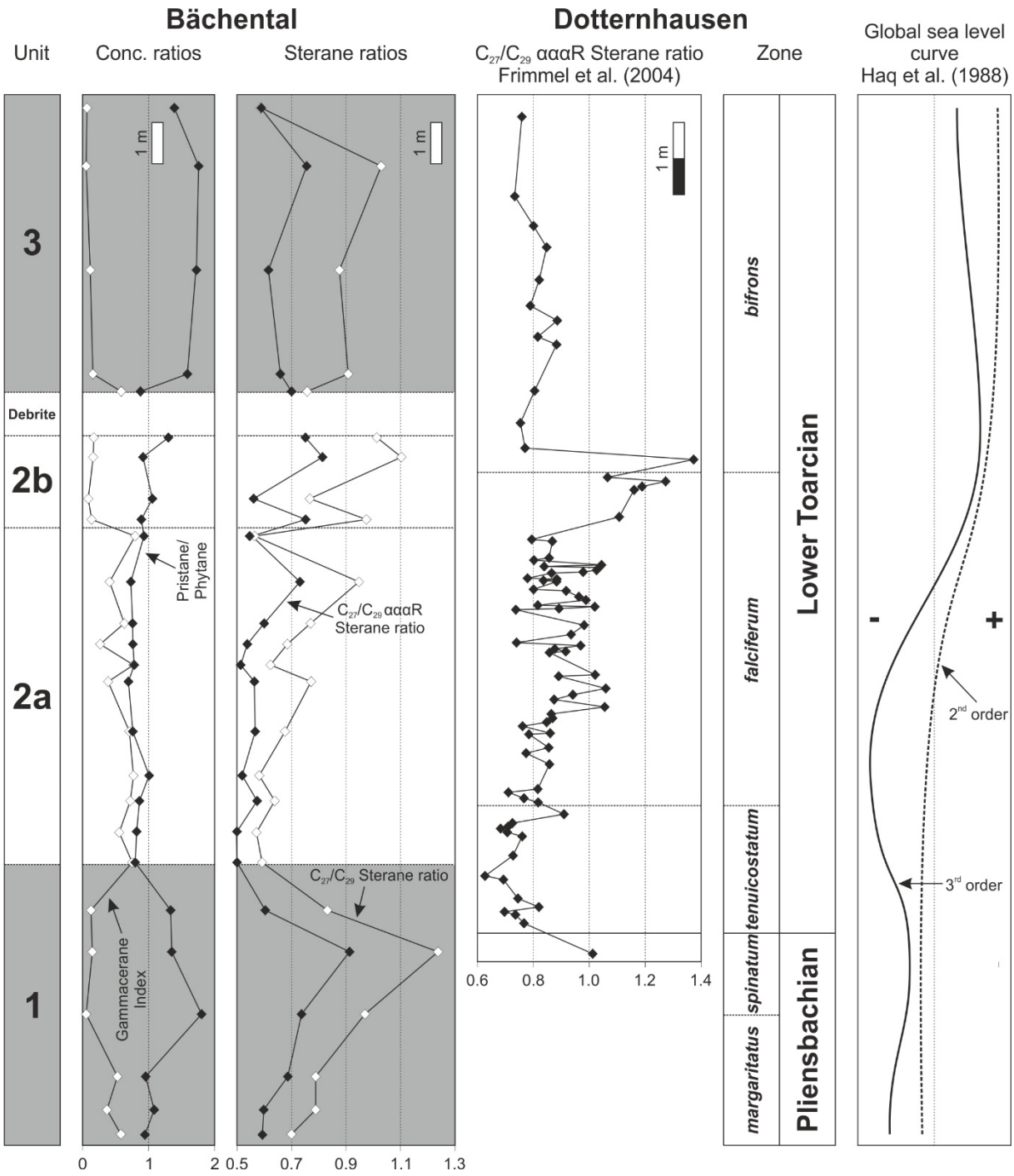

Fig. 10.1: Influence of sea-level changes on depositional environment and correlation of Lower Jurassic OM-rich sediments of Alpine (Bächental) and epicontinental (Dotternhausen; Frimmel et al., 2004) settings with global sea-level curve (Haq et al., 1988) using sterane ratios. See text for explanations.

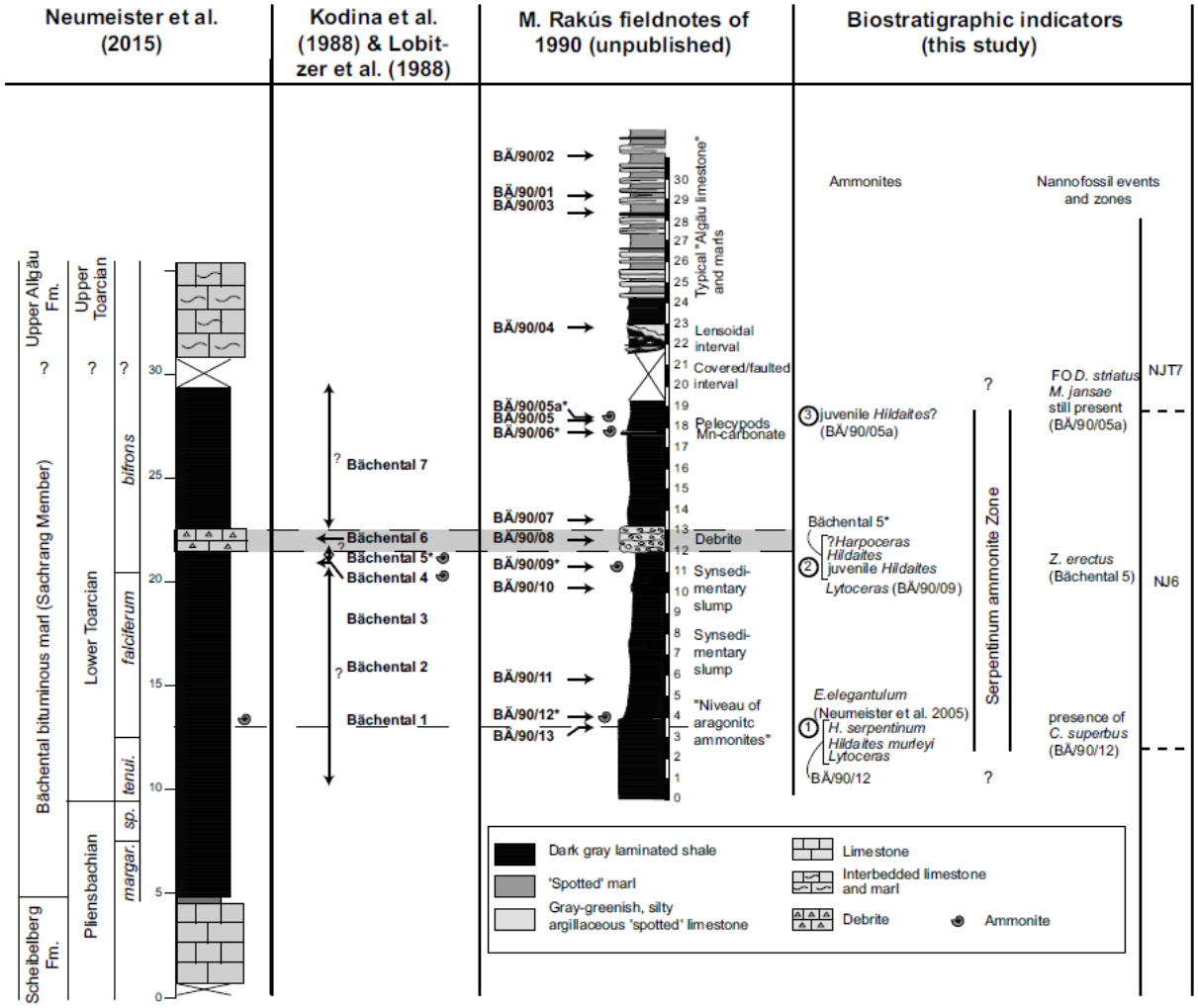

Fig. 10.2: Correlation between the various studies of the Bächental sections from Suan et al. (2016). Data from Neumeister et al. (2015), Kodina et al. (1988), Lobitzer et al. (1988) and M. Rakús fieldnotes of 1990 (originally unpublished, included in Suan et al., 2016), and Suan et al. (2016). The ammonites published by Kodina et al. (1988) and labelled as "Bächental 5" derive from an interval shortly below the debrite layer and, hence, several meters above the ammonite *Cleviceras exaratum* reported by Neumeister et al. (2015).

The recent re-examination of ammonite material previously published by Kodina et al. (1988) and Neumeister et al. (2015) along with new biostratigraphic data based on nannofossils and ammonites from the Bächental section resulted in a revised stratigraphic classification of the study section (Table 10.1; Suan et al., 2016). Furthermore, the authors could reliably attribute the position of the ammonites originally published by Kodina et al. (1988) to an interval directly below the debrite layer (ca. at 19-22 m; Fig. 10.2).

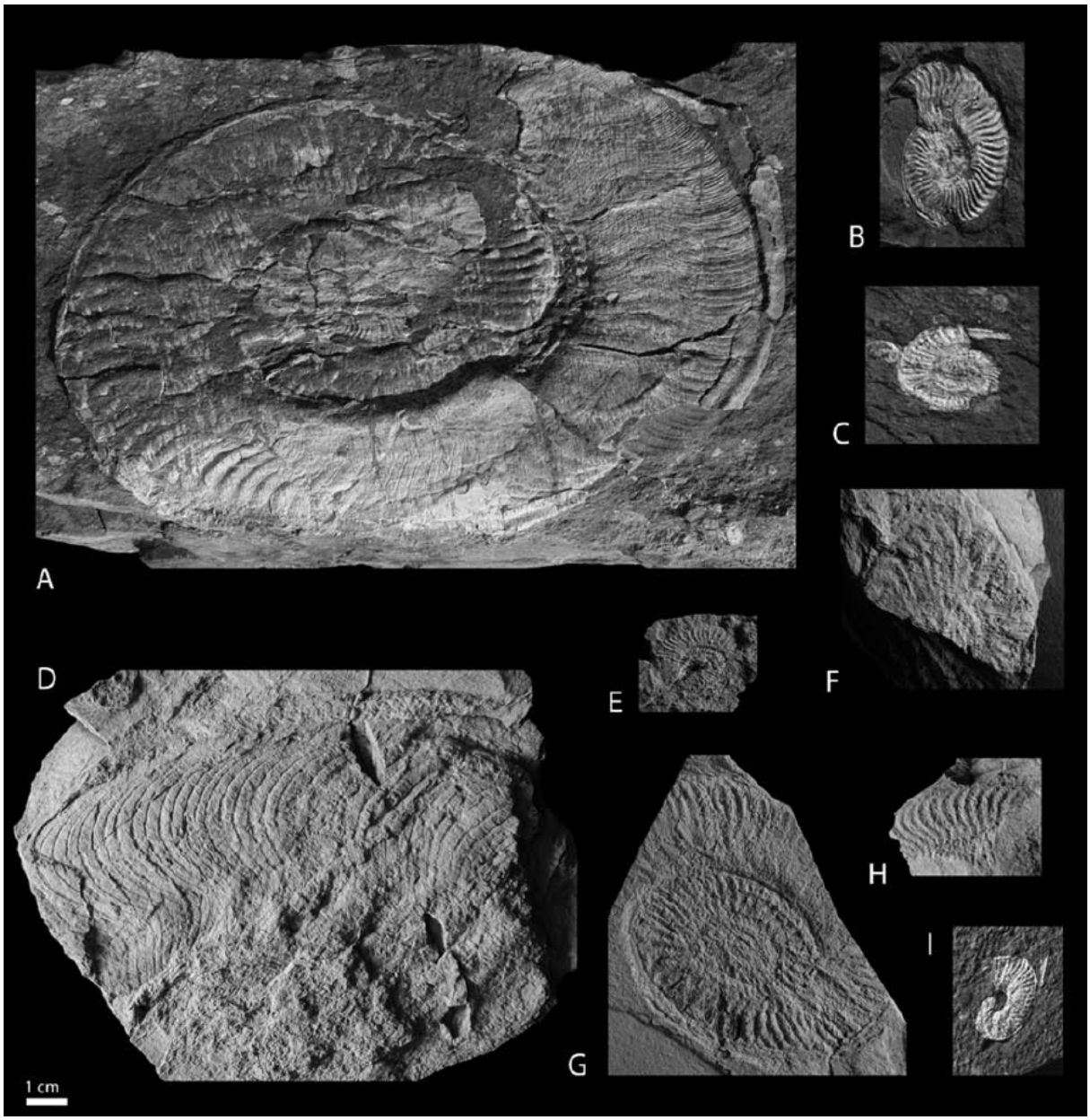

Fig. 10.3: Ammonite specimens from the Bächental locality published by Suan et al., 2016. (A, D) *Harpoceras serpentinum* (Schlotheim, 1813), coll. Rakús, 1990; (B) *Hildaites murleyi* (Moxon, 1841), coll. Rakús, 1990; (C, E) *Hildaites* sp. juv., coll. Rakús, 1990; (F) *Hildaites* sp., GBA 1988/5/3; (G) *Hildaites* sp., GBA 1988/5/2; (H) cf. *Harpoceras* sp., GBA 1988/5/4; I) *Hildaites* sp. juv., GBA 1988/5/5. The likely provenance of these specimens is indicated in Fig. 10.2.

Ammonites	Calcareous nannofossils
Eleganticeras elegantulum	*Schizosphaerella* spp.
Harpoceras serpentinum	*several species of Lotharingius* including *L. sigillatus*, *L. crucicentralis* and *L.* aff. *L. velatus*
Lytoceras	*Crepidolithus cavus/impontus*
Hildaites, including one specimen of Hildaites murleyi	*Biscutum intermedium*
	Zeugrhabdotus erectus
	Carinolithus superbus
	Mitrolithus jansae
	Discorhabdus striatus

Table 10.1: Ammonite and calcareous nannofossils assemblages published by Suan et al. (2016). The mentioned ammonite are diagnostic for the Early Toarcian according to Howarth (1992), Elmi et al. (1997), Page (2004), and Bécaud (2006). Calcareous nannofossils cover a time interval between Upper Pliensbachian and Lower Toarcian (Bown, 1987; Mattioli et al., 2013).

On the basis of ammonite and nannofossil assemblages (Table 1), Suan et al. (2016) suggested an age of Lower Toarcian *serpentinum/falciferum* Zone for the interval between ~13.4 and 28 m in the Bächental section including Unit 2 and large parts of Unit 3 (Fig. 10.2). For Unit 2, this biostratigraphic interpretation of Suan et al. (2016) is rather consistent with that published by Neumeister et al. (2015), considering the origin of the sample material from two independent sampling campaigns with a time lag of almost 30 years.

In contrast to Neumeister et al. (2015), Suan et al. (2016) allocate the upper part of the section into the *serpentinum/falciferum* Zone based on the finding of a juvenile ammonite (probably *Hildaites*) and the FO of *Discorhabdus striatus* both derived from the investigation of one single sample (Fig. 10.2). Regarding the stratigraphic data of Suan et al. (2016) for Unit 3 has to be mentioned that [i] the FO of *Discorhabdus striatus* is only “commonly described” (Suan et al., 2016) from the upper part of the *levisoni*/*serpentinum* Zone, [ii] the published ammonite in that interval is a juvenile specimen which could not be identified with absolute certainty, and [iii] the authors do not provide any data from the lower ~5 m of Unit 3

and, hence, an actual FO of *Discorhabdus striatus* at a lower level in the section cannot be fully excluded.

Furthermore, biostratigraphic data for the lower part of the Bächental section (ca. 12 m, including ca. 7.5 m of Unit 1; Fig. 10.2) is missing in the publication of Suan et al. (2016), making biostratigraphic interpretations impossible regarding this interval for their part.

Neumeister et al. (2015) stated a duration of bituminous marl sedimentation from late Pliensbachian (*margaritatus* Zone) to early Toarcian (*bifrons* Zone) on the basis of a chemostratigraphic correlation of sterane ratios from Bächental and time-equivalent Dotternhausen sections and the sea-level curve for the Lower Jurassic and, thereby, assigned Unit 3 into the *bifrons* Zone (Fig. 10.1). Although stratigraphic correlation based on biomarker data is a rather untested and unconventional technique, the Bächental bituminous marls exhibit an almost identical pattern of stratigraphic variation in sterane ratios and sea level relative to the biostratigraphically well-dated Dotternhausen section (Fig. 10.1). The data shows a well-defined fit in Units 1 and 2 and a fair correlation in Unit 3. Furthermore, agreement between the sea-level curve and variations in redox and salinity conditions inferred by independent proxies demonstrate the strong influence of sea-level fluctuations on watermass exchange and ventilation of the Bächental basin (Fig. 10.1; Neumeister et al., 2015). This supports the reliability of the suggested correlation between sterane ratios and sea level and, hence, the associated stratigraphic interpretation of Neumeister et al. (2015). Suan et al. (2016) neither mentioned the sterane-based chemostratigraphic correlation nor the stratigraphic variations of redox and salinity conditions and their well-defined fit to the sea-level curve published by Neumeister et al. (2015). Consequently, the authors obviously did not consider this information for their interpretation.

In a further step, Suan et al. (2016) propose a time interval of 200.000 to 450.000 years for deposition of the Bächental bituminous marls based on $\delta^{13}C$ isotope values of OM. However, based on the discussion in Section 10.2 (see below) this assumption has to be revised. Nevertheless, the stated onset of OM accumulation in the late Pliensbachian (*margaritatus* Zone) has to be questioned. According to Ebli et al. (1998) the deposition of the Sachrang Member at its type locality in Bavaria commenced at the base of the *tenuicostatum* Zone and continued through the entire early Toarcian. In the author's opinion this stratigraphic interpretation can be cautiously adopted for the Sachrang Member in the

Bächental basin considering all the existing data. However, the placement of boundaries at exact levels in the study section for further stratigraphic subdivision (i.e., ?late Pliensbachian – *tenuicostatum* Zone – *falciferum* Zone – ?*bifrons* Zone) in the study section is not possible with an adequate precision at present.

10.2 Stable carbon isotopes in the Bächental section: A record of the Lower negative Toarcian carbon isotope excursion?

A pronounced negative carbon isotope excursion (CIE) that is recorded in both marine carbonates and marine and terrestrial OM is widely regarded as a defining characteristic of the Toarcian oceanic anoxic event (T-OAE) and a global chemostratigraphic marker for the uppermost *tenuicostatum* and lower *falciferum* zones. This negative CIE has been reported from sections in NW Europe and the Mediterranean (e.g., Röhl et al., 2001; Jenkyns et al., 2001; Kemp et al., 2005; Hesselbo et al., 2007; Sabatino et al., 2009; Kafousia et al., 2014), the NE paleo-Pacific ocean (Caruthers et al., 2011), South America (Al-Suwaidi et al., 2010; Mazzini et al., 2010; Sell et al., 2014), and northwestern Panthalassa (Izumi et al., 2012) and is followed by a positive CIE toward the top of *falciferum/serpentinum* Zone (Röhl et al., 2001; Kemp et al., 2005; Hesselbo et al., 2007; Suan et al., 2011; Suan et al., 2015). The two Toarcian CIE couplets have been used to correlate poorly dated OM-rich successions of the Alpine Tethys area with NW European basins and to define the interval of the T-OAE in ammonite-poor deposits (Jenkyns et al., 1991; Sabatino et al., 2009, 2011, 2013; Kafousia et al., 2014). The negative CIE has been related to a rapid release of biogenic methane by dissociation of methane hydrates (e.g., Hesselbo et al., 2000, 2007; Jenkyns et al., 2002; Kemp et al., 2005), release of large volumes of CO_2 due to the emplacement of the Karoo-Ferrar large igneous province (LIP; e.g., Palfy and Smith, 2000; Mazzini et al., 2010), thermogenic methane resulting from the intrusion of igneous rocks into Gondwanan coals (McElwain et al., 2005; Svensen et al., 2007), recycling of OM ("recycling model"; Küspert, 1982, 1983; Röhl et al., 2001), and to the contribution of OM deriving either from calcareous or organic-walled plankton (Jenkyns and Clayton, 1986). Although Caruthers et al. (2011) inferred that the early Toarcian negative CIE was a global signal that had been imprinted on all active global reservoirs of the exchangeable carbon cycle, Neumeister et al. (2015) stated that both the organic and inorganic carbon isotope profiles of the Bächental section do not show the typical early Toarcian negative CIE (Fig. 10.4).

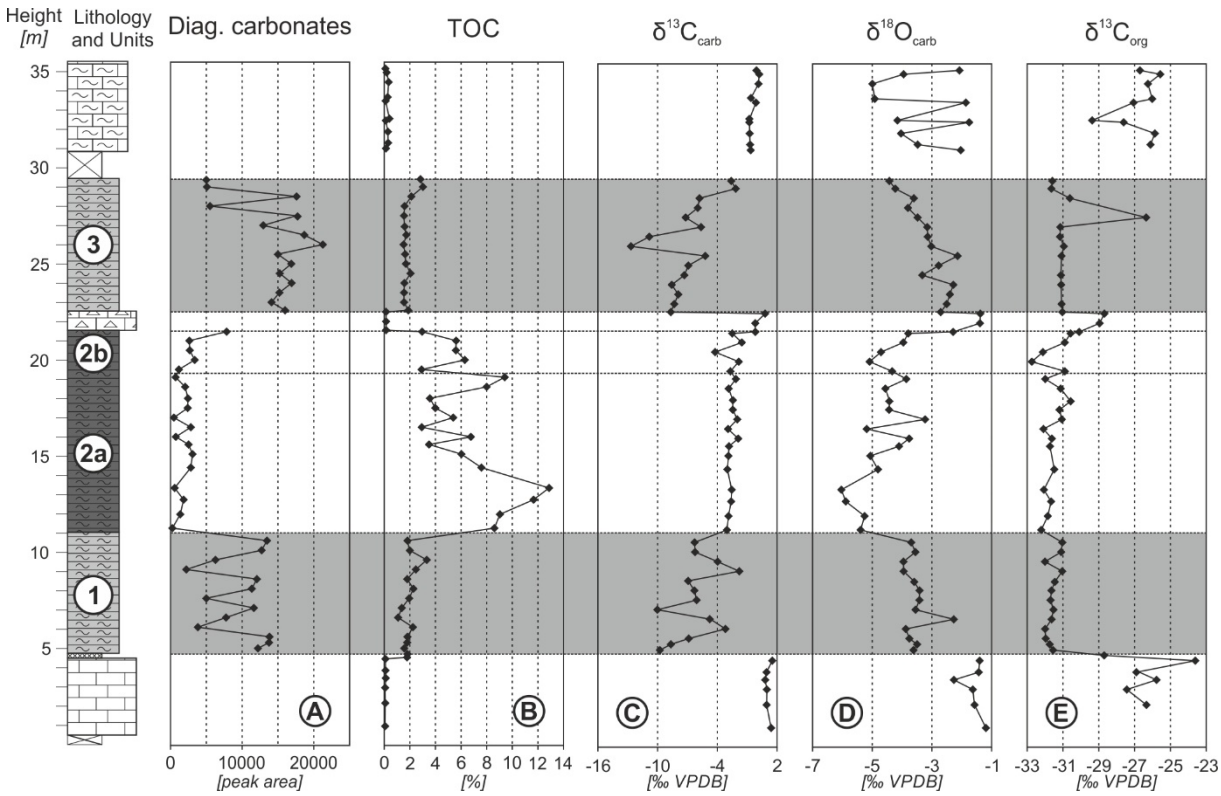

Fig. 10.4: Vertical variation of (A) diagenetic carbonates (peak area), (B) total organic carbon (TOC, %), (C) inorganic carbon isotope composition ($\delta^{13}C_{carb}$, ‰ VPDB), (D) oxygen isotope composition of carbonate ($\delta^{18}O_{carb}$, ‰ VPDB), (E) organic carbon isotope composition ($\delta^{13}C_{org}$, ‰ VPDB) for samples of the study section. The distinguished units within the Bächental bituminous marl are highlighted.

In contrast, Suan et al. (2016) [i] record the Lower Toarcian negative CIE in both the carbonate C-isotope (~3 ‰) and the organic C-isotope (~6-7 ‰) signal of Bächental bituminous marls, [ii] correlate the study section with several Lower Toarcian deposits by means of isotope chemostratigraphy, and finally [iii] suggest a time interval of 200.000 to 450.000 years for deposition of Bächental bituminous marls on the basis of stable isotope data published by Neumeister et al. (2015).

Suan et al. (2016) claim that a 3 ‰ negative CIE is evident from bulk carbonate $\delta^{13}C$ data after the removal of samples most likely to contain diagenetic carbonates. Accordingly, the authors removed samples from Units 1 and 3 and the debrite which, in their opinion, were diagenetically overprinted (cf. Figs. 10.4 and 10.5).

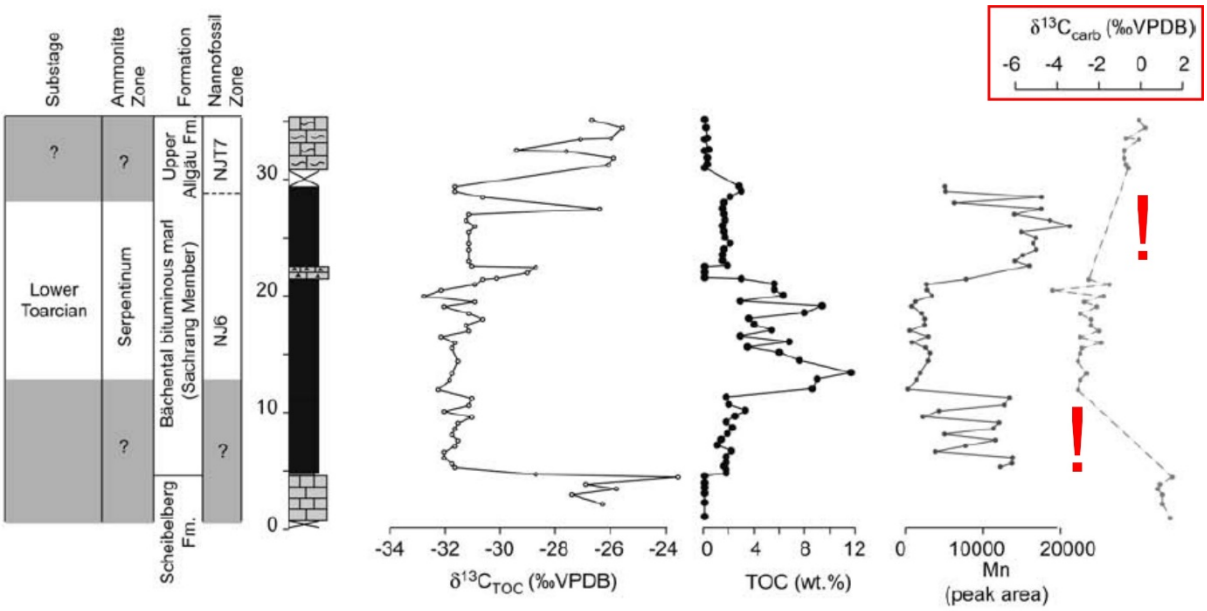

Fig. 10.5: Comparisons of the revised biostratigraphy and geochemical data of Bächental by Suan et al. (2016). Note that carbonate C-isotope values for samples from Units 1 and 3 were removed.

However, the interpretation of the carbonate C-isotope signal of Bächental bituminous marls by Suan et al. (2016) is biased. Bächental bituminous marls generally were affected by early diagenetic processes and contain almost exclusively secondary carbonate minerals (Neumeister et al., 2015). The dominant processes were markedly redox-dependent and varied strongly between sediments that accumulated under suboxic (Unit 1 and 3) versus anoxic-euxinic (Unit 2) conditions (Neumeister et al., submitted). During deposition of Units 1 and 3 Mn reduction was the dominant OM oxidation process. The release of dissolved Mn and isotopically light C triggered Mn supersaturation in pore waters and the formation of abundant kutnohorite (Fig. 10.6), representing the main carbonate phase in samples from Units 1 and 3, at the chemocline. Kutnohorite incorporated varying amounts of isotopically light organic-derived C during its formation, inducing the observed abnormally low carbonate-C isotope values in suboxic Units 1 and 3 (Fig. 10.4). In contrast, sulfate reduction was the main OM oxidation process during deposition of anoxic-euxinic Unit 2. The process caused an increase of alkalinity and pH conditions in porewaters resulting in the precipitation of diagenetic Mn-bearing calcite which is the dominant carbonate phase in Unit 2 (Fig. 10.6). This phase incorporated small fractions of isotopically light C provided by sulfate reduction and inducing a shift of bulk carbonate $\delta^{13}C$ data to slightly lower values interpreted as negative CIE by Suan et al. (2016). The relative significance of Mn reduction and sulfate reduction under suboxic and anoxic-euxinic conditions, respectively, and their impact on OM

oxidation and carbonate formation and, hence, carbonate C-isotope values is clearly visible for samples from the study section (cf. Neumeister et al., submitted). Accordingly, Suan et al. (2016) detected their negative CIE by the invalid comparison of the carbonate C-isotope signals of the OM-poor carbonates and marls from the Scheibelberg and Upper Allgäu Formations on the one hand and of bituminous marls from Unit 2 which contain almost exclusively diagenetic Mn-bearing calcite featuring low amounts of organic-derived C on the other hand.

Anoxic-euxinic Unit 2 was conclusively dated into the *falciferum* Zone corresponding to the time interval of the T-OAE (Neumeister et al., 2015; Suan et al., 2016). A massive perturbation of the global carbon cycle should be recorded in the carbonate C-isotope signal of Unit 2 despite the occurrence of early diagenetic carbonates especially as the values are rather constant in that interval. However, the shift of 3 ‰ observed by Suan et al. (2016) is evidently attributed to incorporation of organic-derived C in Mn-bearing calcite whereas an additional potentially global effect is not visible. Consequently the Lower Toarcian negative CIE cannot be observed in the study section questioning its applicability as ubiquitous chemostratigraphic marker for this time interval.

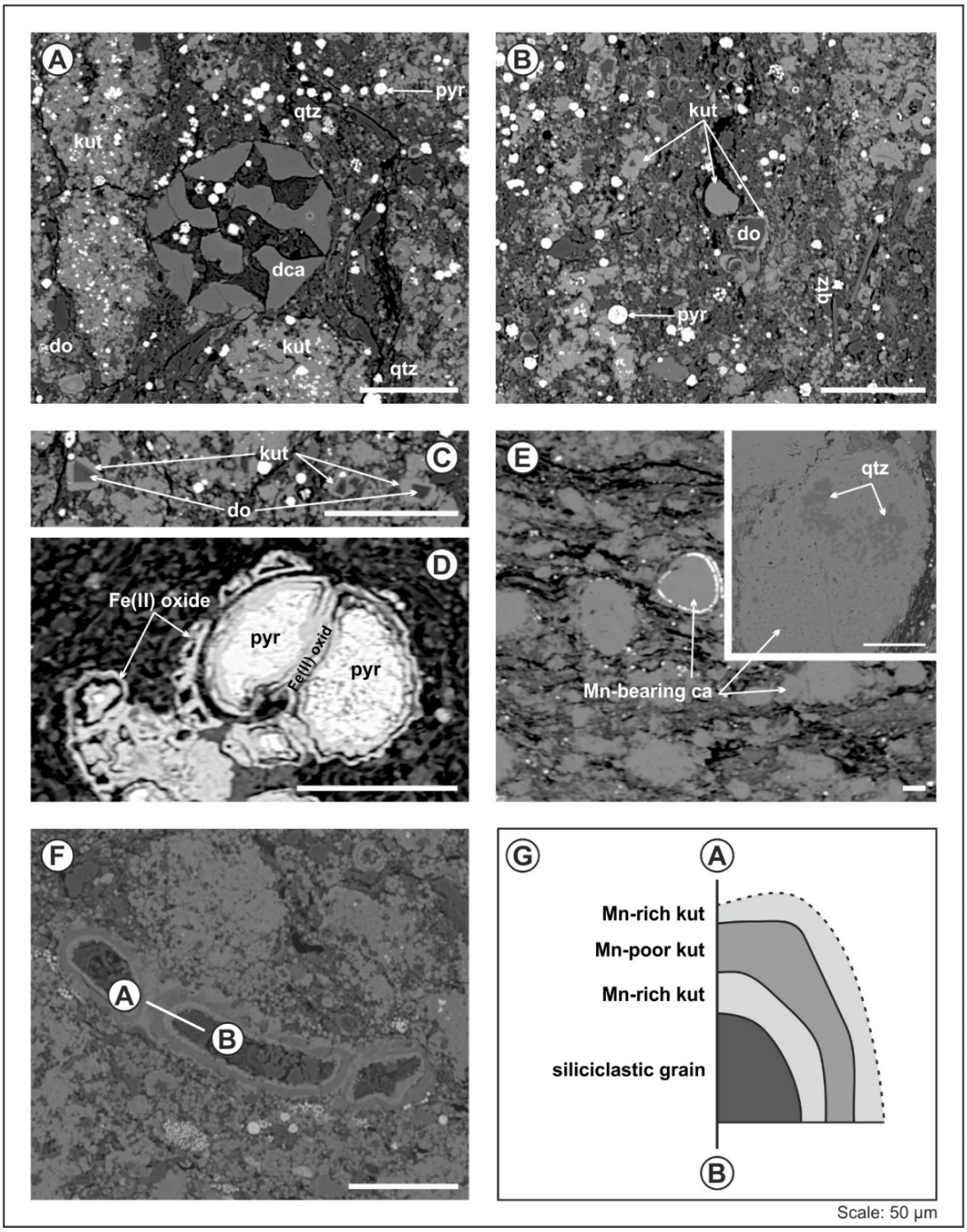

Fig. 10.6: Microphotographs of selected samples using the microprobe: (A-C) BT 9 (Unit 1), (D) BT 25 (Subunit 2a), (E) BT 29 (Subunit 2a), (F) BT 45 (Unit 3), and (G) sketch showing carbonate zonation surrounding a siliciclastic grain (for position, see line a-b in F). Indicated mineral phases: detrital calcite (dca), Mn-bearing calcite (Mn-bearing ca), kutnohorite (kut), dolomite (do), quartz (qtz), pyrite (pyr), and iron (II) oxide (Fe (II) oxide). Note that the samples almost exclusively contain diagenetic carbonate phases. Scale: 50 µm.

Organic C-isotope compositions for the Bächental bituminous marls are considerably lighter (-32.7 to -30.6 ‰ VPDB; Fig. 10.4) than typical values for modern marine plankton (-24 to -18 ‰ VPDB; e.g., Lewan, 1986; Tyson, 1995). They are also significantly lighter than average values of other lower Toarcian profiles as the $\delta^{13}C_{org}$ values of the entire Bächental bituminous marls succession are in the range of the lower Toarcian negative organic CIE (Hesselbo et al., 2000; Röhl et al., 2001; Kemp et al., 2005; Sabatino et al., 2009; Al-Suwaidi et al., 2010; Caruthers et al., 2011; Gröcke et al., 2011). In contrast, OM-poor rocks of Scheibelberg and Upper Allgäu Formations show heavier $\delta^{13}C_{org}$ isotope values (-29.4 to -23.6 ‰ VPDB) that are similar to correlative strata in other Toarcian sections (see above for references). Suan et al. (2016) concluded that the entire OM-rich interval in the Bächental basin was deposited during the time interval of the T-OAE due to the low $\delta^{13}C_{org}$ compositions for the bituminous marls. However, as noted above, the negative CIE is not recorded in the carbonate C-isotope values of the study section also questioning a potential global impact on the organic C-isotope signal. The ratio of C_{27} versus C_{29} steranes is commonly used for determination of OM sources as algae are the predominant producers of C_{27} sterols whereas C_{29} sterols are more typically associated with land plants (Volkman and Maxwell, 1986). Hence, the positive correlation between $\delta^{13}C_{org}$ values and C_{27}/C_{29} ratios indicate an influence of local OM sources (i.e., variations of marine versus terrestrial sources) on the measured organic C-isotope signal and cast doubt on a dominant influence of global perturbations (Fig. 10.7).

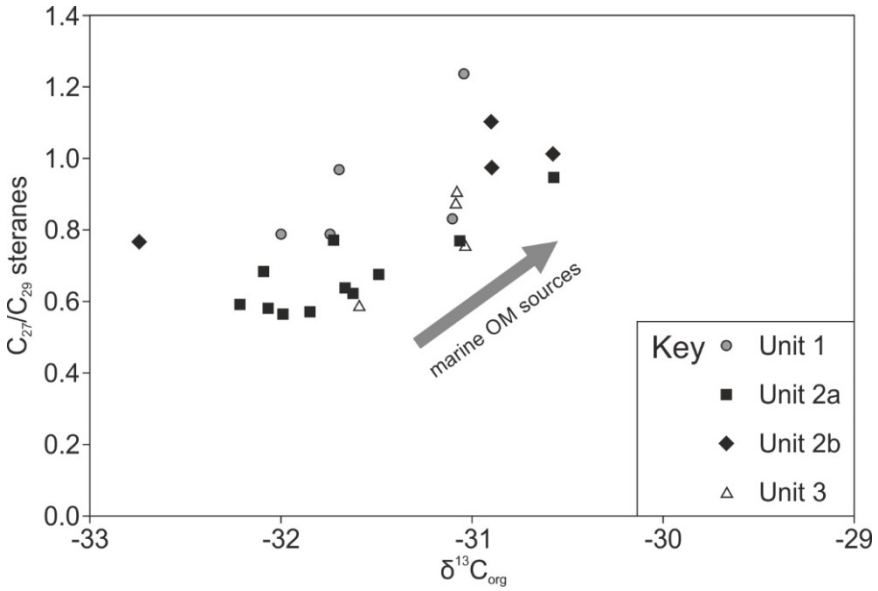

Fig. 10.7: The plot of $\delta^{13}C_{org}$ values versus C_{27}/C_{29} ratios indicate that the organic C-isotope signal of Bächental bituminous marls was influenced by variations of local OM sources.

Summing up, both the chemostratigraphic interpretation of the study section and the correlation of the Bächental section with several Lower Toarcian deposits on the basis of stable isotope data published by Suan et al. (2016) and using the dataset of Neumeister et al. (2015) has to be revised. Hence, the interpretation of the latter, suggesting that the inorganic C-isotope profile of the Bächental section do not show the typical early Toarcian negative CIE, is still valid. Although the organic C-isotope signal of Bächental bituminous marls is characterized by low values similar to deposits corresponding to the time interval of the T-OAE and probably also reflects global variations (global injection of ^{12}C-enriched carbon in all exchangeable reservoirs – Hesselbo et al. 2000, 2007), it obviously was mainly controlled by regional factors (i.e., variations in OM sources). Thus, both the organic and inorganic carbon isotope profiles of the Bächental section cannot be used for widespread stratigraphic correlations.

10.3 References

Al-Suwaidi, A.H., Angelozzi, G.N., Baudin, F., Damborenea, S.E., Hesselbo, S.P., Jenkyns, H.C., Manceñido, M.O., Riccardi, A.C. (2010). First record of the Early Toarcian Oceanic Anoxic Event from the Southern Hemisphere, Neuquén Basin, Argentina. Journal of the Geological Society, London 167, 633-636.

Bécaud, M. (2006). Les Harpoceratinae, Hildoceratinae et Paroniceratinae du Toarcien de la Vendée et des Deux-Sèvres (France). Documents des laboratoires de Géologie de Lyon. U.F.R. des Sciences de la Terre – Université Claude Bernard Lyon 1 Lyon, p. 245.

Bown, P. R. (1987). Taxonomy, evolution, and biostratigraphy of the late Triassic–early Jurassic calcareous nannofossils. The Palaeontological Association, London.

Caruthers, A.H., Gröcke, D.R., Smith, P.L. (2011). The significance of an Early Jurassic (Toarcian) carbon-isotope excursion in Haida Gwaii (Queen Charlotte Islands), British Columbia, Canada. Earth and Planetary Science Letters 307, 19-26.

Ebli, O., Vetö, I., Lobitzer, H., Sajgò, C., Demény, A., Hetényi, M. (1998). Primary productivity and early diagenesis in the Toarcian Tethys on the example of the Mn rich black shales of the Sachrang Formation, Northern Calcareous Alps. Organic Geochemistry 29, 1635-47.

Elmi, S., Rulleau, L., Gabilly, J., Mouterde, R. (1997). Toarcien. In: Cariou, E., Hantzpergue, P. (Eds.), Biostratigraphie du Jurassique ouest-européen et méditerranéen: zonations parallèles et distribution des invertébrès et microfossiles. Bulletin des centres de recherches Exploration- production Elf-Aquitaine, Mémoire 17, Pau, France, 25–36.

Frimmel, A., Oschmann, W., Schwark, L. (2004). Chemostratigraphy of the Posidonia Shale, SW Germany I. Influence of sea-level variation on organic facies evolution. Chemical Geology 206, 199-230.

Gröcke, D.R., Hori, R.S., Trabucho-Alexandre, J., Kemp, D.B., Schwark, L. (2011). An open ocean record of the Toarcian oceanic anoxic event. Solid Earth 2, 245-57.

Haq, B.U., Hardenbol, J., Vail, P.R. (1988). Mesozoic and Cenozoic chronostratigraphy and cycles of sea-level change. In: Wilgus, C.K., Hastings, B.S., Posamentier, H., Wagoner, J.V., Ross, C.A., Kendall, C.G.S.C. (Eds.), Sea-Level Changes - An Integrated Approach. SEPM Special Publications 42, pp. 71-108.

Hesselbo, S.P., Gröcke, D.R., Jenkyns, H.C., Bjerrum, C.J., Farrimond, P., Morgans Bell, H.S., Green, O.R. (2000). Massive dissociation of gas hydrate during a Jurassic oceanic anoxic event. Nature 406, 392-395.

Hesselbo, S.P., Jenkyns, H.C., Duarte, L.V., Oliviera, L.C.V. (2007). Carbon-isotope record of the Early Jurassic (Toarcian) Oceanic Anoxic Event from fossil wood and marine carbonate (Lusitanian Basin, Portugal). Earth and Planetary Science Letters 253, 455-470.

Howarth, M.K. (1992). The Ammonite Family Hildoceratidae in the Lower Jurassic of Britain. Part 1. Monograph of the Palaeontographical Society. Palaeontographical Society, London.

Izumi, K., Miyaji, T., Tanabe, K. (2012). Early Toarcian (Early Jurassic) oceanic anoxic event recorded in the shelf deposits in the northwestern Panthalassa: Evidence from the Nishinakayama Formation in the Toyora area, west Japan. Palaeogeography, Palaeoclimatology, Palaeoecology 315-316, 100-108.

Jenkyns, H.C., Clayton, C.J. (1986). Black shales and carbon isotopes in pelagic sediments from the Tethyan Lower Jurassic. Sedimentology 33, 87-106.

Jenkyns, H. C., Geczy, B., Marshall, J. D. (1991). Jurassic manganese carbonates of central-Europe and the early Toarcian anoxic event. Journal of Geology 99, 137–149.

Jenkyns, H.C., Gröcke, D.R., Hesselbo, S.P. (2001). Nitrogen isotope evidence for water mass denitrification during the early Toarcian (Jurassic) ocean anoxic event. Paleoceanography 16, 593–603.

Jenkyns, H.C., Jones, C.E., Gröcke, D.R., Hesselbo, S.P., Parkinson, D.N. (2002). Chemostratigraphy of the Jurassic System: applications, limitations and implications for palaeoceanography. Journal of the Geological Society of London 159, 351-378.

Kafousia, N., Karakitsios, V., Mattioli, E., Kenjo, S., Jenkyns, H.C. (2014). The Toarcian Oceanic Anoxic Event in the Ionian Zone, Greece. Palaeogeography, Palaeoclimatology, Palaeoecology 393, 135-145.

Kemp, D.B., Coe, A.L., Cohen, A.S., Schwark, L. (2005). Astronomical pacing of methane release in the early Jurassic period. Nature 437, 396-399.

Klebelsberg, R.v. (1935). Geologie von Tirol. Gebr. Borntraeger, Berlin.

Kodina, L.A., Bogatecheva, M.P., Lobitzer, H. (1988). An anorganic geochemical study of Austrian bituminous rocks. Jb. Geol. B.-A. 131, 291-300, Wien.

Küspert, W. (1982). Environmental changes during oil shale deposition as deduced from stable isotope ratios. In: Einsele, G., Seilacher, A. (Eds.), Cyclic and Event Stratification. Springer, Berlin, pp. 482-501.

Küspert, W. (1983). Faziestypen des Posidonienschiefers (Toarcium, Süddeutschland): Eine isotopen-geologische, organisch-chemische und petrographische Studie. Ph.D. Thesis, Tübingen University.

Lewan, M.D. (1986). Stable carbon isotopes of amorphous kerogens from Phanerozoic sedimentary rocks. Geochim. Cosmochim. Acta 50, 1583-1591.

Mattioli, E., Pittet, B., Suan, G., Mailliot, S. (2008). Calcareous nannoplankton changes across the early Toarcian oceanic anoxic event in the Western Tethys. Paleoceanography 23, PA3208.

Mazzini, A., Svensen, H., Leanza, H.A., Corfu, F., Planke, S. (2010). Early Jurassic shale chemostratigraphy and U–Pb ages from the Neuquén Basin (Argentina): implications for the Toarcian Oceanic Anoxic Event. Earth Planet. Sci. Lett. 297, 633–645.

McElwain, J.C., Murphy, J.W., Hesselbo, S.P. (2005). Changes in carbon dioxide during an oceanic anoxic event linked to intrusion of Gondwana coals. Nature 435, 479-483.

Neumeister, S., Gratzer, R., Algeo, T.J., Bechtel, A., Gawlick, H.-J., Newton, R.J., Sachsenhofer, R.F. (2015). Oceanic response to Pliensbachian and Toarcian magmatic events: Implications from an organic-rich basinal succession in the NW Tethys. Global and Planetary Change 126, 62-83.

Neumeister, S., Algeo, T.J., Bechtel, A., Gawlick, H.-J., Gratzer, R., Sachsenhofer, R.F. (2016). Redox conditions and depositional environment of the Lower Jurassic Bächental bituminous marls (Tyrol, Austria). Austrian Journal of Earth Sciences.

Neumeister, S., Algeo, T.J., Gawlick, H.-J., Gratzer, R., Sachsenhofer, R.F. (2016). Diagenesis of organic-rich marls under shifting suboxic to euxinic conditions. Submitted for publication in the International Journal of Earth Sciences.

Pálfy, J., Smith, P.L. (2000). Synchrony between Early Jurassic extinction, oceanic anoxic event, and the Karoo–Ferrar flood basalt volcanism. Geology 28, 747-750.

Page, K.N. (2004). A sequence of biohorizons for the subboreal province Lower Toarcian in Northern Britain and their correlation with a submediterranean standard. Riv. Ital. Paleontol. Stratigr. 110, 109–114.

Röhl, H.J., Schmid-Röhl, A., Oschmann, W., Frimmel, A., Schwark, L. (2001). The Posidonia Shale (Lower Toarcian) of SW-Germany: an oxygen-depleted ecosystem controlled by sea level and palaeoclimate. Palaeogeography, Palaeoclimatology, Palaeoecology 165, 27-52.

Sabatino, N., Neri, R., Bellanca, A., Jenkyns, H.C., Baudin, F., Parisi, G., Masetti, D. (2009). Carbon-isotope records of the Early Jurassic (Toarcian) Oceanic Anoxic Event from the Valdorbia (Umbria-Marche Apennines) and Monte Mangart (Julian Alps) sections: palaeoceanographic and stratigraphic implications. Sedimentology 56, 1307-1328.

Sabatino, N., Neri, R., Bellanca, A., Jenkyns, H. C., Masetti, D., Scopelliti, G. (2011). Petrography and high-resolution geochemical records of Lower Jurassic manganese-rich deposits from Monte Mangart, Julian Alps. Palaeogeography, Palaeoclimatology, Palaeoecology 299, 97–109.

Sabatino, N., Vlahović, I., Jenkyns, H.C., Scopelliti, G., Neri, R., Prtoljan, B., Velić, I. (2013). Carbon-isotope record and palaeoenvironmental changes during the early Toarcian oceanic anoxic event in shallow-marine carbonates of the Adriatic Carbonate Platform in Croatia. Geological Magazine 150, Issue 6, 1085-1102.

Sell, B., Ovtcharova, M., Guex, J., Bartolini, A., Jourdan, F., Spangenberg, J.E., Vicente, J.-C., Schaltegger, U. (2014). Evaluating the temporal link between the Karoo LIP and climatic-biologic events of the Toarcian Stage with high-precision U-Pb geochronology. Earth and Planetary Science Letters 408, 48-56.

Suan, G., Nikitenko, B. L., Rogov, M. A., Baudin, F., Spangenberg, J. E., Knyazev, V. G., Glinskikh, L. A., Goryacheva, A. A., Adatte, T., Riding, J. B., Föllmi, K. B., Pittet, B., Mattioli, E., Lécuyer, C. (2011). Polar record of Early Jurassic massive carbon injection. Earth and Planetary Science Letters 312, 102–113.

Suan, G., van de Schootbrugge, B., Adatte, T., Fiebig, J., Oschmann, W. (2015). Calibrating the magnitude of the Toarcian carbon cycle perturbation. Paleoceanography 30, 495–509.

Suan, G., Schlögl, J., Mattioli, E. (2016). Bio- and chemostratigraphy of the Toarcian organic-rich depsits of some key successions of the Alpine Tethys. Newsletters on Stratigraphy, published online in February 2016.

Svensen, H., Planke, S., Chevalier, L., Malthe-Sørensen, A., Corfu, F., Jamveit, B. (2007). Hydrothermal venting of greenhouse gases triggering Early Jurassic global warming. Earth and Planetary Science Letters 256, 554-566.

Tyson, R.V. (1995). Sedimentary Organic Matter - Organic Facies and Palynofacies. Chapman and Hall, London.

Volkman, J.K., Maxwell, J.R. (1986). Acyclic isoprenoids as biological markers. In: Johns, R.B. (Eds.), Biological Markers in the Sedimentary Record. Elsevier, Amsterdam, pp. 1-42.

APPENDIX

11.1 Photographs of the Bächental section

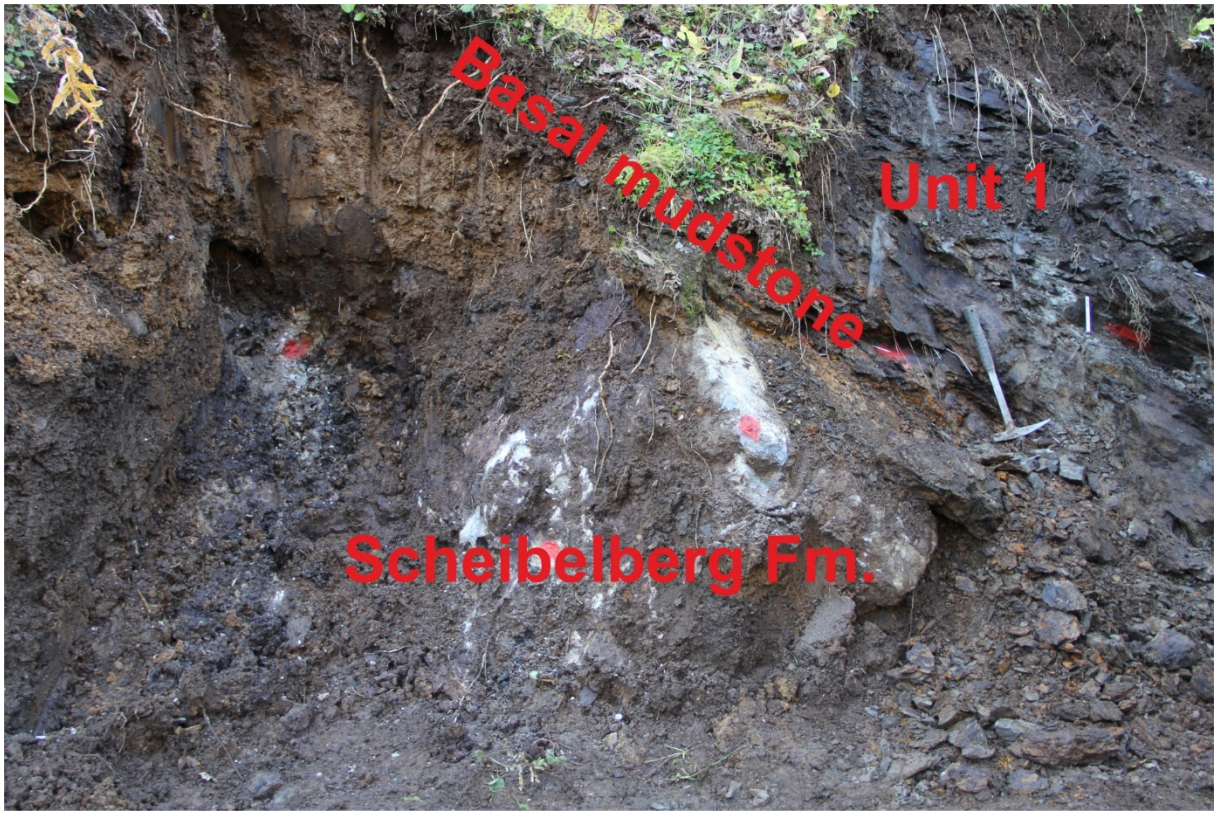

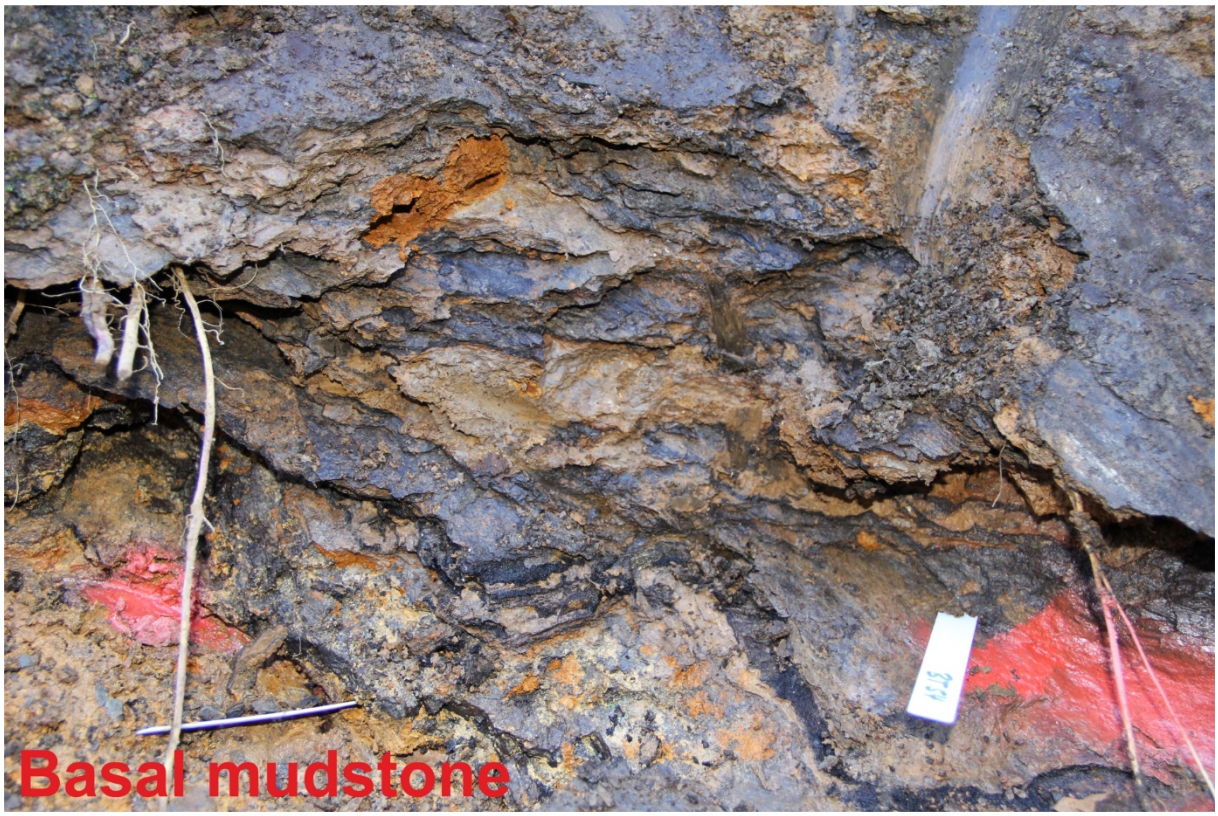
Basal mudstone

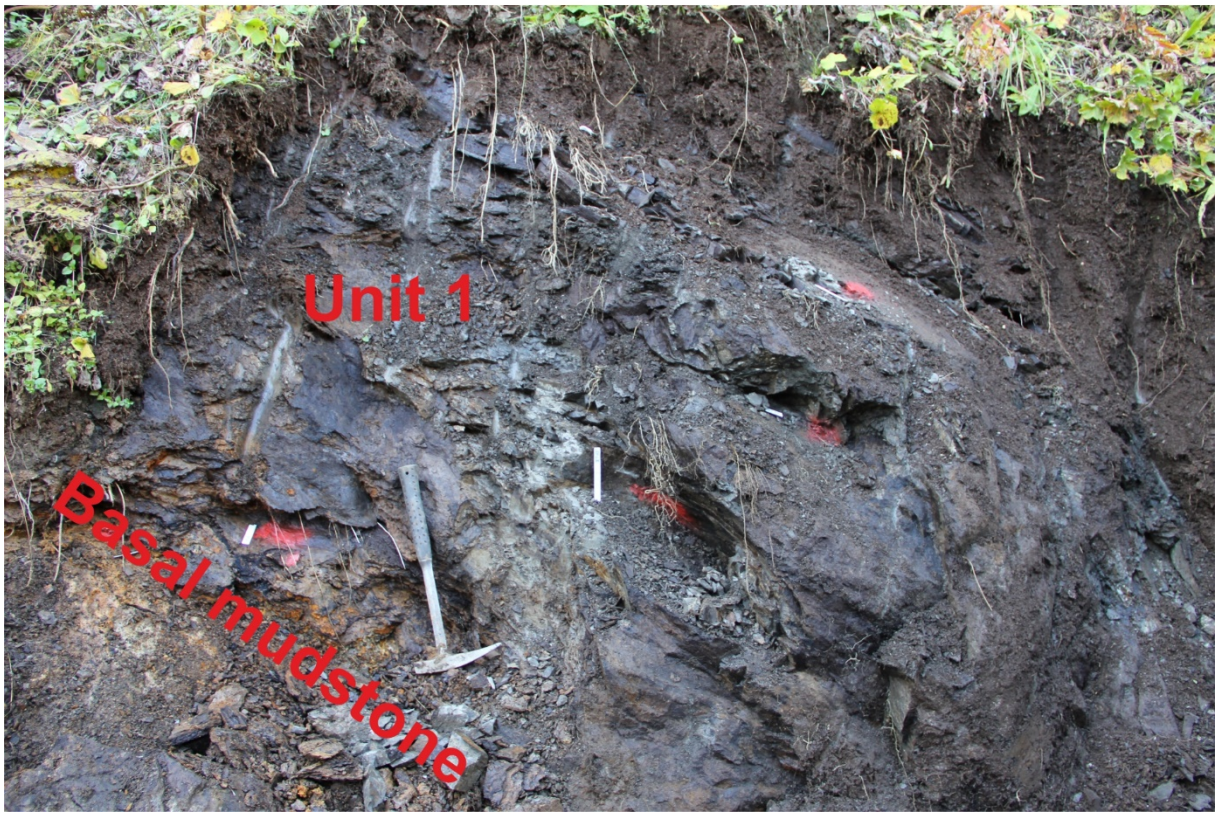
Unit 1
Basal mudstone


Debrite
Unit 3
Unit 2
Unit 1
900


Unit 3
Debrite
Unit 2
900


Debrite
Unit 2
Unit 3

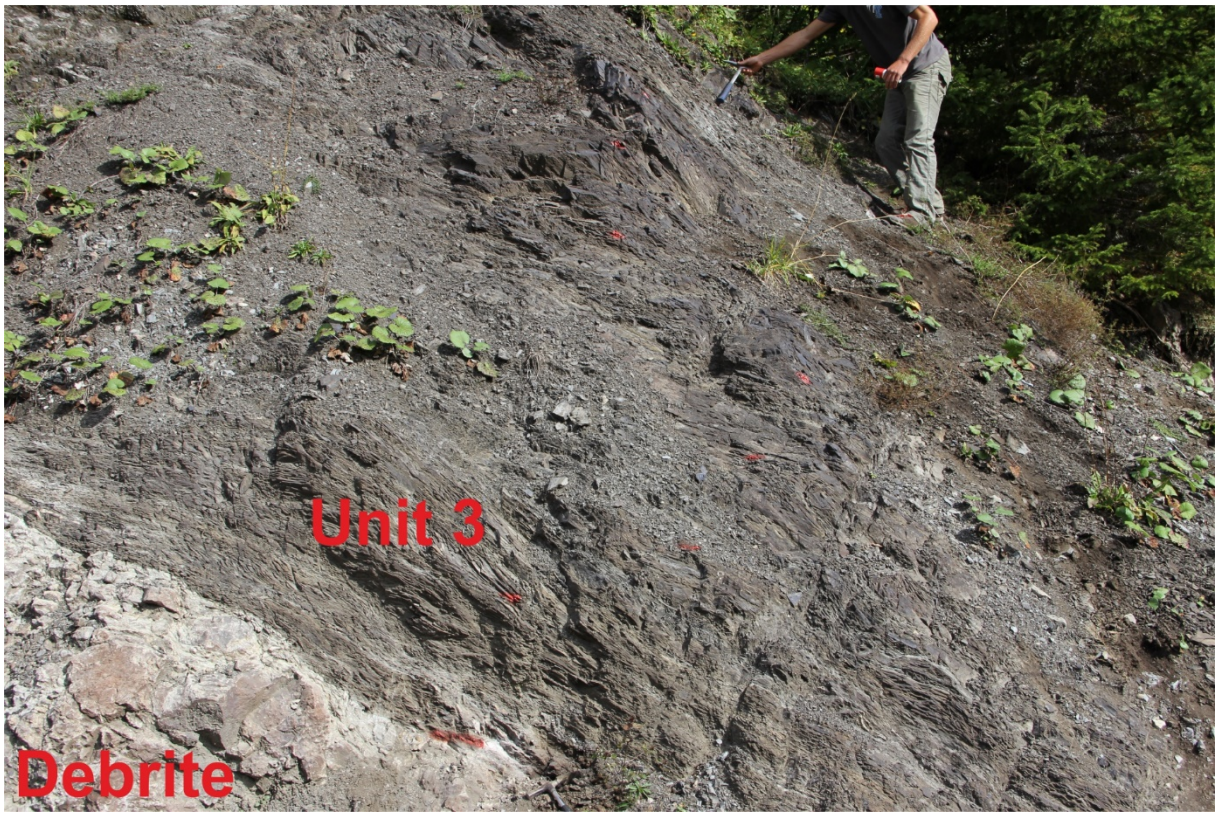
Unit 3
Debrite


Unit 3
Covered
Upper Allgäu Fm.


Covered
Upper Allgäu Fm.


Digging a trench for sampling

11.2 Selected photographs of thin sections (Scale: 0.5 mm)

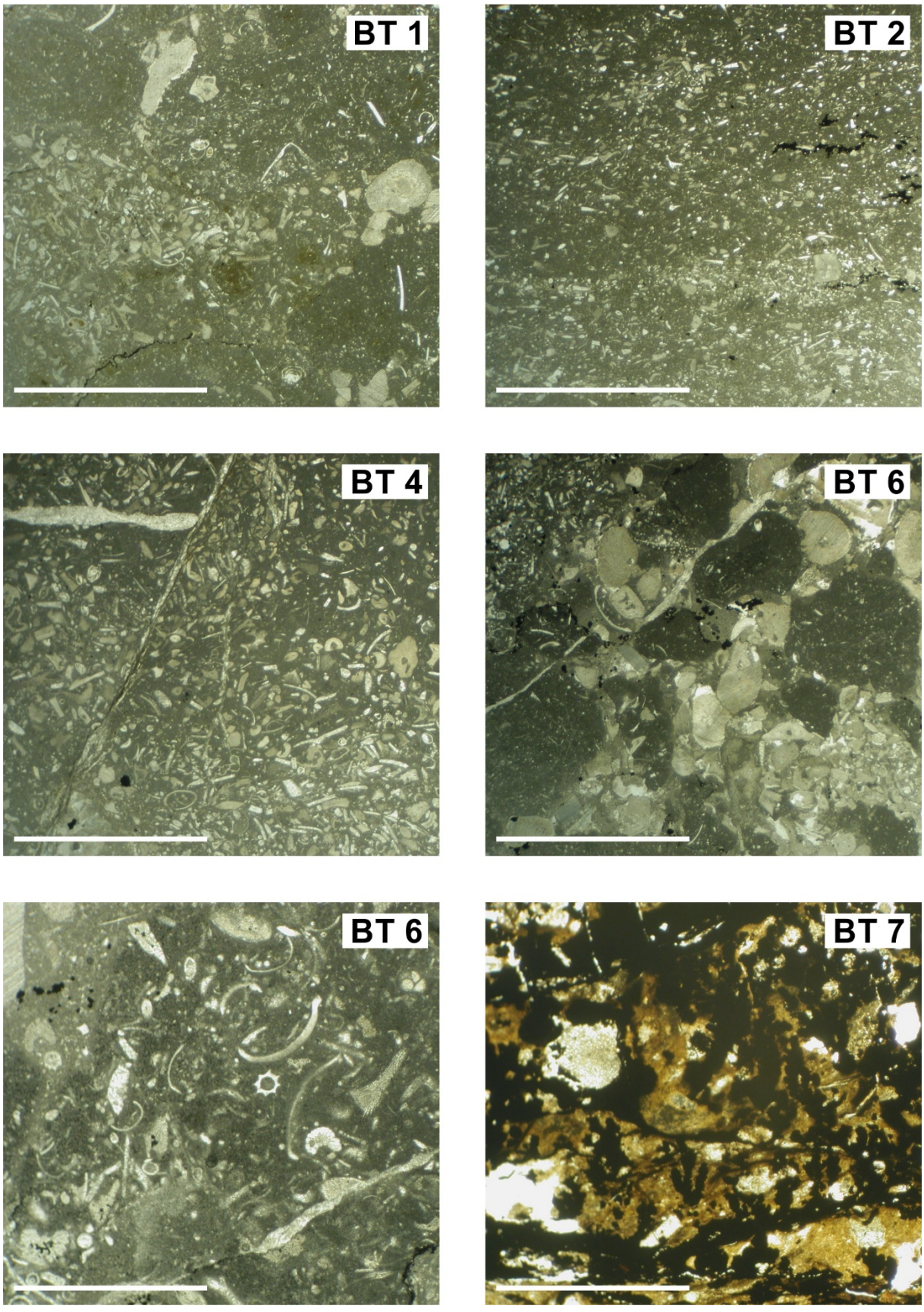

Scheibelberg Formation: samples BT 1, BT 2, BT 4, and BT 6; basal mudstone: sample BT 7.

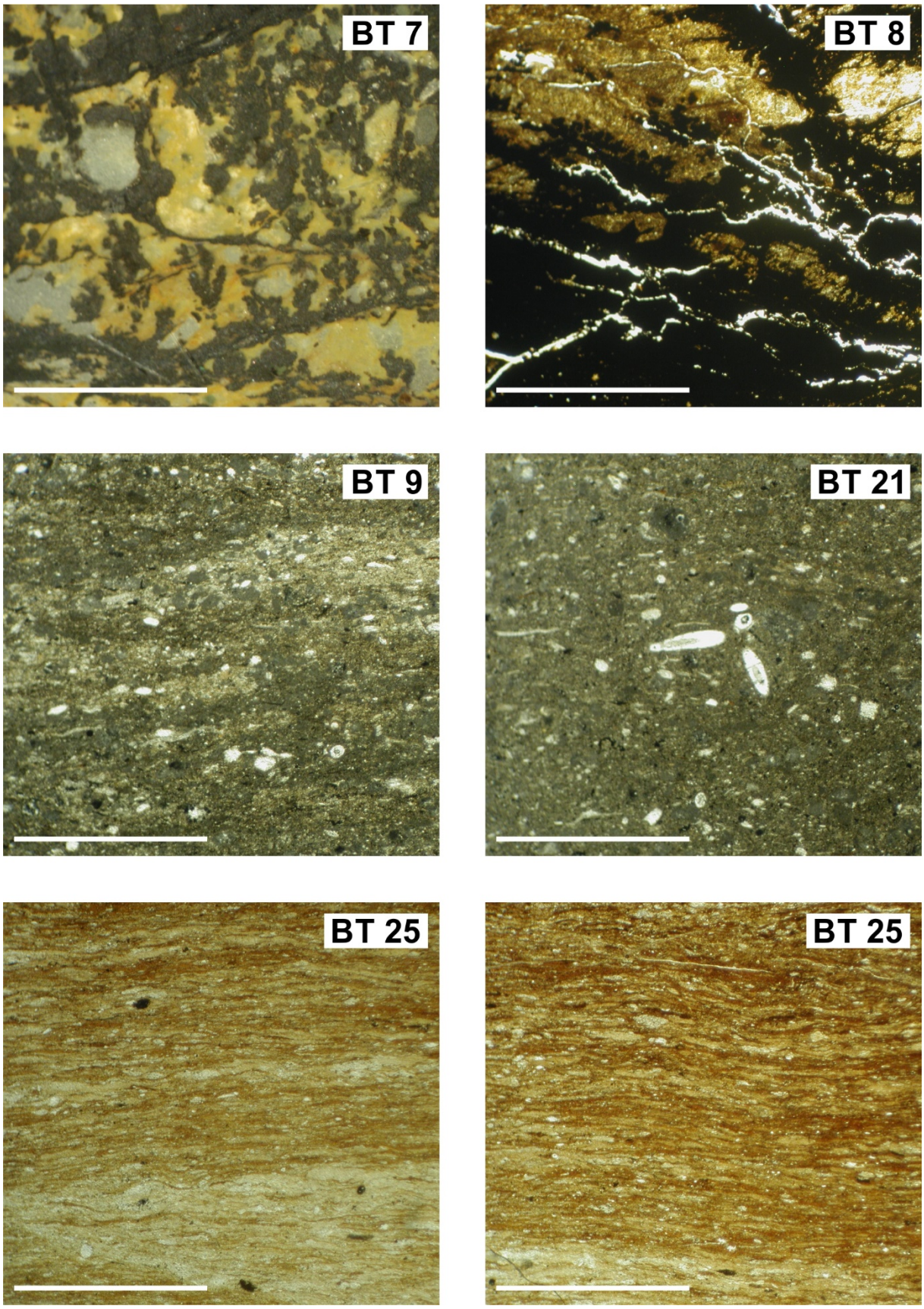

Basal mudstone: samples BT 7 and BT 8; Unit 1: samples BT 9 and BT 21; Subunit 2a: sample BT 25.

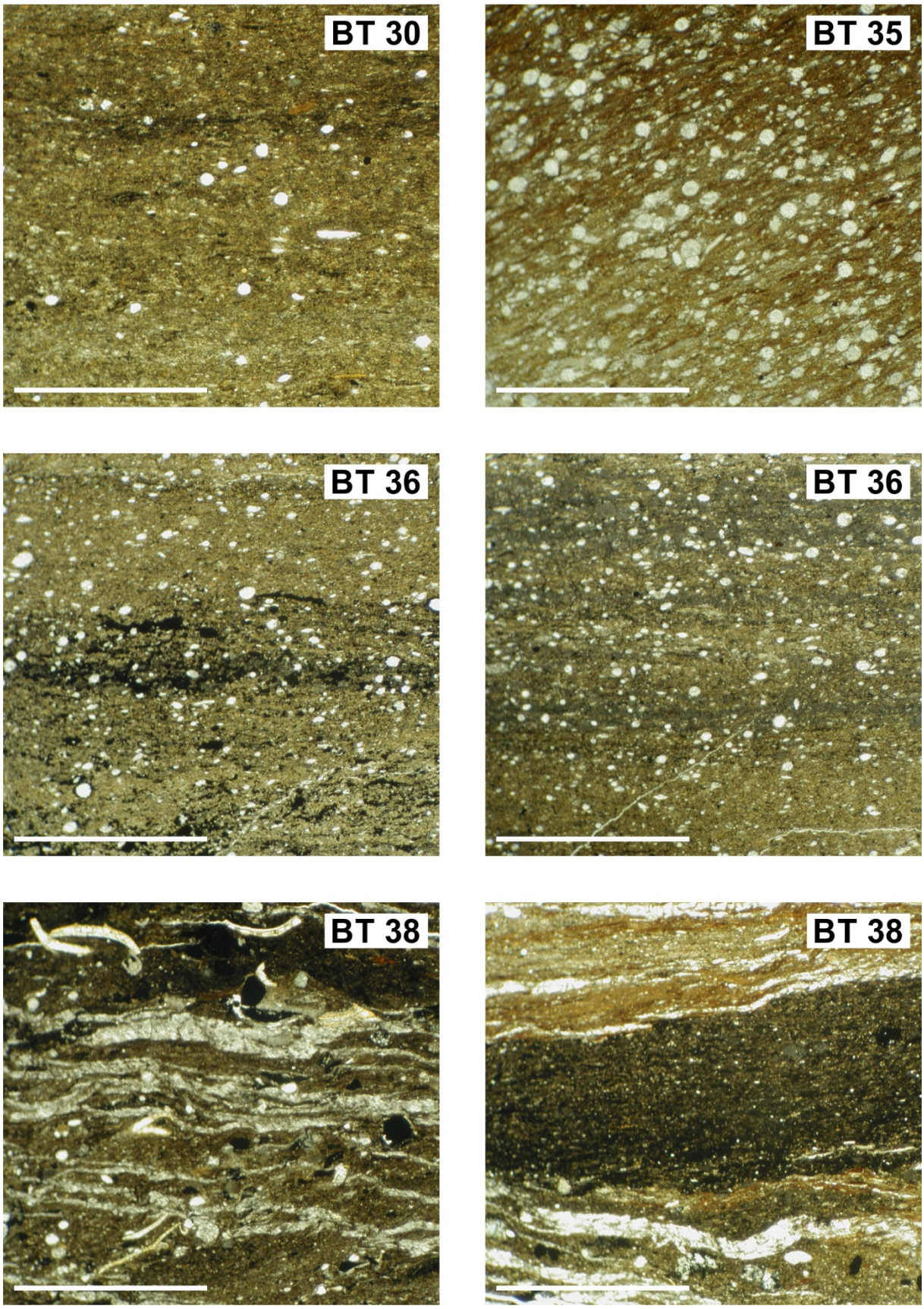

Subunit 2a: samples BT 30 and BT 35; Subunit 2b: samples BT 36 and BT 38.

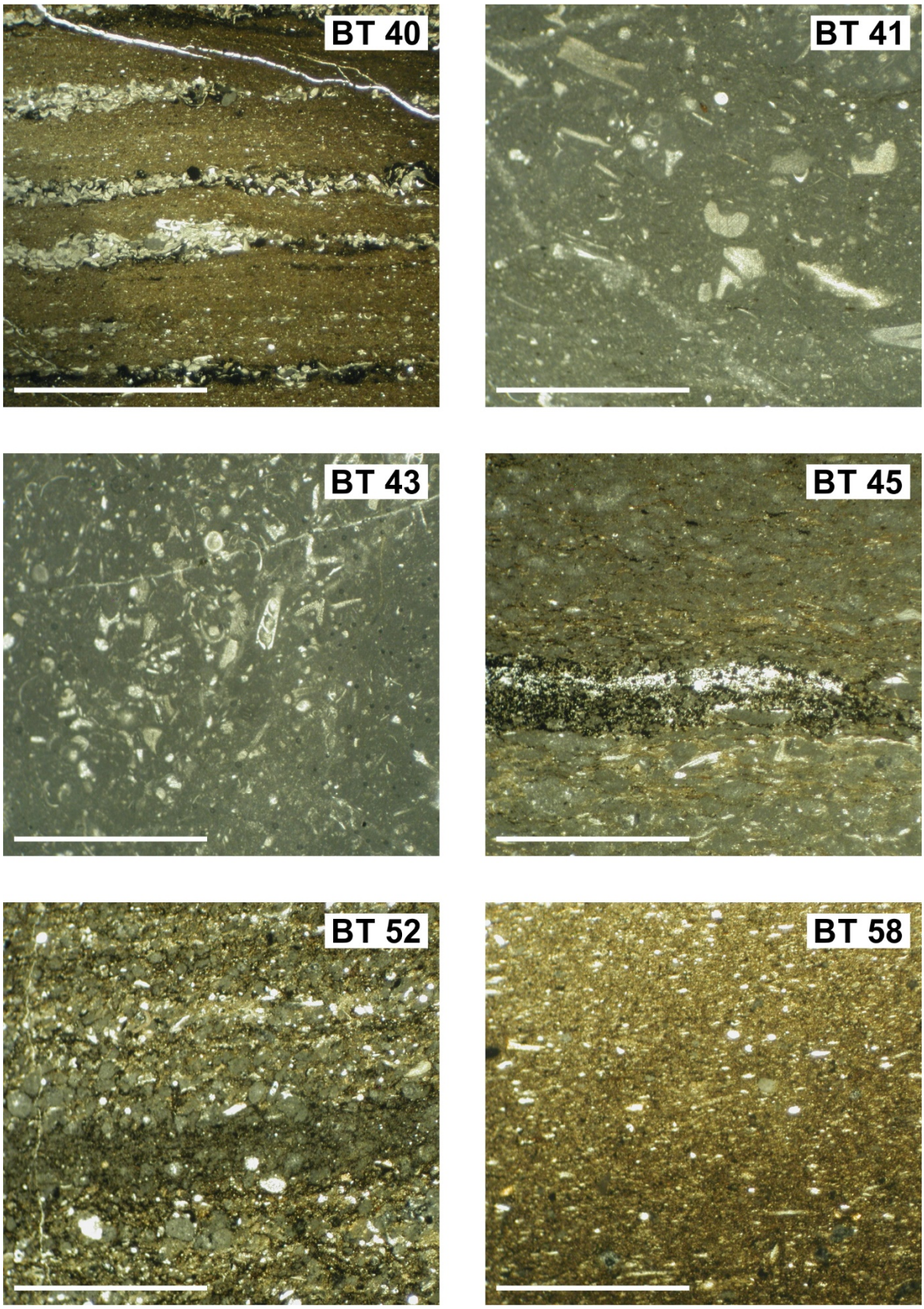

Subunit 2b: sample BT 40; Debrite: samples BT 41 and BT 43; Unit 3: samples BT 45, BT 52, and BT 58.

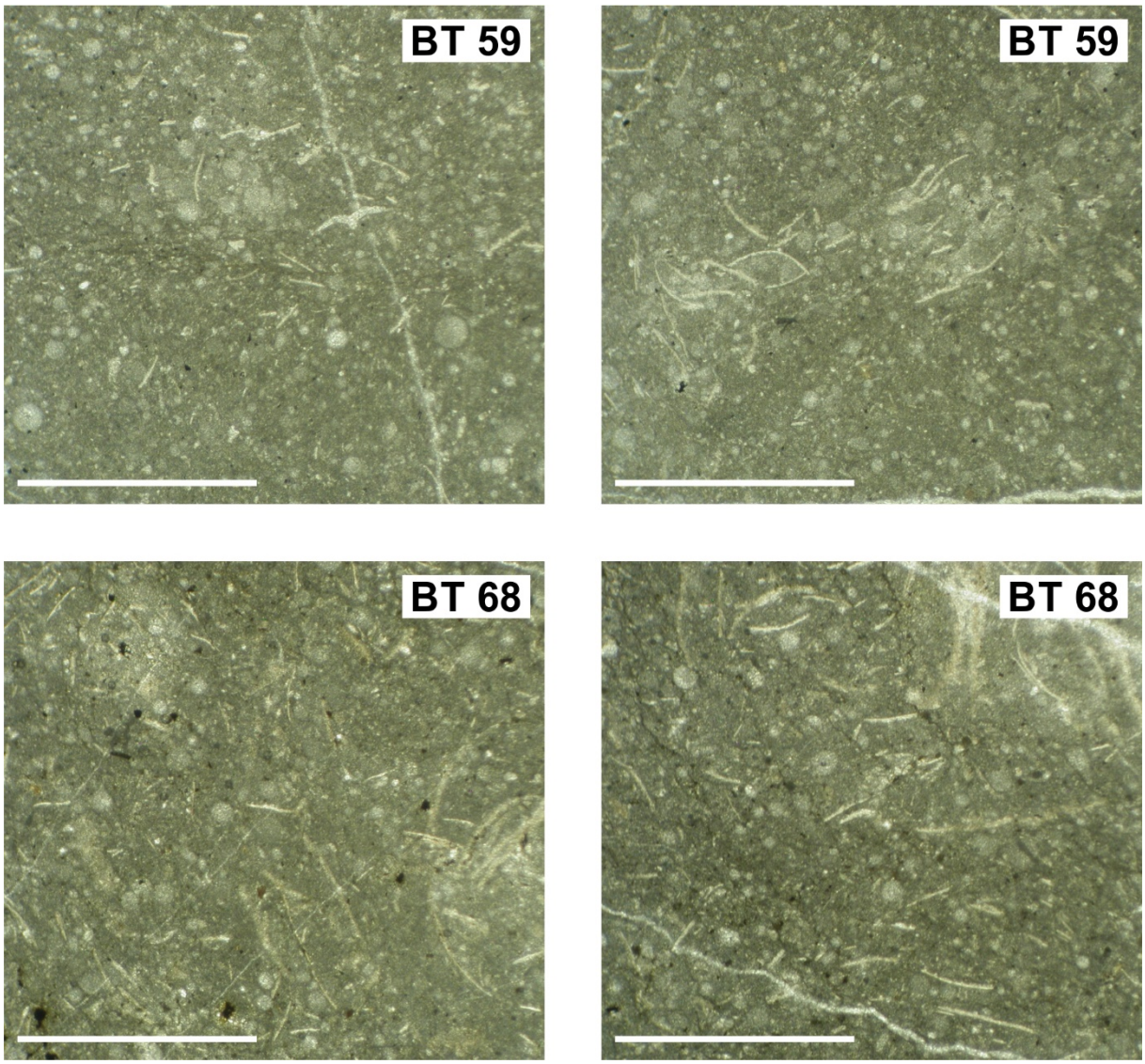

Upper Allgäu Formation: samples BT 59 and BT 68.

11.3 X-ray diffractograms of bituminous marl samples

Unit 1: samples BT 9 to BT 21; Subunit 2a: samples BT 22 to BT 35; Subunit 2b: samples BT 36 to BT 40; Unit 3: samples BT 44 to BT 58. Light grey rectangles mark the peak areas of detrital calcite, Mn-bearing calcite, kutnohorite, dolomite, Mn-bearing siderite, and pyrite in the samples. Also shown are the positions of the standard peaks of (1) calcite, (2) kutnohorite, (3) dolomite, (4) rhodochrosite, and (5) siderite. Note that relative intensities of the individual chromatograms are not adjusted to a common scale.

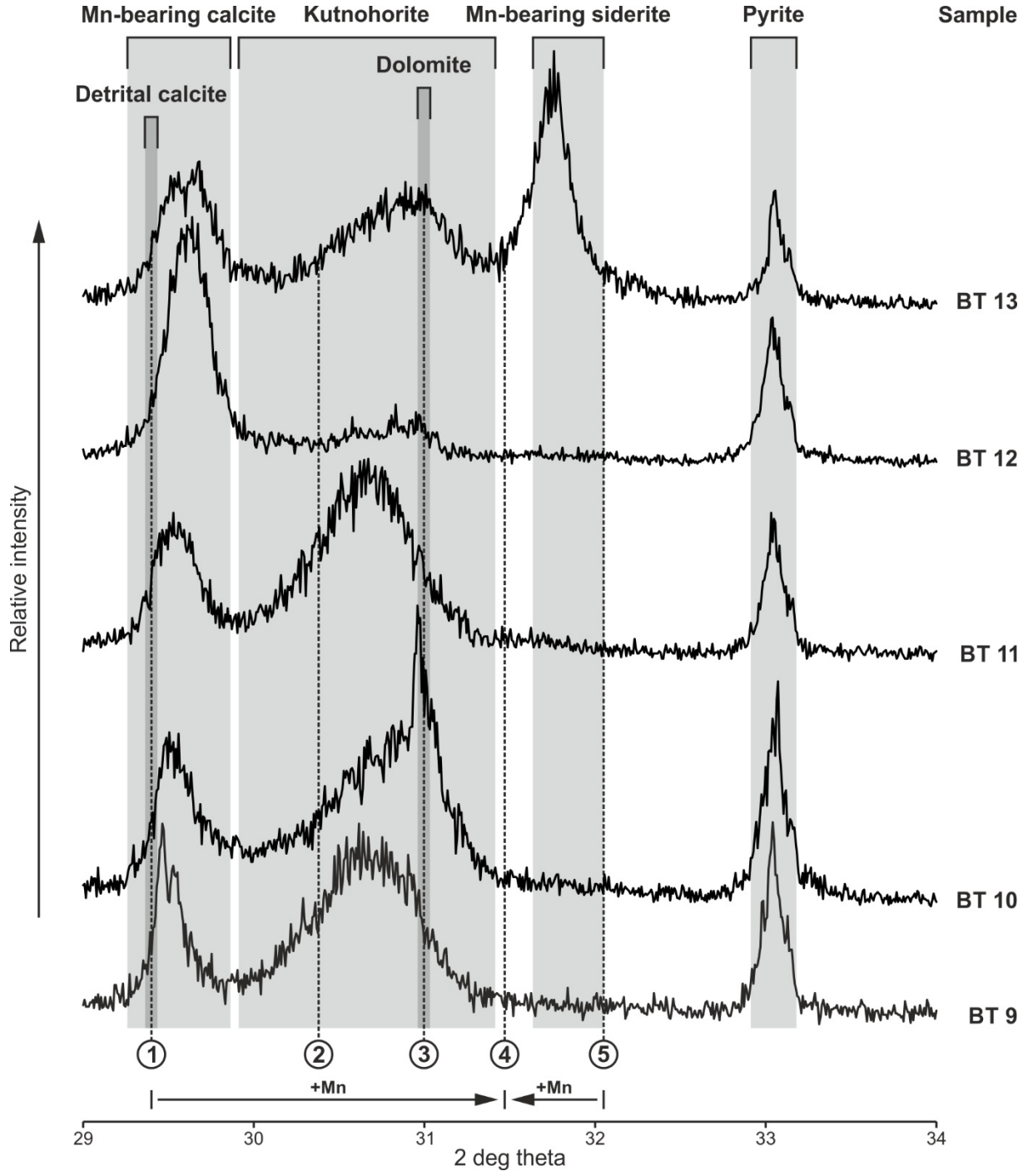

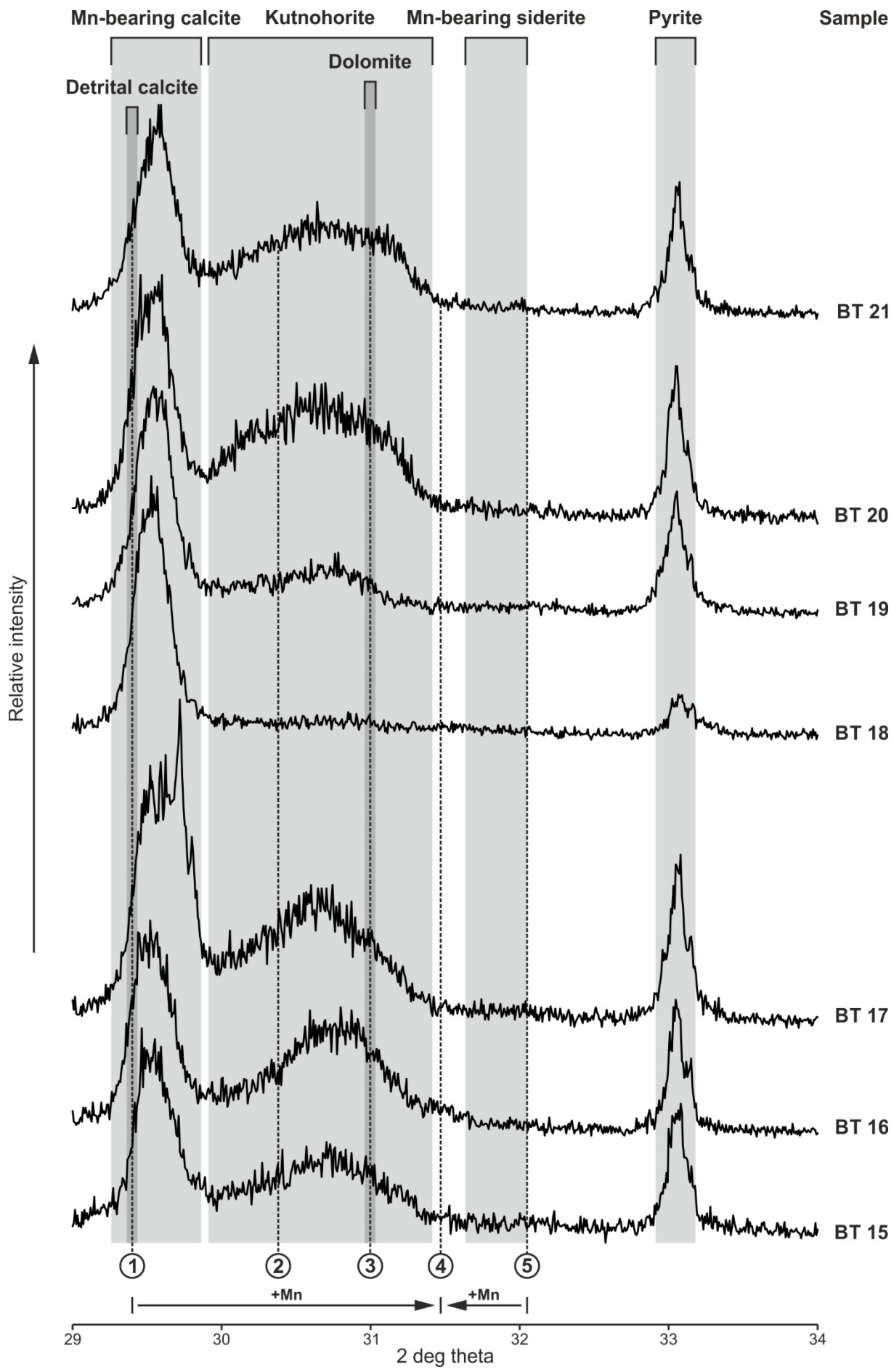
Mn-bearing calcite
Kutnohorite
Mn-bearing siderite
Pyrite
Sample
Dolomite
Detrital calcite
BT 21
BT 20
BT 19
BT 18
BT 17
BT 16
BT 15
Relative intensity
1
2
3
4
5
+Mn
+Mn
29
30
31
32
33
34
2 deg theta

[203]

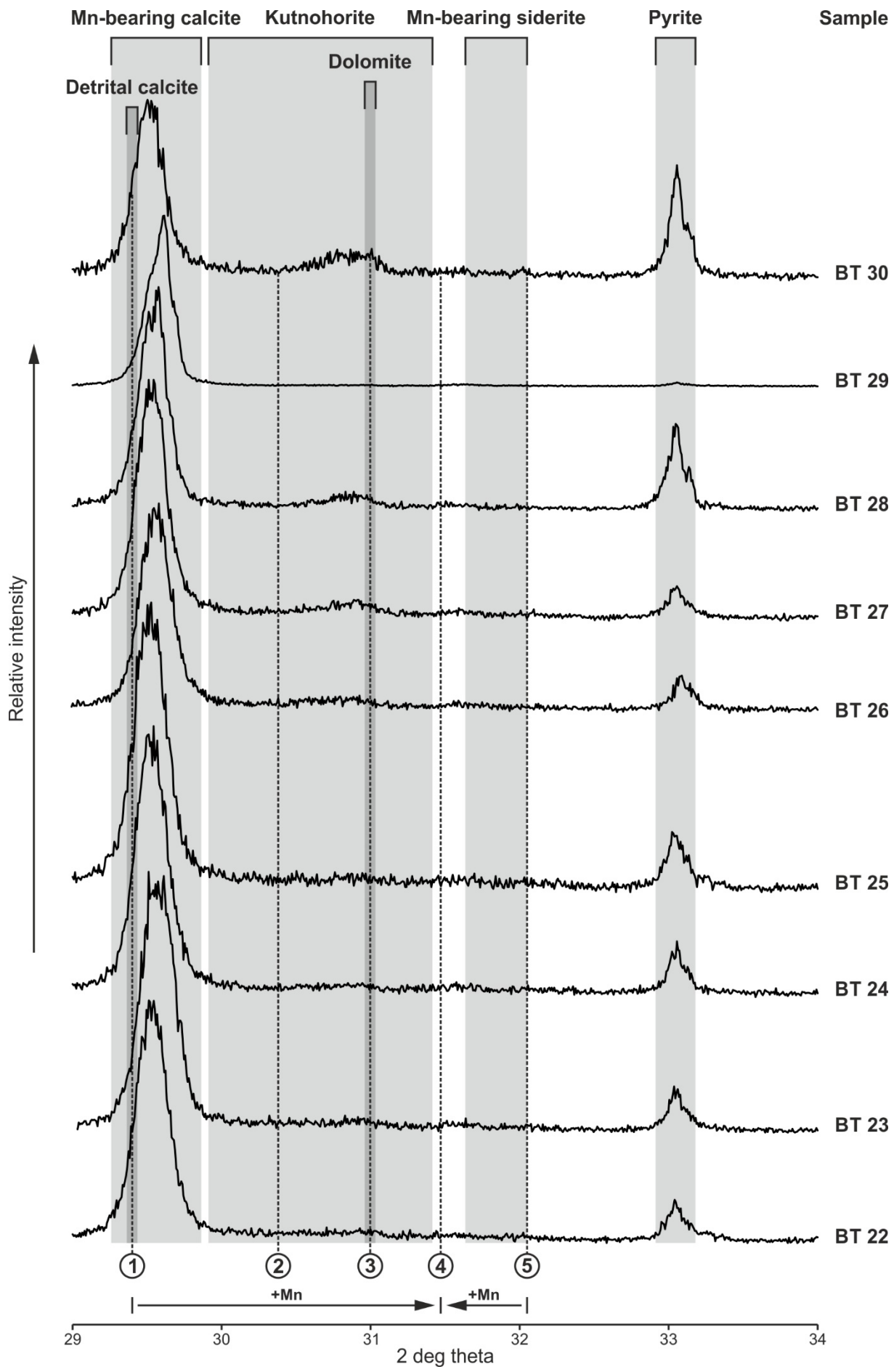
Mn-bearing calcite
Kutnohorite
Mn-bearing siderite
Pyrite
Sample
Dolomite
Detrital calcite
BT 30
BT 29
BT 28
BT 27
BT 26
BT 25
BT 24
BT 23
BT 22
Relative intensity
1
2
3
4
5
+Mn
+Mn
29
30
31
32
33
34
2 deg theta

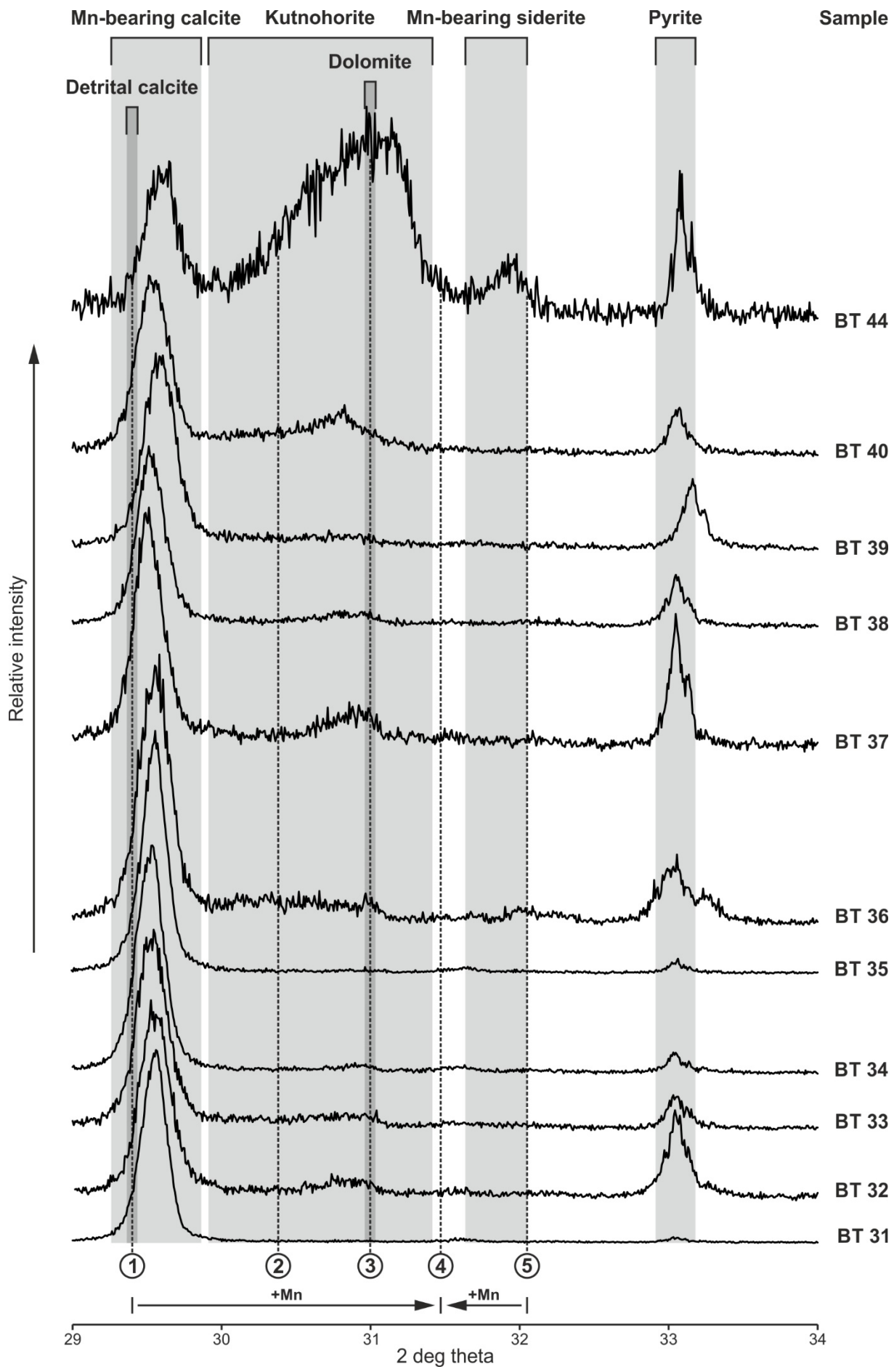
Mn-bearing calcite
Kutnohorite
Mn-bearing siderite
Pyrite
Sample
Dolomite
Detrital calcite
BT 44
BT 40
BT 39
BT 38
BT 37
BT 36
BT 35
BT 34
BT 33
BT 32
BT 31
Relative intensity
1
2
3
4
5
+Mn
+Mn
29
30
31
32
33
34
2 deg theta

[205]

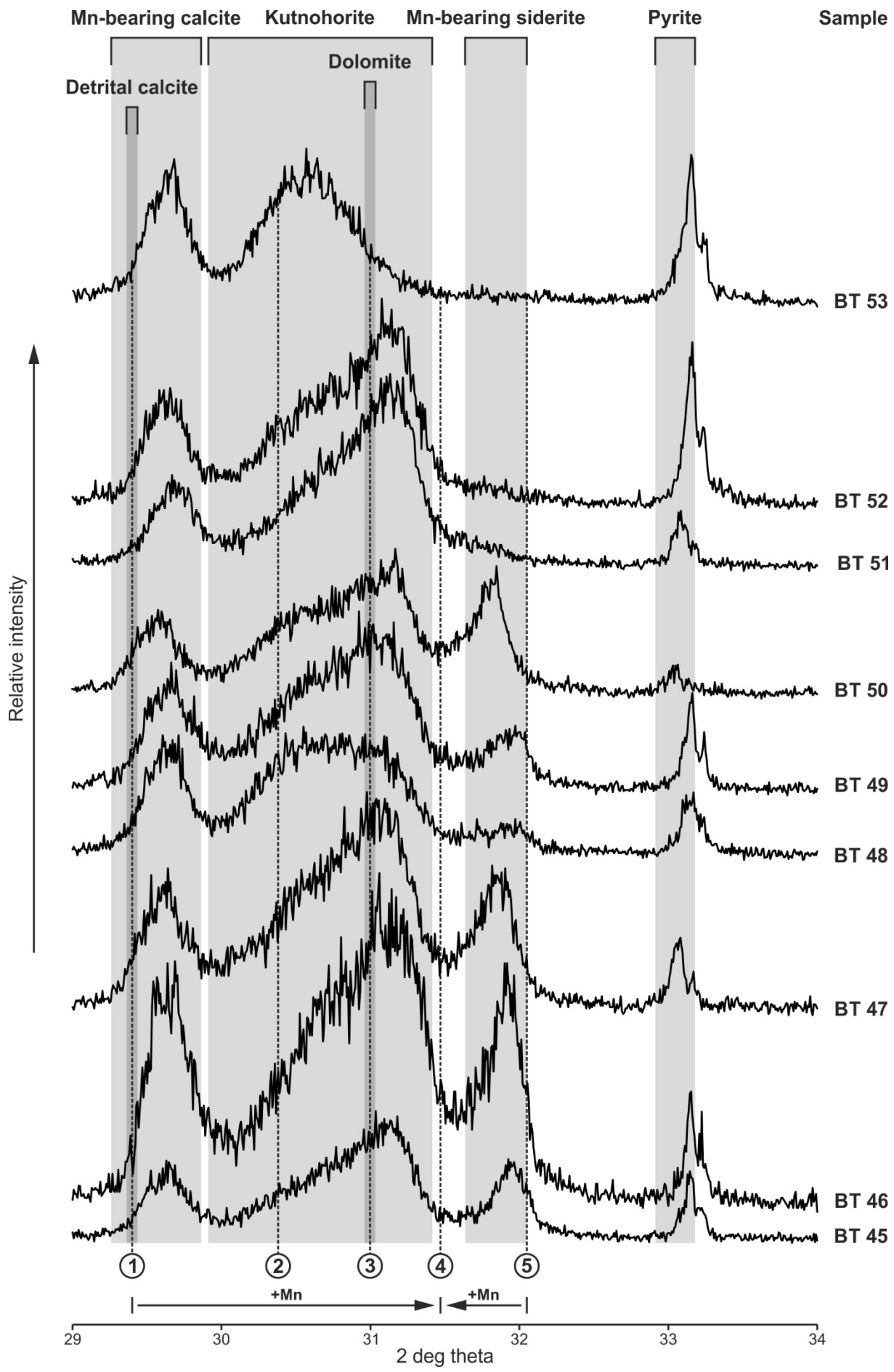
Mn-bearing calcite
Kutnohorite
Mn-bearing siderite
Pyrite
Sample
Dolomite
Detrital calcite
BT 53
BT 52
BT 51
BT 50
BT 49
BT 48
BT 47
BT 46
BT 45
Relative intensity
1
2
3
4
5
+Mn
+Mn
29
30
31
32
33
34
2 deg theta

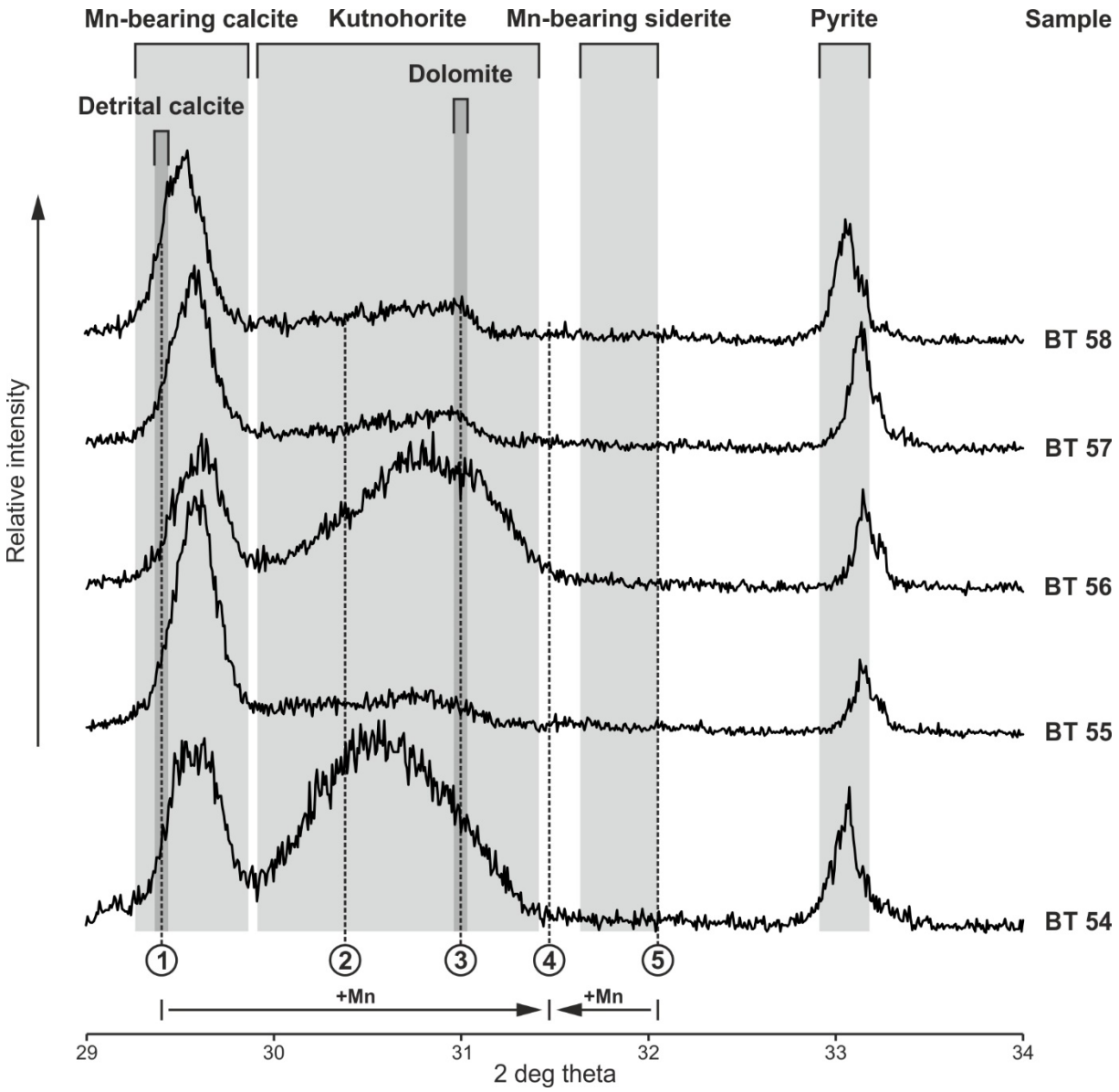

11.4 Chromatograms of saturated hydrocarbon fractions of bituminous marl samples

Total ion current gas chromatograms, partial mass chromatograms of steranes (m/z 217), and partial mass chromatograms of hopanes (m/z 191). Unit 1: samples BT 9 to BT 21; Subunit 2a: samples BT 22 to BT 35; Subunit 2b: samples BT 36 to BT 40; Unit 3: samples BT 44 to BT 58.

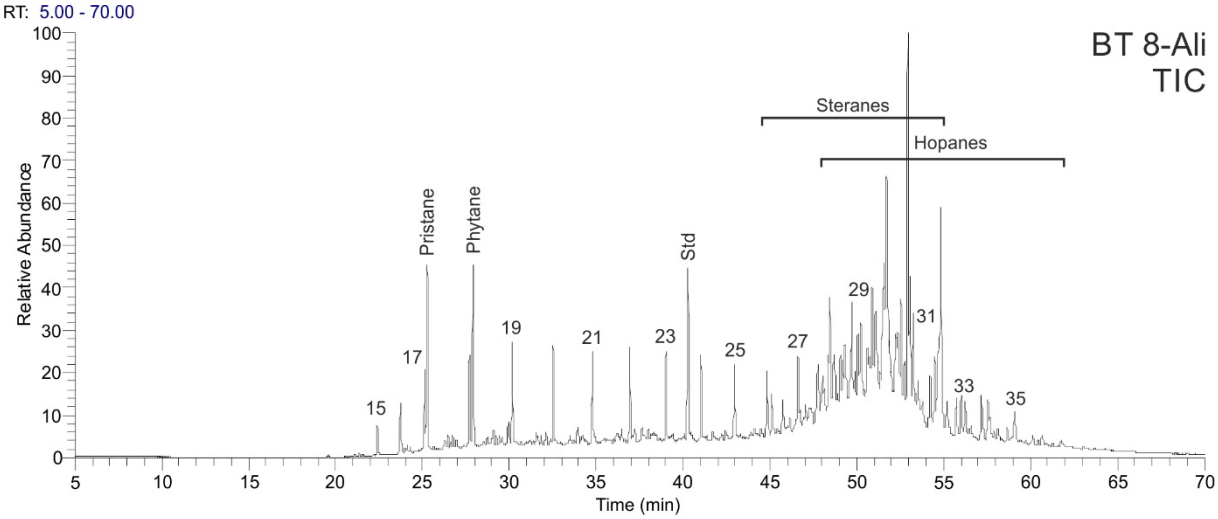
RT: 5.00 - 70.00
BT 8-Ali
TIC
Steranes
Hopanes
Pristane
Phytane
Std
15
17
19
21
23
25
27
29
31
33
35
Relative Abundance
Time (min)

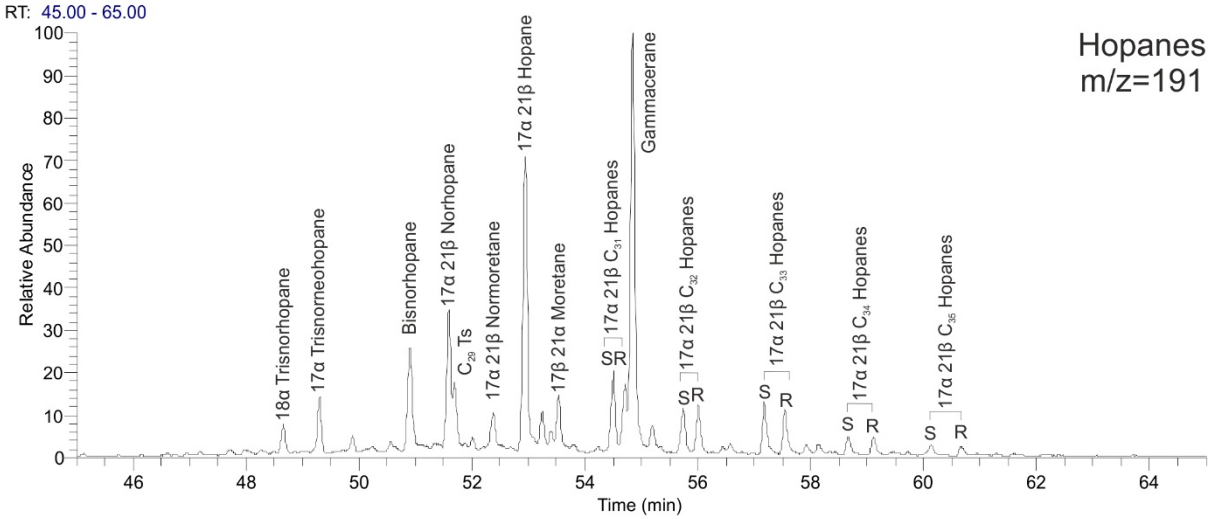
RT: 45.00 - 65.00
Hopanes
m/z=191
18α Trisnorhopane
17α Trisnorneohopane
Bisnorhopane
17α 21β Norhopane
C29 Ts
17α 21β Normoretane
17α 21β Hopane
17β 21α Moretane
17α 21β C31 Hopanes
SR
Gammacerane
17α 21β C32 Hopanes
SR
17α 21β C33 Hopanes
S R
17α 21β C34 Hopanes
S R
17α 21β C35 Hopanes
S R
Relative Abundance
Time (min)

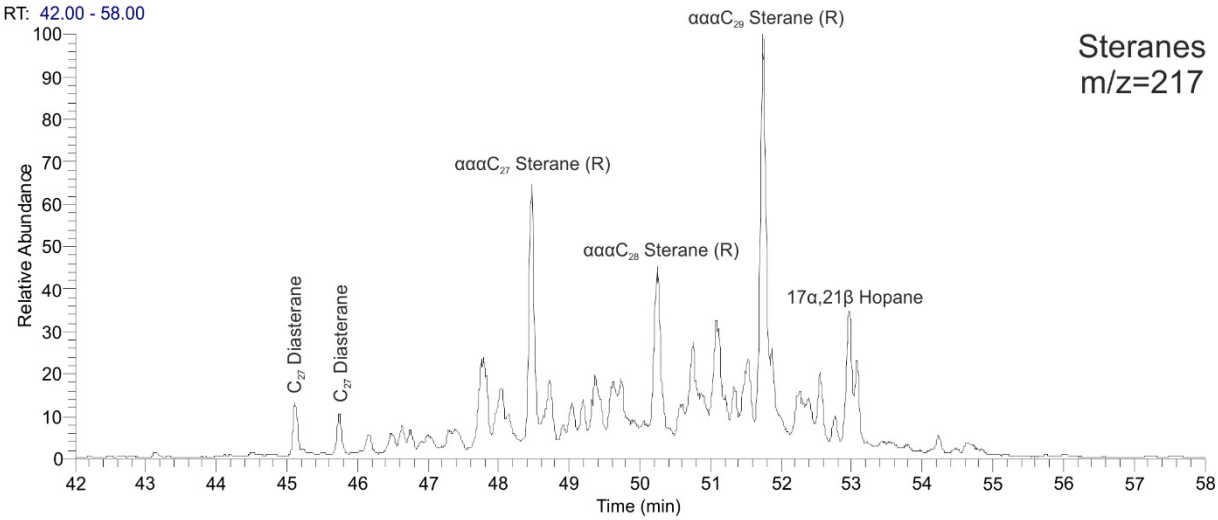
RT: 42.00 - 58.00
αααC29 Sterane (R)
Steranes
m/z=217
αααC27 Sterane (R)
αααC28 Sterane (R)
17α,21β Hopane
C27 Diasterane
C27 Diasterane
Relative Abundance
Time (min)

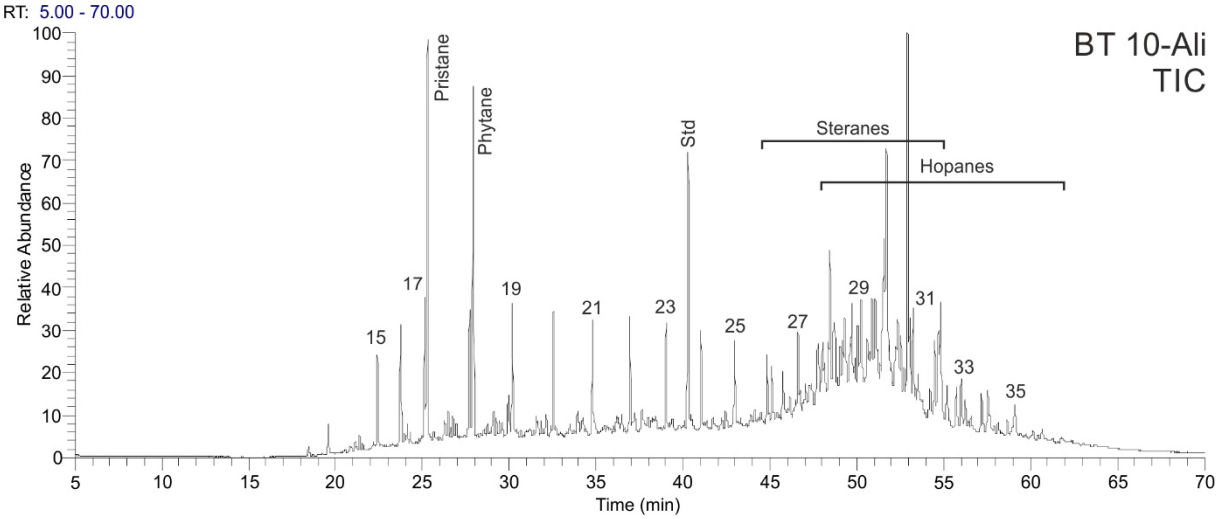
RT: 5.00 - 70.00
BT 10-Ali
TIC
Relative Abundance
Time (min)
Pristane
Phytane
Std
Steranes
Hopanes
15
17
19
21
23
25
27
29
31
33
35

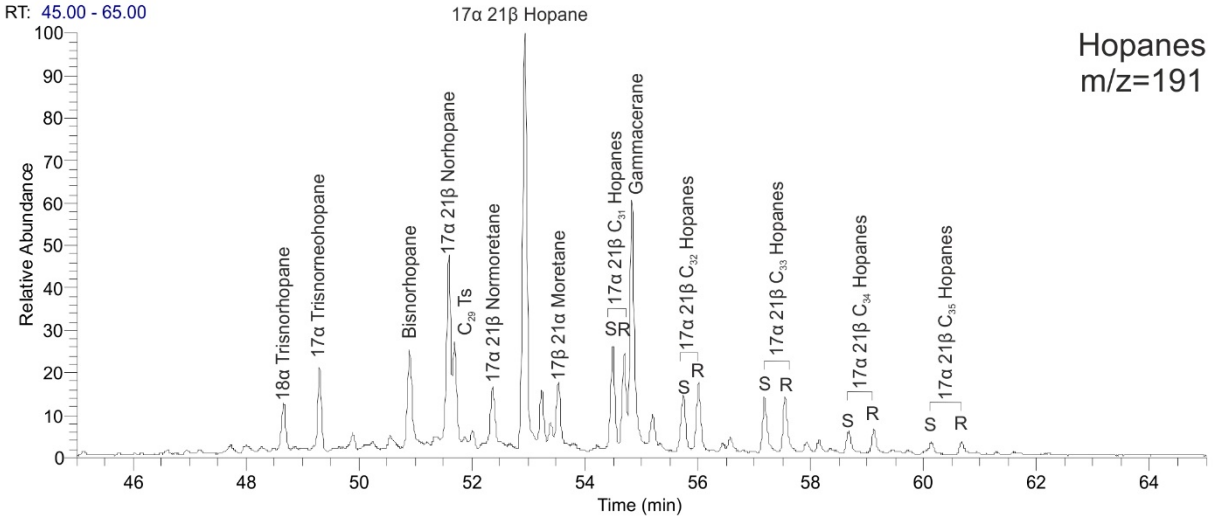
RT: 45.00 - 65.00
Hopanes
m/z=191
Relative Abundance
Time (min)
17α 21β Hopane
18α Trisnorhopane
17α Trisnorneohopane
Bisnorhopane
17α 21β Norhopane
C29 Ts
17α 21β Normoretane
17β 21α Moretane
17α 21β C31 Hopanes
Gammacerane
17α 21β C32 Hopanes
17α 21β C33 Hopanes
17α 21β C34 Hopanes
17α 21β C35 Hopanes
S
R

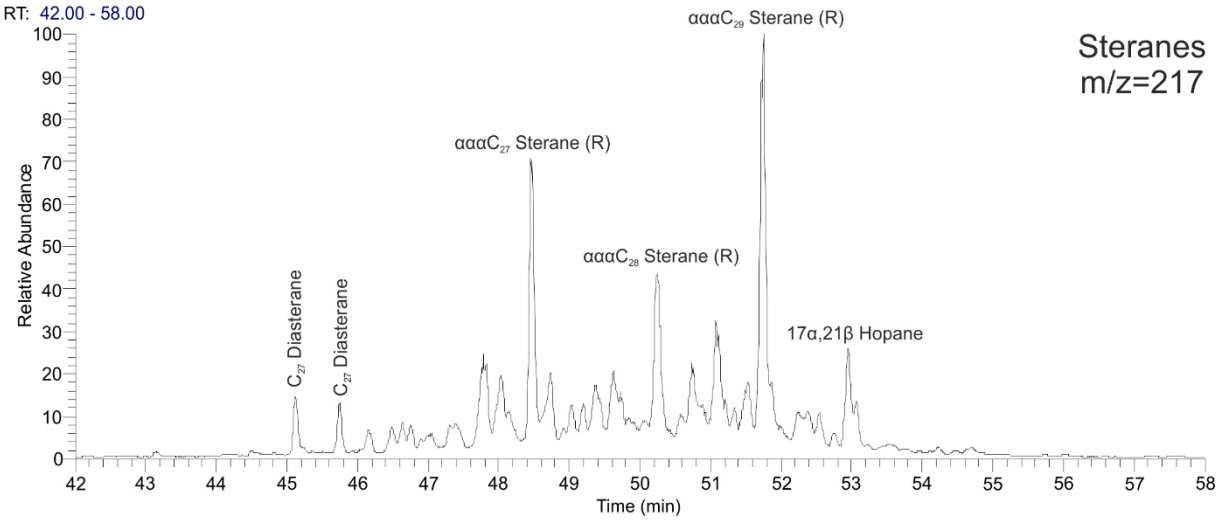
RT: 42.00 - 58.00
Steranes
m/z=217
Relative Abundance
Time (min)
αααC29 Sterane (R)
αααC27 Sterane (R)
αααC28 Sterane (R)
C27 Diasterane
C27 Diasterane
17α,21β Hopane

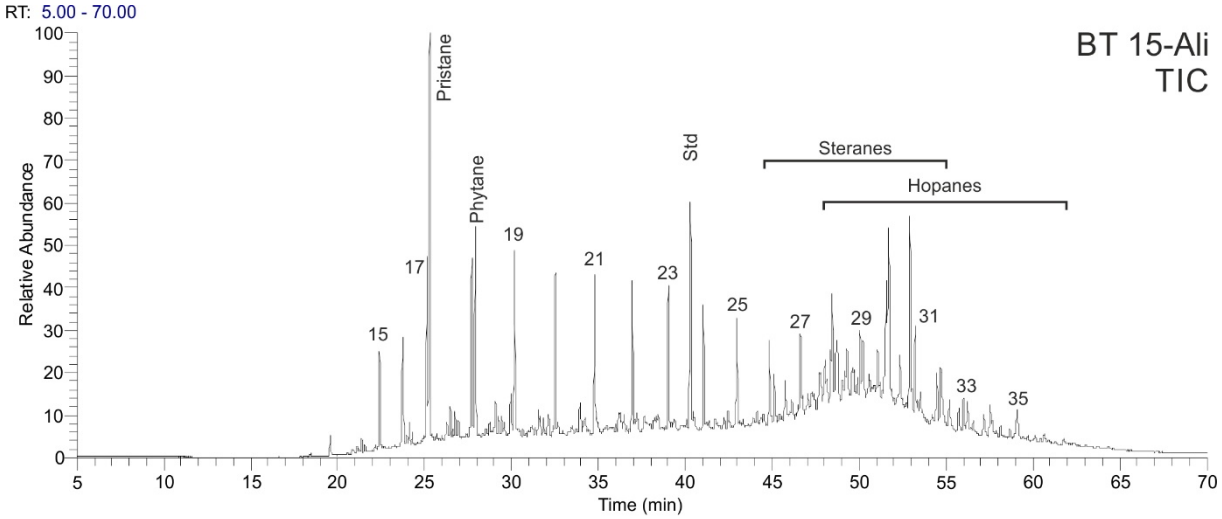
RT: 5.00 - 70.00
BT 15-Ali
TIC
Relative Abundance
Time (min)
Pristane
Phytane
Std
Steranes
Hopanes
15
17
19
21
23
25
27
29
31
33
35

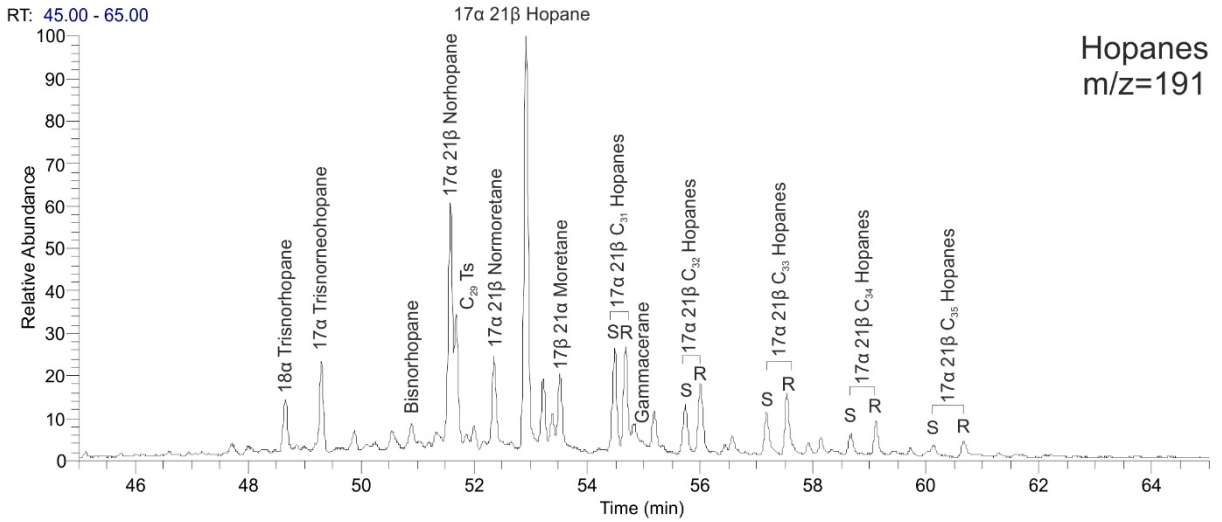
RT: 45.00 - 65.00
Hopanes
m/z=191
Relative Abundance
Time (min)
18α Trisnorhopane
17α Trisnorneohopane
Bisnorhopane
17α 21β Norhopane
C29 Ts
17α 21β Normoretane
17α 21β Hopane
17β 21α Moretane
17α 21β C31 Hopanes
S R
Gammacerane
17α 21β C32 Hopanes
S R
17α 21β C33 Hopanes
S R
17α 21β C34 Hopanes
S R
17α 21β C35 Hopanes
S R

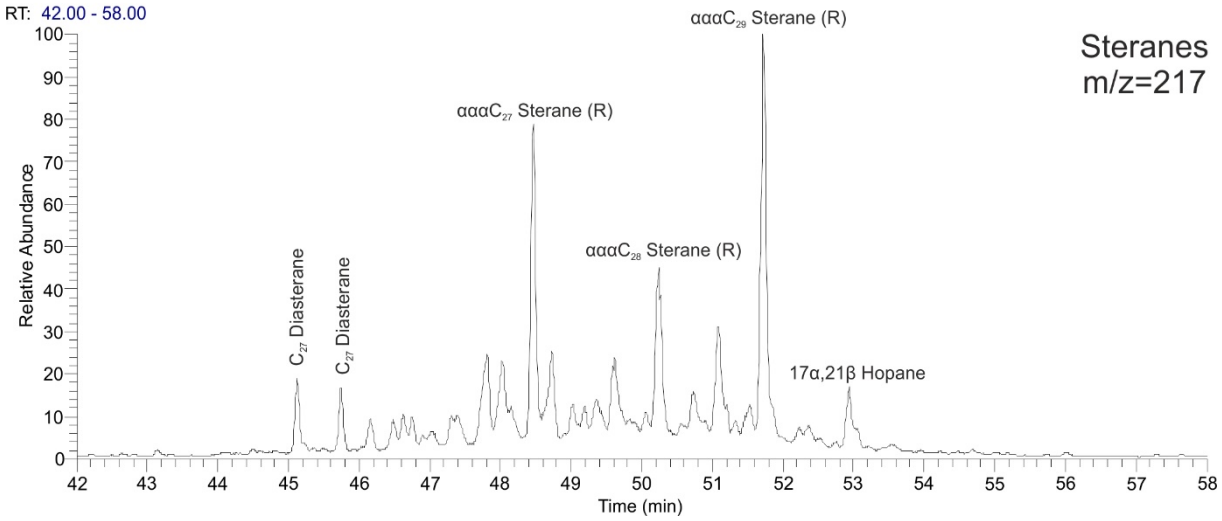
RT: 42.00 - 58.00
Steranes
m/z=217
Relative Abundance
Time (min)
C27 Diasterane
C27 Diasterane
ααα C27 Sterane (R)
ααα C28 Sterane (R)
ααα C29 Sterane (R)
17α,21β Hopane

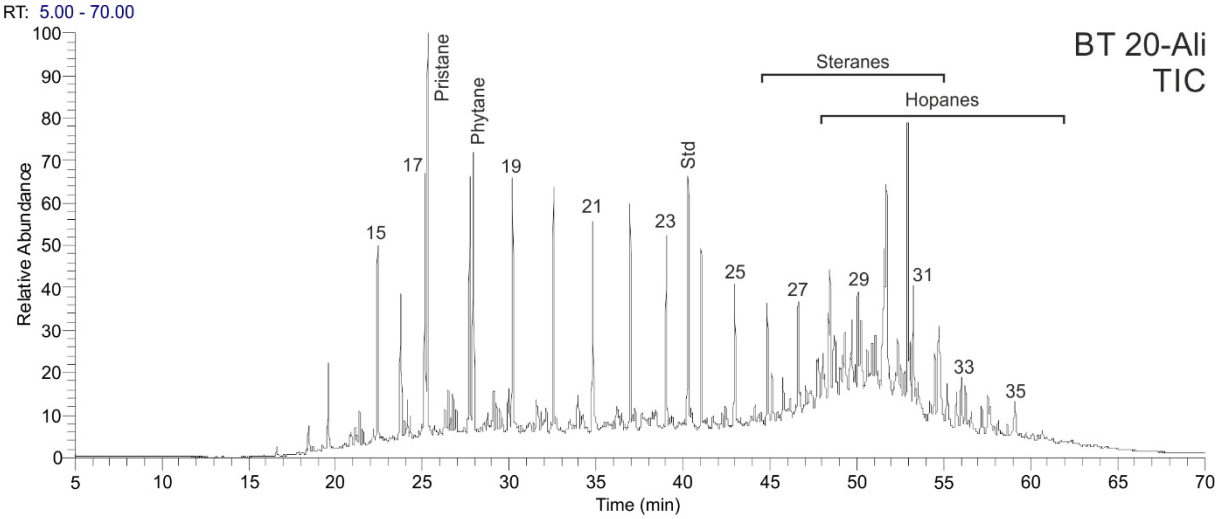
RT: 5.00 - 70.00
BT 20-Ali
TIC
Relative Abundance
Time (min)
Pristane
Phytane
Std
Steranes
Hopanes
15
17
19
21
23
25
27
29
31
33
35

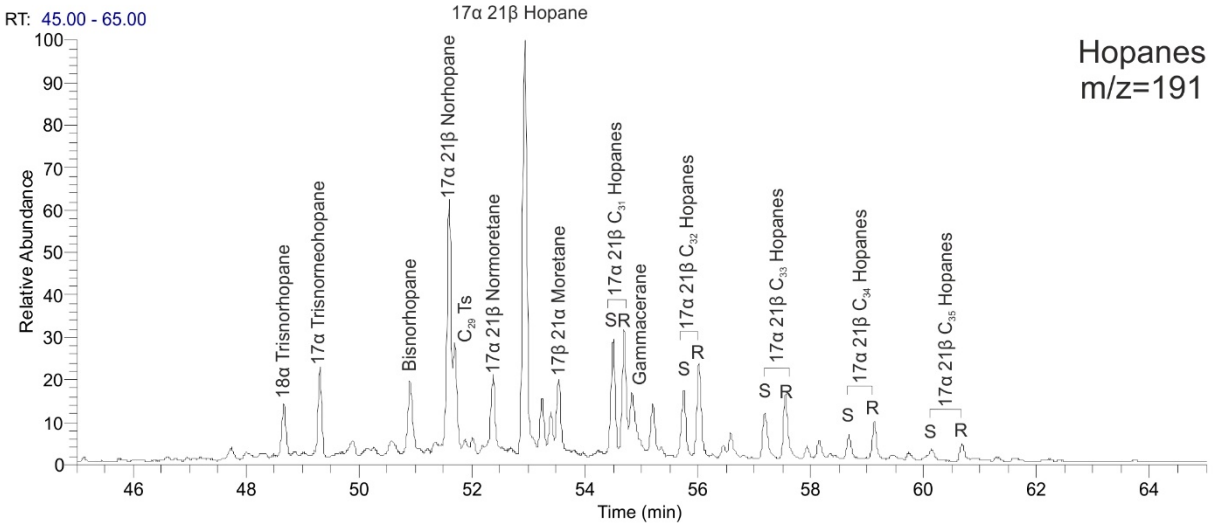
RT: 45.00 - 65.00
Hopanes
m/z=191
Relative Abundance
Time (min)
17α 21β Hopane
18α Trisnorhopane
17α Trisnorneohopane
Bisnorhopane
17α 21β Norhopane
C29 Ts
17α 21β Normoretane
17β 21α Moretane
17α 21β C31 Hopanes
S R
Gammacerane
17α 21β C32 Hopanes
S R
17α 21β C33 Hopanes
S R
17α 21β C34 Hopanes
S R
17α 21β C35 Hopanes
S R

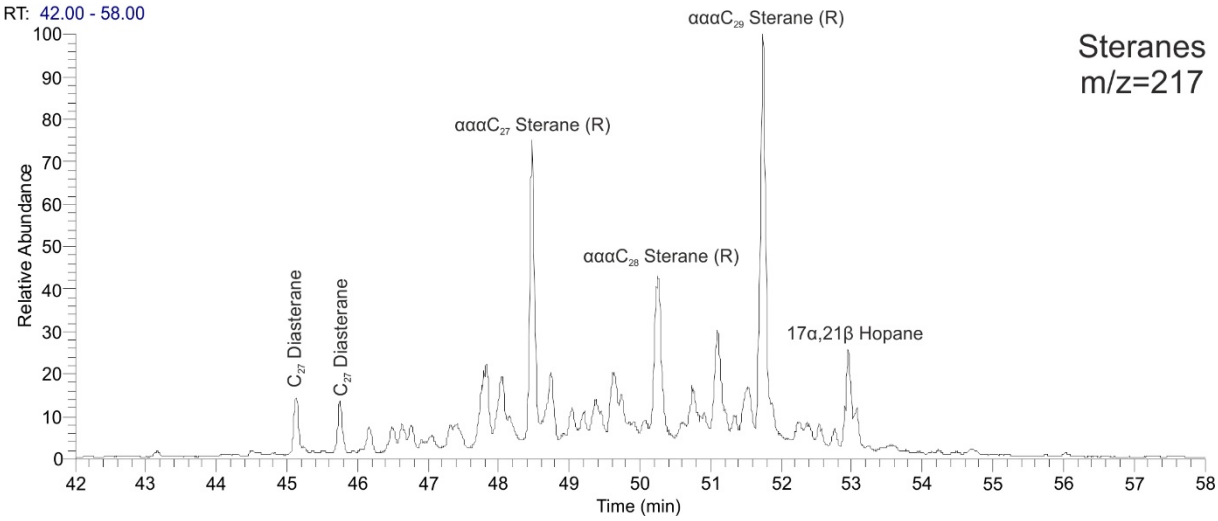
RT: 42.00 - 58.00
Steranes
m/z=217
Relative Abundance
Time (min)
αααC29 Sterane (R)
αααC27 Sterane (R)
αααC28 Sterane (R)
C27 Diasterane
C27 Diasterane
17α,21β Hopane

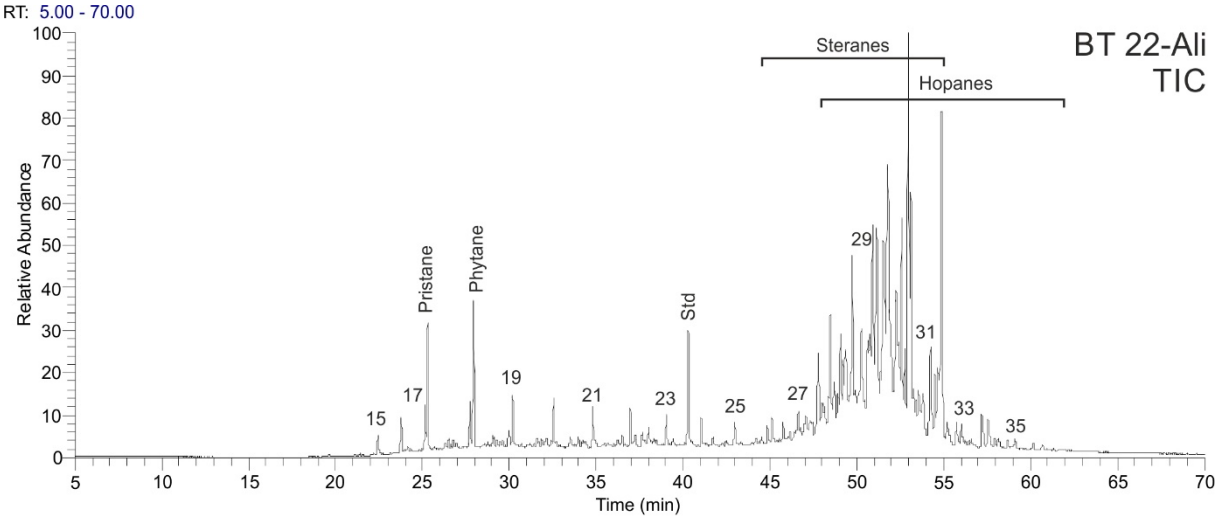
RT: 5.00 - 70.00
BT 22-Ali
TIC
Steranes
Hopanes
Relative Abundance
Time (min)
Pristane
Phytane
Std
15
17
19
21
23
25
27
29
31
33
35

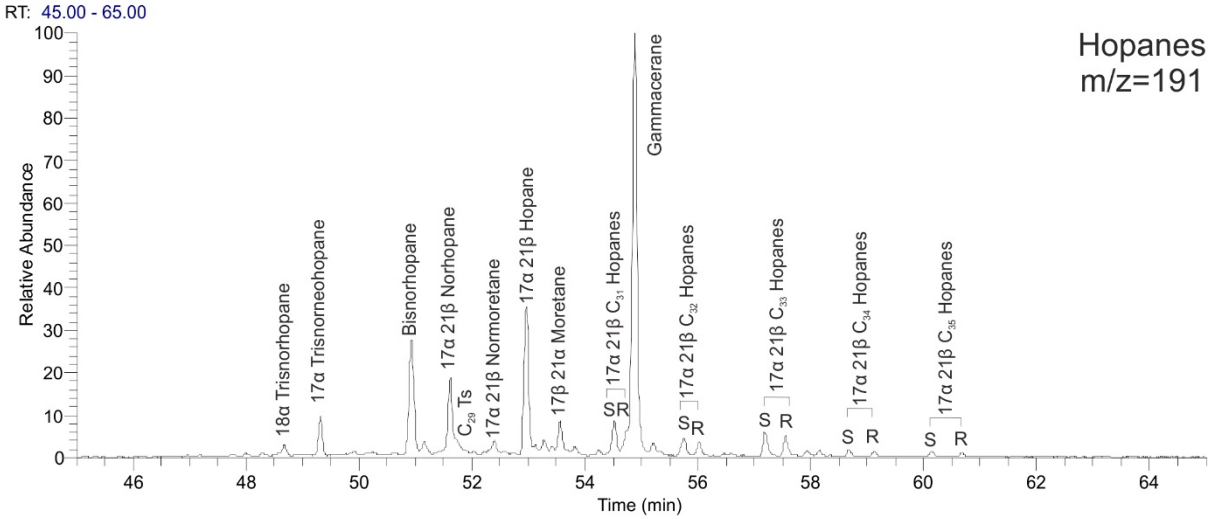
RT: 45.00 - 65.00
Hopanes
m/z=191
Relative Abundance
Time (min)
18α Trisnorhopane
17α Trisnorneohopane
Bisnorhopane
17α 21β Norhopane
C29 Ts
17α 21β Normoretane
17α 21β Hopane
17β 21α Moretane
17α 21β C31 Hopanes
Gammacerane
17α 21β C32 Hopanes
17α 21β C33 Hopanes
17α 21β C34 Hopanes
17α 21β C35 Hopanes
S R

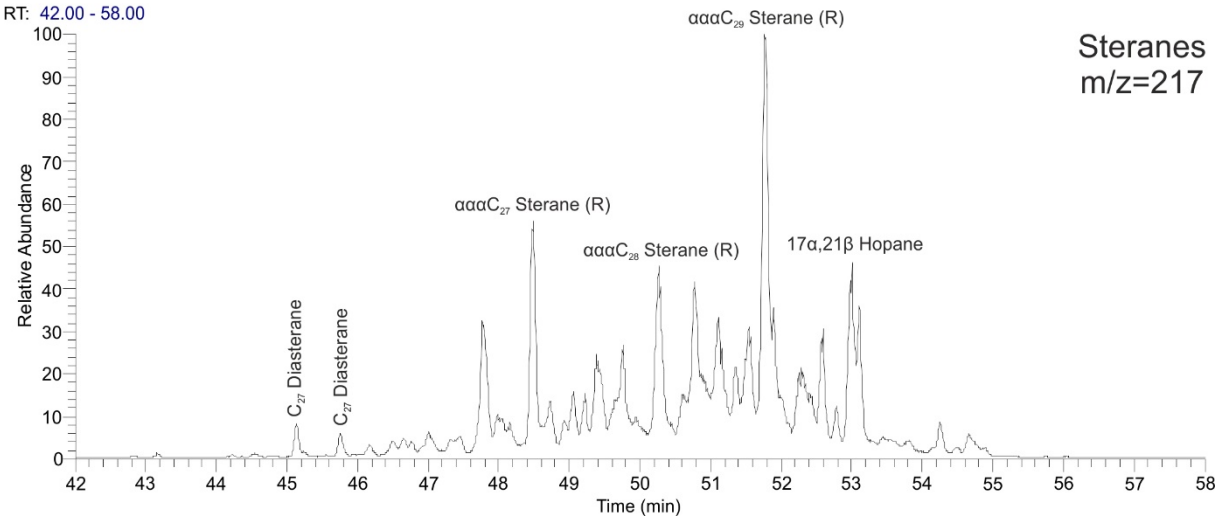
RT: 42.00 - 58.00
Steranes
m/z=217
Relative Abundance
Time (min)
αααC29 Sterane (R)
αααC27 Sterane (R)
αααC28 Sterane (R)
17α,21β Hopane
C27 Diasterane
C27 Diasterane

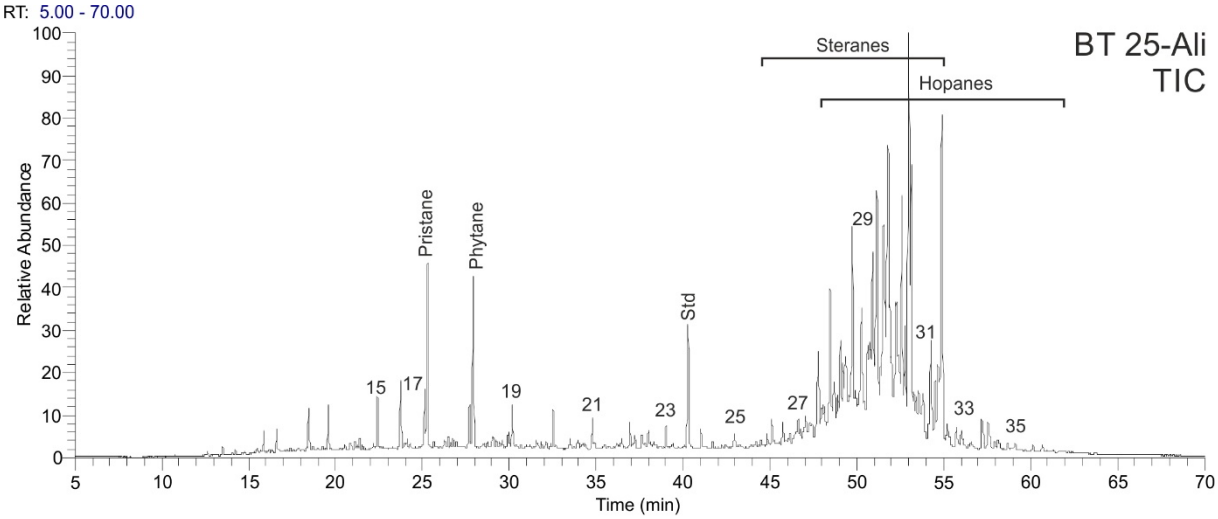
RT: 5.00 - 70.00
BT 25-Ali
TIC
Steranes
Hopanes
Pristane
Phytane
Std
15
17
19
21
23
25
27
29
31
33
35
Relative Abundance
Time (min)

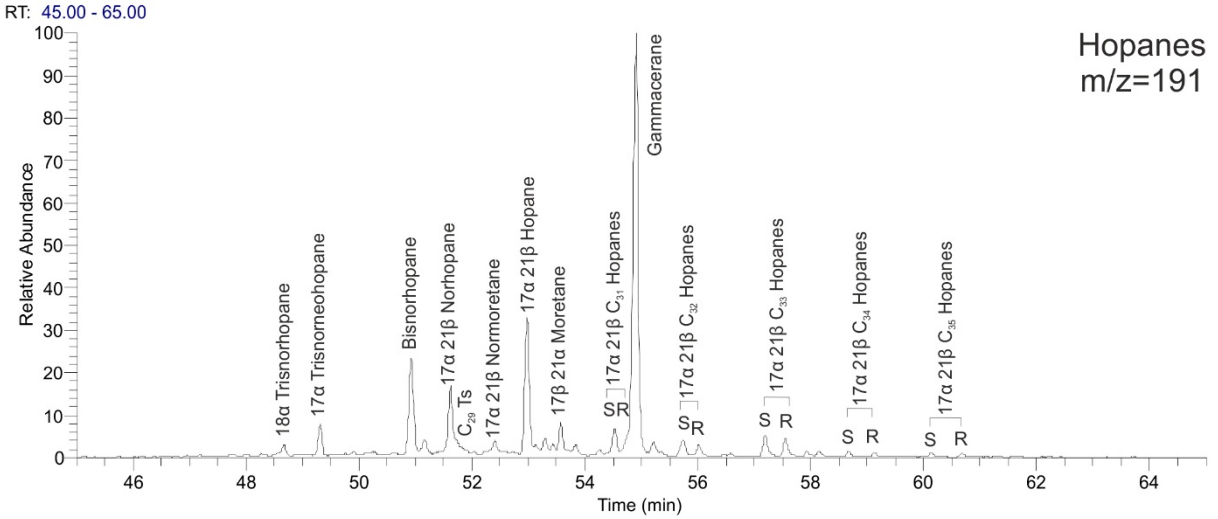
RT: 45.00 - 65.00
Hopanes
m/z=191
18α Trisnorhopane
17α Trisnorneohopane
Bisnorhopane
17α 21β Norhopane
C29 Ts
17α 21β Normoretane
17α 21β Hopane
17β 21α Moretane
17α 21β C31 Hopanes
Gammacerane
17α 21β C32 Hopanes
17α 21β C33 Hopanes
17α 21β C34 Hopanes
17α 21β C35 Hopanes
S R
Relative Abundance
Time (min)

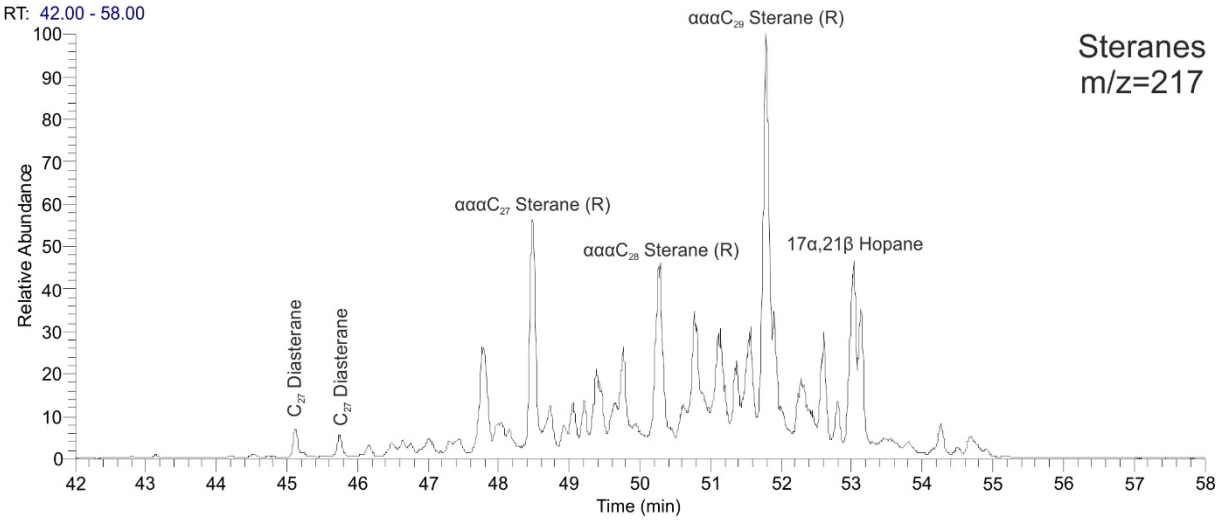
RT: 42.00 - 58.00
Steranes
m/z=217
αααC29 Sterane (R)
αααC27 Sterane (R)
αααC28 Sterane (R)
17α,21β Hopane
C27 Diasterane
C27 Diasterane
Relative Abundance
Time (min)

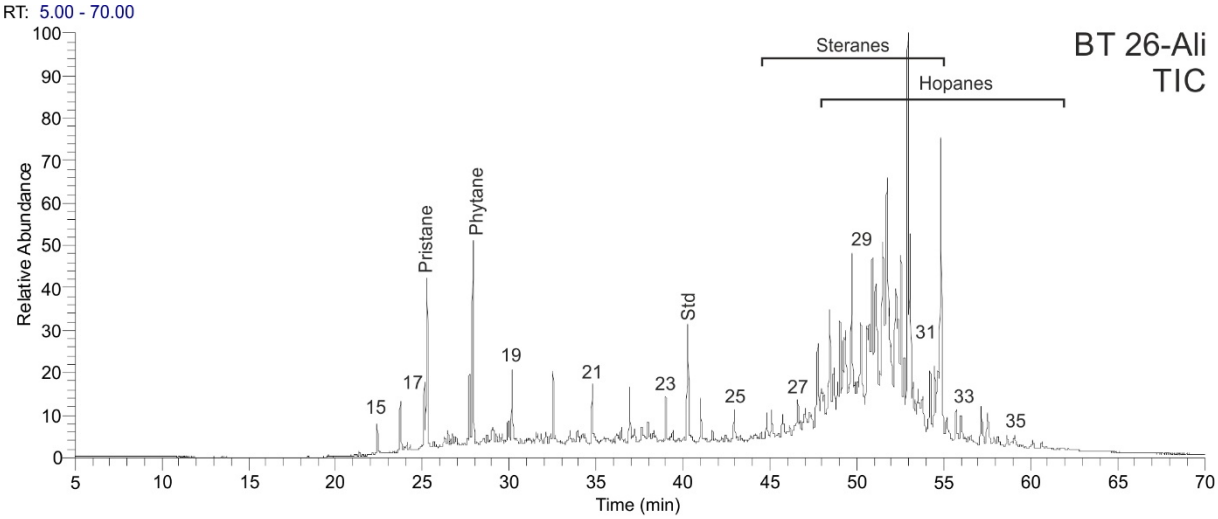
RT: 5.00 - 70.00
BT 26-Ali
TIC
Steranes
Hopanes
Pristane
Phytane
Std
15
17
19
21
23
25
27
29
31
33
35
Relative Abundance
Time (min)

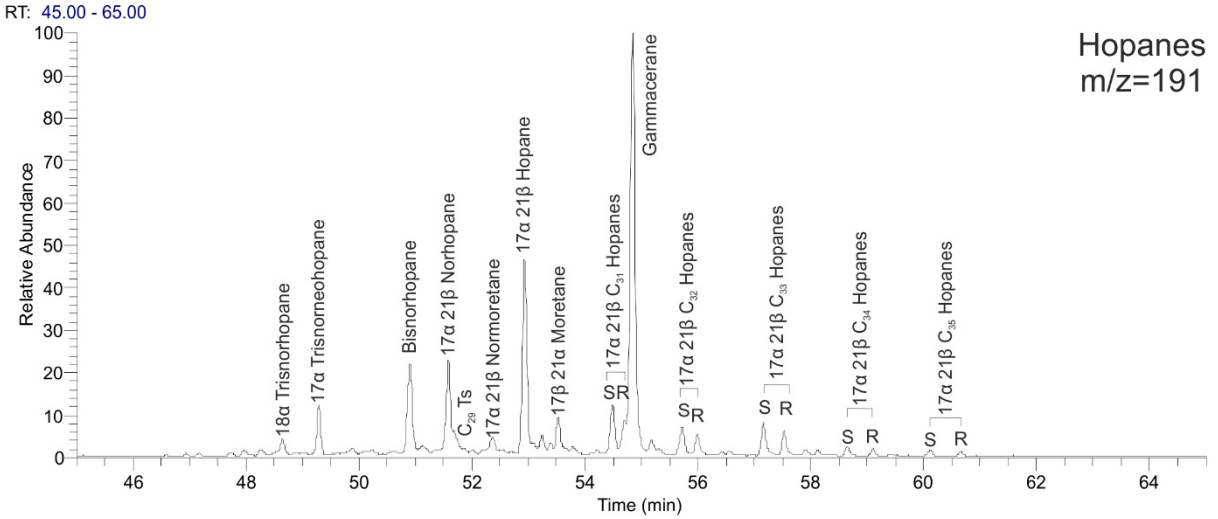
RT: 45.00 - 65.00
Hopanes
m/z=191
18α Trisnorhopane
17α Trisnorneohopane
Bisnorhopane
17α 21β Norhopane
C29 Ts
17α 21β Normoretane
17α 21β Hopane
17β 21α Moretane
17α 21β C31 Hopanes
Gammacerane
17α 21β C32 Hopanes
17α 21β C33 Hopanes
17α 21β C34 Hopanes
17α 21β C35 Hopanes
S R
Relative Abundance
Time (min)

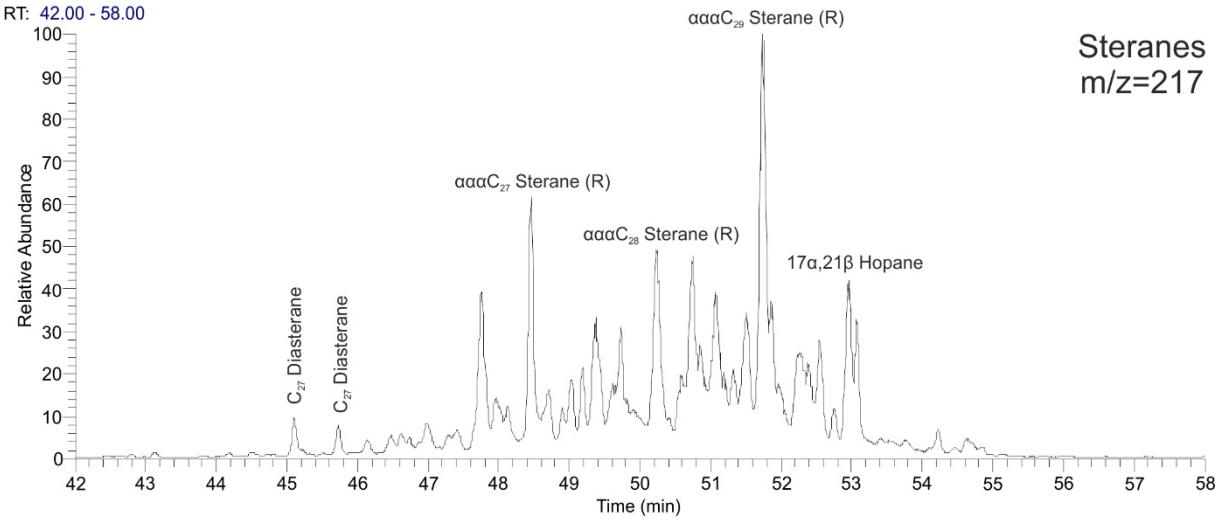
RT: 42.00 - 58.00
Steranes
m/z=217
αααC29 Sterane (R)
αααC27 Sterane (R)
αααC28 Sterane (R)
17α,21β Hopane
C27 Diasterane
C27 Diasterane
Relative Abundance
Time (min)

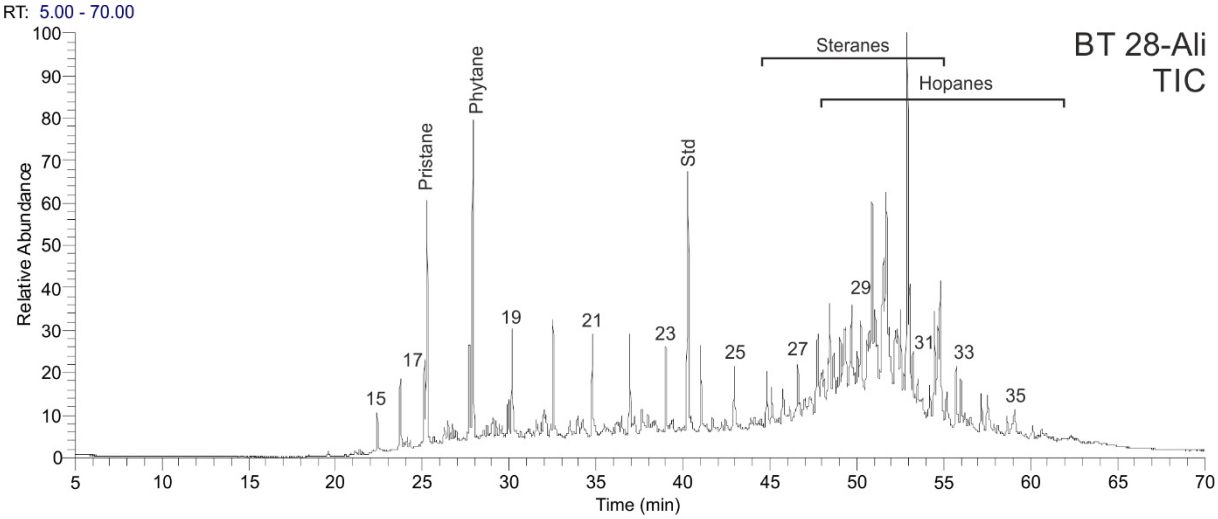
RT: 5.00 - 70.00
BT 28-Ali
TIC
Steranes
Hopanes
Pristane
Phytane
Std
15
17
19
21
23
25
27
29
31
33
35
Relative Abundance
Time (min)

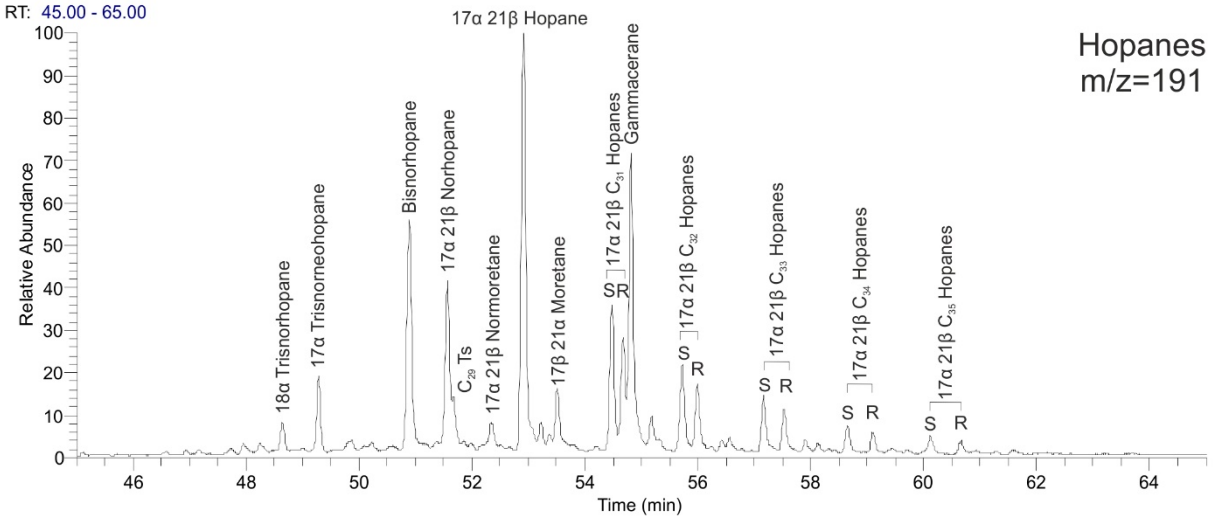
RT: 45.00 - 65.00
Hopanes
m/z=191
17α 21β Hopane
18α Trisnorhopane
17α Trisnorneohopane
Bisnorhopane
17α 21β Norhopane
C29 Ts
17α 21β Normoretane
17β 21α Moretane
17α 21β C31 Hopanes
Gammacerane
17α 21β C32 Hopanes
17α 21β C33 Hopanes
17α 21β C34 Hopanes
17α 21β C35 Hopanes
S R
Relative Abundance
Time (min)

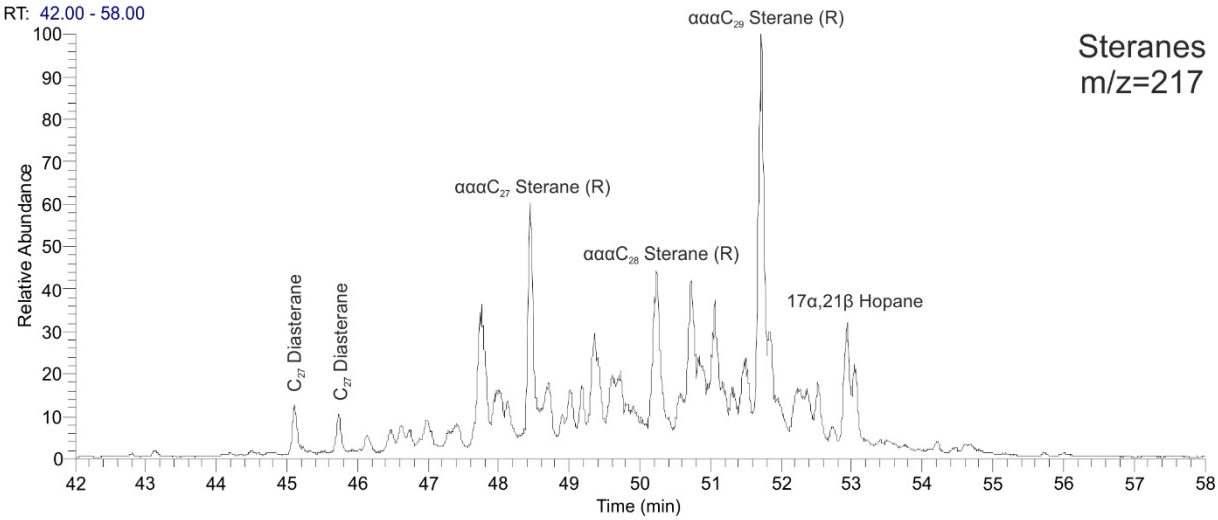
RT: 42.00 - 58.00
Steranes
m/z=217
ααα C29 Sterane (R)
ααα C27 Sterane (R)
ααα C28 Sterane (R)
17α,21β Hopane
C27 Diasterane
C27 Diasterane
Relative Abundance
Time (min)

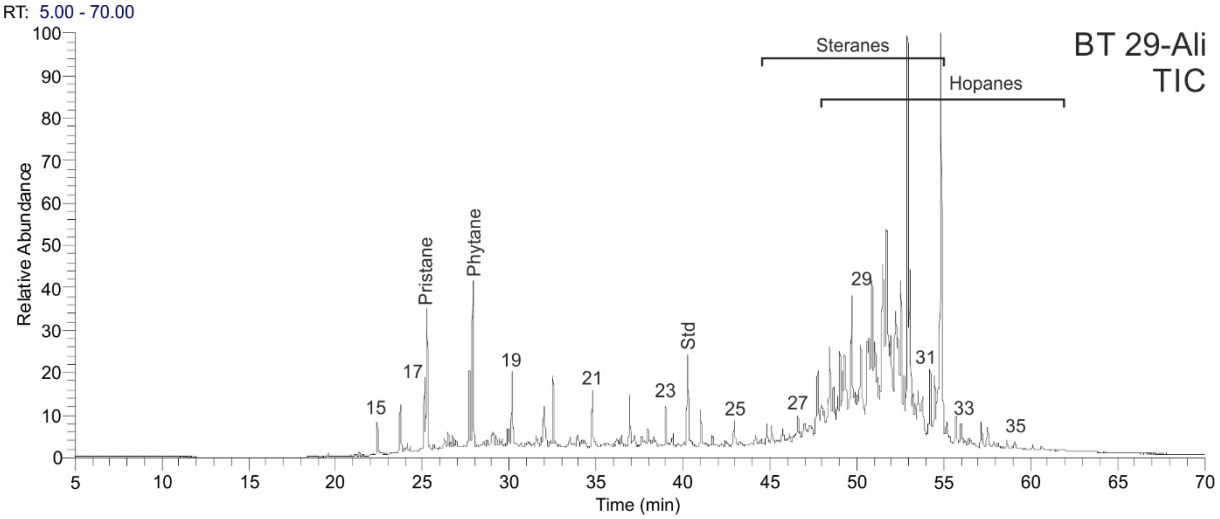
RT: 5.00 - 70.00
BT 29-Ali
TIC
Steranes
Hopanes
Relative Abundance
Time (min)
Pristane
Phytane
Std
15
17
19
21
23
25
27
29
31
33
35

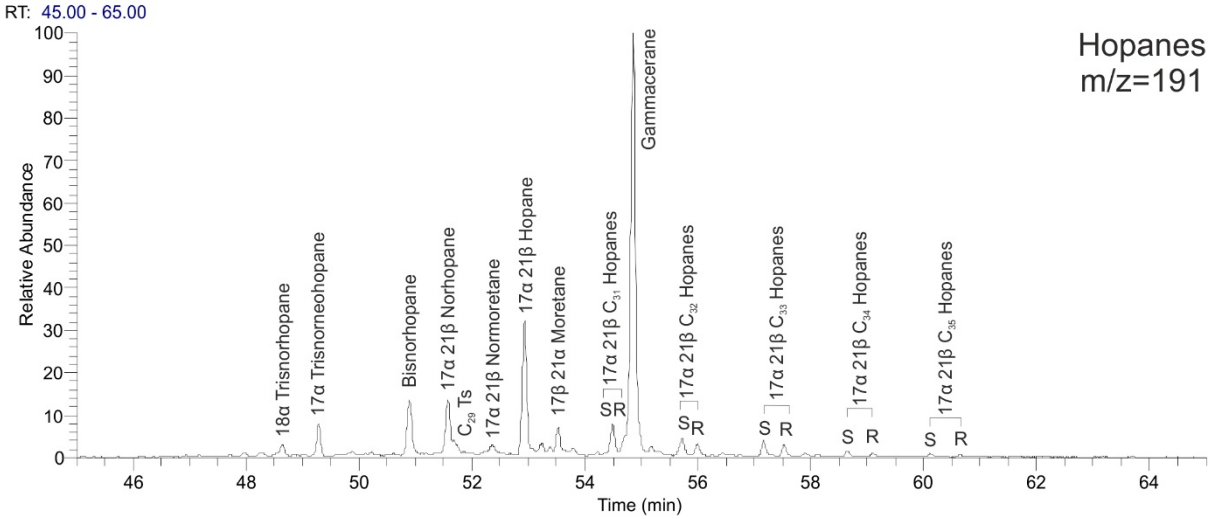
RT: 45.00 - 65.00
Hopanes
m/z=191
Relative Abundance
Time (min)
18α Trisnorhopane
17α Trisnorneohopane
Bisnorhopane
17α 21β Norhopane
C29 Ts
17α 21β Normoretane
17α 21β Hopane
17β 21α Moretane
17α 21β C31 Hopanes
Gammacerane
17α 21β C32 Hopanes
17α 21β C33 Hopanes
17α 21β C34 Hopanes
17α 21β C35 Hopanes
S R

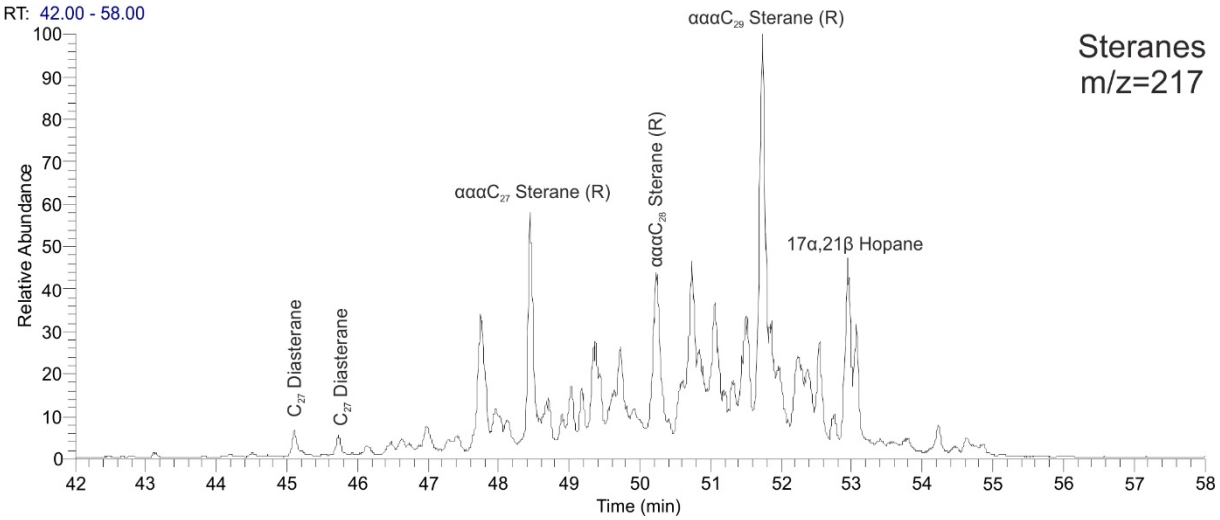
RT: 42.00 - 58.00
Steranes
m/z=217
Relative Abundance
Time (min)
C27 Diasterane
C27 Diasterane
αααC27 Sterane (R)
αααC28 Sterane (R)
αααC29 Sterane (R)
17α,21β Hopane

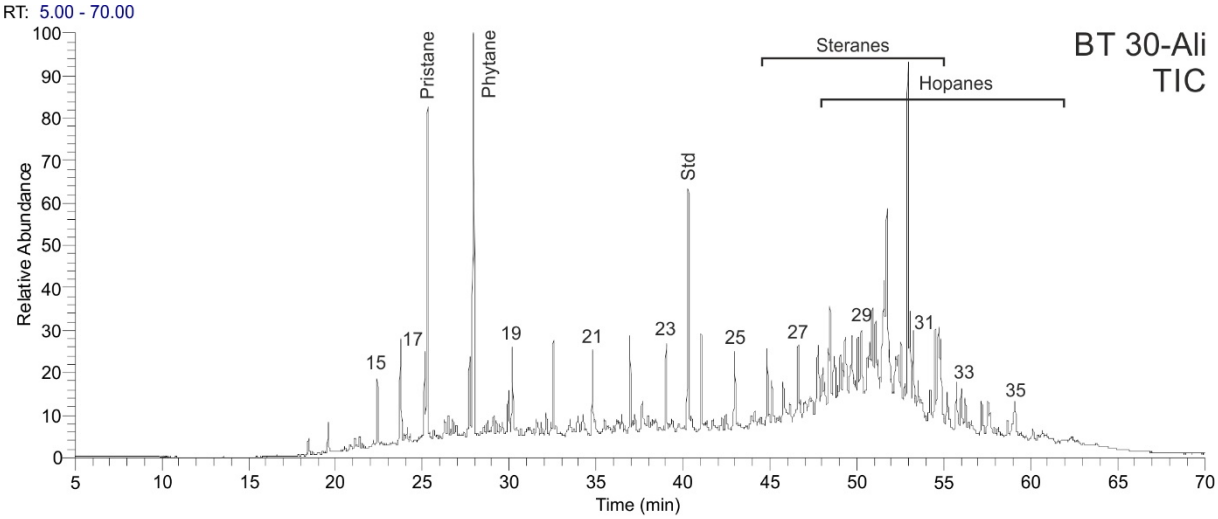
RT: 5.00 - 70.00
BT 30-Ali
TIC
Steranes
Hopanes
Pristane
Phytane
Std
15
17
19
21
23
25
27
29
31
33
35
Relative Abundance
Time (min)

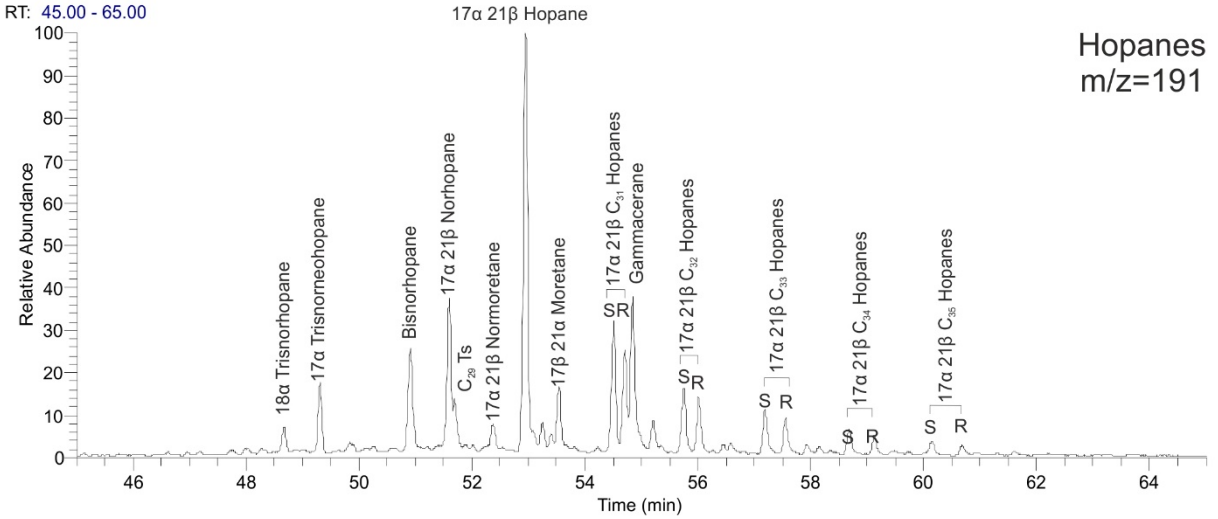
RT: 45.00 - 65.00
Hopanes
m/z=191
17α 21β Hopane
18α Trisnorhopane
17α Trisnorneohopane
Bisnorhopane
17α 21β Norhopane
C29 Ts
17α 21β Normoretane
17β 21α Moretane
17α 21β C31 Hopanes
Gammacerane
17α 21β C32 Hopanes
17α 21β C33 Hopanes
17α 21β C34 Hopanes
17α 21β C35 Hopanes
S R
Relative Abundance
Time (min)

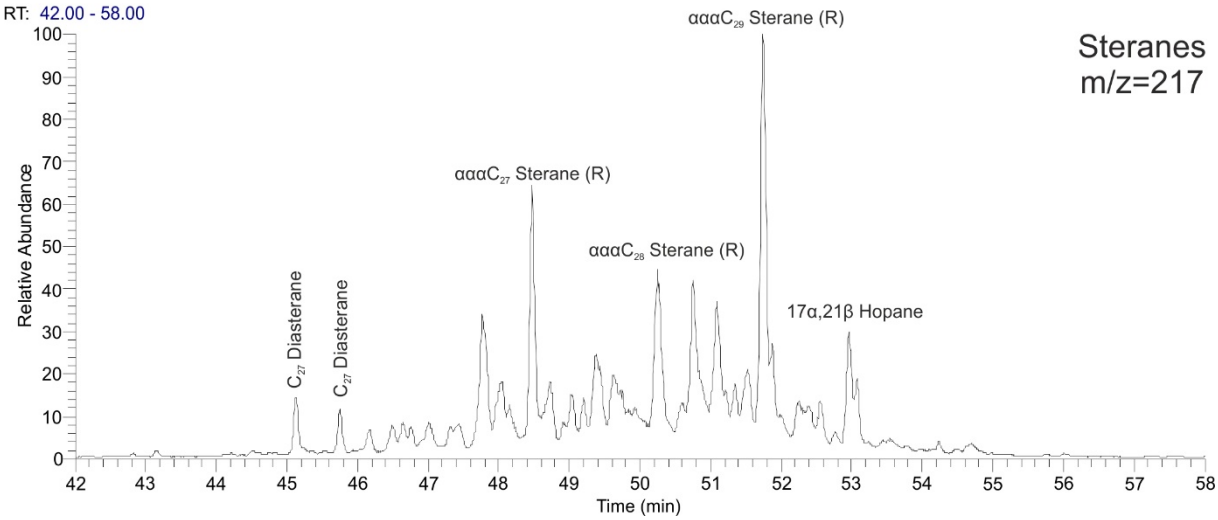
RT: 42.00 - 58.00
Steranes
m/z=217
ααα C29 Sterane (R)
ααα C27 Sterane (R)
ααα C28 Sterane (R)
C27 Diasterane
C27 Diasterane
17α,21β Hopane
Relative Abundance
Time (min)

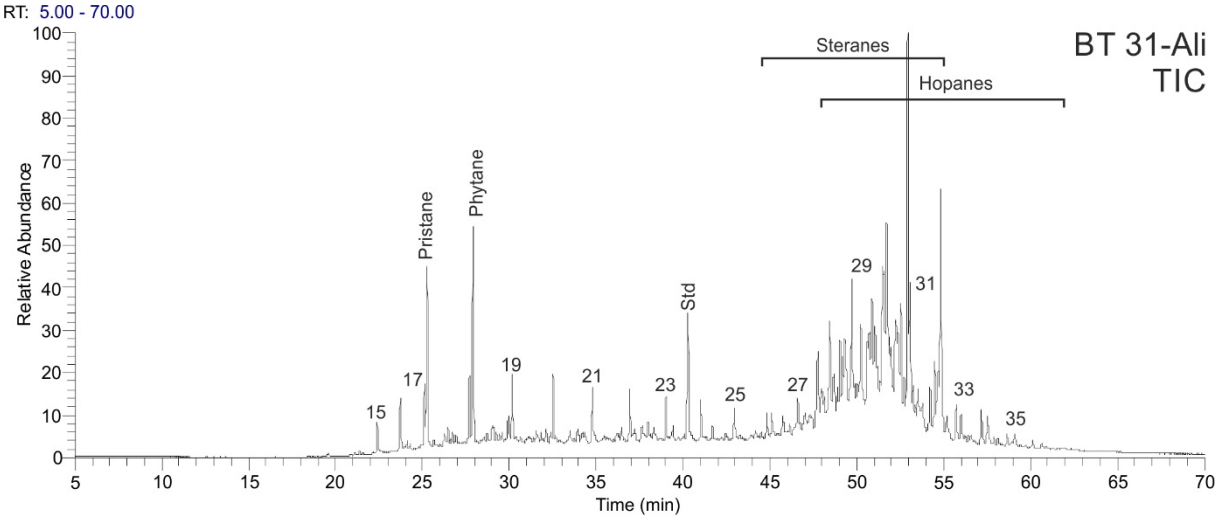
RT: 5.00 - 70.00
BT 31-Ali
TIC
Steranes
Hopanes
Pristane
Phytane
Std
15
17
19
21
23
25
27
29
31
33
35
Relative Abundance
Time (min)

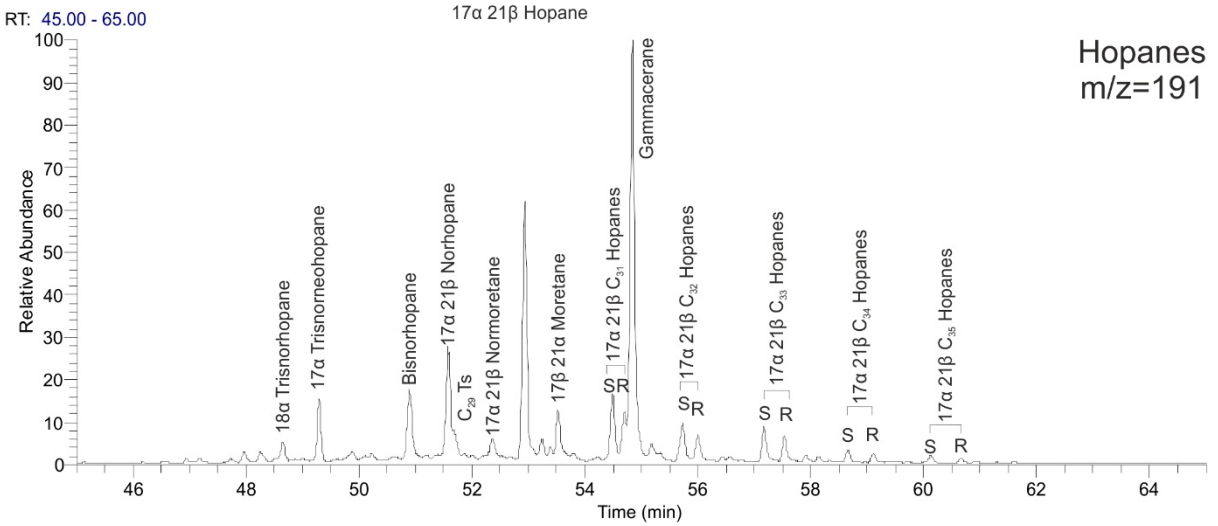
RT: 45.00 - 65.00
Hopanes
m/z=191
17α 21β Hopane
18α Trisnorhopane
17α Trisnorneohopane
Bisnorhopane
17α 21β Norhopane
C29 Ts
17α 21β Normoretane
17β 21α Moretane
17α 21β C31 Hopanes
Gammacerane
17α 21β C32 Hopanes
17α 21β C33 Hopanes
17α 21β C34 Hopanes
17α 21β C35 Hopanes
S R
Relative Abundance
Time (min)

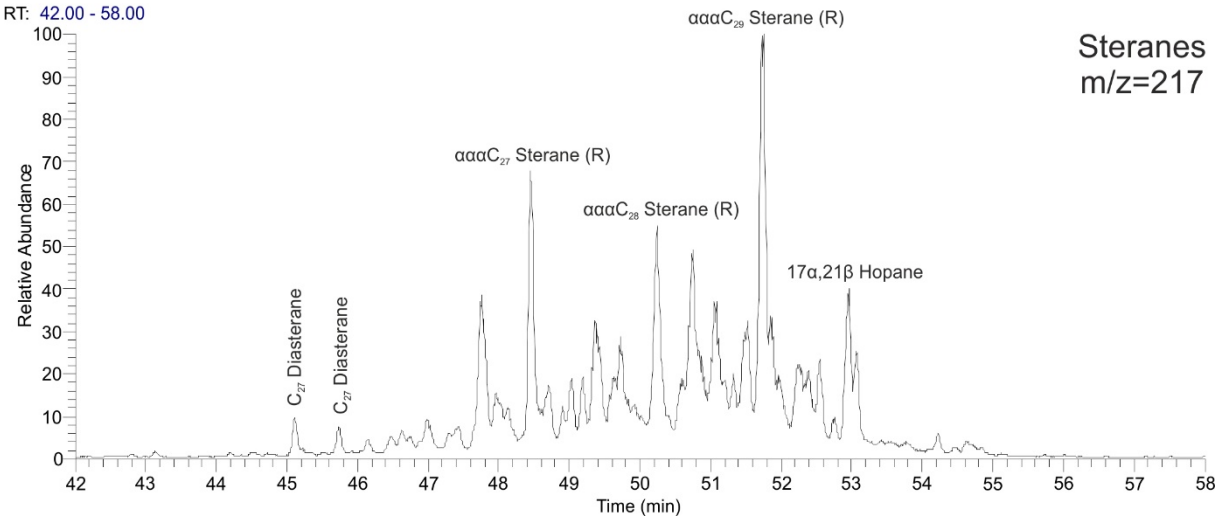
RT: 42.00 - 58.00
Steranes
m/z=217
αααC29 Sterane (R)
αααC27 Sterane (R)
αααC28 Sterane (R)
17α,21β Hopane
C27 Diasterane
C27 Diasterane
Relative Abundance
Time (min)

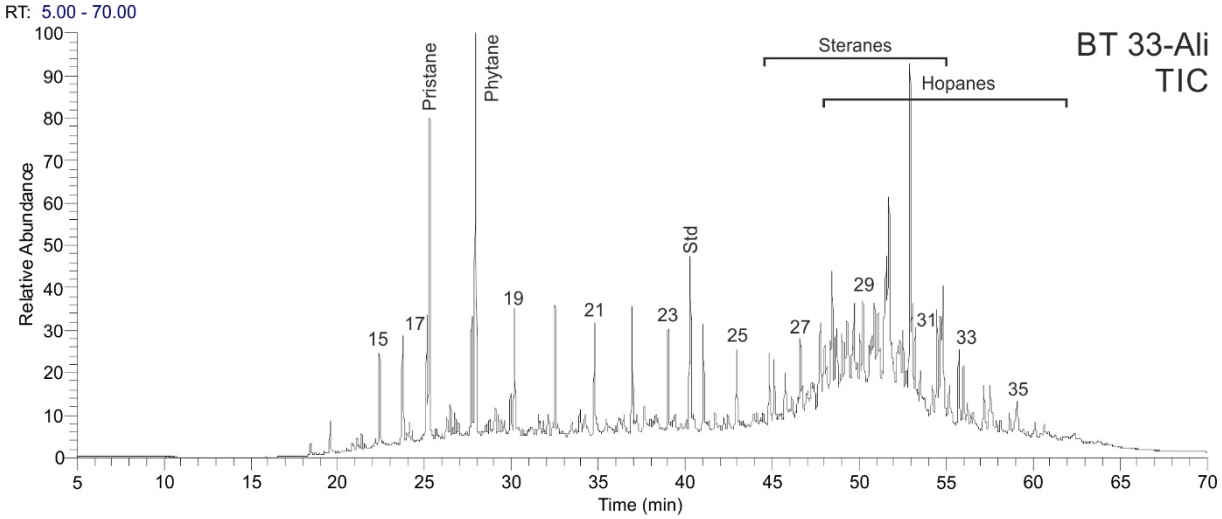
RT: 5.00 - 70.00
BT 33-Ali
TIC
Steranes
Hopanes
Pristane
Phytane
Std
15
17
19
21
23
25
27
29
31
33
35
Relative Abundance
Time (min)

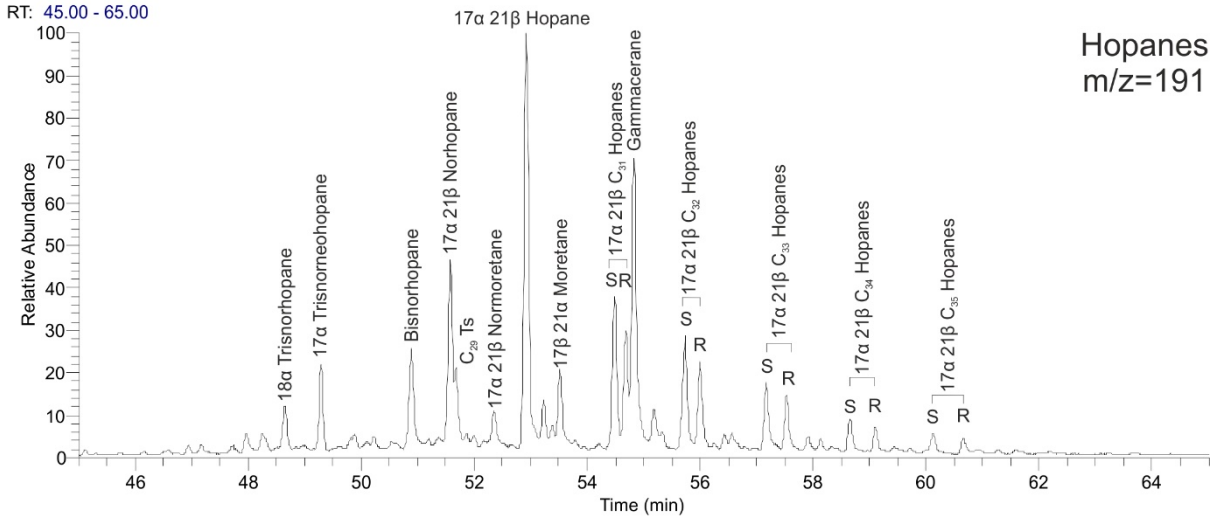
RT: 45.00 - 65.00
Hopanes
m/z=191
17α 21β Hopane
18α Trisnorhopane
17α Trisnorneohopane
Bisnorhopane
17α 21β Norhopane
C29 Ts
17α 21β Normoretane
17β 21α Moretane
17α 21β C31 Hopanes
Gammacerane
17α 21β C32 Hopanes
17α 21β C33 Hopanes
17α 21β C34 Hopanes
17α 21β C35 Hopanes
S
R
Relative Abundance
Time (min)

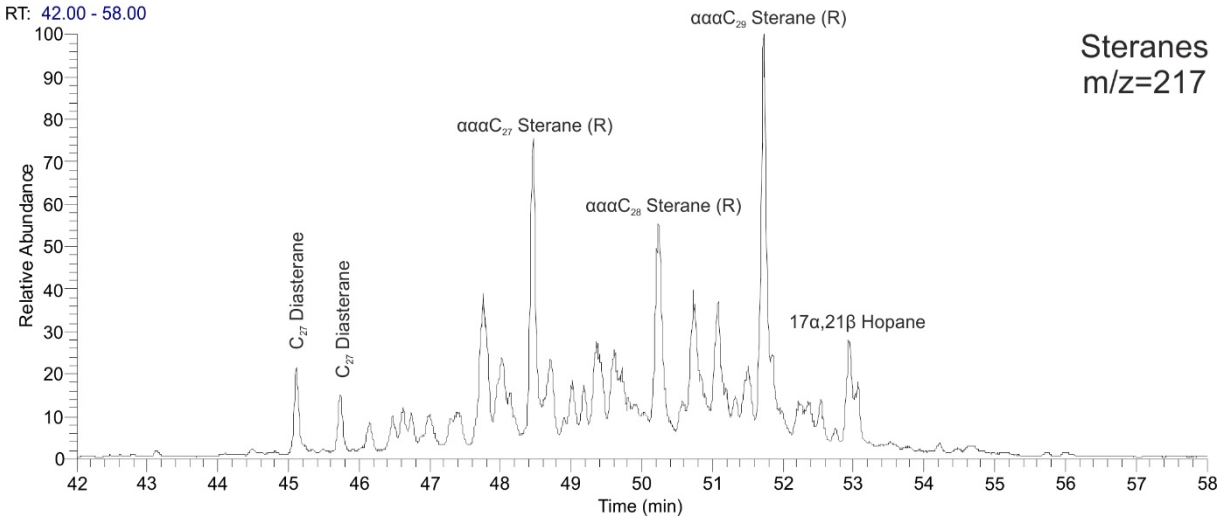
RT: 42.00 - 58.00
Steranes
m/z=217
αααC29 Sterane (R)
αααC27 Sterane (R)
αααC28 Sterane (R)
C27 Diasterane
C27 Diasterane
17α,21β Hopane
Relative Abundance
Time (min)

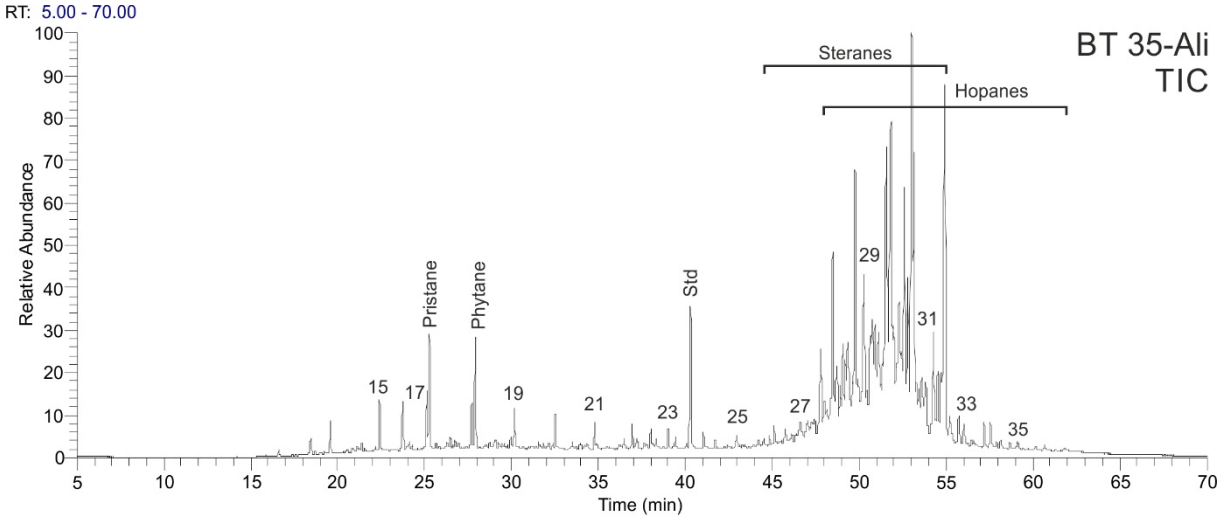
RT: 5.00 - 70.00
BT 35-Ali
TIC
Steranes
Hopanes
Relative Abundance
Time (min)
Pristane
Phytane
Std
15
17
19
21
23
25
27
29
31
33
35

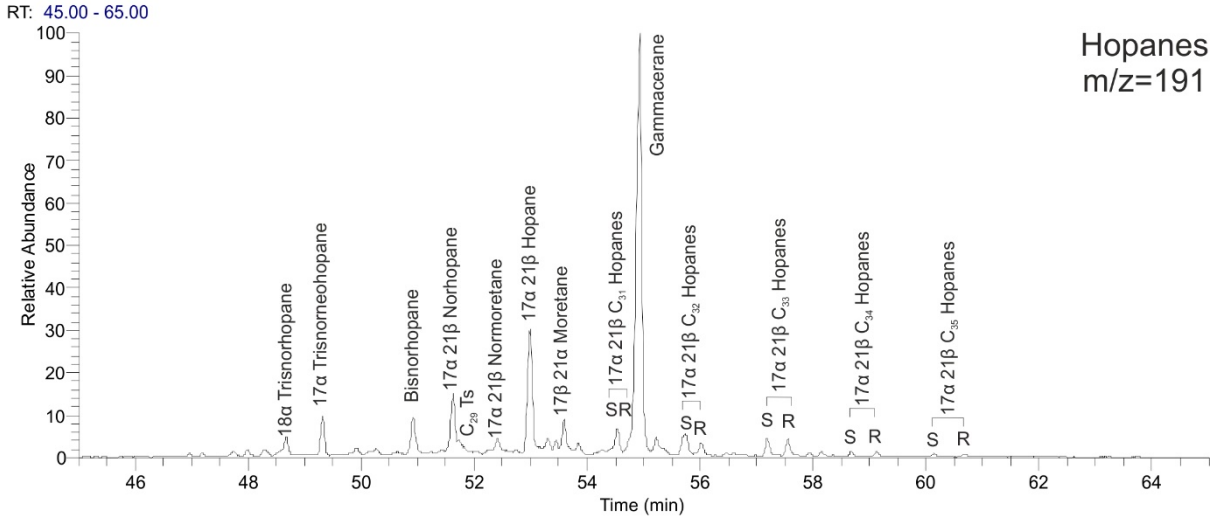
RT: 45.00 - 65.00
Hopanes
m/z=191
Relative Abundance
Time (min)
18α Trisnorhopane
17α Trisnorneohopane
Bisnorhopane
17α 21β Norhopane
C29 Ts
17α 21β Normoretane
17α 21β Hopane
17β 21α Moretane
17α 21β C31 Hopanes
SR
Gammacerane
17α 21β C32 Hopanes
S R
17α 21β C33 Hopanes
S R
17α 21β C34 Hopanes
S R
17α 21β C35 Hopanes
S R

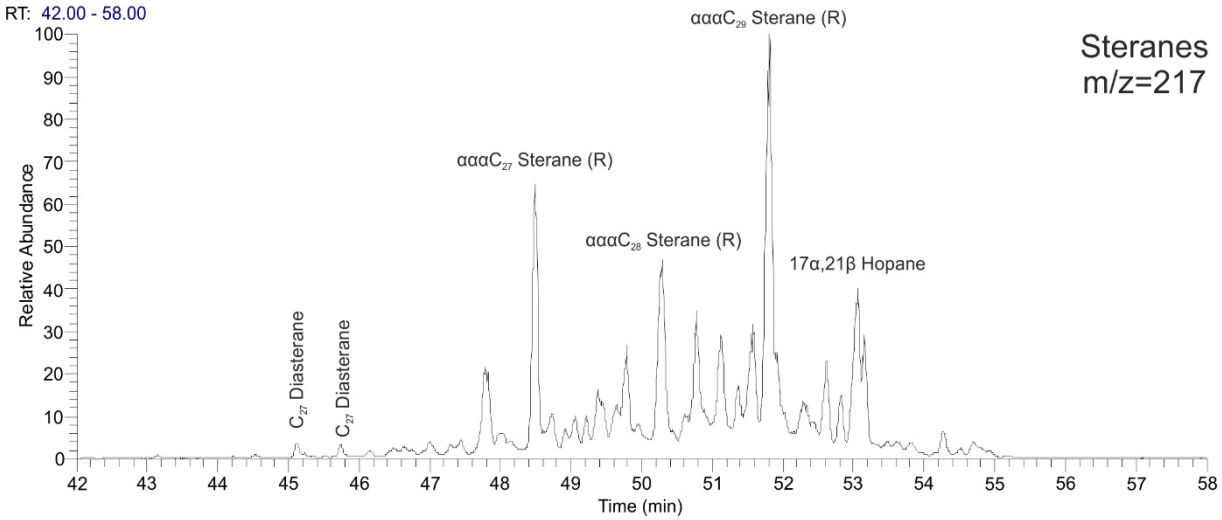
RT: 42.00 - 58.00
Steranes
m/z=217
Relative Abundance
Time (min)
αααC29 Sterane (R)
αααC27 Sterane (R)
αααC28 Sterane (R)
17α,21β Hopane
C27 Diasterane
C27 Diasterane

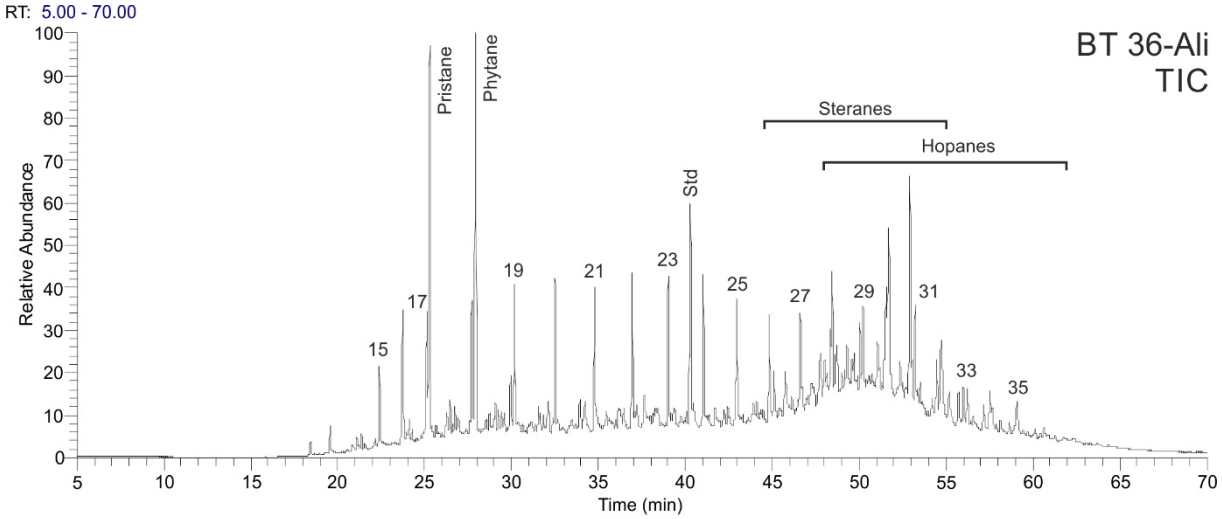
RT: 5.00 - 70.00
BT 36-Ali
TIC
Relative Abundance
Time (min)
Pristane
Phytane
Std
Steranes
Hopanes
15
17
19
21
23
25
27
29
31
33
35

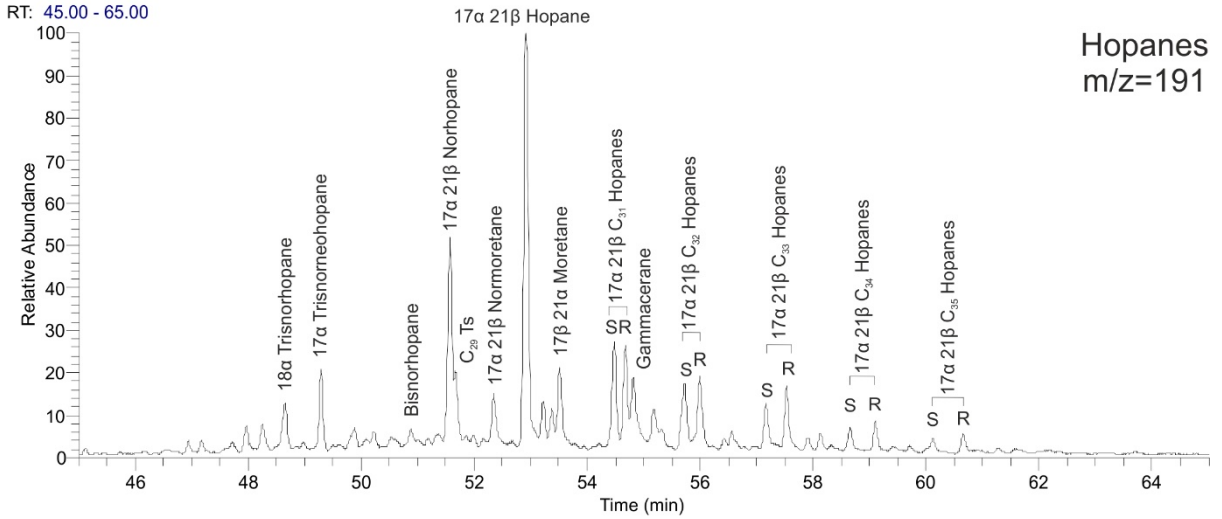
RT: 45.00 - 65.00
Hopanes
m/z=191
Relative Abundance
Time (min)
18α Trisnorhopane
17α Trisnorneohopane
Bisnorhopane
17α 21β Norhopane
C29 Ts
17α 21β Normoretane
17α 21β Hopane
17β 21α Moretane
17α 21β C31 Hopanes
S R
Gammacerane
17α 21β C32 Hopanes
S R
17α 21β C33 Hopanes
S R
17α 21β C34 Hopanes
S R
17α 21β C35 Hopanes
S R

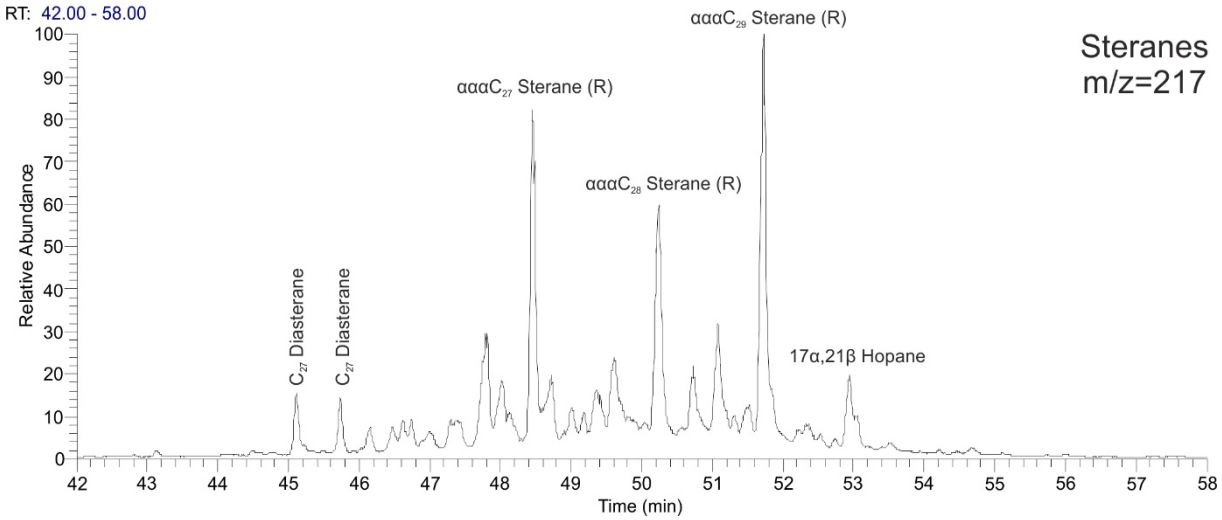
RT: 42.00 - 58.00
Steranes
m/z=217
Relative Abundance
Time (min)
αααC29 Sterane (R)
αααC27 Sterane (R)
αααC28 Sterane (R)
C27 Diasterane
C27 Diasterane
17α,21β Hopane

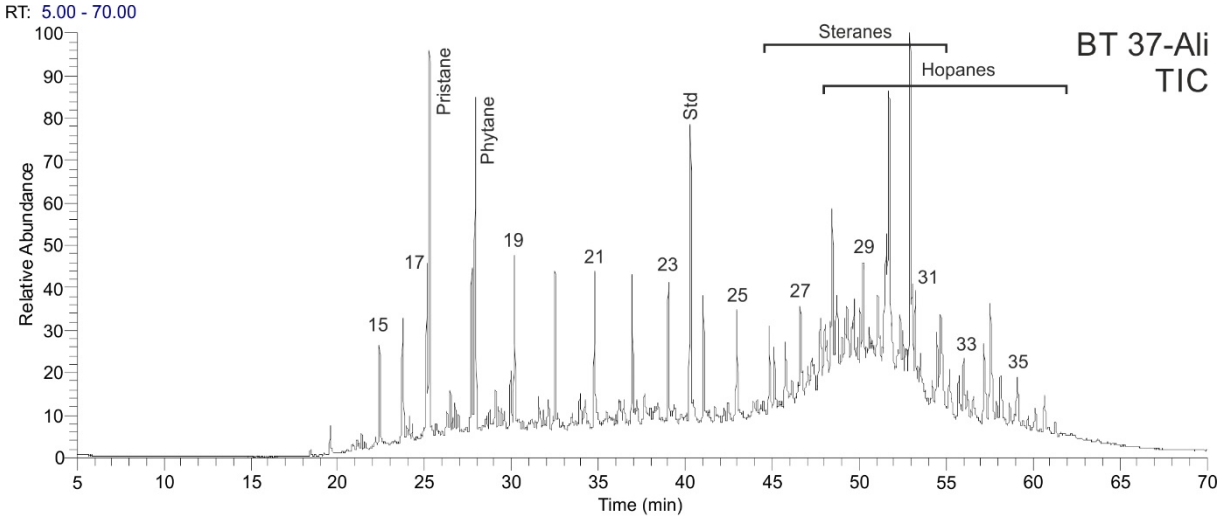
RT: 5.00 - 70.00
BT 37-Ali
TIC
Steranes
Hopanes
Pristane
Phytane
Std
15
17
19
21
23
25
27
29
31
33
35
Relative Abundance
Time (min)

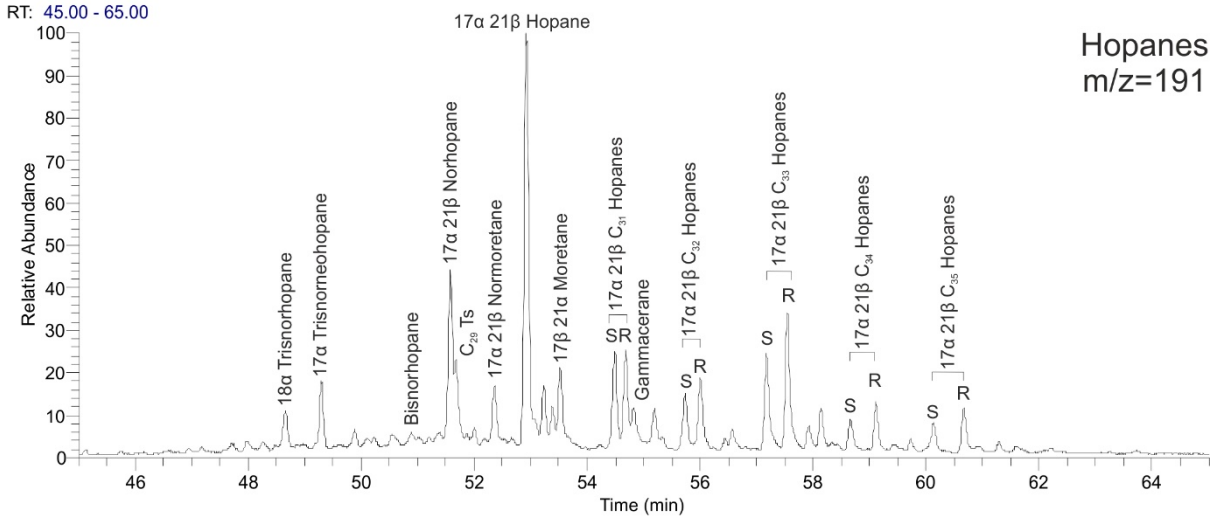
RT: 45.00 - 65.00
Hopanes
m/z=191
17α 21β Hopane
18α Trisnorhopane
17α Trisnorneohopane
Bisnorhopane
17α 21β Norhopane
C29 Ts
17α 21β Normoretane
17β 21α Moretane
17α 21β C31 Hopanes
Gammacerane
17α 21β C32 Hopanes
17α 21β C33 Hopanes
17α 21β C34 Hopanes
17α 21β C35 Hopanes
S
R
Relative Abundance
Time (min)

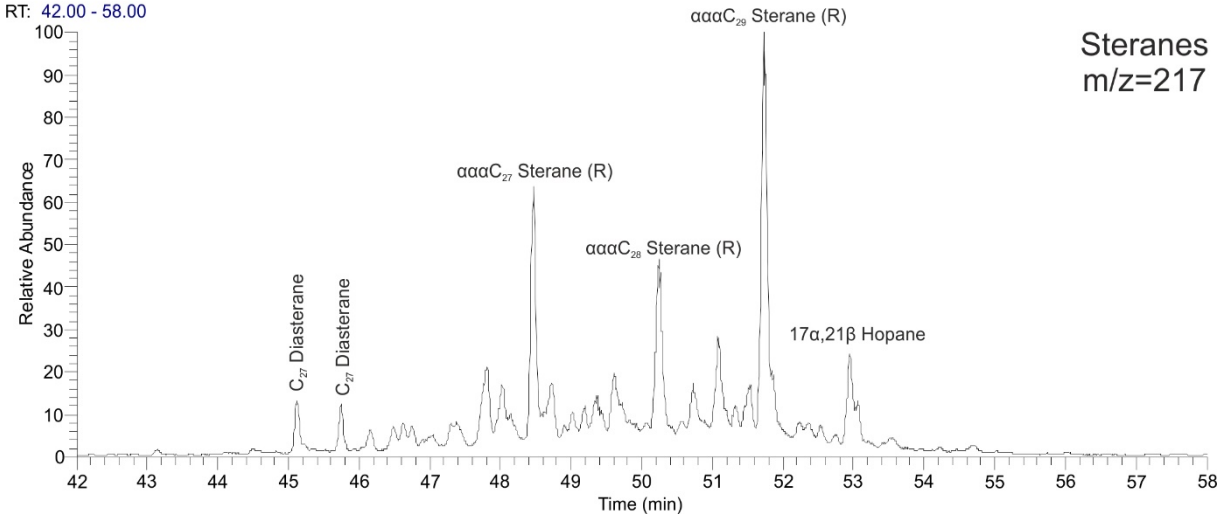
RT: 42.00 - 58.00
Steranes
m/z=217
αααC29 Sterane (R)
αααC27 Sterane (R)
αααC28 Sterane (R)
C27 Diasterane
C27 Diasterane
17α,21β Hopane
Relative Abundance
Time (min)

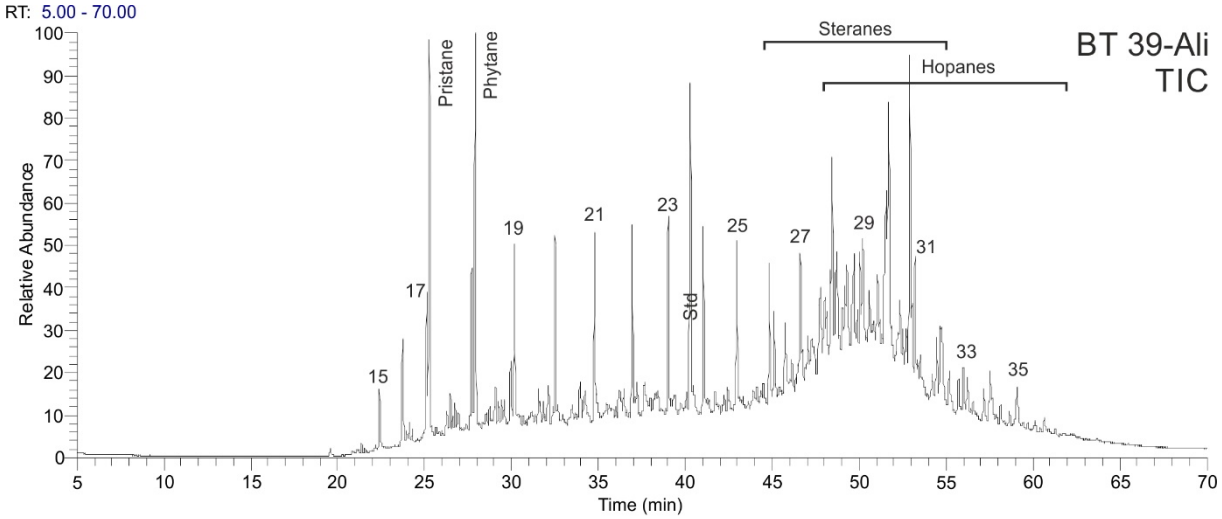
RT: 5.00 - 70.00
BT 39-Ali
TIC
Steranes
Hopanes
Pristane
Phytane
Std
15
17
19
21
23
25
27
29
31
33
35
Relative Abundance
Time (min)

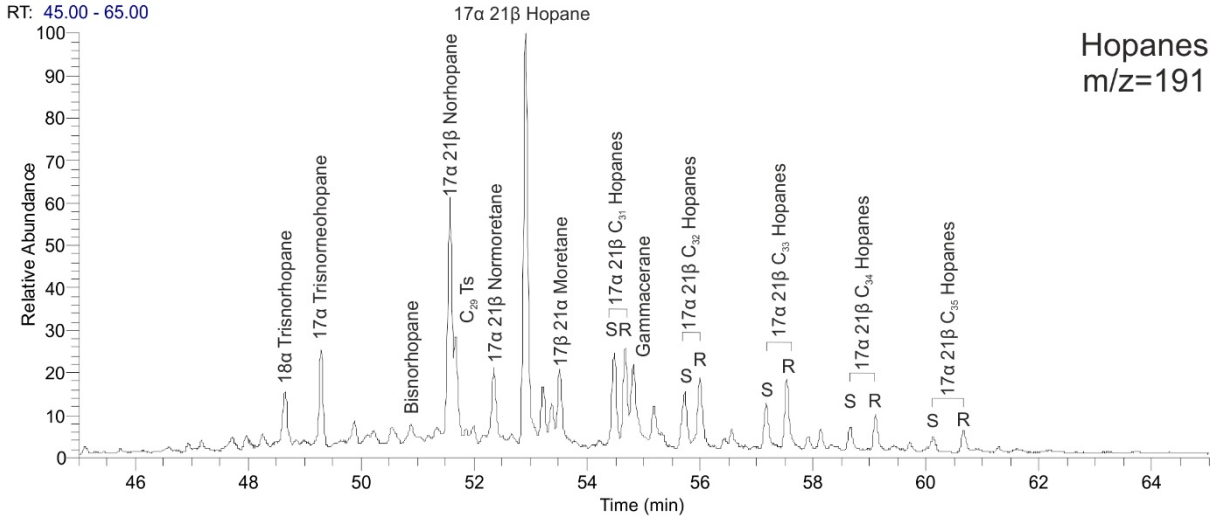
RT: 45.00 - 65.00
Hopanes
m/z=191
17α 21β Hopane
18α Trisnorhopane
17α Trisnorneohopane
Bisnorhopane
17α 21β Norhopane
C29 Ts
17α 21β Normoretane
17β 21α Moretane
17α 21β C31 Hopanes
SR
Gammacerane
17α 21β C32 Hopanes
S R
17α 21β C33 Hopanes
S R
17α 21β C34 Hopanes
S R
17α 21β C35 Hopanes
S R
Relative Abundance
Time (min)

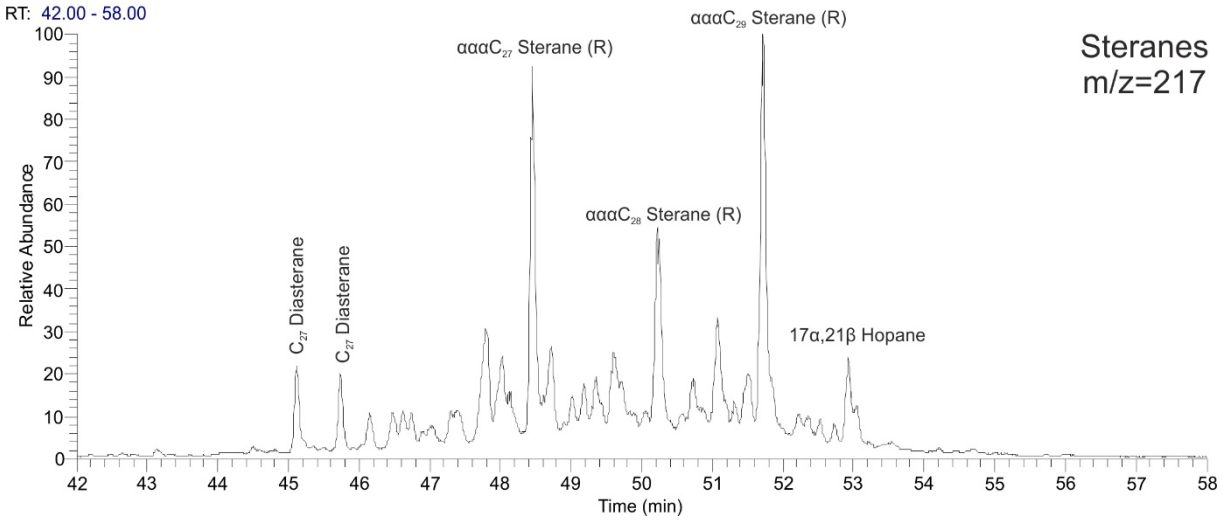
RT: 42.00 - 58.00
Steranes
m/z=217
αααC29 Sterane (R)
αααC27 Sterane (R)
αααC28 Sterane (R)
C27 Diasterane
C27 Diasterane
17α,21β Hopane
Relative Abundance
Time (min)

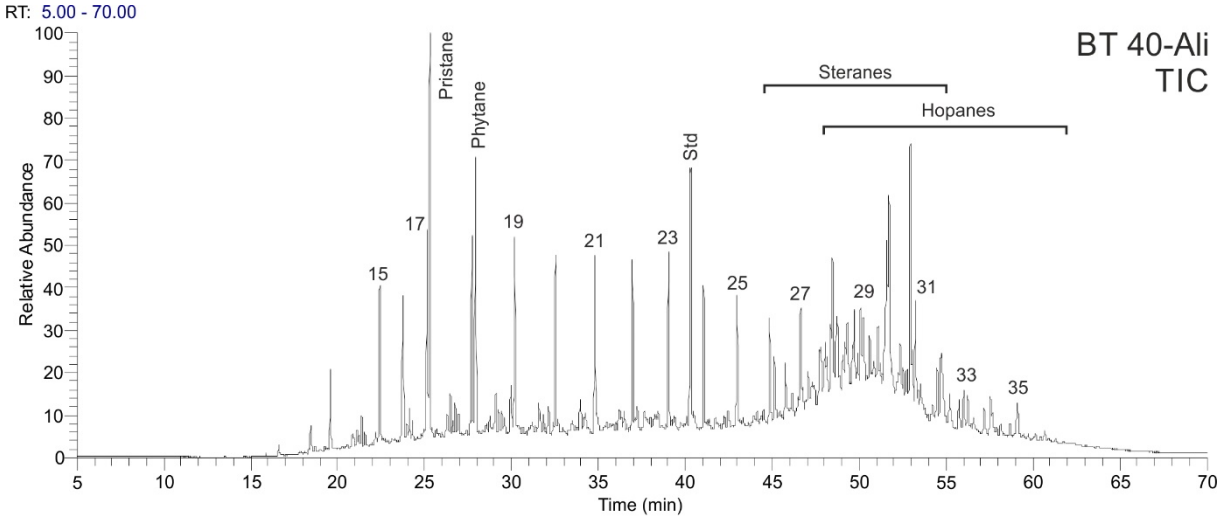
RT: 5.00 - 70.00
BT 40-Ali
TIC
Relative Abundance
Time (min)
Pristane
Phytane
Std
Steranes
Hopanes
15
17
19
21
23
25
27
29
31
33
35

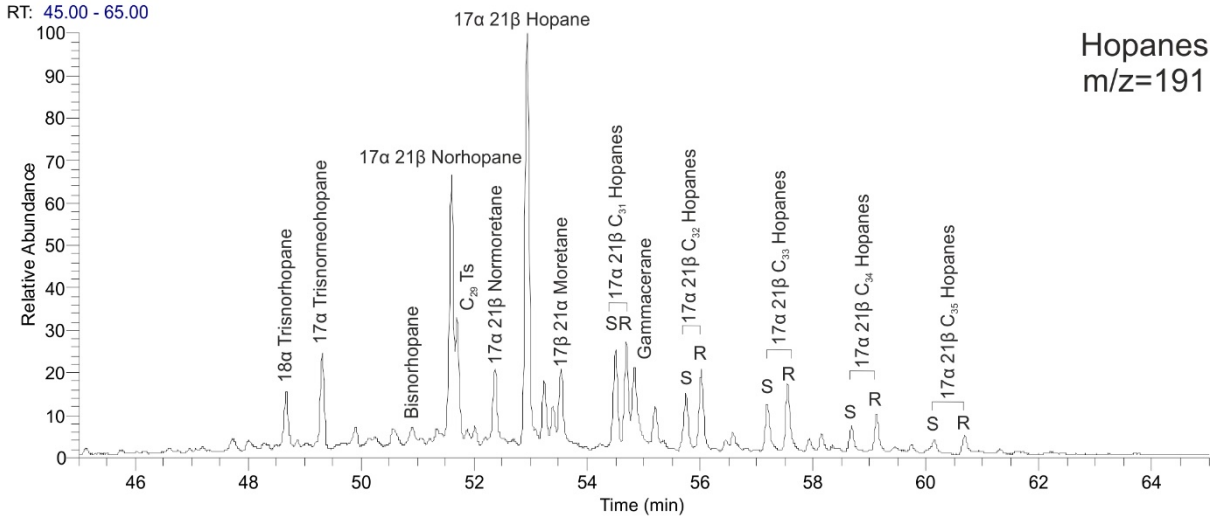
RT: 45.00 - 65.00
Hopanes
m/z=191
Relative Abundance
Time (min)
18α Trisnorhopane
17α Trisnorneohopane
Bisnorhopane
17α 21β Norhopane
C29 Ts
17α 21β Normoretane
17α 21β Hopane
17β 21α Moretane
17α 21β C31 Hopanes
SR
Gammacerane
17α 21β C32 Hopanes
S
R
17α 21β C33 Hopanes
17α 21β C34 Hopanes
17α 21β C35 Hopanes

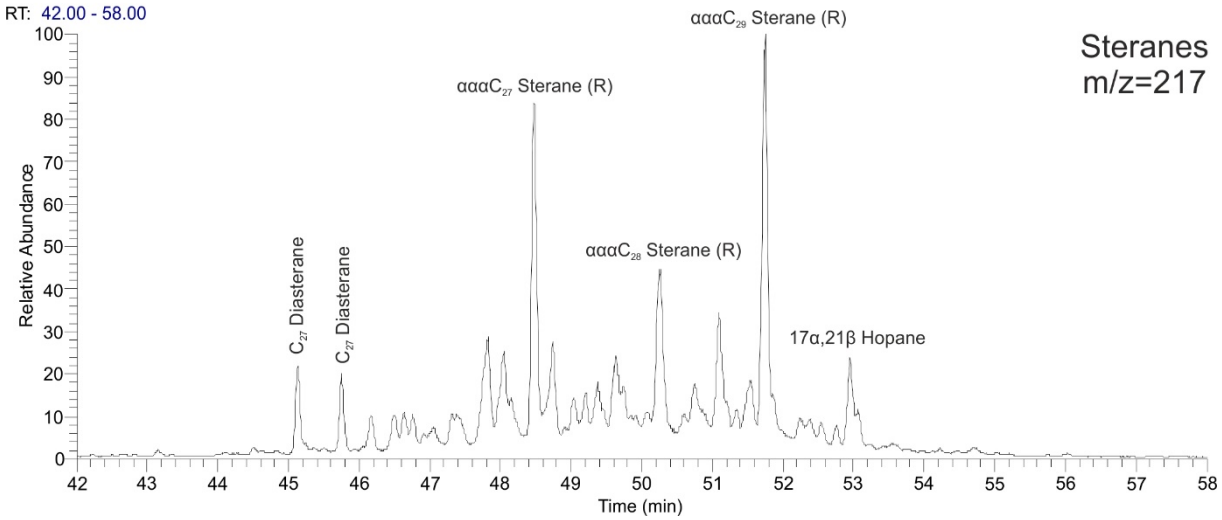
RT: 42.00 - 58.00
Steranes
m/z=217
Relative Abundance
Time (min)
C27 Diasterane
C27 Diasterane
αααC27 Sterane (R)
αααC28 Sterane (R)
αααC29 Sterane (R)
17α,21β Hopane

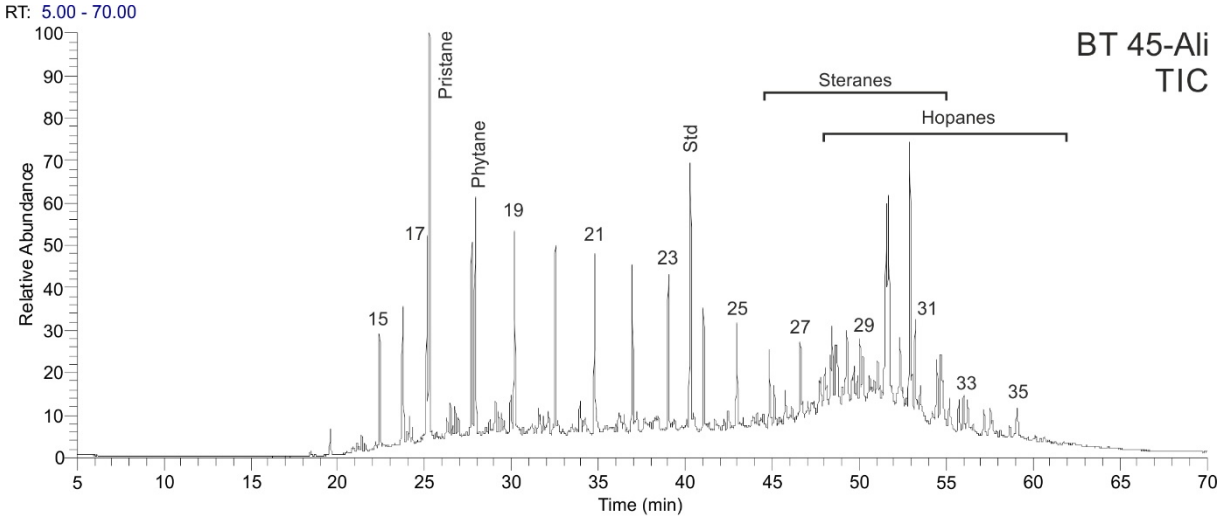
RT: 5.00 - 70.00
BT 45-Ali
TIC
Relative Abundance
Time (min)
Pristane
Phytane
Std
Steranes
Hopanes
15
17
19
21
23
25
27
29
31
33
35

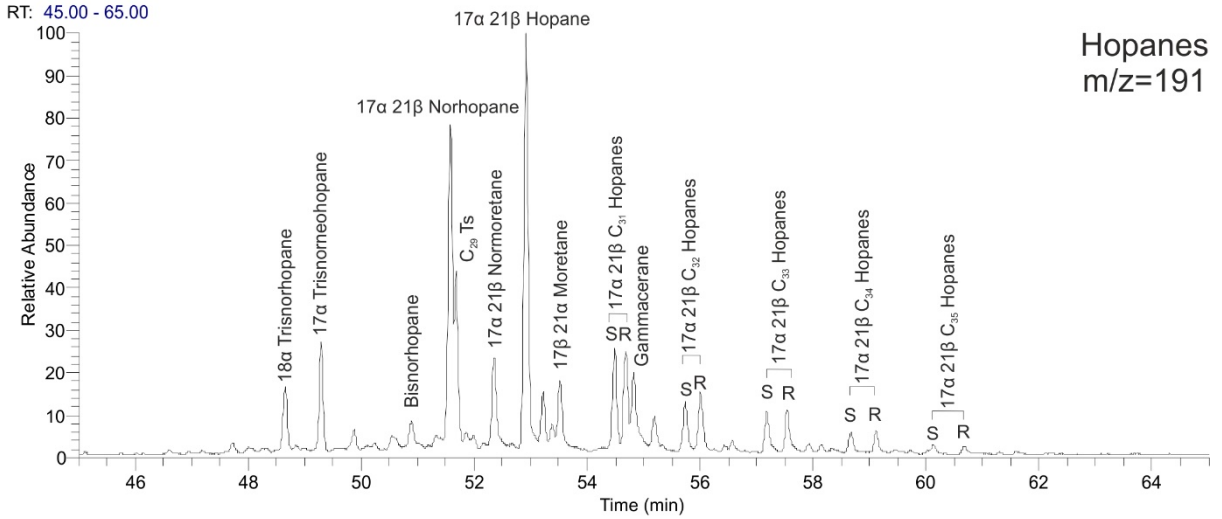
RT: 45.00 - 65.00
Hopanes
m/z=191
Relative Abundance
Time (min)
18α Trisnorhopane
17α Trisnorneohopane
Bisnorhopane
17α 21β Norhopane
C29 Ts
17α 21β Normoretane
17α 21β Hopane
17β 21α Moretane
17α 21β C31 Hopanes
S R
Gammacerane
17α 21β C32 Hopanes
17α 21β C33 Hopanes
17α 21β C34 Hopanes
17α 21β C35 Hopanes

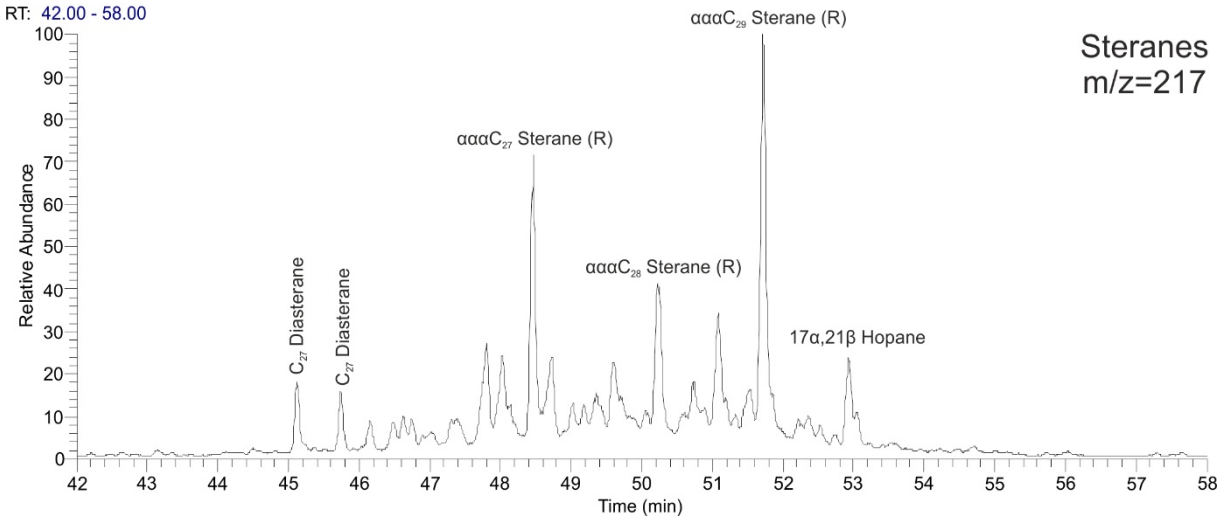
RT: 42.00 - 58.00
Steranes
m/z=217
Relative Abundance
Time (min)
C27 Diasterane
C27 Diasterane
αααC27 Sterane (R)
αααC28 Sterane (R)
αααC29 Sterane (R)
17α,21β Hopane

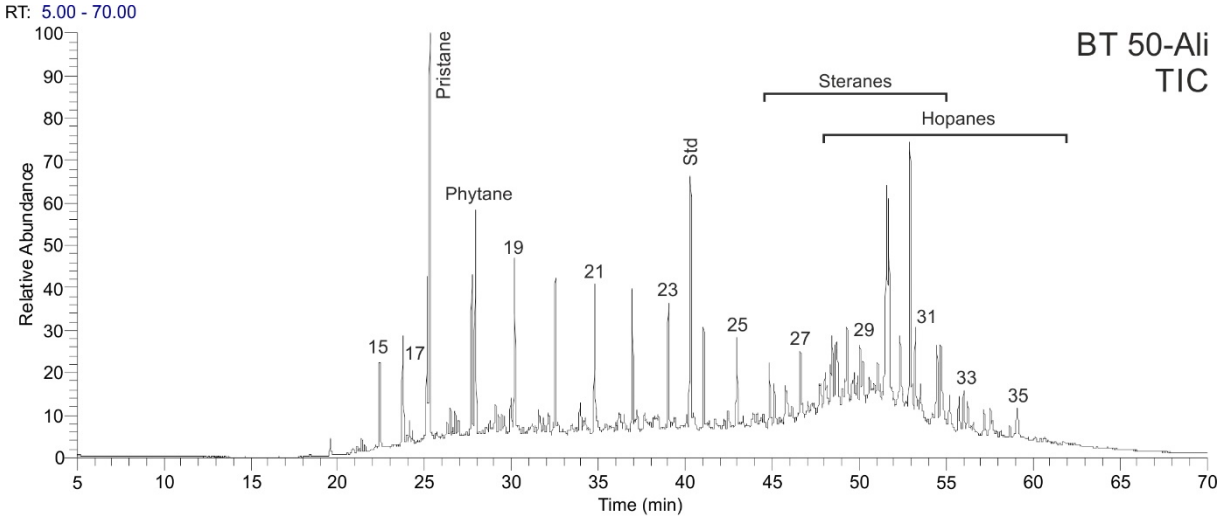
RT: 5.00 - 70.00
BT 50-Ali
TIC
Relative Abundance
Time (min)
Pristane
Phytane
Std
Steranes
Hopanes
15
17
19
21
23
25
27
29
31
33
35

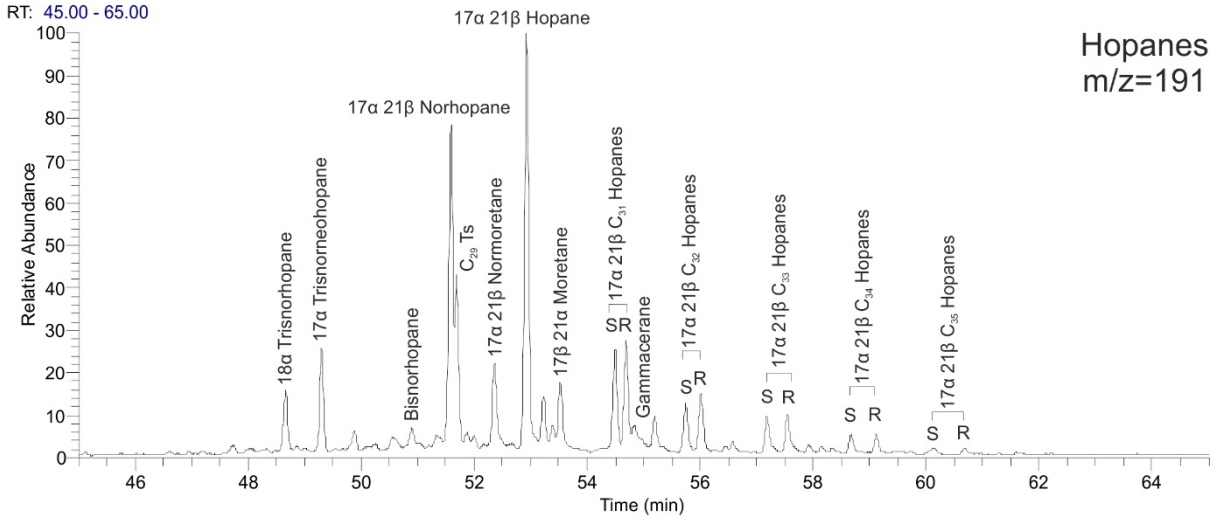
RT: 45.00 - 65.00
Hopanes
m/z=191
Relative Abundance
Time (min)
18α Trisnorhopane
17α Trisnorneohopane
Bisnorhopane
C29 Ts
17α 21β Norhopane
17α 21β Normoretane
17α 21β Hopane
17β 21α Moretane
17α 21β C31 Hopanes
S R
Gammacerane
17α 21β C32 Hopanes
17α 21β C33 Hopanes
17α 21β C34 Hopanes
17α 21β C35 Hopanes

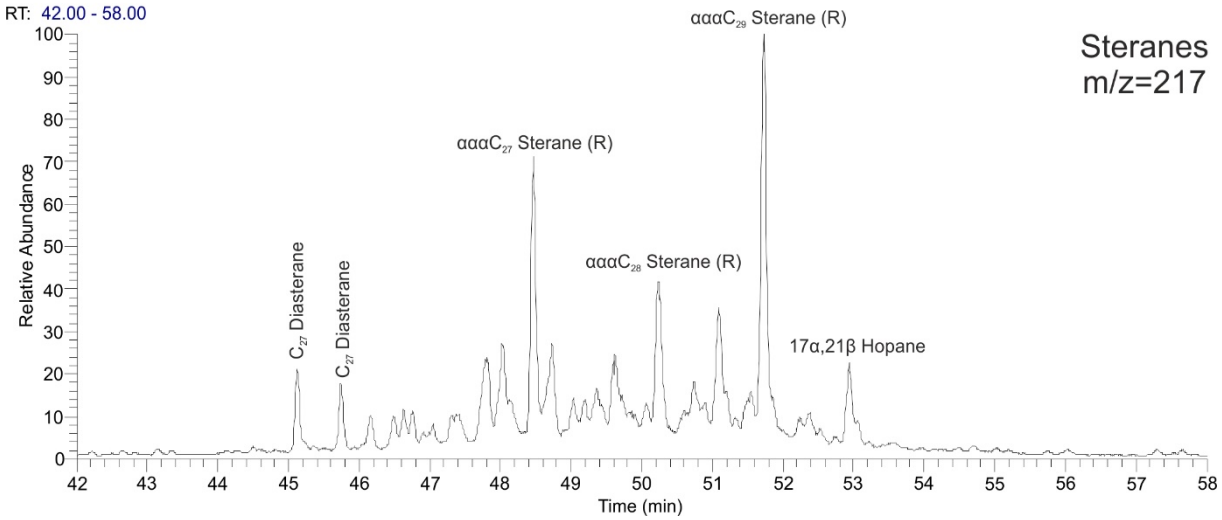
RT: 42.00 - 58.00
Steranes
m/z=217
Relative Abundance
Time (min)
C27 Diasterane
C27 Diasterane
ααα C27 Sterane (R)
ααα C28 Sterane (R)
ααα C29 Sterane (R)
17α,21β Hopane

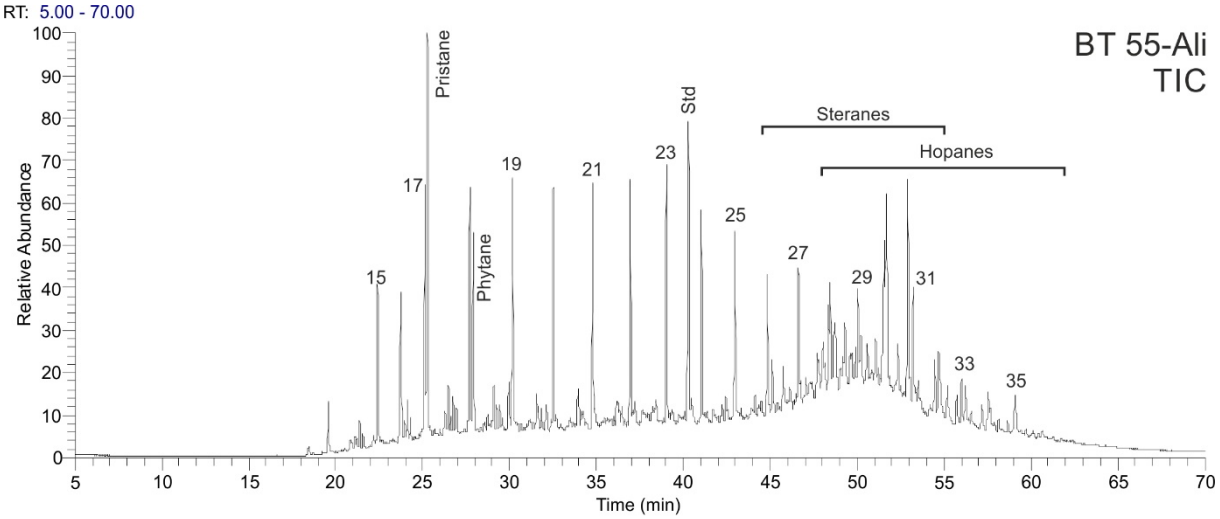
RT: 5.00 - 70.00
BT 55-Ali
TIC
Relative Abundance
Time (min)
Pristane
Phytane
Std
Steranes
Hopanes
15
17
19
21
23
25
27
29
31
33
35

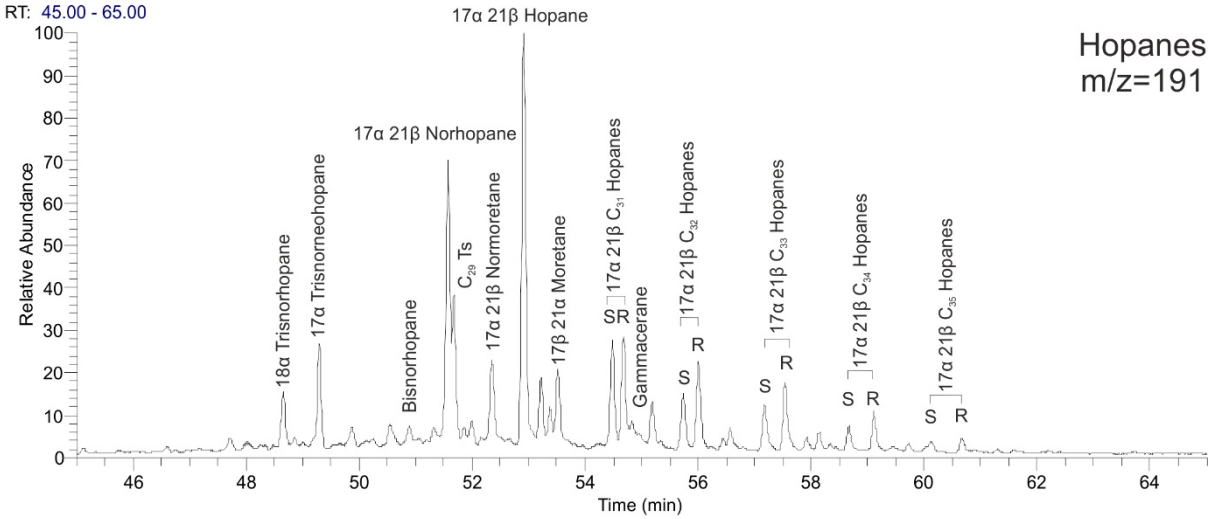
RT: 45.00 - 65.00
Hopanes
m/z=191
Relative Abundance
Time (min)
17α 21β Hopane
17α 21β Norhopane
18α Trisnorhopane
17α Trisnorneohopane
Bisnorhopane
C29 Ts
17α 21β Normoretane
17β 21α Moretane
17α 21β C31 Hopanes
SR
Gammacerane
17α 21β C32 Hopanes
S
R
17α 21β C33 Hopanes
17α 21β C34 Hopanes
17α 21β C35 Hopanes

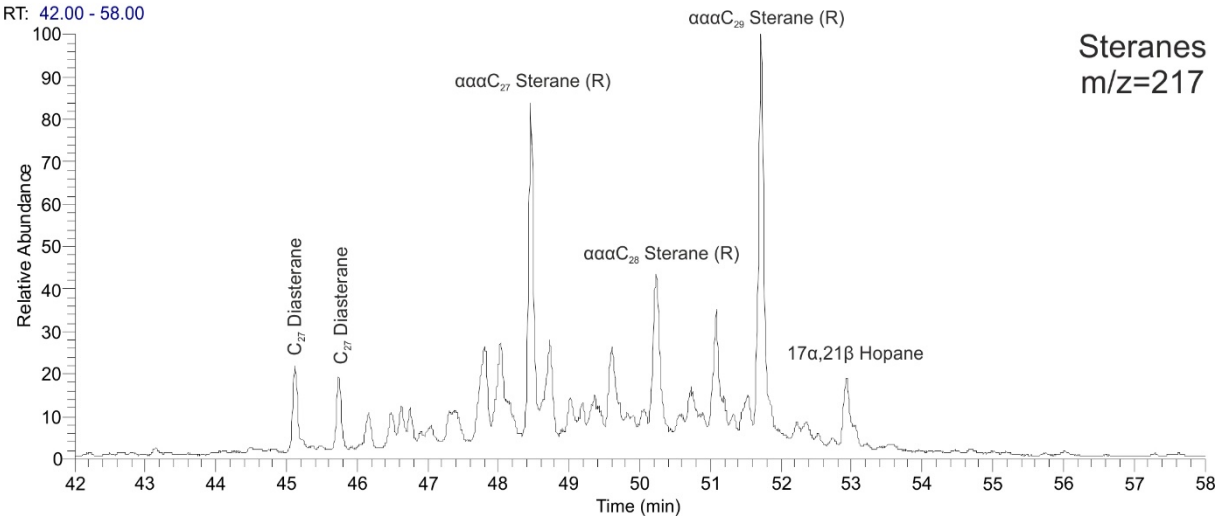
RT: 42.00 - 58.00
Steranes
m/z=217
Relative Abundance
Time (min)
αααC29 Sterane (R)
αααC27 Sterane (R)
αααC28 Sterane (R)
C27 Diasterane
C27 Diasterane
17α,21β Hopane

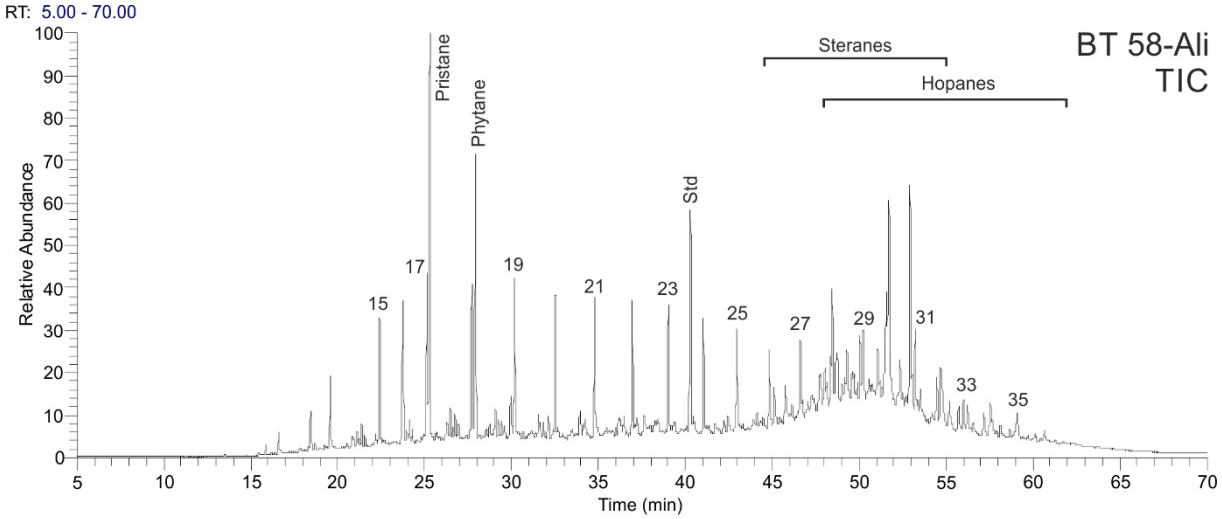
RT: 5.00 - 70.00
BT 58-Ali
TIC
Steranes
Hopanes
Pristane
Phytane
Std
15
17
19
21
23
25
27
29
31
33
35
Relative Abundance
Time (min)

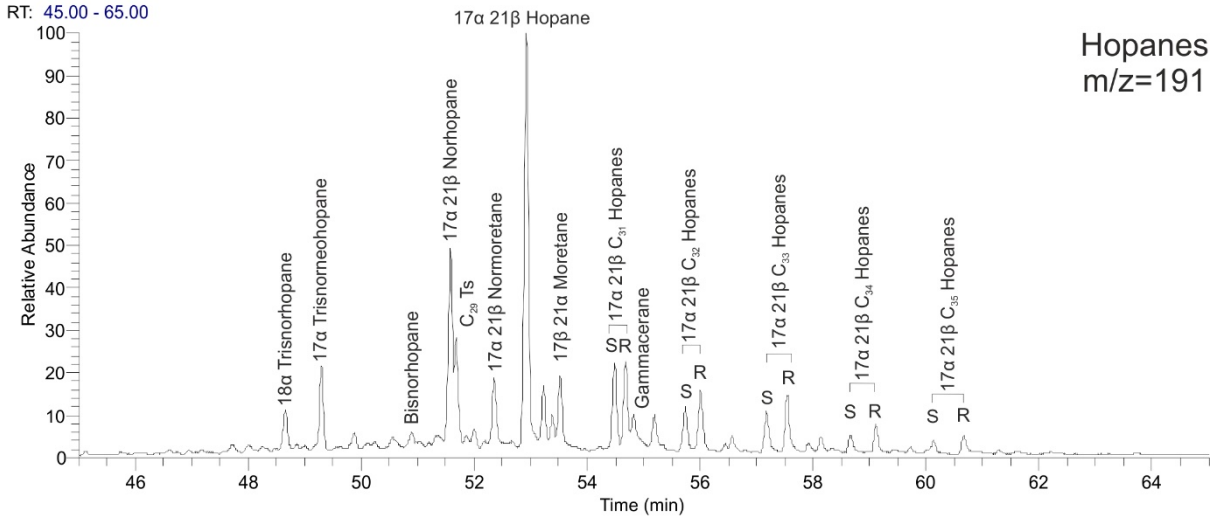
RT: 45.00 - 65.00
Hopanes
m/z=191
17α 21β Hopane
18α Trisnorhopane
17α Trisnorneohopane
Bisnorhopane
17α 21β Norhopane
C29 Ts
17α 21β Normoretane
17β 21α Moretane
17α 21β C31 Hopanes
SR
Gammacerane
17α 21β C32 Hopanes
S R
17α 21β C33 Hopanes
S R
17α 21β C34 Hopanes
S R
17α 21β C35 Hopanes
S R
Relative Abundance
Time (min)

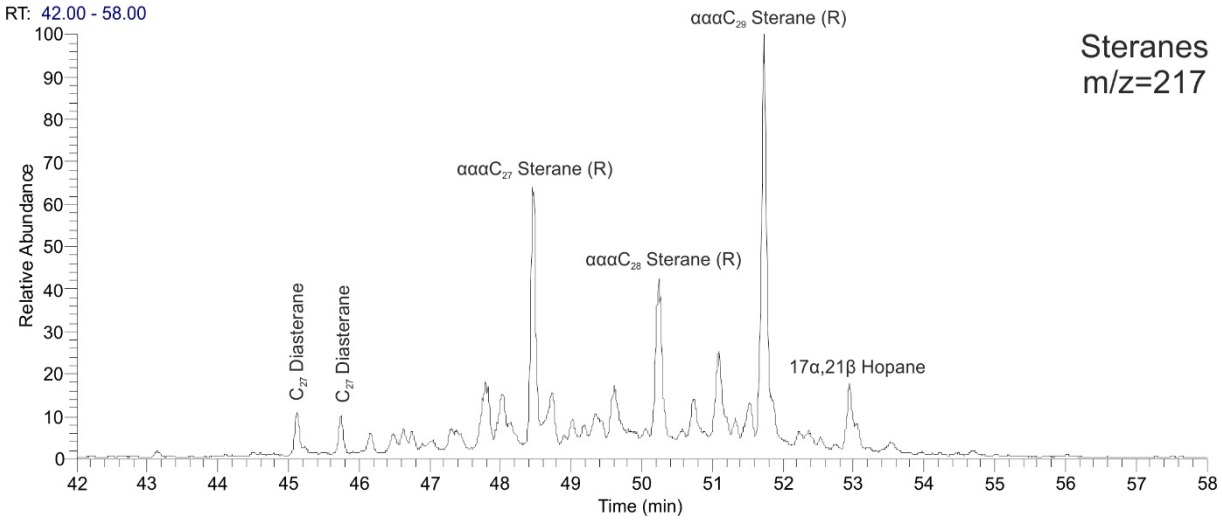
RT: 42.00 - 58.00
Steranes
m/z=217
ααα C29 Sterane (R)
ααα C27 Sterane (R)
ααα C28 Sterane (R)
C27 Diasterane
C27 Diasterane
17α,21β Hopane
Relative Abundance
Time (min)